Interpretation of the gravity anomalies of Bahia state Brazil

Ussami, Naomi

INTERPRETATION OF THE GRAVITY ANOMALIES OF BAHIA STATE, BRAZIL

by

Naomi Ussami

A thesis submitted for the degree of Doctor of Philosophy

University of Durham

Graduate Society *August 1986*

TABLE OF CONTENTS

ABSTRACT

This thesis describes the gravity interpretation of Bahia State, Brazil, which comprises the northern São Francisco craton, the Upper Proterozoic fold belts and the basins adjacent to the continental margin. The study centres on the isostatic analysis of the region and on the interpretation of large and high amplitude negative anomalies which occur over the Precambrian and the sedimentary basins.

The isostatic analysis of the northern São Francisco craton was carried out using the isostatic response function technique. Taking into account subsurface loads, an elastic plate with a minimum effective thickness of 20-40 km explains the observed isostatic response function. The subsurface loads are (1) a slight thickening of the crust under the Espinhaço Fold System and (2) five to ten kilometres of low density rocks in the upper crust.

A large and high amplitude (~ 50 mGal) negative anomaly of shallow origin, centred near the western border of the Paramirim complex and parallel to the Espinhaço fold belt, is interpreted as caused by a large and mainly unexposed granite batholith. The granite substantially underlies the fold belt and extends towards the centre of the Paramirim complex. The minimum density contrast between the granite and the country rocks is estimated to be -0.06 g cm^{-3} . The thickness of the granite is 8 to 13 km for density contrasts of -0.15 g cm^{-3} to -0.10 g cm^{-3}.

A series of high amplitude negative anomalies (50 to 100 mGal), without flanking positive anomalies, characterizes the onshore Reconcavo, Tucano and Jatoba basins, which were all formed in connection with the South Atlantic opening. The gravity interpretation indicates up to 7 km of sediments infilling these basins and no significant Moho upwarp beneath. In contrast, the gravity anomalies over the offshore Jacuipe and Sergipe-Alagoas basins are explained by a thick accumulation of sediments on a strongly attenuated crust. The onshore basins show short-lived subsidence (< 25 Ma) with little, if any thermal subsidence. Syn-rift and post-rift (thermal) sedimentation is observed only in the continental margin basins. A mechanism in which upper crustal extension in one region (onshore basins) is compensated and balanced against lower extension in another region (offshore basins), through a detachment fault, may explain the way these basins formed.

ACKNOWLEDGEMENTS

I would like to thank Professor Martin Bott for suggestions, criticism and advice throughout the development of this project.

I would like also to thank

Fundação de Amparo a Pesquisa do Estado de São Paulo, Conselho Nacional de Desenvolvimento Cientifico e Tecnologico (CNPq) and Overseas Research Student Award (ORS Award) for financial assistance.

Departamento de Geofisica of São Paulo University for allowing me to remain on leave throughout the course of this project. In particular, to my colleague Nelsi Cogo de Sá who patiently organized the computer data base of the Brazilian gravity data, including the Bahia State.

PETROBRAS, in particular to Dr. Walter C. M. Campos and Dr. Marco Polo P. Boa Hora, for providing the gravity and well data of the coastal basins.

Dr. Umberto G. Cordani for providing the rock samples of Bahia State and the literature on the local geology.

Garry Karner, Webster Mohriak and Emmanuel Jardim de Sá for many discussions, comments and criticisms on different parts of this thesis.

Special thanks to Chris Bentley, who was prepared to give up his time in dealing with philosophical and theological questions, for proof reading several versions of the manuscript and to Dona Teruko Ussami, in Brazil, for her valuable support and assistance.

CHAPTER 1

Introduction

Bahia State, Brazil comprises an area of approximately 677,600 km^2, between latitude 8^0 and 14^0 S and longitude 38^0 and 46^0 W. This State includes almost all of the northern São Francisco craton, part of the surrounding fold belts and the onshore Mesozoic to Tertiary sedimentary basins adjacent to the South Atlantic continental margin.

Within the Brazilian territory, Bahia State is the region with the largest amount of geological information, which has resulted from an intensive program of mineral exploration in its Precambrian terrain and oil exploration in the onshore and offshore basins. However, in spite of a systematic program of radiometric dating (Brito Neves et al., 1980) in order to understand the complex Archean and Proterozoic histories of the northern São Francisco craton, the density of geological information for most of the region is still of reconnaissance type. The most recent account of Bahia State geology (Inda and Barbosa, 1978) is mainly based on 1:250,000 scale surveys.

Apart from the present study, there has not been a previous interpretational geophysical study in the northern São Francisco

craton. Gravity and seismic studies are restricted to the southern part of the São Francisco craton. An unreversed seismic profile, between 17^{0}-19^{0}S and 42^{0}-44^{0}W, located the Moho at about 42 km (Giese and Schütte, 1975). This profile runs across the southeastern boundary of the São Francisco craton, near the south end of the Espinhaço fold belt. Blitzkow et al. (1978) interpreted a large and high amplitude negative gravity anomaly, in the same region, as caused by a relative crustal thickening of about 5 km across the fold belt. A gravity study in the southern São Francisco craton and across its southern and southwestern borders was carried out by Lesquer et al. (1981). The objective of their study was to define the boundaries of the craton which are partially covered by the metasediments of the marginal fold belts. They also estimated the thickness of the Upper Proterozoic pelitic-calcareous sequence which covers the interior of the craton.

The present research project aims to interpret the gravity data obtained by Gomes and Motta (1978) in the northern São Francisco craton and the gravity data of the eastern coast of Bahia State, provided by PETROBRAS (Brazilian Oil Company).

A Bouguer anomaly map of Bahia State was published by Motta et al. (1981) using a Bouguer density of 2.60 g cm^{-3}. In the present study, density measurements on crystalline rocks of the Precambrian basement of Bahia State yielded an average density of 2.71 g cm^{-3}, which is characteristic of a granodioritic

rather than granitic upper crust. A new Bouguer anomaly map was constructed using a more appropriate density in the Bouguer correction. The results together with a geological account of Bahia State are presented in Chapter 2.

The interpretation of the gravity data of Bahia State is subdivided into three parts.

1.1 The Isostatic Analysis of the Northern São Francisco Craton.

In Chapter 3, the isostatic analysis of the northern São Francisco craton using the isostatic response function technique (Dorman and Lewis, 1970) is discussed.

In recent years, an advance in understanding the thermal and mechanical properties of the oceanic and continental lithospheres has been obtained by studying how the lithosphere responds to geological time scale loads (Forsyth, 1979; Kirby, 1983; McNutt, 1980; Watts et al., 1982; Karner and Watts, 1982, 1983). Flexural and isostatic response function studies of oceanic regions assuming an elastic plate rheology proved to be adequate in explaining the gravity and bathymetric features. Studies in continental areas, which are generally characterized by complex geological history, have used both elastic and viscoelastic rheologies. Low flexural rigidities obtained for continental lithosphere (Banks et al., 1977; McNutt and Parker, 1978), using the isostatic response function technique,

apparently contradicted the inference from oceanic studies of an increase of flexural rigidity with the thermal age of the plate (Watts, 1978). Because the continental lithosphere is older, higher rigidity was expected. Viscous relaxation of the continental lithosphere was then proposed by McNutt and Parker (1978) in order to explain the apparent low flexural rigidity of an old and stable continental lithosphere. However, studies of lithospheric flexure on single tectonic features (Walcott, 1970; Karner and Watts, 1982; 1983) show that an elastic plate with relatively high flexural rigidity explains the gravity and geomorphological features in some continental regions. This suggests that the lithosphere is capable of maintaining stress for periods of time longer than 10^9 years without necessarily undergoing viscous relaxation. An apparent inconsistency is therefore evident between the flexural rigidity of the continental lithosphere obtained from flexural studies ("forward" problem) and the results obtained by using the isostatic function technique ("inverse" problem). Possible reasons for obtaining low flexural rigidities in continental areas using the response function technique were suggested by Forsyth (1985). Firstly, in the studies of Banks et al. (1977) and McNutt and Parker (1978), the observed topography was supposed to be the only load acting on the plate and its compensation was situated at a single depth at the Moho. If there are other sources of compensation which are not taken into account in interpreting the observed isostatic response function, the estimated rigidity of the plate may be biased

towards lower values. These other sources of compensation are generally referred to as subsurface loads. Secondly, Forsyth (1985) showed that the application of the response function technique to continental wide areas may be biased towards low flexural rigidity because different provinces with variable topographic signals are averaged together. This process favours provinces of higher topography which generally are situated over weaker plate.

In Chapter 3, the isostatic response function technique is applied to a single tectonic province, the São Francisco craton, taking into account the existence of subsurface loads as suggested by Forsyth (1985). It is shown that this technique can give useful information on the compensation mechanism.

1.2 The Gravity Study of the Paramirim Complex Granite.

Following the isostatic analysis, a gravity study of a large and high amplitude (-50 mGal) negative gravity anomaly situated in the centre of the northern São Francisco craton was carried out (Chapter 4). Local negative gravity anomalies are generally ascribed to low density granites or sedimentary basins. However, in the present case, there is no direct indication of the possible source of the observed negative gravity anomaly. By combining the available geological information with the aeromagnetic data and density measurements together with quantitative techniques of gravity interpretation such as the

maximum depth rule of gravitating bodies (Bott and Smith, 1958), the source of this anomaly was investigated. The gravity anomaly is situated along the Espinhaço fold belt of Middle Proterozoic age to the east and it extends westwards towards the centre of the Paramirim complex. The mostly likely source of this large and high amplitude negative anomaly is low density granite. This seems to be another of many common cases of granite batholith associated with orogeny. Gravity method is useful in finding and mapping granitic bodies which are not exposed on the surface (Bott et al., 1958; Bott, 1967). In spite of the ambiguity of the gravity method, it is possible to obtain useful structural information of granitic bodies by placing bounds on density and depth of gravitating bodies (Bott and Smithson, 1967). The subsurface shape of the granitic body obtained from the gravity modelling provides, to a first approximation, the structural relationship between the emplaced granite and the deformation of the fold belt.

1.3 Gravity and Stratigraphic Studies of the Mesozoic-Tertiary Basins.

Chapter 5 deals with the integrated gravity and stratigraphic studies of the onshore Reconcavo, Tucano, Jatoba and offshore Sergipe-Alagoas basins, which were formed in connection with the South Atlantic opening.

The onshore Reconcavo, Tucano and Jatoba basins, which are separated from the continental margin by a segment of Precambrian terrain, are all characterized by high amplitude negative anomalies (50 to 110 mGal). Such negative anomalies are usually ascribed to low density sediments. The absence of positive gravity anomalies flanking the sides of the basins suggests a flat Moho topography beneath these basins. The stratigraphy of the onshore basins indicates a short lived subsidence of less than 25 Ma which was synchronous with the rift phase of the South Atlantic opening (Upper Jurassic to Aptian). The Jacuipe and Sergipe-Alagoas continental margin basins are situated upon a strongly attenuated crust and contain both the syn and post-rift sedimentation.

It is now of general consensus (see review by Scrutton,1982; Bally, 1981) that continental rifted margins initiate and evolve according to the mechanism proposed by Artemjev and Artyushkov (1971) and McKenzie (1978). Lithospheric extension, accompanied with crustal attenuation, normal faulting in the brittle upper crust and ductile deformation of the lower crust, characterizes the initial subsidence. The amount of extension controls the amount of heat input into the thinned lithosphere. At the cessation of the extensional regime, following the onset of the sea floor spreading, the lithosphere cools and contracts initiating the stage of thermal subsidence of the margins, which decreases exponentially with time. Whilst this model accounts reasonably well with the thermal subsidence during the drifting

stage, there are still some complex features related to the rifting stage which are not predicted by the simple extensional model (Bott, 1982; Keen, 1982). The amount of extension estimated from reconstruction of faults in the upper crust (De Charpal et al., 1978) and backstripping of the sediments to estimate the rift phase and thermal subsidences (Royden and Keen, 1980) appears to be incompatible with the estimated amount of lower crust attenuation beneath the rifted area. Therefore, it is not fully understood how the rifting process leading to lithospheric failure actually occurs. Because the onshore Reconcavo, Tucano and Jatoba basins were entirely formed during the rifting phase of the South Atlantic, a comparative study of the evolution of these onshore basins with the adjacent continental margin, complemented with deep crustal information inferred from gravity data, may provide new evidence on the mechanism of continental rifting. There is an intimate connection between the evolution of these onshore basins with the rift phase of the South Atlantic opening. However, when the drifting stage initiated the onshore basins stopped subsiding and the continental margin basins went into the thermal stage. An extensional process in the lines of Wernicke's "simple shear" model, in which upper crustal extension on one region is connected and balanced against lower lithospheric extension in another region, may explain the way the Brazilian onshore and offshore basins and their complementary African basins formed during the rifting stage.

CHAPTER 2

Gravity Data and Geology of Bahia State

2.1 Gravity Data

2.1.1 Data Acquisition

The gravity data of Bahia State were obtained by two Brazilian organizations. During the years of 1977 and 1978, the Brazilian Mineral Production Department (DNPM/CPRM) carried out the first regional gravity survey, comprising 2084 gravity stations, which covered almost of all of Bahia State and its Precambrian terrain. A complete description of the development of this project and the listing of the acquired data are reported in Gomes and Motta (1978).

Of the stations, 548 are located at bench marks, 387 had the altitude determined by using barometers and the altitudes and coordinates of the remaining 1023 stations were obtained from contours on the 1:100,000 and 1:250,000 scale topographic maps. In order to avoid large errors, the sites of the stations, which had the altitude determined using barometers and topographic contours, were carefully chosen to be located in regions of

smooth topography and easy recognition in the field. The altitudes obtained from contours on 1:250,000 scale maps have an estimated error of ±20 metres, whereas the error is about ±5 metres for altitudes determined by using barometers. The estimated error of heights at bench marks is less than one metre.

The eastern part of Bahia State, along the Atlantic coast, was surveyed by the Brazilian oil company (PETROBRAS) during the 1960's. The gravity survey covered the Cenozoic-Mesozoic sedimentary basins with an average spacing of 500 metres between the stations. 2470 stations from the survey, with an average distance of one kilometre, were provided for the present study. The coordinates and altitudes are accurately known to a few centimetres.

Fig. 2.1 shows the distribution of the gravity stations of Bahia State. It also includes some stations of the neighbouring States of Minas Gerais in the south and Sergipe and Alagoas in the northeast.

2.1.2 Data Reduction

All the gravity values are referenced to the International Gravity System Network 1971. The survey carried out by the DNPM/Brazil and by PETROBRAS, are both related to the same

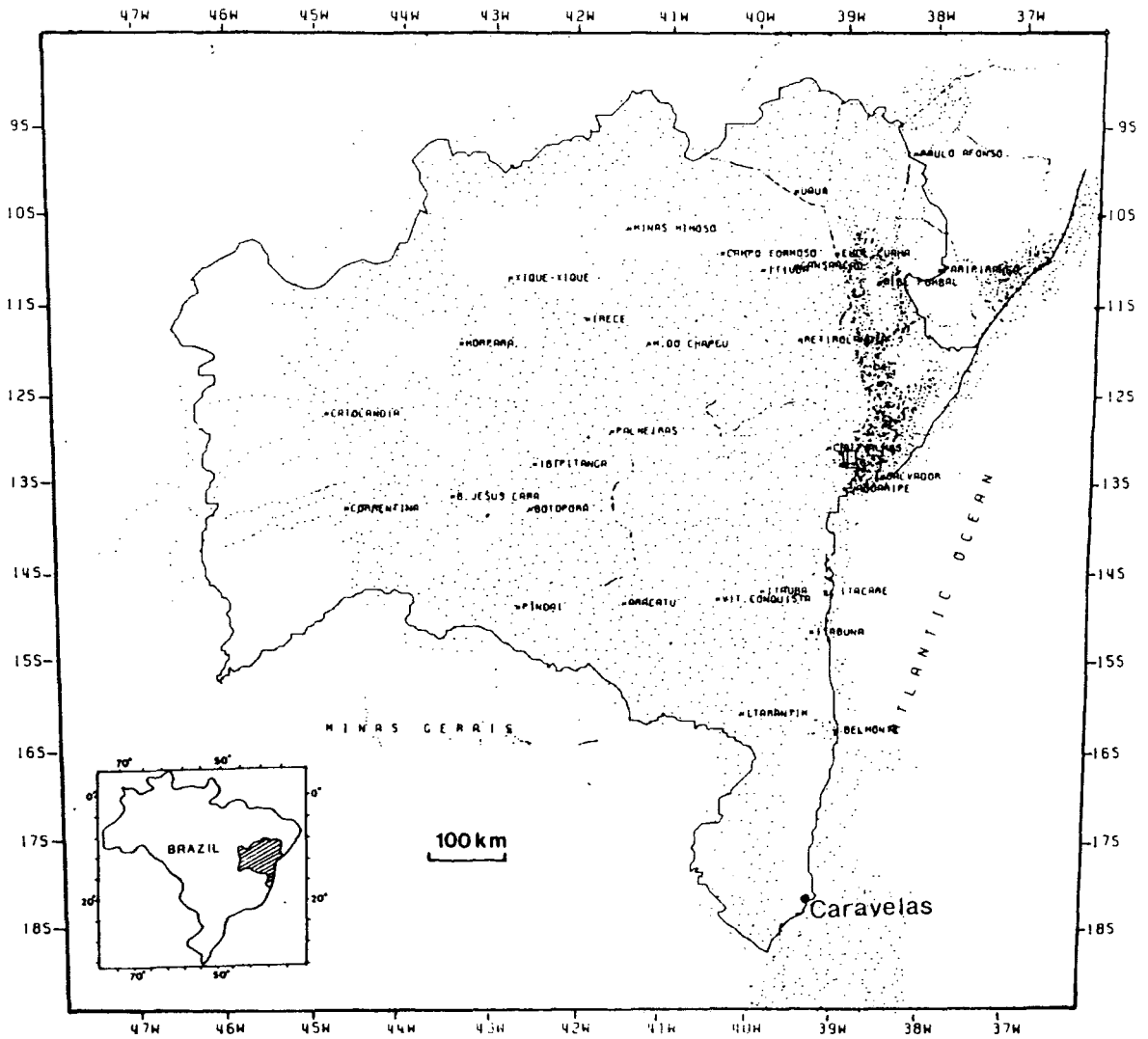

Fig. 2.1 - Distribution of gravity stations in Bahia State and neighbouring States.

IGSN-71 base station named Caravelas J situated at Caravelas city, shown in Fig. 2.1.

The area covered by these two gravity surveys extends from 8^{o}S to 18^{o} S. The latitude correction was carried out using the 1967 International Gravity Formula. The accuracy in the latitude of the stations varies from a few centimetres to two hundred metres. Therefore, a maximum error of ± 0.07 mGal is estimated for the latitude correction.

The free-air correction was calculated using a vertical gradient of -0.3086 mGal m^{-1} . The main source of error in evaluating the gravity reduction is the uncertainty in the altitude. The error in the combined elevation correction can be as much as ± 3 mGal for stations which had the altitude determined from contours on the 1:250,000 scale maps. Whilst the error due to the uncertainty in the altitude is regarded as random, an incorrect choice of the density value in the Bouguer correction introduces a systematic error. In regions of significant topographic variation, a correlation between Bouguer anomalies and short wavelength topographic features may be observed. The average altitude of Bahia State is about 800 metres. An error of ± 0.05 g cm^{-3} in the Bouguer density introduces a systematic error of ± 1.7 mGal.

A Bouguer anomaly map of Bahia State has previously been published by Gomes and Motta (1978) and by Motta et al. (1981).

2.60 g cm^{-3} was assumed as the density for the Bouguer correction. Because this value seemed too low to be representative of the Precambrian terrain of Bahia State, density measurements on 158 crystalline rock samples of Bahia State basement were carried out by Ussami and Padilha (1982) in order to obtain a more appropriate density value for the Bouguer reduction. The description of the rocks samples and the results of the measurements are presented in Appendix A.

The density measurements were made on dry rocks, disregarding the effects of porosity, which is expected to be negligible in igneous and metamorphic rocks. The samples were weighed in the air and in water, and the density was obtained using the formula:

$$d_r = [M_1 - M_2]^{-1} \; M_1 \; d_w$$

where M_1 = mass in the air (in grams)

M_2 = mass in water (in grams)

$d_w = 1.03$ g cm^{-3}

The estimated accuracy in the density measurements is ± 0.02 g cm^{-3}. The results are summarized in the histogram shown in Fig. 2.2(a), for different types of rocks. A weighted average (see

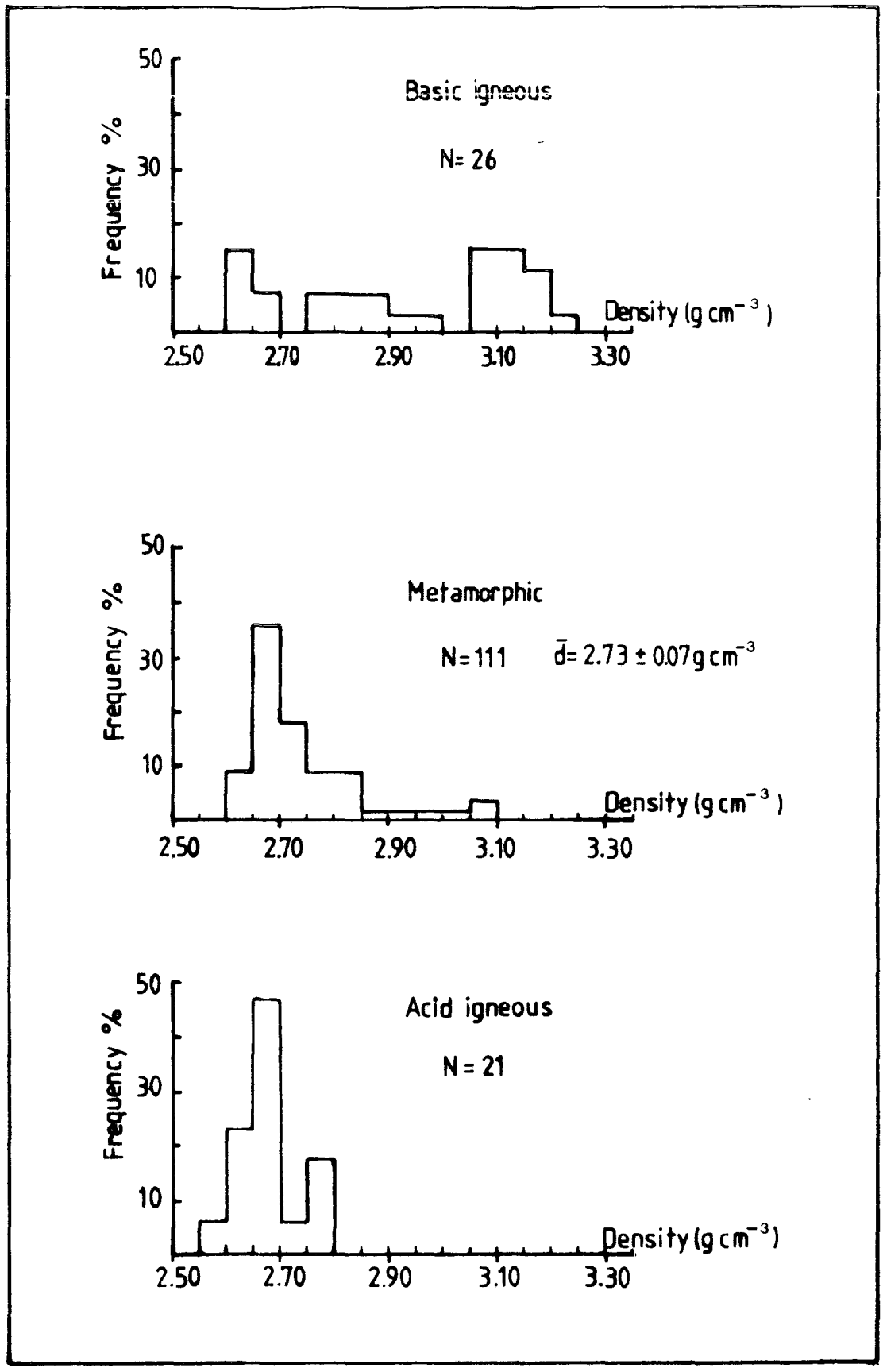

Fig. 2.2a - Histogram of density measurements for different types of rock from the crystalline basement of Bahia State. d is the average density. The standard deviation is only calculated for the metamorphic rocks.

Appendix A) was calculated from the histogram of Fig. 2.2(b), assuming the high density rocks (> 2.85 g cm^{-3}) constitute 5% of the total composition of the upper crust.

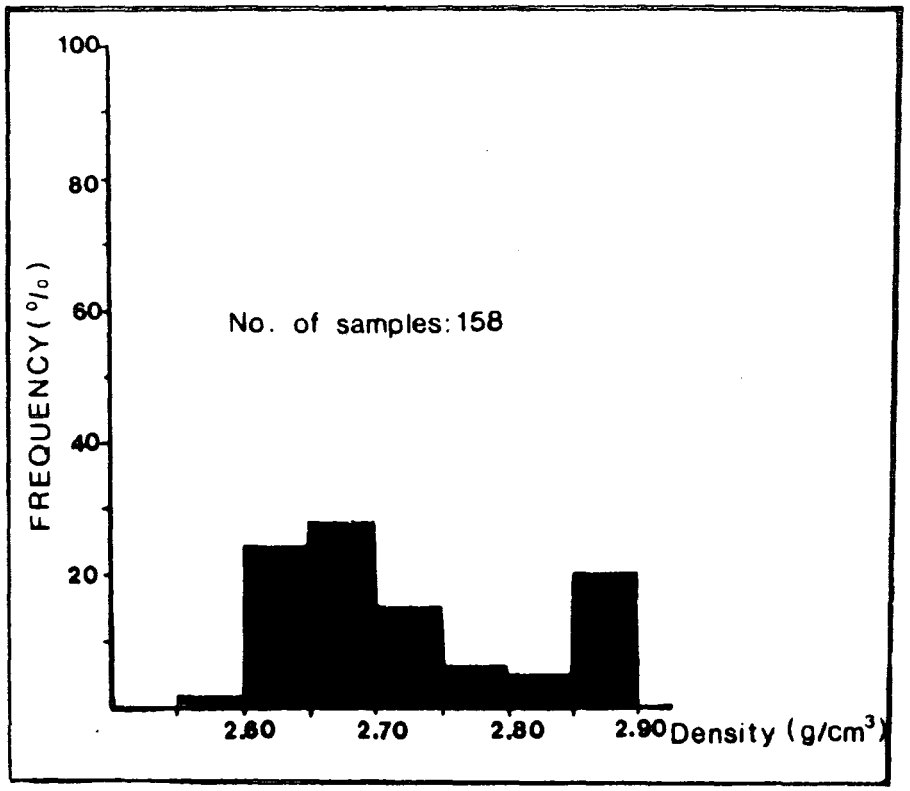

Fig. 2.2b - Histogram of density measurements on crystalline rocks of Bahia State.

The result of this calculation yielded an average density of 2.71 ± 0.06 g cm^{-3}. A similar result has been reported by Gibbs (1968) for the Canadian Shield. This value characterizes an upper crust of granodioritic to dioritic composition.

A Bouguer density of 2.67 g cm^{-3} was therefore assumed, since this value is closer to the one obtained for the Precambrian terrain of Bahia State and it is also the most commonly used density for Bouguer correction over large continental areas.

The Bouguer anomalies were calculated with an accuracy of ±0.1 mGal for stations situated at bench marks. The same accuracy is estimated for stations located over the sedimentary basins. An error of ±1 mGal is estimated for stations in which the altitude was measured using barometers and 1:100,000 scale topographic maps. The stations which had the altitude obtained from 1:250,000 topographic maps have an error of about ±3 mGal.

Terrain corrections were calculated by Motta et al. (1981), using the Hammer's table up to 15 km from the station, in regions of rough topography. The maximum terrain correction does not exceed 3 mGal. The accuracy of these corrections has not been reported but it is probably about 10%.

To summarize, the maximum random error in the Bouguer anomalies is 3 mGal for stations where the heights were obtained from contours of 1:250,000 scale maps. The maximum systematic error does not exceed 2 mGal.

2.1.3 The Free-air and Bouguer Anomaly Maps

In order to obtain the free-air and Bouguer anomaly maps, it was necessary to have the data points distributed on a regular grid.

Due to the large extent of the area covered by the present gravity survey, the stations were initially projected onto a plane by transforming the geocentric coordinates into conical coordinates, using the Lambert conical projection with standard parallel at 13^{0} S. The chosen projection made it possible to compare directly the gravity map with the available geological maps of Bahia State. The Lambert conical projection computer program is listed in Appendix B and the mathematical formulae for the projection were obtained from Richardus and Adler (1972).

The irregularly distributed data were interpolated on a regular grid of 20 km x 20 km, using a two dimensional interpolation routine provided by the GPCP (General Purpose Contouring Package, 1973). The algorithm is based on the local least squares polynomial approximation, in which the point to be interpolated is determined by fitting a local smooth surface. The surface coefficients are calculated based on the neighbouring data points situated within a region defined by a circle of radius R and centred in the point to be interpolated. A weighting function, with maximum value of one at its origin

and zero at the circunference of radius R, is also defined and applied to the neighbouring data points, prior to calculating the coefficients of the local least square polynomial. In this particular application, the radius R was chosen to include sixteen data points, which resulted from the combination of two factors. Firstly, the average distance between the gravity stations (15-20 km) and secondly the "smoothness" of the desired interpolated surface. This guaranteed that no short wavelength anomaly was created in regions of poor data coverage and where the coverage was good, a more accurate estimate was obtained. The GPCP computer program control commands used to produce the maps are listed in Appendix B and the free-air and Bouguer anomaly maps are shown in Figs. 2.3 and 2.4, with contour interval of 20 mGal and Bouguer density of 2.67 g cm^{-3} .

2.2 Geology of Bahia State

The main tectonic features of the Brazilian Platform (Fig. 2.5), which occupies the major part of the South American Platform, were formed by the beginning of the Phanerozoic on the termination of the Proterozoic geosynclinal evolution (Almeida et al., 1981).

The Archean basement of the Brazilian Platform is composed of metamorphic rocks of amphibolite to granulite facies, granitoids

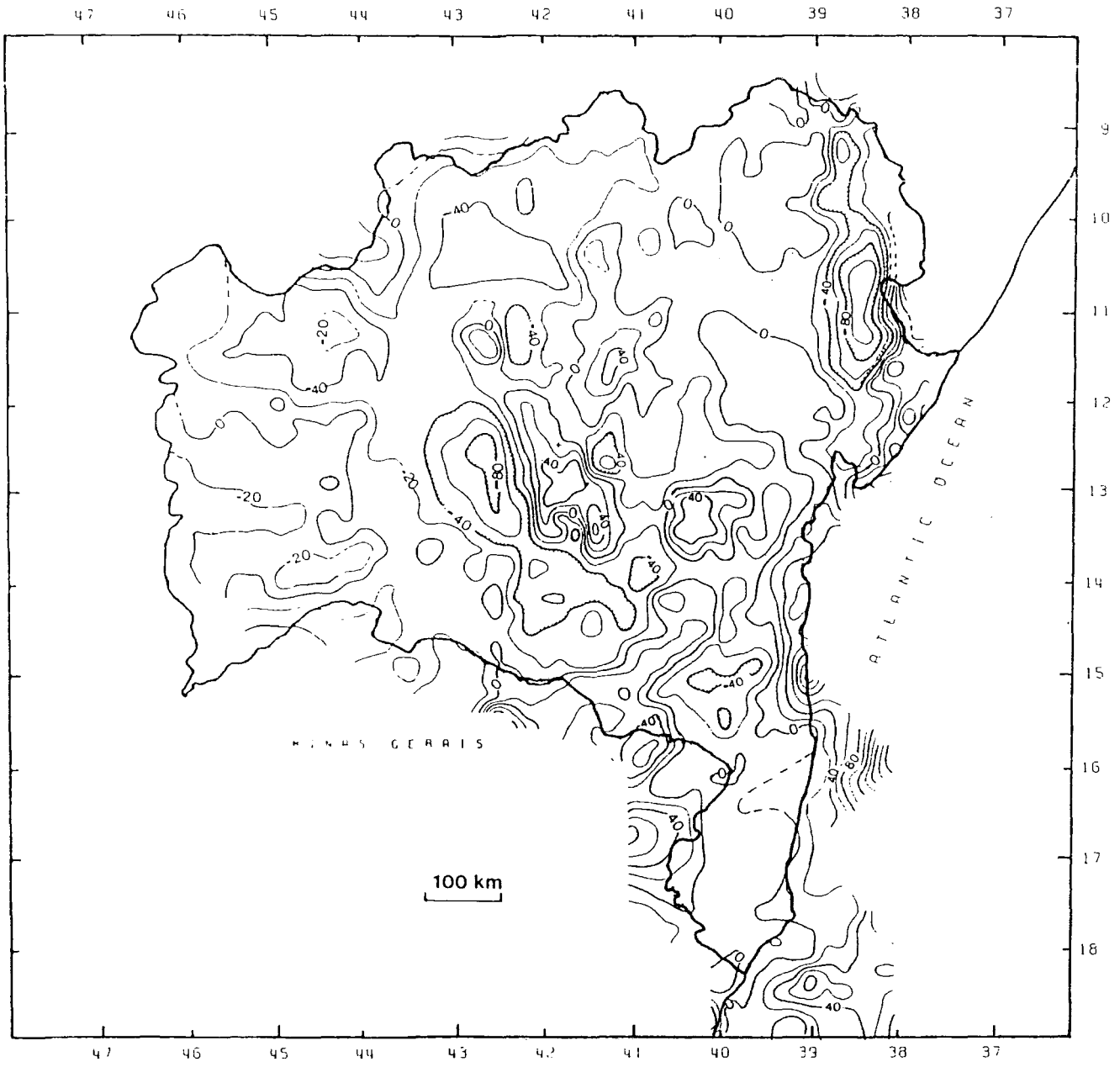

Fig. 2.3 - Free-air anomaly map of the Bahia State. Contour interval 20 mGal. IGSN-71, IGF-1967.

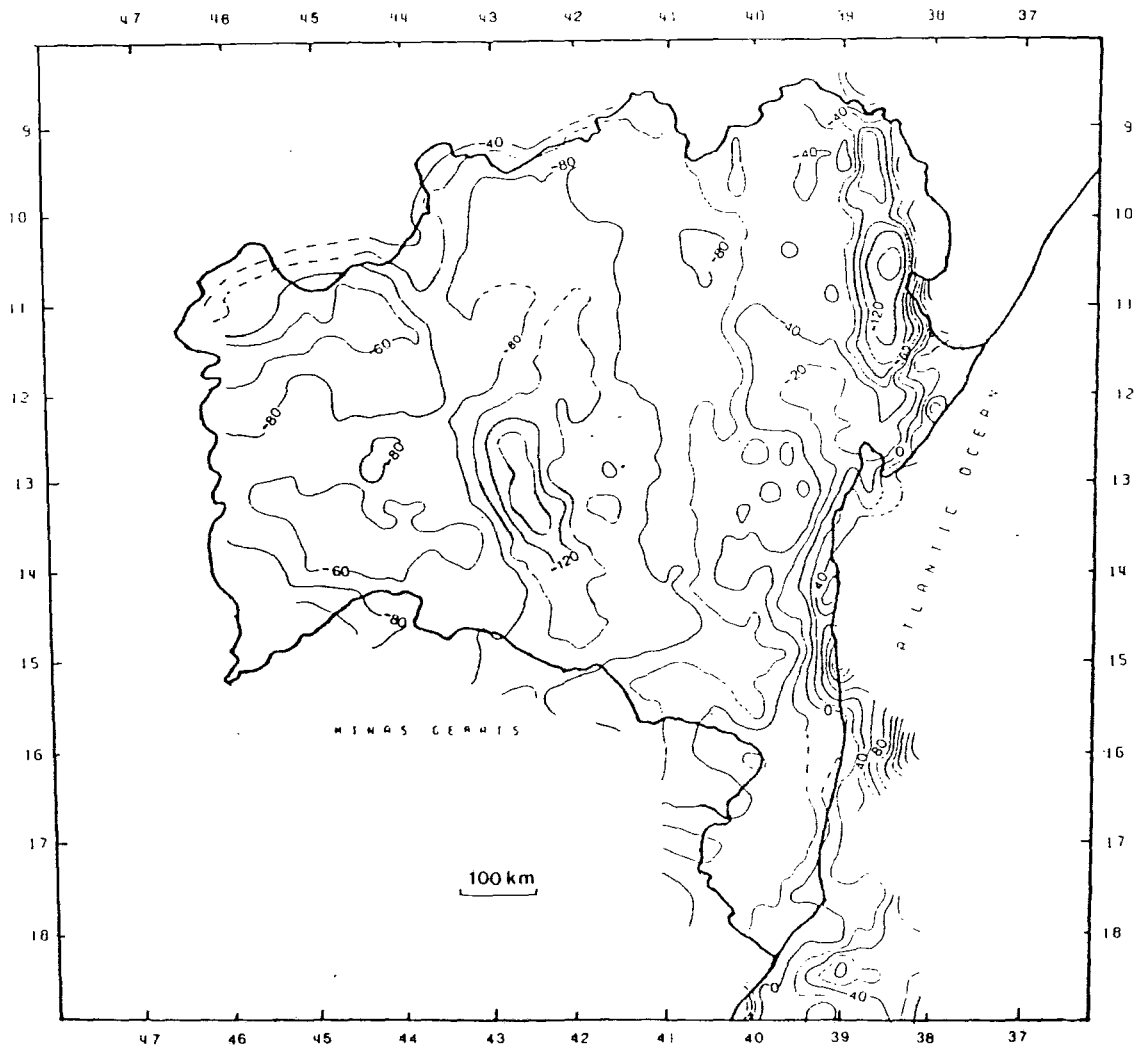

Fig. 2.4 - Bouguer anomaly map of the Bahia State. Contour interval 20 mGal. IGSN-71, IGF-1967.

and mafic-ultramafic complexes. This basement was subsequently affected by intense magmatism, migmatization and high grade metamorphism in the Lower Proterozoic. In Brazil, the end of this period is referred to as the Transamazonian cycle which lasted from 2200 to 1800 Ma (Brito Neves et al., 1980).

During the Middle Proterozoic (1800 - 1000 Ma), a dominantly continental sedimentation occurred which was accompanied by acid and intermediate volcanism. The sediments were then deformed and metamorphosed (greenschist facies) during the last stage of this cycle (Espinhaço orogeny).

The Upper Proterozoic is characterized by the evolution of the fold belts which surround the cratonic nuclei and by the development of the sedimentary covers within the cratons. The sedimentation was initiated at about 1000 Ma and deformation and metamorphism (greenschist facies) occurred during the tectono-magmatic events of the Brasiliano cycle (ca. 500 Ma).

Bahia State comprises almost all of the northern part of the São Francisco craton (Almeida, 1977) and part of the marginal fold belts. The location of the São Francisco craton, in relation to others Brazilian tectonic provinces, is shown in Fig. 2.5.

According to the definition of Almeida (1977), the São Francisco craton extends from the latitude 9° S to 20° S, with

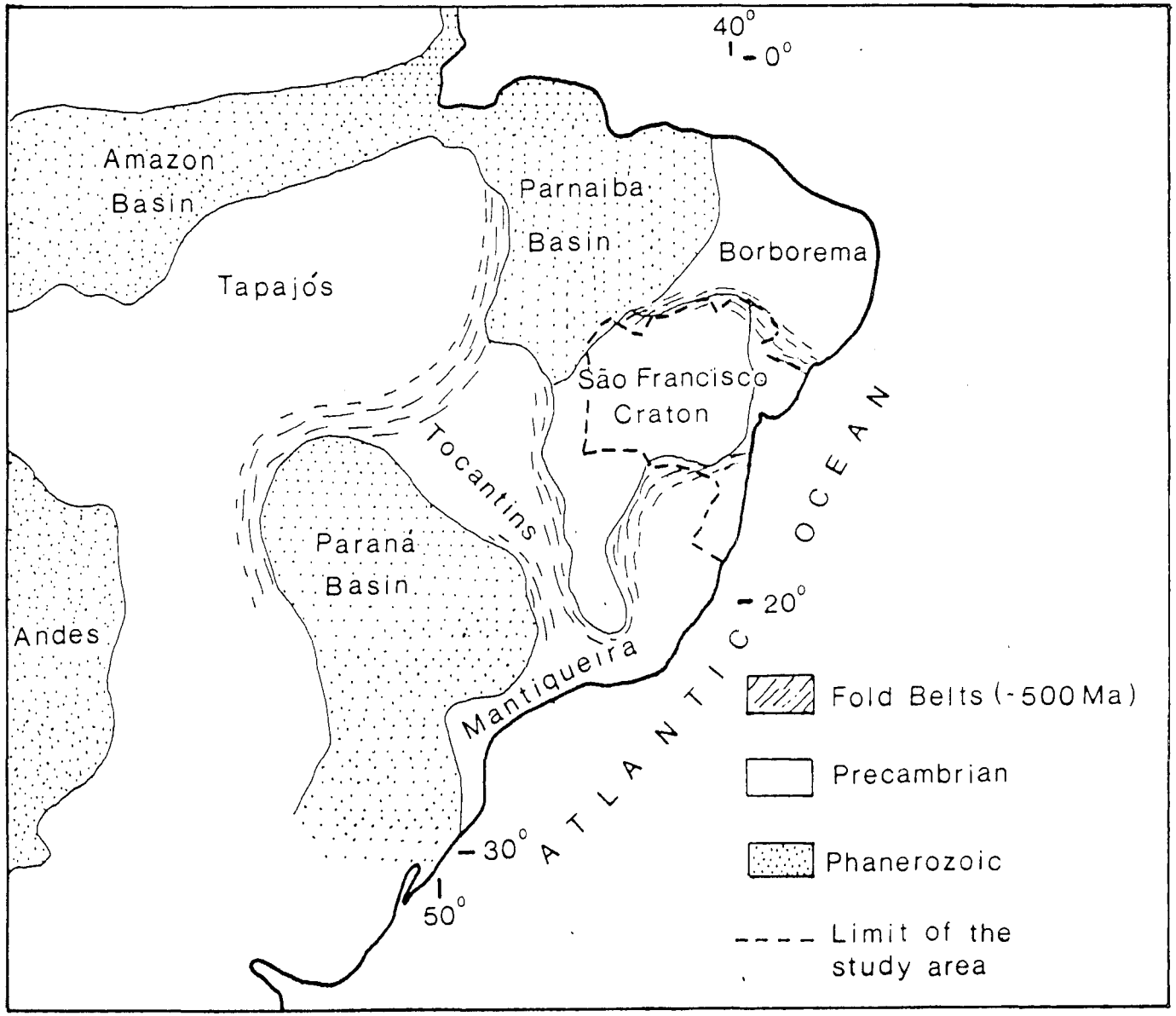

Fig. 2.5 - The São Francisco craton and the Brazilian structural provinces. From Almeida et al. (1981).

its borders conventionally situated at the fold belts of Brasiliano age (ca. 500 Ma) and at the Atlantic continental margin on the eastern side.

The craton acted as a foreland during the geosynclinal evolution of the marginal fold belts in the Upper Proterozoic (Fig. 2.6). The basement is composed of granitic and gneissic complexes, highly migmatized and metamorphosed (high amphibolite to granulite facies), and it is structurally very complex. By the end of the Transamazonian cycle, the basement was completely formed and it was only affected by paratectonic deformation in the Middle Proterozoic.

The basement cover is subdivided into two main complexes, separated by an angular unconformity. The older complex is Middle Proterozoic and it belongs to the Espinhaço orogenic cycle (1800 to 1300 Ma). The sedimentation is essentially clastic, psammitic and pelitic, with thickness of at least 3000 metres in the central part of the northern São Francisco craton. The younger complex was deposited during the Brasiliano cycle (900 - 500 Ma). The basal sequence is composed of remnants of glacial deposits, including tillites. An erosional period followed the deposition of this sequence. The upper sequence is the Bambui group, which covers nearly half of the São Francisco craton. It is composed of pelitic and calcareous rocks, deposited in an epicontinental sea. This upper sequence is overlain by siltstones and sandstones with arkose intercalation

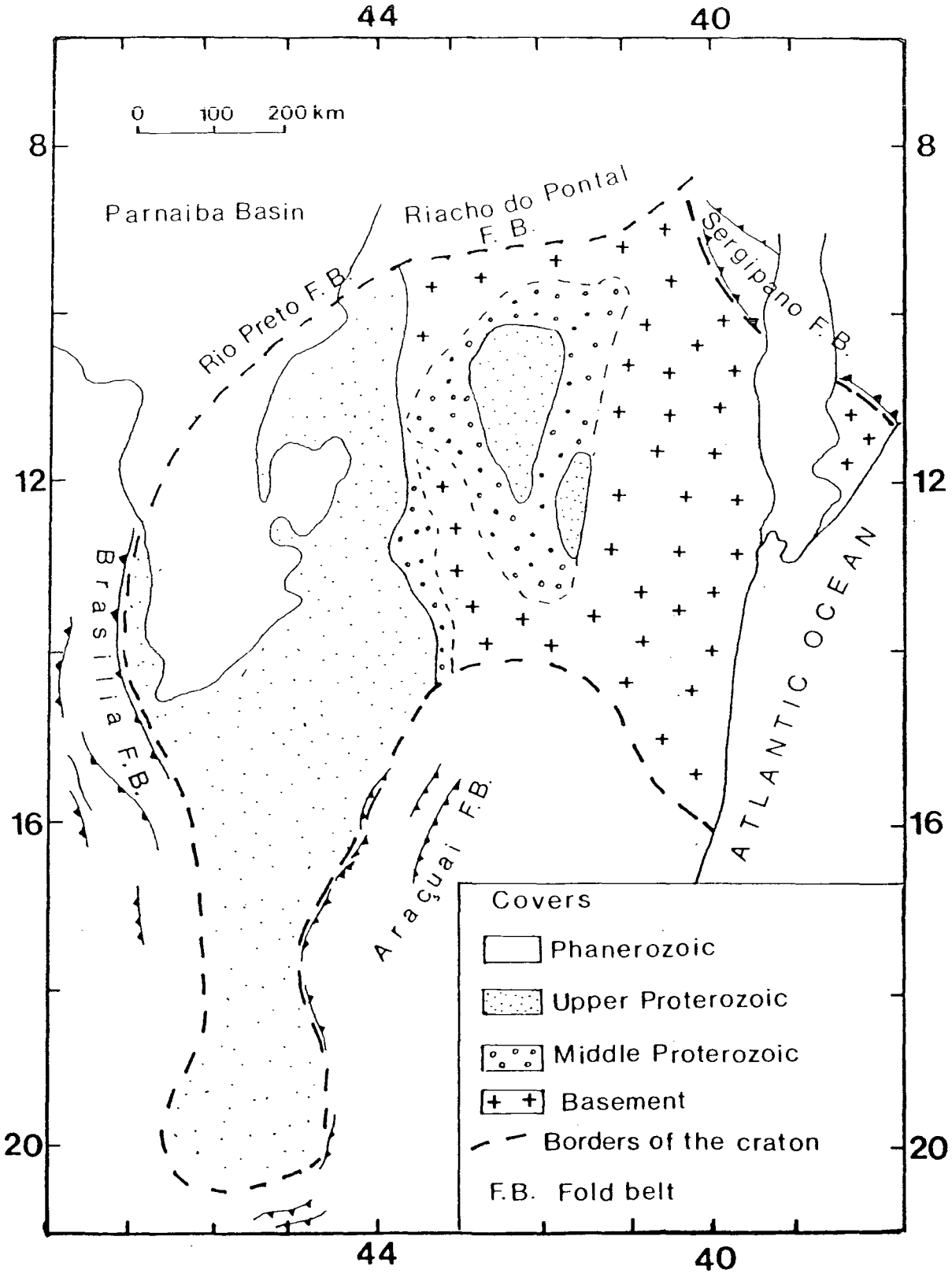

Fig. 2.6 - The São Francisco craton and its marginal fold belts as defined by Almeida (1977).

which represents the molasse sedimentation following the Brasiliano orogeny (500 Ma). Near the western and northern borders of the craton, the Upper Proterozoic cover is deformed with fold axes and faults paralleling the belts. Towards the centre of the craton, the degree of metamorphism decreases and the sedimentary sequences are nearly horizontal. A non-depositional phase followed until the Lower Cretaceous when sandstones (Areado Fm.), volcanics (Mata da Corda Fm.) and aeolian and fluvial sandstones (Urucuia Fm.) were deposited. The last two sequences are believed to be synchronous and they were deposited at 80 Ma ago (Hasui and Cordani, 1968).

Fig. 2.7, modified from Inda et al. (1984) provides a more detailed account of the geology of the Sao Francisco craton, including the Archean and the Lower Proterozoic terrains. According to Inda and Barbosa (1978), Bahia State can be subdivided into seven geological regions (Fig. 2.8), based on geochronological, structural and petrogenetic information. Four of the regions, the São Francisco basin (II), the Espinhaço Fold System (III), the Lençois basin (IV) and the Eastern Bahia Shield (V), are situated within the craton. The remaining regions (I, VI, VII) are the marginal fold belts of the Upper Proterozoic age.

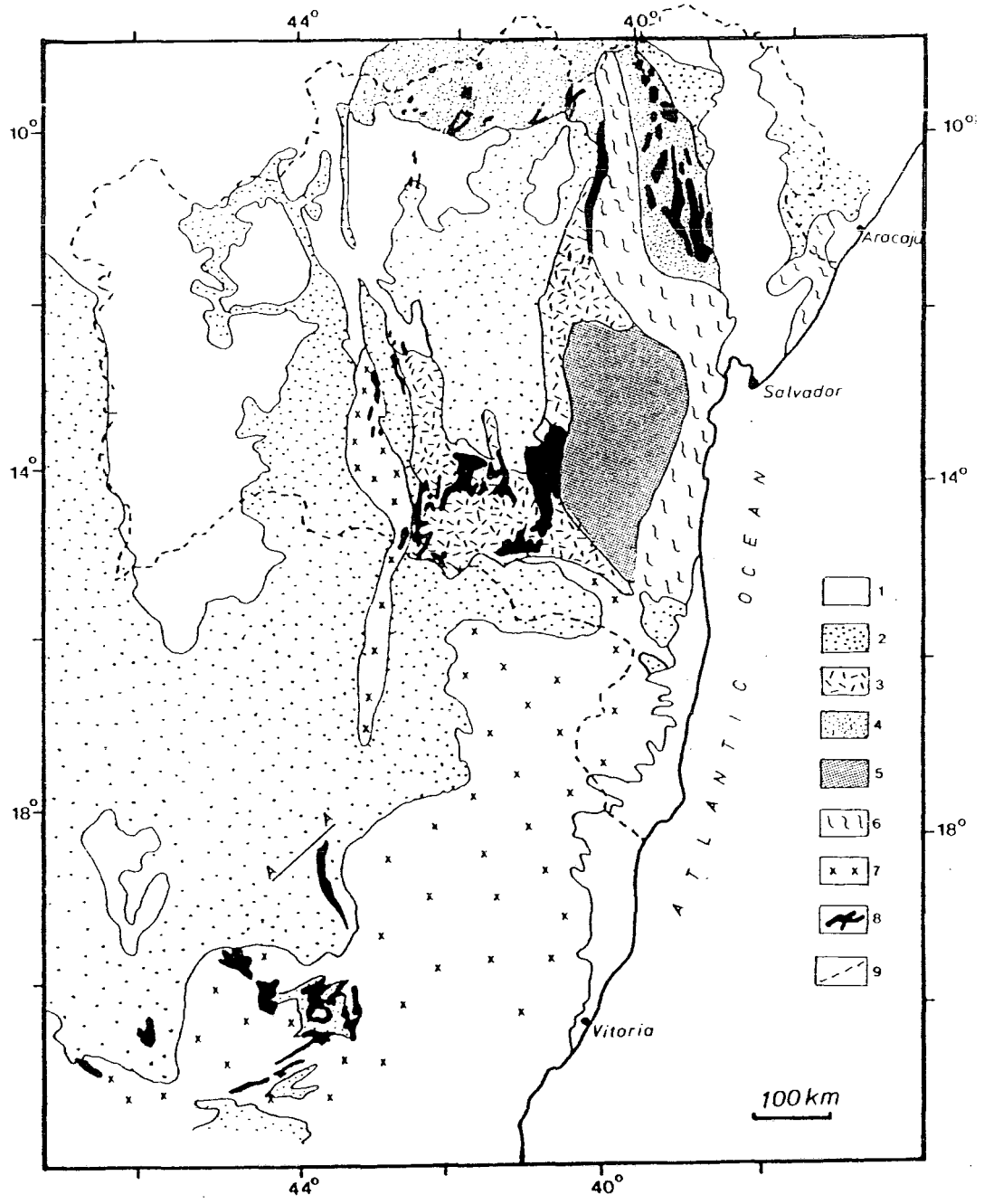

Fig. 2.7 -

Simplified geology of the São Francisco craton. Modified from Inda et al. (1984). (1) Phanerozoic covers; (2) Middle and Upper Proterozoic covers; (3) granitic and greenstone terrains; (4) same as (3) but rejuvenated during the Transamazonian cycle (1.8 - 2.2 Ga); (5) granulitic terrain; (6) granulitic terrain totally or partially rejuvenated during the Transamazonian cycle; (7) Non-differentiated Archean terrain rejuvenated during the Transamaz. and Brasiliano cycles; (8) differentiated greenstone belts; (9) Bahia State political boundaries.
A - A' is the profile shown in Fig. 2.10.

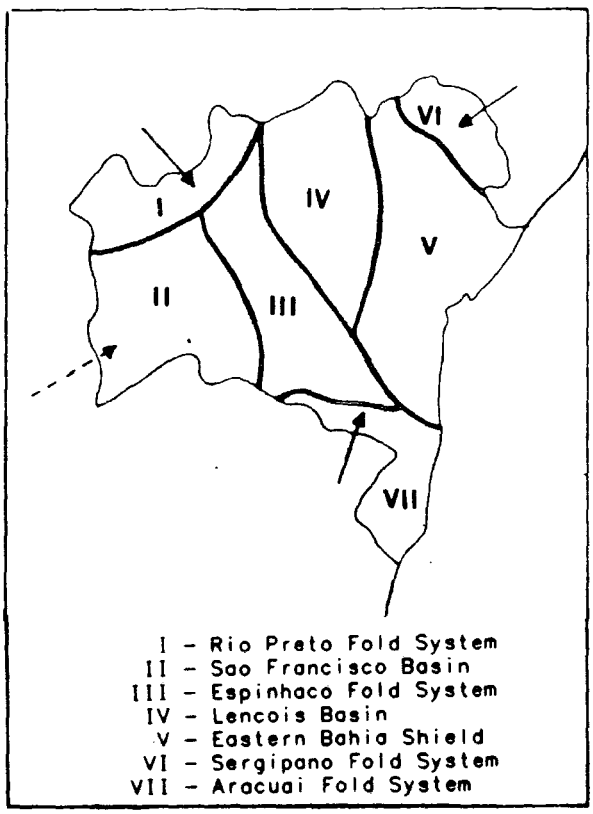

Fig. 2.8 - Bahia State and its geological subregions as defined by Inda and Barbosa (1978).

The arrows in Fig. 2.8 represent the vergence of the fold belts. The intracratonic regions, apart from the Espinhaço Fold System, were stabilized at the end of the Lower Proterozoic. The Archean basement presents widespread records of crustal remobilization during the Transamazonian cycle (1800 to 2200 Ma). Tectonic quiescence prevailed after the end of the Lower Proterozoic, during the deposition of the sedimentary cover in the regions II and IV. The crustal stability of the Eastern Bahia Shield (region V) is suggested by the lack of post-Transamazonian radiometric ages.

The gravity survey of Bahia State does not include the western border of the São Francisco craton, the Brasilia fold belt (Fig. 2.6). This belt contains sedimentation of miogeosynclinal character and the molasse of the final stage extends into the São Francisco basin (region II). The belt verges towards the craton and the metamorphism is of greenschist facies. Burke et al. (1977) have proposed a suture zone along the Brasilia fold belt in an attempt to apply the Wilson cycle to the Proterozoic of the South America. However, this hypothesis has not yet been tested by the Brazilian geologists.

A geological description of each of the regions, as defined by Inda and Barbosa (1978), is now given, starting with the intracratonic regions and followed by the marginal fold belts.

2.2.1 São Francisco Basin (Region II)

This region comprises the western part of the São Francisco craton, extending into the southern State of Minas Gerais. The western border is situated in the Brasilia fold belt, the northern border is the Rio Preto Fold System and to the east the boundary is defined by a sequence of faults associated with the Espinhaço Fold System. The basement of Archean age is composed of felsic and intermediate plutons, granites, metamorphic, volcanic-sedimentary, basic and ultrabasic rocks. The oldest sedimentary cover is Middle Proterozoic.

The metasediments of this Middle Proterozoic sequence, the Espinhaço Supergroup, are mostly greenschist facies clastic quartzites with little deformation, in contrast to the metasediments of similar age in the Espinhaço Fold System. The thickness and the distribution of this Middle Proterozoic sequence in Bahia State are not known. In the south of Minas Gerais State, the thickness is as much as 4 km, thinning towards the north.

The Upper Proterozoic (900 - 500 Ma) cover is the São Francisco Supergroup which lies unconformably over the Middle Proterozoic sequence. It is subdivided into two major groups, the Macaubas and the Bambui groups.

The Macaubas group extends from south of Bahia State, towards the Minas Gerais State. The glacial event which occurred during the Late Proterozoic, is registered in this sequence. The orientation of the area of deposition is approximately north-south and it parallels the Araçuai fold belt (Fig. 2.6). The east-west geographical extension has not yet been defined. According to Almeida (1977), the Macaubas group in Minas Gerais State represents geosynclinal sedimentation of highly diversified lithofacies. It is composed of at least one kilometre of pelites, sandstones, greywake, arkoses, conglomerates, subordinate limestones and itabirates (iron formation). The conglomerates, conglomeratic greywackes and tillites represent the remnant of glacial deposition. The metamorphism of greenschist facies increases from west to east and it has been dated at 600 Ma. The contact between the Macaubas group and the overlain sediments is still controversial. As summarized by Inda et al. (1984), this contact is either described as conformable with intermixing of the Macaubas and Bambui groups (Hettich, 1977) or as an angular unconformity (Dardenne and Walde, 1979).

The Bambui group is composed of calcareous and pelitic rocks deposited in an epicontinental sea, reflecting the high stability of the craton at that time. The thickness of this sequence in Bahia State averages 500 metres but it reaches more than 1000 metres in Minas Gerais State (DNPM/CPRM Bambui Drilling Project, 1980). In Fig. 2.9, the lithostratigraphic

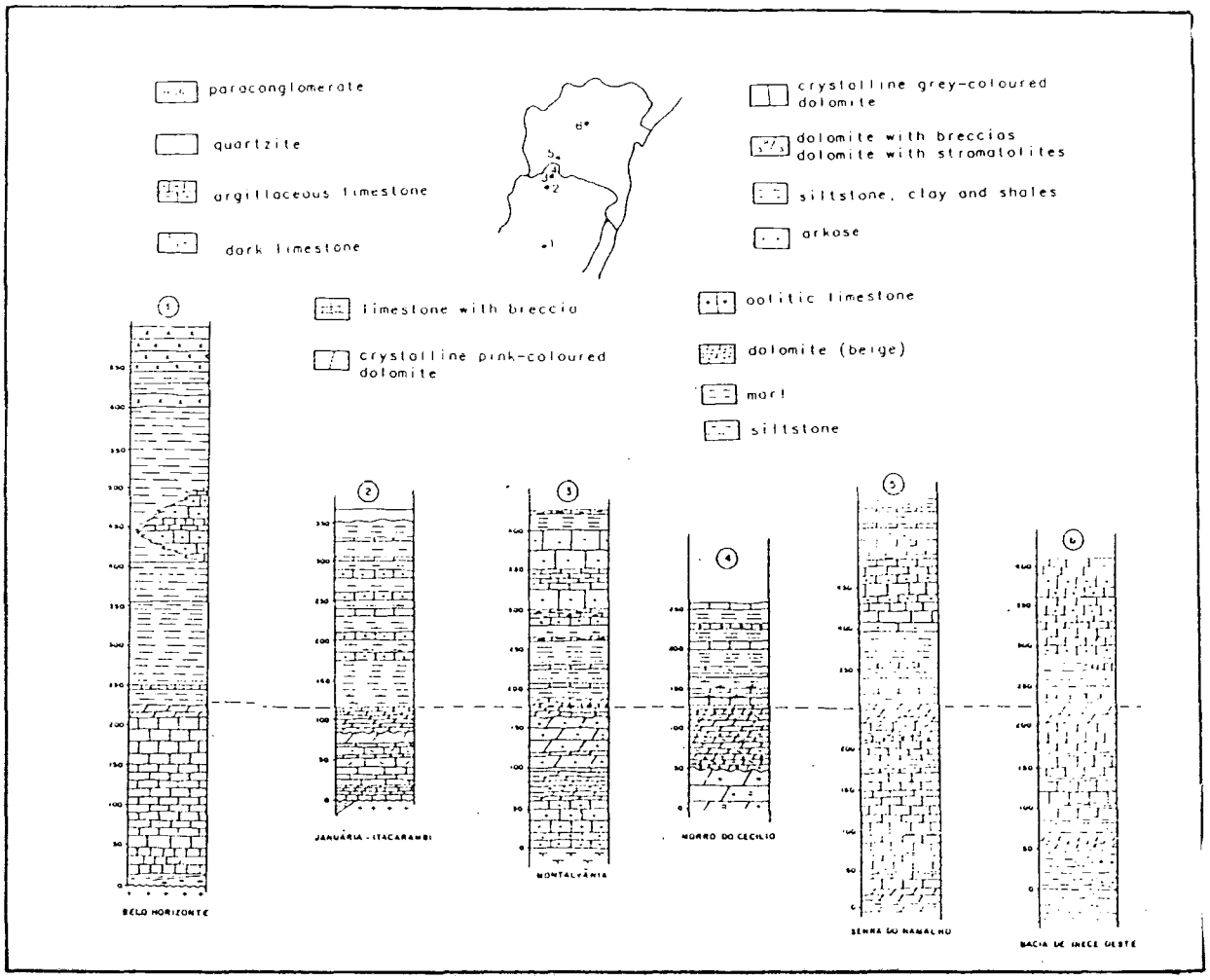

Fig. 2.9 - Stratigraphical correlation of the Bambuí group in Minas Gerais and Bahia States. Reproduced from Inda et al. (1984). Thickness in metres.

correlation of the Bambui group in Bahia and Minas Gerais State is presented, based on wells compiled from different authors (see Inda et al., 1984 for reference). The sedimentary sequence is subdivided into three megacycles of regressive sedimentation after the glacial retreat. The first two megacycles are characterized by shaly-limy sediments and the third, the molasse, is characterized by sandy-shaly sediments. Each of these megacycles started with a regional transgression followed by the development of sublittoral marine facies, becoming littoral to supra littoral, and eventually reaching, in some places, continental facies.

Linear folding observed in the Upper Proterozoic sequences near the borders of the craton, is associated with the compression of the marginal fold belts. A section across the Araçuai fold belt is presented in Fig. 2.10. The older sequences, the Espinhaço supergroup and the Macaubas group, are folded over the younger sequences of the Bambui group. In Bahia State, the Bambui group was only affected by the north-south compression of the Rio Preto Fold System. The low grade metamorphism which affected the Bambui group was dated at 600 Ma (Amaral and Kawashita, 1967) but the stromatolites of the calcareous sequences indicates a minimum age for the beginning of the sedimentation at 900 Ma (Cloud and Dardenne, 1968).

The Phanerozoic sedimentation in the São Francisco basin began in the Lower Cretaceous, following the regional uplift of

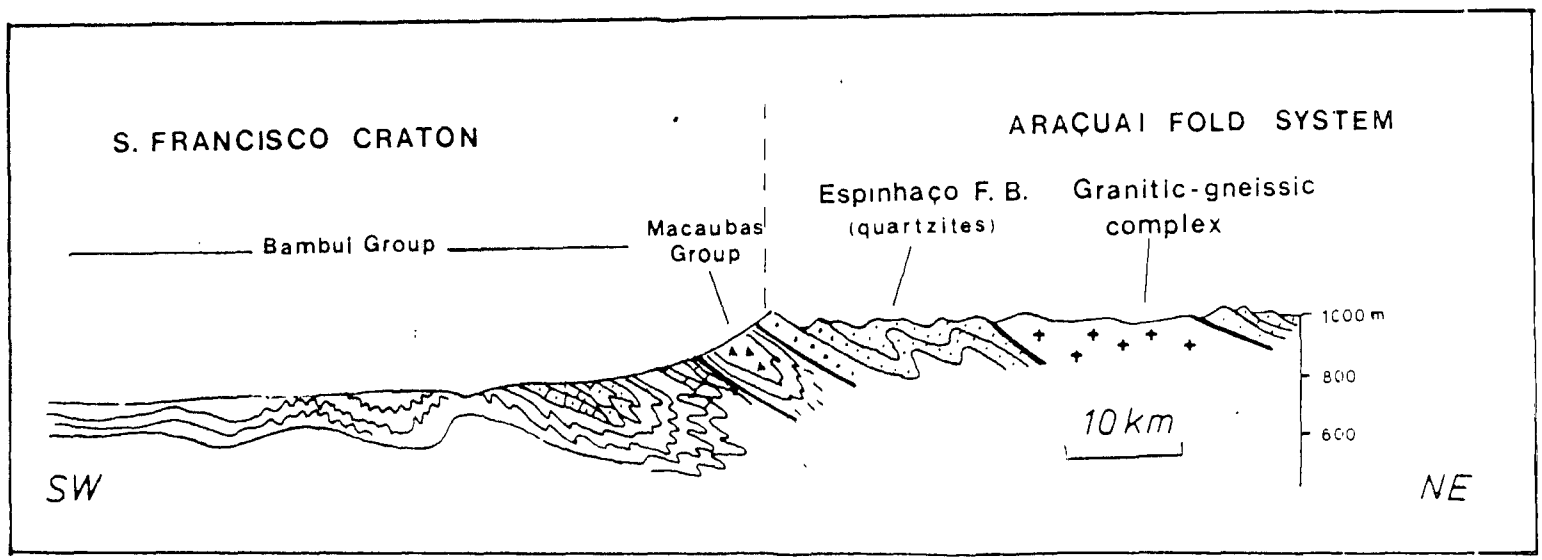

Fig. 2.10 - Schematic section across the southern Espinhaço fold belt (Minas Gerais State) showing the Bambuí and the Macaubas groups. From Inda et al. (1984).

the southern part of the São Francisco craton. The sediments are virtually absent in the western, southwestern and southern parts of the craton. Three units are recognized: Areado, Mata da Corda and Urucuia formations. The Areado formation, of about 200 metres of sandstone sequence, was deposited in an initial desert condition changing to fluvial-deltaic. The age, based on fossil analysis, is considered to be Aptian - Albian (ca. 108 Ma). The Mata da Corda formation has a thickness of approximately 150 metres. Hasui and Cordani (1968) dated the volcanics of this formation at 80 Ma. The area of outcrop is restricted to the south of the craton. The Urucuia formation is essentially composed of sandstones and its thickness ranges from 360 metres in Bahia State to 70 metres in Minas Gerais State. The environment of deposition changed from aeolian in the south to fluvial in Bahia State. Lima and Leite (1978) have dated this formation as Albian-Cenomanian, therefore establishing a similar age to that of the Mata da Corda formation. The Lower Cretaceous sedimentation in the São Francisco basin appears to be synchronous with the rifting phase of the opening of the South Atlantic, which occurred further to the east. Thin continental alluvial detritic deposits and arenaceous rocks constitute the Tertiary and Quaternary sedimentation. The thickness is about 30-40 metres.

2.2.2 Lençois Basin (Region IV)

The Lençois basin is situated at the centre of the northern São Francisco craton and it includes nearly all the eastern part of the physiographic region named "chapada" (tableland) Diamantina. This triangular shaped region is bordered by the Espinhaço fold belt to the west, the Eastern Bahia Shield to the east and the Riacho do Pontal Fold System to the north. A geological map of the region is shown in Fig. 2.11. The northeastern basement is of Archean age (2.7-2.6 Ga) and it was described by Jardim de Sa' et al. (1976a) as composed of migmatites, gneisses, granites and basic-ultrabasic rocks. The rocks present metamorphism of amphibolite facies. The structures are very complex, with folding along different axial planes. At the southeast of the "chapada" Diamantina, the basement is dominantly composed of gneisses of granulite facies. The radiometric age ranges from 3.2 Ga (Cordani and Iyer, 1979) to 2.7 Ga (Jardim de Sa' et al., 1976a). The basement was extensively remobilized during the Transamazonian events (2.2 to 1.8 Ga). Above this high grade basement, the Middle and Upper Proterozoic covers were deposited. As in the São Francisco basin, the Middle Proterozoic sequence is the Espinhaço Supergroup. Its thickness is estimated as 2-3 km.

According to Montes et al. (1981), the Middle Proterozoic stratigraphical column of the Lençois basin can be summarized as shown in Fig. 2.12. Jardim de Sá (1981) discusses the two

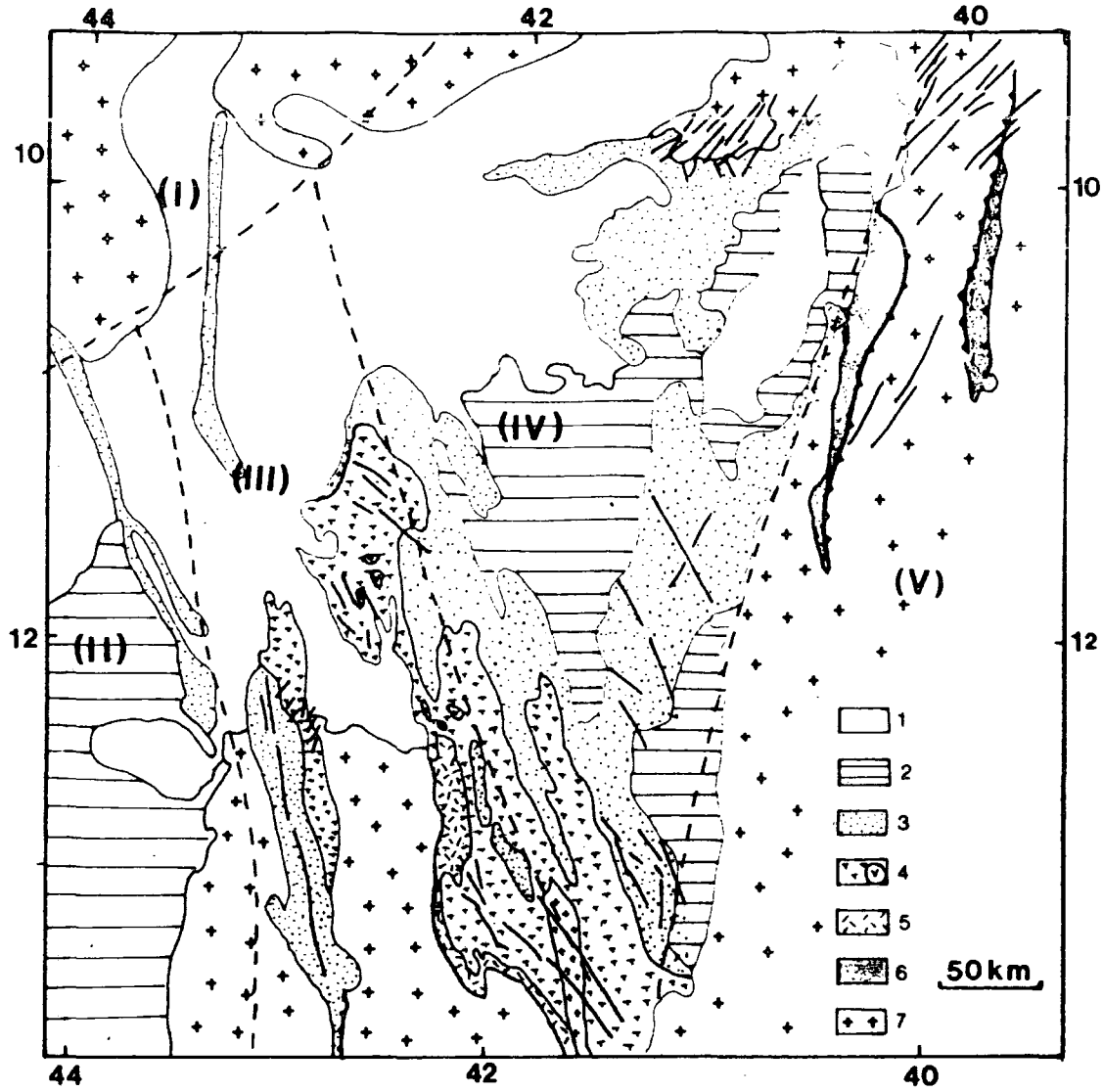

Fig. 2.11 - Geology of Lencois Basin. Modified from Inda et al. (1984).
(1) Phanerozoic cover; (2) Upper Proterozoic cover (S. Francisco Supergroup);
Middle Proterozoic cover: (3) Chapada Diamantina group;
(4) Paraguacu group; (5) Rio dos Remedios group;
(6) Lower Proterozoic : volcano-sedimentary complexes;
(7) Crystalline basement.
Roman numbers are the sub-regions according to the definition of Inda and Barbosa (1978).

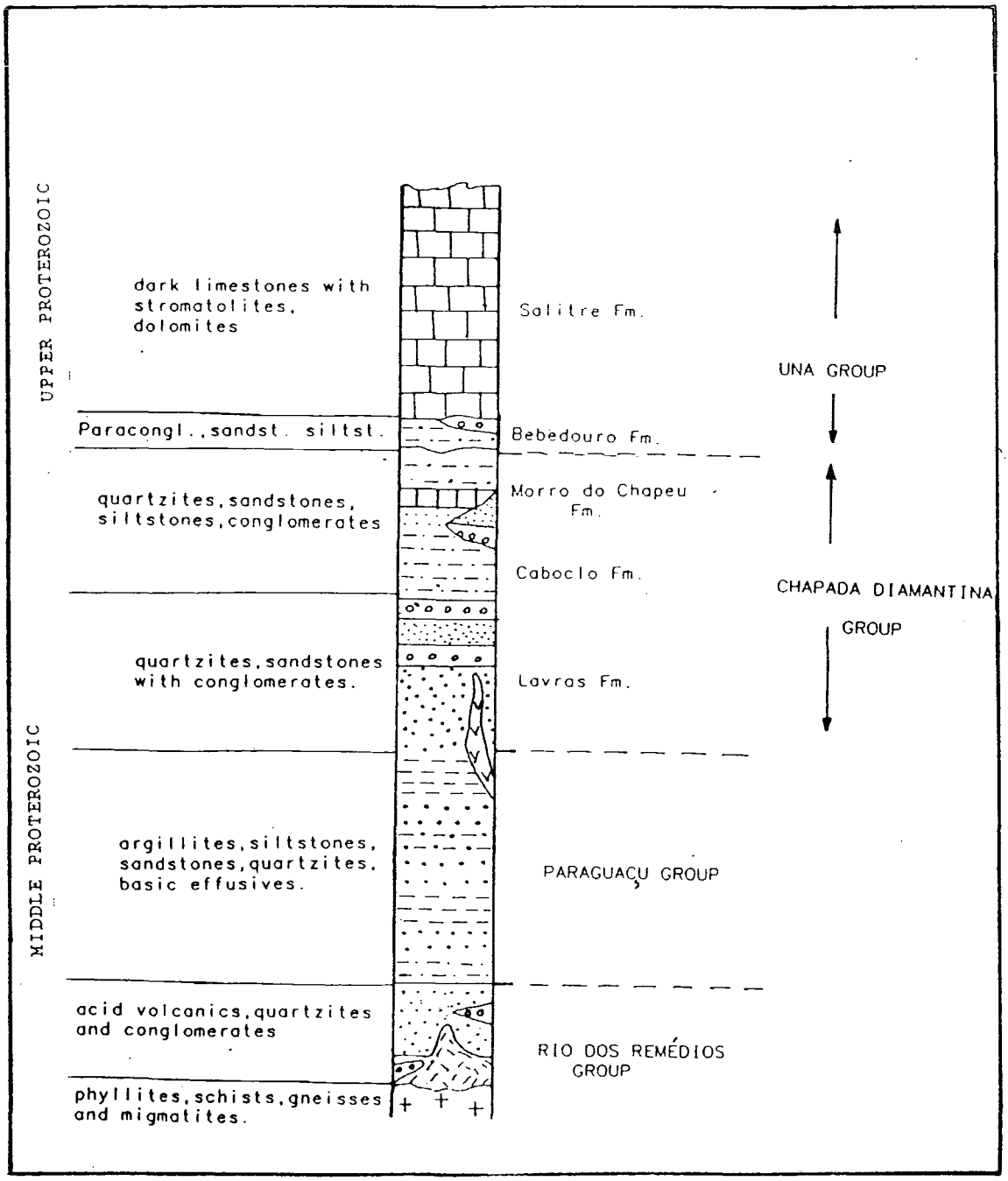

Fig. 2.12 - Stratigraphy of the Lençois basin, according to Montes et al. (1981).

models which have been proposed so far. The first model proposes that the three groups are separated by stratigraphical and structural unconformities and that only the upper Chapada Diamantina group is present in the northeastern part of the basin. Inda and Barbosa (1978) and Inda et al. (1984) propose that the other two groups were deposited only in the western border of the Lençois basin. The second model (see references in Jardim de Sá, 1981) does not recognize a regional unconformity, but only local movement of the basement during the sedimentation. Variations in the stratigraphy, at different parts of the basin, are ascribed to facies change.

The following presentation of the stratigraphy of the Lençois basin is based on Inda et al. (1984). The basal sequence is the Rio dos Remedios group, which is composed of acid volcanics, fluvial quartzites and conglomerates. The group is particularly thick at the western "chapada" Diamantina which, according to the criteria adopted to subdivide Bahia State into geological regions, is included in the Espinhaço Fold system.

The Paraguaçu group is composed of sandstones, argillaceous rocks, conglomerates, acid volcanics and basic intrusives related to the final phase of deposition. The thickness is about one kilometre in the centre of the basin thinning towards the north. Discordantly over this group the last sedimentation of the Middle Proterozoic, the Chapada Diamantina group, was deposited which occurs at the north-northeastern part of the

Lençois basin. It is composed of quartzites, conglomerates, sandstones, shales and siltstones. The deposition was transgressive over the Paraguaçu group. The Chapada Diamantina group is subdivided into three formations. The Tombador formation is essentially composed of quartzites with ample facies variation and it is deposited throughout the entire basin. The estimated thickness is about 300 metres, thickening towards the west and southwest of the "chapada" Diamantina. The Caboclo formation, which is restricted to the central part of the "chapada", is essentially composed of siltstones and argillites with intercalations of oolitic cherts and limestones which indicates a shallow marine condition. The thickness is about 700 metres. The Morro do Chapeu formation, in the central part of the "chapada", is composed of fine to intermediate grained sandstones, changing locally to quartzites with well preserved primary structures. The sediments were deposited in a shallow coastal marine condition with small transgression. The estimated thickness is about 350 metres.

The structural features of the "chapada" Diamantina show different characteristics between the western and eastern parts. As discussed in Jardim de Sá et al. (1976a), these two regions are separated by NNW trend faults. In the western "chapada", the metasediments are more deformed and verge towards the east. The synclinoria are well developed and have open folds, whereas the anticlinoria have tightly folded core and they are often cut by west to east inverse faults. Further details regarding the

Middle Proterozoic deformation are presented in the next section (2.2.3)

The tectonic style of the Lençois basin (eastern "chapada") is relatively simple and it is characterized by long wavelength folds caused by the movement of the incompetent layers of shales and siltites over the quartzitic sequence, as suggested by Mascarenhas (1973). The metamorphism is almost non-existent.

The Upper Proterozoic deposition is represented by the Una group, which is equivalent to the Bambui group of the São Francisco basin. The group lies discordantly over the Morro do Chapeu formation and shows very little deformation. The basal sequence comprises the Bebedouro formation, which is composed of paraconglomerates intercalated with sandstones and siltstones. The upper sequence, the Salitre formation, was deposited under very stable and shallow epicontinental sea. It is composed of dark limestones and dolomites. Its thickness is about 350 metres.

2.2.3 Espinhaço Fold System (Region III)

On the western border of the Lençois basin, there is a long and narrow region which was affected by a series of tectonic events at the end of the Middle Proterozoic. This region was named the Espinhaço Fold System by Inda and Barbosa (1978). It

comprises the Middle Proterozoic metasediments of the western "chapada" Diamantina (east) and the Espinhaço orogenic belt (west). These are separated by a zone of Archean basement named the Paramirim complex (see Fig. 2.13).

The basement, of Archean age, is composed of gneissic and migmatitic complexes which were affected by the magmatism and high grade metamorphism of the Transamazonian cycle (1.8 - 2.2 Ga). Volcanic-sedimentary complexes (schists, quartzites and iron banded quartzites) occur together with the plutonic complexes.

The Middle Proterozoic cover is considered to be similar to the sedimentary sequences of the Espinhaço Supergroup deposited in the Lençois basin. The following diagram shows the possible correlation between the sequences of the Espinhaco fold belt and the "chapada" Diamantina.

		ESPINHAÇO FOLD BELT	"CHAPADA" DIAMANTINA	Lithology
PROTEROZOIC	Middle (1.0 Ga)	Upper	Chapada Diamantina	Sandstones, siltstones and conglomerates.
		Middle	Paraguaçu	Continental pelitic sediments cut by sills of diabase. Quartzites intercalated by schists and phyllites.
	Lower (1.8 Ga)	Lower	Rio dos Remedios	Acid and intermediate volcanic rocks and clastic sediments.
		Volcanic-sedimentary complexes		micaschists, meta-sandstones overlain by phyllites and fine meta sandstones. amphibolites, marbles, quartzites, micaschists. migmatites and charnockites.
ARCHEAN		Basement		gneissic and migmatitic complexes.

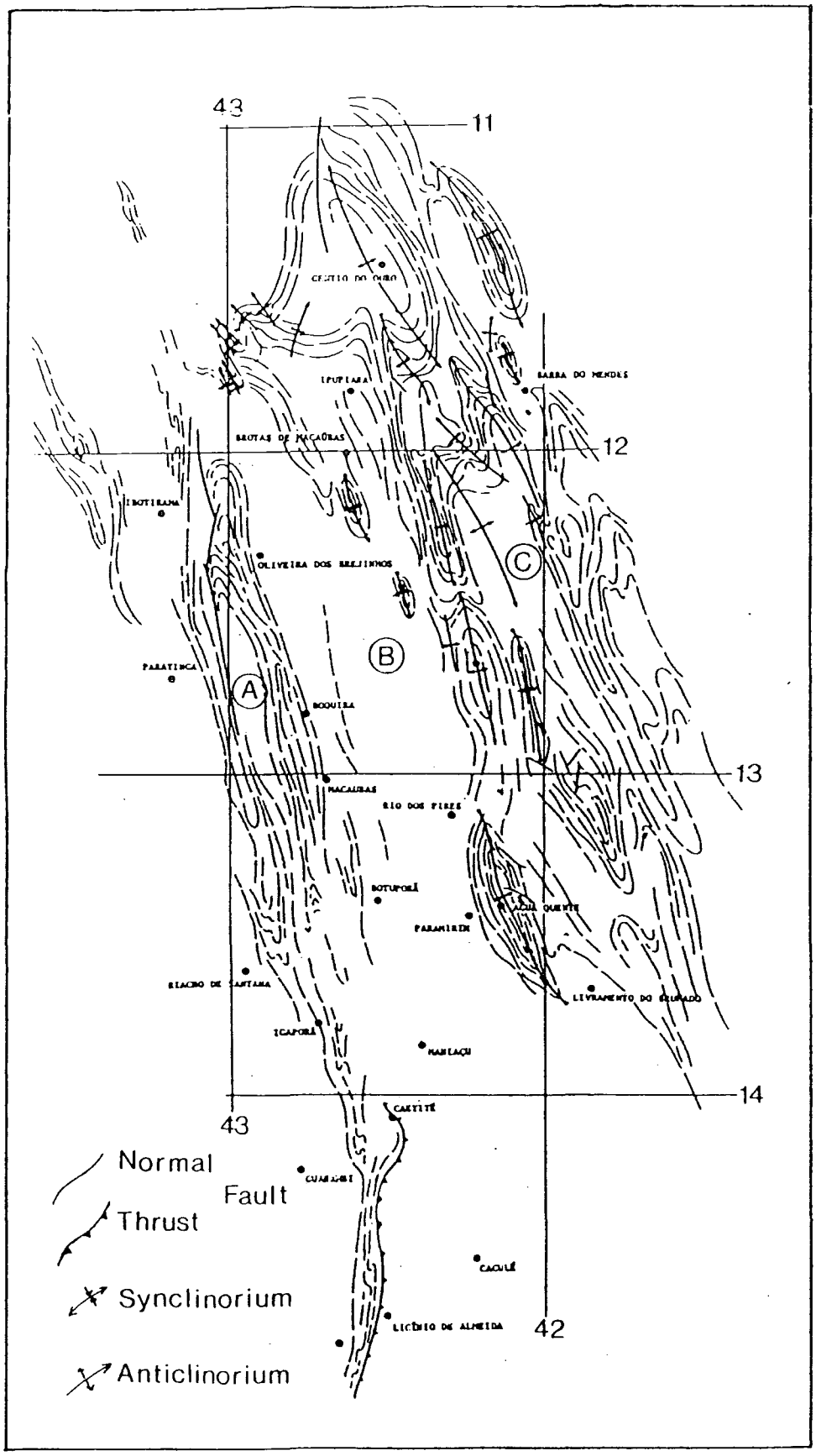

Fig. 2.13 - Main regional structural lineaments of the northern Espinhaço fold belt and western border of the Chapada Tableland. From Inda and Barbosa (1978).
A = Espinhaco fold belt
B = Paramirim complex
C = Western "chapada" Diamantina

Due to the long duration of the deposition, from 1.8 to 1.0 Ga, this correlation is still uncertain and solely based on lithological similarity (Inda and Barbosa, 1978). The metasediments present metamorphism of greenschist facies and they were deformed during the Espinhaço orogeny (1.3 - 1.0 Ga). K/Ar dates show the overprint of the Brasiliano event (600-450 Ma), as determined by Tavora et al. (1967), Jardim de Sá et al. (1976a) and Brito Neves et al. (1980). However, structural or metamorphic feature which could be ascribed to this event has not yet been recognized. According to these authors, the young ages may reflect regional uplift and hydrothermal activity at the end of the Proterozoic.

The Middle Proterozoic evolution of this region is very controversial (Inda et al., 1984), particularly if one attempts to include the southern part of the Espinhaço fold belt, situated in Minas Gerais State. These belts extend from southern Minas Gerais State up to the north of Bahia State, for about 1000 km. Cordani (1973), using geochronological data, has postulated a suture zone along the Paramirim complex, with final development at the end of the Brasiliano orogeny (ca. 500 Ma). Sighinolfi and Conceição (1974) have associated the acid volcanism of the "chapada" Diamantina to this collision. This model has been questioned by recent geological and geochemical studies carried out by Jardim de Sá et al. (1976a). According to these authors, the acid and intermediate volcanism was accompanied by clastic and volcano-clastic sedimentation. This

occurred during the intraplate events, when the lithosphere started rifting in this part of the São Francisco craton. The uplift of the central block, defined by the Paramirim complex, created two parallel marginal troughs, where the sediments of the Espinhaço Supergroup were accumulated and subsequently folded and metamorphosed.

In Bahia State, the Espinhaço fold belt is composed of strongly folded metasediments and its borders are limited by NNW trending faults. The degree of metamorphism increases from north to south and from upper to lower sequences. A map of the structural lineaments of the Espinhaço Fold System is shown in Fig. 2.13, reproduced from Inda and Barbosa (1978). Jardim de Sá et al. (1976a) described the contact between the western "chapada" Diamantina and the Paramirim complex as made up of NNW trend cataclasites and mylonites zones. The metasediments lie discordantly over these zones, indicating that they are older than the sedimentation. It appear that they were subsequently reactivated, as evidenced by cataclastic features in the acid volcanics and quartzitic sequences.

The Espinhaço fold belt was affected by the Middle Proterozoic tectonism, since the sequences are strongly folded with westward vergence. Subsequently, normal faulting occurred. The contact with the Paramirim complex, is defined by high angle normal faults but from Caetité city (Fig. 2.13) southwards, thrusts are observed instead. The metamorphism is of

greenschist facies and locally of low amphibolite faceis. More detailed geological aspects of this region are given in Chapter 4, in connection with the interpretation of a large negative gravity anomaly found in the region (Fig. 2.4).

2.2.4 Eastern Bahia Shield (Region V)

This eastern region of the São Francisco craton has its basement extensively exposed. The whole region was consolidated at the end of the Transamazonian cycle (1.7-1.8 Ga) but radiometric data have revealed Archean nuclei which remained unaffected by the Proterozoic orogenies.

The Eastern Bahia Shield is essentially composed of mesozone and catazone plutons of acid composition. The epimetamorphic rocks are represented by sedimentary and volcanic-sedimentary complexes. These are classified as greenstone belts by Mascarenhas (1973).

Inda and Barbosa (1978) subdivided the Eastern Bahia Shield into three sub-regions in order to account for the radiometric and petrological data and the structural characteristics.

The Jequié-Mutuipe zone, the first sub-region, is shown in Fig. 2.7 and identified with number 5 in the caption. It is composed of granulites and migmatites. Part of this region,

dated at 3.2 Ga, can be associated with the first crustal nuclei within the São Francisco craton. Other parts are commonly dated at 2.7 Ga, corresponding to the high grade metamorphic event which occurred in the Archean and was referred to as the Jequie cycle by Cordani (1973). The structural pattern is very complex, reflecting the overprint of several deformational phases. During the Lower Proterozoic, the region was affected by feldspathization, migmatization and granitic-granodioritic intrusion.

The second sub-region is the Contendas-Uaua-Jacobina fold zone (number 4 in Fig. 2.7) . Transamazonian age predominates in this part of the Eastern Bahia Shield. It is composed of high grade metamorphic rocks, volcanic and acid intrusives and basic-ultrabasic rocks. The structures have fold axes and foliations trending north-south.

The Salvador-Juazeiro is the third sub-region (number 6 in Fig. 2.7). It is possible that the basement is Archean. The similarity of the granulite facies rocks of this region with the rocks found in the Jequie-Mutuipe sub-region can be taken as evidence for this. Migmatization and granitization occurred at about 1.9 2.0 Ga.

Middle Proterozoic sedimentation has not been found so far in this part of Bahia State. The Phanerozoic is represented by the Cenozoic-Mesozoic sedimentary basins of Reconcavo, Tucano and

Jatoba. Details of the stratigraphy and evolution of these basins is presented in Chapter 5.

2.2.5 The Marginal Fold Systems (Regions I,VI,VII)

Three fold systems which surround the São Francisco craton in Bahia State are briefly described..

The Rio Preto Fold System, the region I of Inda and Barbosa (1978), is situated at the north-northwestern border of the State. The basement of granitic-gneissic composition is Archean and it is overlain by sequences deposited in the Middle and Upper Proterozoic. The lower sequence is correlated with the Espinhaço Supergroup (Mid-Proterozoic) and it is composed of micaschist with biotite and garnet. The Upper Proterozoic sequence is composed of metasiltstones, arkoses and greywacke of the Bambui group. During the Brasiliano orogeny (500 Ma), the sediments were metamorphosed (low to intermediate grade) and deformed. The structural pattern is characterized by NW-SE vergence towards the craton.

The Sergipano Fold System (Region VI) is situated at the northeastern border of the State, and it is possibly an extension of the Pan - African belt (Burke et al., 1977). This system is composed of four zones trending WNW-ESE. The degree of deformation increases northeastwards. The metasediments

which compose the belt (pelitic and psammitic rocks) were deformed during the Brasiliano cycle. A more detailed account of this unit is given in Chapter 5, in connection with the evolution of the Cenozoic-Mesozoic sedimentary basins.

The Araçuai Fold System (Region VII) is situated at the south-southeastern border of Bahia State, continuing into Minas Gerais State (Fig. 2.6). The basement of Archean age is composed of granitic gneisses and gneisses. Some remnants of granulitic and charnockitic nuclei are also found. In the State of Minas Gerais, this belt is covered by the Middle Proterozoic sediments of the Espinhaço fold belt. It is composed of quartzites of Middle Proterozoic (Espinhaço Supergroup) and Upper Proterozoic sequences (Macaubas and Bambui groups). During the Brasiliano orogeny (ca. 500 Ma), the sediments were affected by greenschist facies metamorphism, folded and thrust against the craton (Fig. 2.10).

CHAPTER 3

The Isostatic Analysis of Bahia State

The isostatic response function technique was used to study the isostasy of the northern São Francisco craton. The following constitute adequate conditions for the application of this technique: the area covered by the present gravity survey, a fairly uniform distribution of the gravity stations and a region of relatively high topography (Espinhaço Fold System).

One of the aims in applying the response function technique is to get some information about the rheology of the lithosphere, in particular, to study how the lithosphere responds to geological time scale loads. The results of the response function studies in continental areas are difficult to be interpreted, due to the complexity of the geological history of the regions covered by the gravity and topographic data. The response function technique requires the data to cover a large area which often involves several different tectonic provinces. By applying this technique to a single tectonic unit, the São Francisco craton, an attempt is made to assess the application of the response function in an old continental area, where topography is highly attenuated due to erosion and where the lithosphere has been affected by an overprint of successive geological episodes.

3.1 The Isostatic Response Function Technique.

The isostatic response function technique, also referred to as the admittance or linear transfer function, was proposed by Dorman and Lewis (1970) to study the isostasy of continental wide areas. In particular, the technique was applied on United States gravity and topographic data (Lewis and Dorman, 1970) in order to estimate the deep crust and upper mantle density distribution associated with topographic variation.

Assuming that topographic masses are added loads produced by some tectonic process, the principle of isostasy states that mass variation at the surface is compensated by mass variation at some depth below the surface. It is usual to assume that topographic masses are compensated at depths where significant density variation occurs, such as at the Moho. Otherwise, if the depth of compensation is assumed constant, the topographic variation is compensated by lateral density variation, as in the case of Pratt model of isostasy. The way these two quantities, the topographic masses and their compensating masses, are interrelated depends on a particular mechanism of compensation.

As discussed by Dorman and Lewis (1970), the gravity effect of the compensating masses on the total measured gravity field

is non-linear. This fact has forced the use of numerical techniques in order to calculate the gravity effect of compensating masses predicted by a particular isostatic model. These techniques can sometimes be laborious and time consuming. However, as estimated by Dorman and Lewis (1970), the quadratic term of the compensating gravity field in the Airy compensation model generally does not exceed 10% of the linear term. Based on this result, they proposed an isostatic model in which, regardless of the mechanism of compensation, the response of the Earth to a surface load is linear. In this way, a linear approximation for the compensating gravity field is obtained.

The linear compensation model of Dorman and Lewis (1970) is based on the assumption that density variation ($\Delta\rho$) at a given depth r_1 under a point P_1 (Fig. 3.1), in response to topographic mass variation at a point P_2 at the surface can be expressed as

$$\Delta\rho(\theta_1, \phi_1, r_1) = \iint_S \Delta\sigma(\theta_2, \phi_2)\, K(\psi, r_1)\, d\Omega_2 \qquad (1)$$

where

$\Delta\rho$ = density variation at a depth r_1 under a point P_1;

$\Delta\sigma$ = mass per unit surface topographic area;

r_1 = depth of compensation, measured from the centre of the Earth;

$d\Omega_2 = \sin\theta_2 d\theta_2 d\phi_2$ = element of surface area;

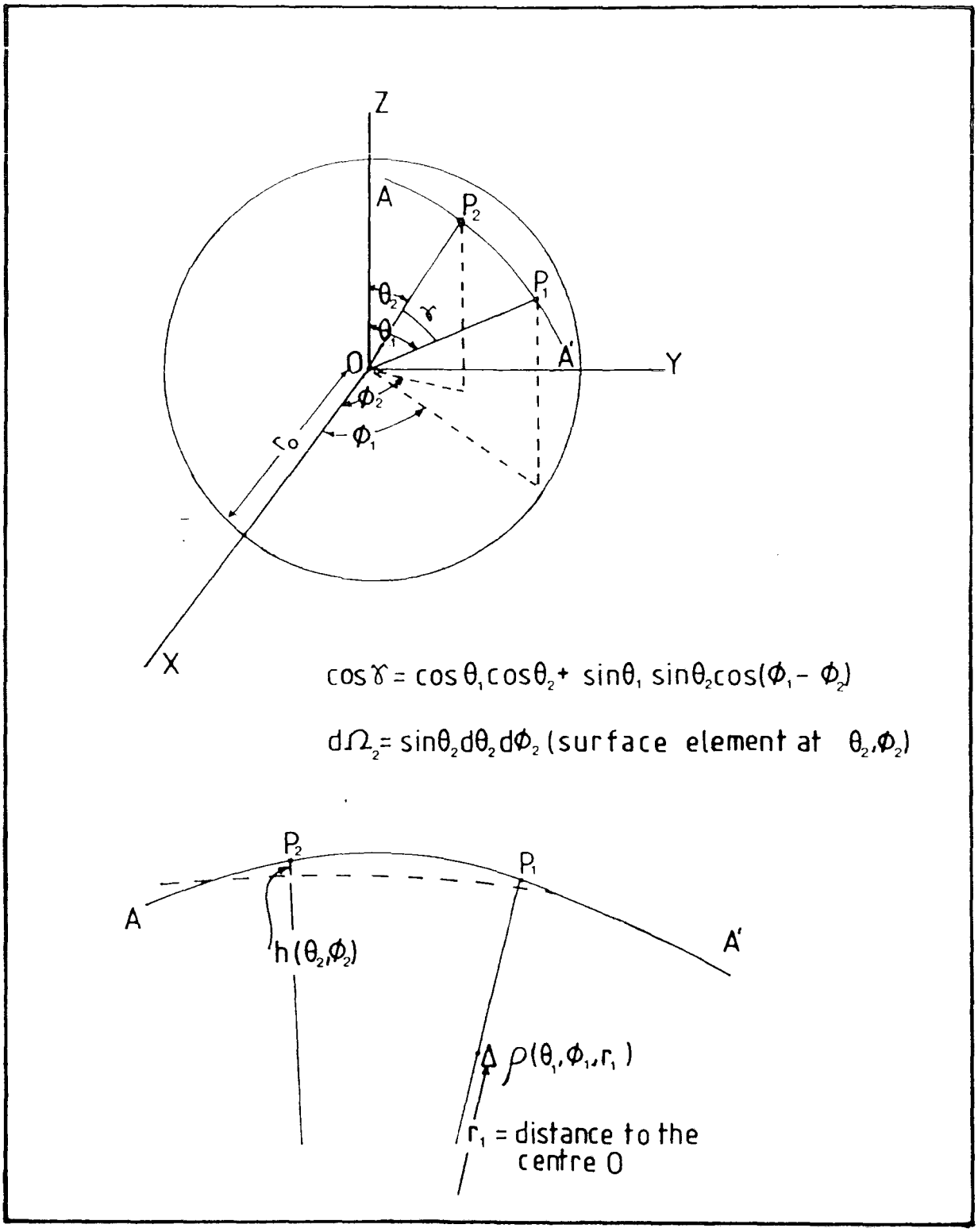

Fig. 3.1 - Spherical coordinates system assumed in the Dorman and Lewis (1970) linear isostatic compensation model.

$$\cos\psi = \cos\theta_1\cos\theta_2 + \sin\theta_1\sin\theta_2\cos(\phi_1 - \phi_2).$$

$K(\psi, r_1)$, the isostatic function due to a unit topographic load, is defined to be only dependant on the relative distance between the topographic masses and the point P_1 and on the depth of compensation r_1. If $K(\psi, r_1)$ is a delta function, the expression (1) reduces to a local compensation model. Therefore, K is a function which weights the surface density variation over the whole Earth. Assuming that the density of the topographic masses is constant and equal to ρ_0,

$$\Delta\sigma(\theta_2, \phi_2) = \rho_0\, h(\theta_2, \phi_2)$$

where h is the altitude at P_2 .

In this case, (1) is written as

$$\Delta\rho(\theta_1, \phi_1, r_1) = \iint_S \rho_0\, h(\theta_2, \phi_2)\, K(\psi, r_1)\, d\Omega_2 \qquad (2)$$

To calculate the gravity effect of the compensating masses, firstly the gravity potential at a point P at the surface, is written as

$$V(\theta, \phi, r) = \iiint_V G \frac{\Delta\rho(\theta_1, \phi_1, r_1)}{p} dr_1 \, d\Omega_1$$

where

G = gravitational constant

$p(\theta, \phi, \theta_1, \phi_1, r)$ = linear distance between the observational point P and P_1 .

$d\Omega_1 = \sin\theta_1 \, d\theta_1 \, d\phi_1$

The vertical component of the attraction is obtained as

$$g_i(\theta, \phi, r_0) = \left[\frac{\partial V}{\partial r}\right]_{r = r_0}$$

$$g_i = \iiint_V G \, \Delta\rho(\theta_1, \phi_1, r_1) \left[\frac{\partial}{\partial r}(1/p)\right]_{r = r_0} dr_1 \, d\Omega_1$$

where r_0 is the average radius of the Earth.

Substituting (2) in (2a) gives

$$g_i = \iiint_V G\rho_0 \iint_S h(\theta, \phi) \, K(\gamma, r_1) d\Omega_2 \left[\frac{\partial}{\partial r}(1/p)\right]_{r=r_0} dr_1 \, d\Omega_1 \qquad (3)$$

By changing the order of integration the attraction g_i is written as

$$g_i = G\rho_0 \iint_S h(\theta_2, \phi_2) \iiint_V K(\gamma, r_1) \left[\frac{\partial}{\partial r}(1/p)\right]_{r=r_0} dr_1 \, d\Omega_1 \, d\Omega_2 \qquad (4)$$

Defining

$$r(\gamma', r_0) = G\rho_0 \iiint_v K(\gamma', r_1) \left[\frac{\partial}{\partial r}(1-p)\right]_{r=r_0} dr_1 \, d\Omega_1$$

where $\cos\gamma' = \cos\theta\cos\theta_2 + \sin\theta\sin\theta_2\cos(\phi - \phi_2)$

the expression (4) is rewritten as

$$g_i(\theta, \phi, r_0) = \iint_S h(\theta_2, \phi_2)\, r(\gamma', r_0)\, d\Omega_2 \qquad (5)$$

Therefore, the vertical gravitational effect produced by the compensating density variation is also written as a linear function of the topographic masses. The expression (5) is the convolution between the topography and the gravity isostatic response function due to a unit topographic load, and it is simply written as

$$g_i = h * r \qquad (6)$$

where * denotes the convolution.

As discussed by Dorman and Lewis (1970), the expression (5) can be approximated to the plane case, even in regions of continental dimension (< 5000 km). In doing so, r, h, Δg_B and g_i become functions of (x,y,z).

In cartesian coordinates,

$$g_i(x,y) = r(x,y,x_2,y_2) * h(x_2,y_2)$$

The isostatic anomaly is defined as

$$\Delta g_i = \Delta g_B - g_i$$

where Δg_B = Bouguer anomaly

Therefore,

$$\Delta g_B - \Delta g_i = r * h \qquad (7)$$

Using the definition of Fourier transform, the convolution in (7) is a simple multiplication in the wavenumber domain. Let us define $R(\underline{k})$, $H(\underline{k})$, $B(\underline{k})$ and $G(\underline{k})$ as the spectral representation of r, h, Δg_B and Δg_i, respectively. Therefore, (7) will be rewritten as

$$B(\underline{k}) - G_i(\underline{k}) = R(\underline{k})\, H(\underline{k}) \qquad (8)$$

where

$$\underline{k} = k_x\, \underline{i} + k_y\, \underline{j}$$

$\underline{i}$ and $\underline{j}$ are the unit vectors

$G_i(\underline{k})$ is the final isostatic anomaly which we expect to be uncorrelated with the topography. If this is the case, the average of the cross-correlation between $G_i(\underline{k})$ and $H(\underline{k})$

approaches zero i.e.

$$\langle G_i(\underline{k})\, H^*(\underline{k}) \rangle = 0$$

where

$H^*(\underline{k})$ = complex conjugate of $H(\underline{k})$

$\langle \quad \rangle$ = average in a wavenumber bandwidth Δk

In this case, (8) can be written as

$$R(k) = \langle B(\underline{k})\, H^*(\underline{k}) \rangle \,/\, \langle H(\underline{k})\, H^*(\underline{k}) \rangle$$

where

$$k = |\underline{k}| = (k_x^2 + k_y^2)^{1/2}.$$

R(k) has no radial dependence, i.e., it is a real and symmetrical function in relation to k =0. This is because $r(\gamma)$, the compensating effect due to a point load, is also a symmetrical function in the space domain.

By cross correlating the observed Bouguer anomaly and the topography, the isostatic response function R(k) is easily obtained. This function provides, to first approximation, information about the possible mechanism by which the topographic masses are compensated at depth.

In order to measure the fraction of the gravity signal, at a particular wavelength k, which is linearly related to the topography, the coherency spectrum is defined as

$$C^2(k) = \langle B\,H^* \rangle^2 \left[\langle B\bar{B}^* \rangle \langle H\,H^* \rangle \right]^{-1}$$

In certain geological situations, the topography is approximately constant along a particular direction, such as in mountain belts or seamount chains. A simple expression for the isostatic function and the compensating gravity field is obtained assuming that the topography only varies along the x-direction

$$g_i(x) = r(x, x_2) * h(x_2)$$

The convolution is one dimensional and consequently also the Fourier transform of the observed Bouguer anomaly and topography.

The numerical aspects of calculating the response function are discussed in the next section, in connection with the application of this technique to the gravity and topographic data of Bahia State.

3.2 The Isostatic Response Function of Bahia State

As presented in Chapter 2, section 2.3, the regional tectonic features within the São Francisco craton trend NNW to N (Fig. 2.7). The Bouguer anomaly map (Fig. 2.4) also shows the same NNW to N trend, indicating a good correlation between geological features and gravity anomalies. However, to the west of longitude 43^{0} W, within the São Francisco basin, the anomalies trend approximately E-W, with wavelength of 400 km and amplitude of about 20 mGal.

The use of the response function technique requires a reasonable topographic signal. The topography of Bahia State, as outlined in Fig. 3.2, was obtained by interpolating the altitudes of the gravity stations. This map is only a first approximation of Bahia State topography. The short wavelength features, and in particular the areas of rough topography, are not well depicted due to the spacing between the stations and because gravity surveys tend to avoid regions of rough topography. Nevertheless, the regional topographic features ($\lambda >$ 20 km) are well reproduced due to a relatively uniform distribution of the gravity stations in this particular survey (see Fig. 2.1). The map shown in Fig. 3.2 was compared with a more detailed topographic map of Bahia State. Topographic features with wavelengths longer than 40 km are in agreement within $\pm$20 metres.

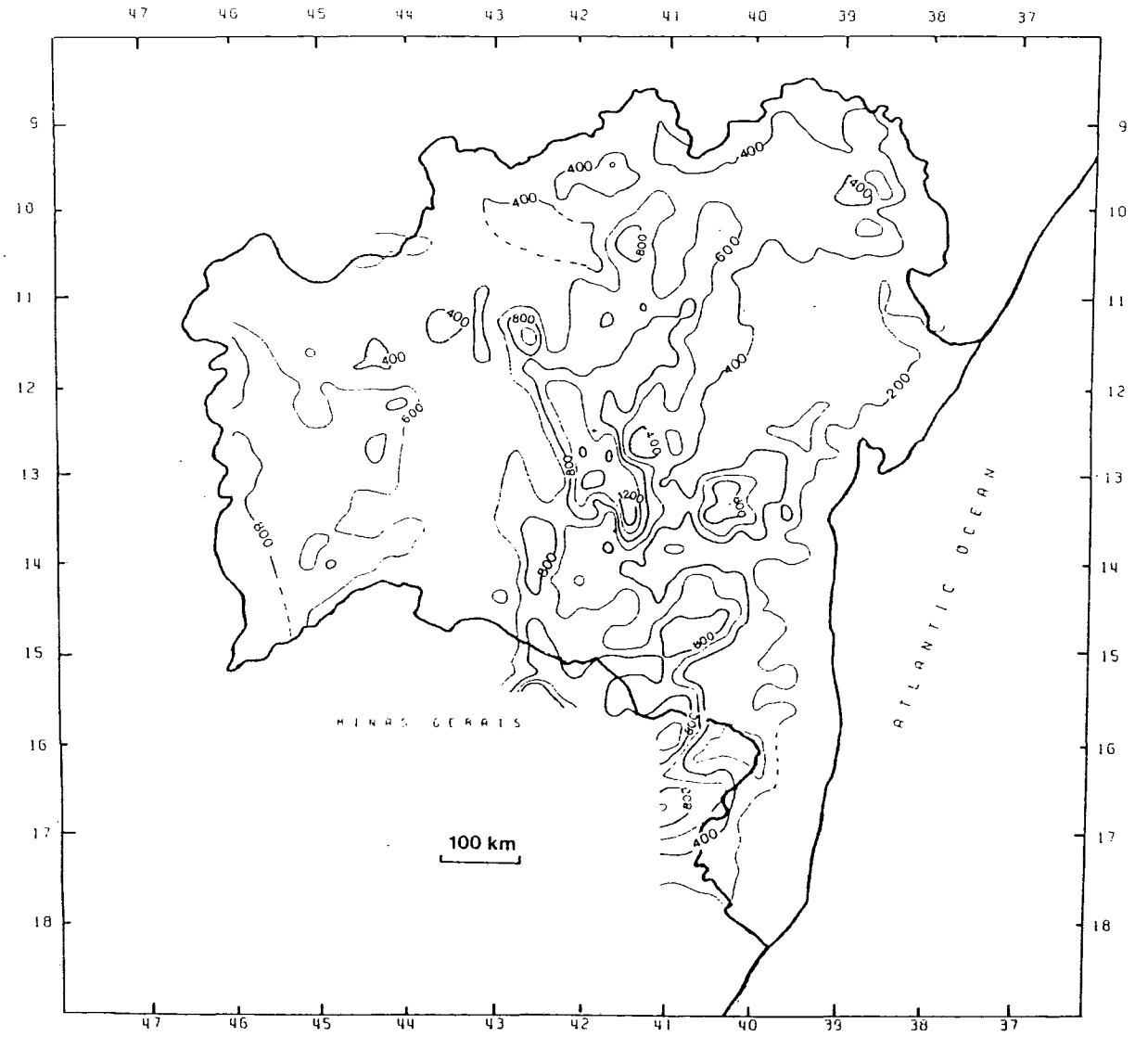

Fig. 3.2 - An outline of Bahia State topography, after the interpolation of altitudes of the gravity stations. Contour interval 200 metres.

The Bouguer and topographic maps (Figs. 2.4 and Fig.3.1) show a narrow region between longitude 41^{0} and 43^{0} W, where gravity and topography show good correlation. Most of the gravity and topographic features are associated with the Espinhaço Fold System. The topography ranges from 400 to 1200 metres above sea level, whereas the Bouguer anomaly ranges from -80 to -110 mGal.

In the present study, the one dimensional isostatic response function technique has been applied to five E-W profiles instead of using the two dimensional approach initially proposed by Dorman and Lewis (1970) and followed by McNutt and Parker (1978), Banks and Swain (1978) and Banks et al. (1977). The one dimensional approach may be justified on the grounds that the main tectonic and gravity features are approximately linear and trend north-south. The response function seeks the linear relationship between two signals. The cross spectrum of these two signals will be composed of random noise if there is not a correlation between them or if the amplitude of the signals is sufficiently low. A stable and unbiased estimate of the response function (Bendat and Piersol, 1966) is obtained by averaging the cross spectrum of the two signals within a wavenumber bandwidth Δk. The average cross spectrum composed of random noise at any Δk is zero. Therefore, for an approximately 2D structure, the average cross spectrum along its strike should be nearly zero and this can be used numerically to justify the use of the one dimensional approximation. This approximation has been previously applied in nearly linear

tectonic settings such as across continental margins (Karner and Watts, 1982), seamount chains (Watts, 1978) and fracture zones (McKenzie and Bowin,1976; Louden and Forsyth, 1982). A stable estimate of the response function is obtained by averaging the cross spectrum over several profiles.

Five gravity and topographic profiles were used in the present study (Fig. 3.3). These are separated from each other by about 55 km. Each of these profiles is composed of data points which are situated within an area extending 10 km on both sides of and parallel to the profile considered. The data within this 20 km window was projected orthogonally onto the profile.

The gravity and topographic profiles show the following main features:

1) The high topographic region is centred around the longitude 42^{0} W, with an average width of 200 km in the northern profiles and 100 km in the south.

2) Associated with the high topography, negative Bouguer anomalies are observed on all profiles. The wavelength of the anomalies is about the same as that of the topographic features.

3) There is a high correlation between free-air anomalies and short wavelength topographic features.

4) The long wavelength Bouguer anomaly, which extends from the centre of the craton towards the continental margin to the east, is inversely correlated with the topography. This can be

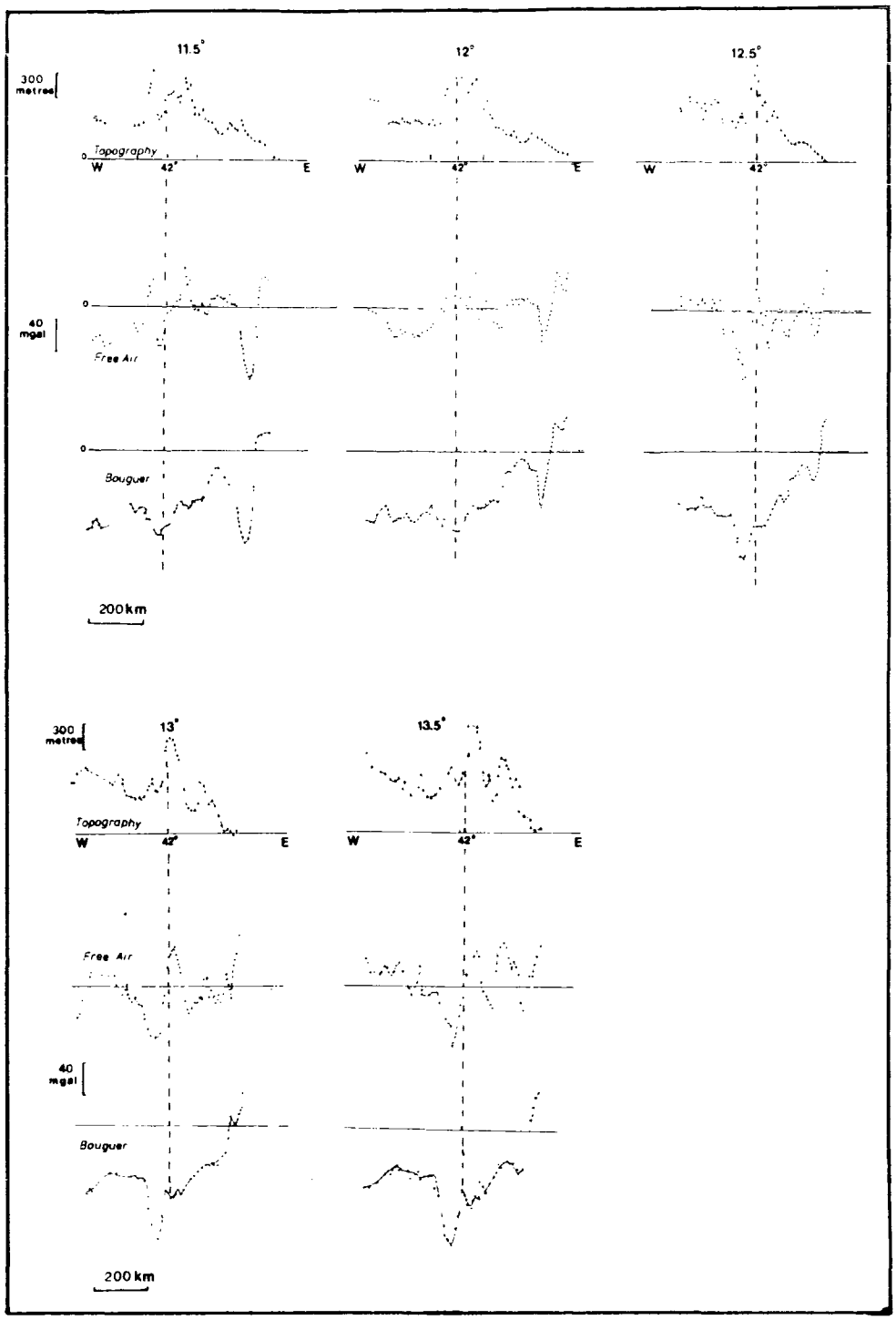

Fig. 3.3 - Five profiles along the west - east direction which were used in the isostatic response function analysis of Bahia State.

accounted for by shallowing of the Moho towards the continental margin.

5) To the west of longitude 42°W, in the São Francisco basin, the free air and Bouguer anomalies show a north-south variation. This is exemplified by two NS profiles shown in Fig. 3.4. The profile at 43.5° W is situated near the border of the São Francisco basin. A second profile (44.5° W), which is situated at a hundred kilometres to the west, shows a similar pattern of Bouguer anomaly. The cross correlation between topography and Bouguer anomaly for both profiles shows a very low coherency. This can be explained by a weak topographic signal in the basin and/or a random phase relationship between topography and gravity. The stratigraphy of the São Francisco basin suggests a NS variation in the thickness of the Middle and Upper Proterozoic metasedimentary cover. Associated with the minimum of the Bouguer anomaly, a thicker sequence of pelitic and calcareous rocks of Upper Proterozoic is observed. The basement outcrops to the north and to the south, as indicated by the positive Bouguer anomaly flanking the central negative anomaly. The long wavelength Bouguer anomaly in the São Francisco basin is thus probably mainly due to a variation of the basement depth within the basin.

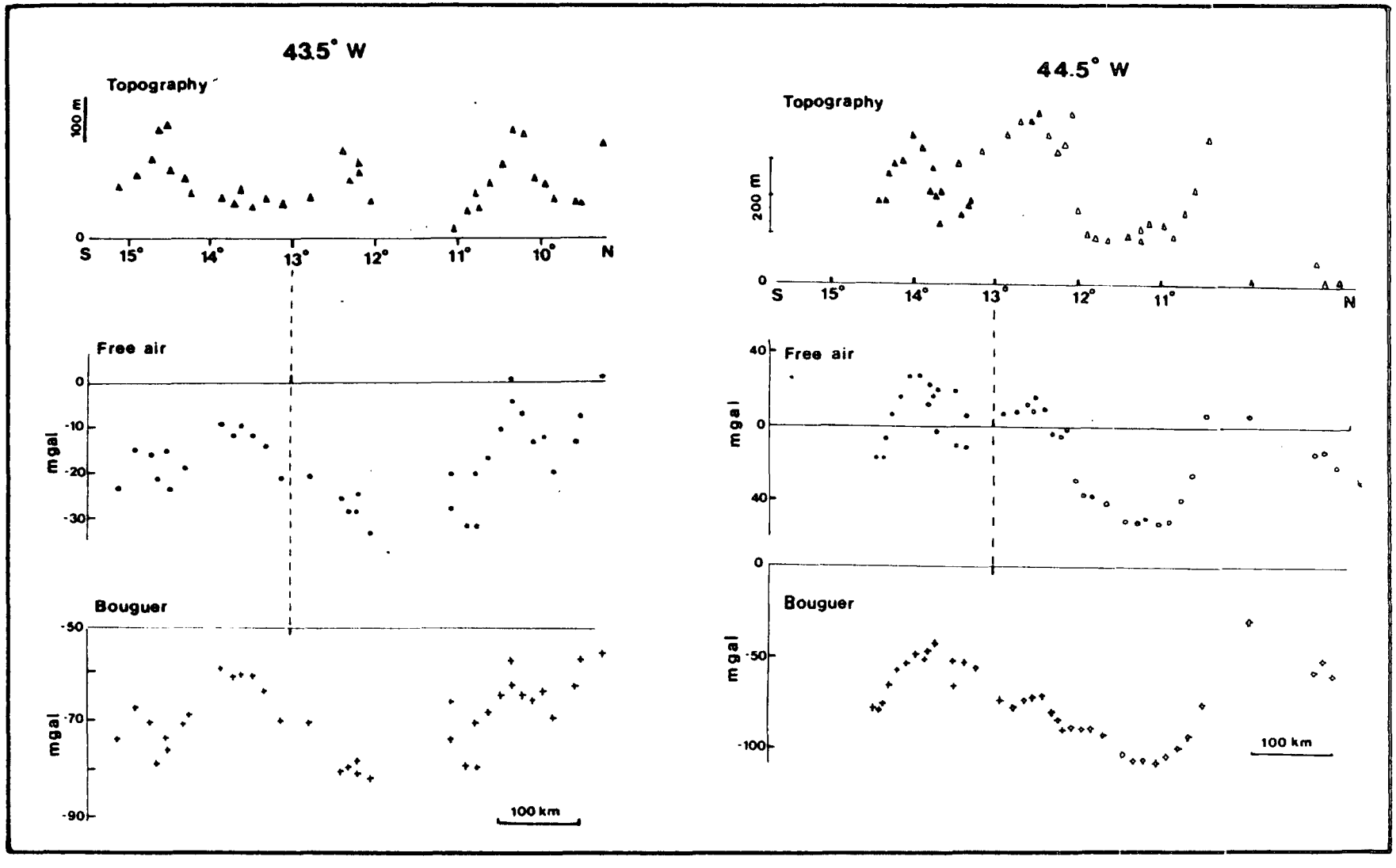

Fig. 3.4 - Two profiles along the south-north direction, in the Sao Francisco basin.

3.2.1 The Response Function, Coherency and Phase Spectra

The cross-spectral analysis of Bahia State gravity and topographic data was carried out on the profiles shown in Fig. 3.3. Linear interpolation yielded data points at interval of 10 km. The profiles have different lengths, which range from 650 to 850 km. The discrete Fourier transform of the data requires the end of the profiles to be smoothed or tapered to avoid the Gibbs phenomenon (Lanczos, 1961). There are different ways of avoiding this numerical problem. A complete discussion of these, with numerical tests within the context of calculating the isostatic response function, is presented by McNutt (1983). The three most common procedures are:

a) linear ramp forcing the values of the opposing ends to the same value;

b) tapering the ends smoothly to zero by applying a pre-defined taper function;

c) mirror image of the profile.

In using synthetic models with random noise, McNutt (1983) found that the most reliable estimate of the response function is obtained by using either the mirror image approach or by extending the ends of the profiles by prediction.

The present study follows the prediction procedure. The profiles were extended westwards to a length of 1280 km which provided 128 data points for the discrete Fourier transform.

The topographic profiles were extended taking data from topographic maps whereas the gravity anomalies were extrapolated following the regional trend, without introducing any short wavelength anomaly.

The isostatic response function, coherency and the phase spectra were calculated using a series of computer routines which are listed in Appendix B. This computer routines package was based on Bloomfield (1975).

An unbiased and stable estimate of the response function is obtained by averaging the cross spectrum $B(k)H^*(k)$ and the auto spectra $H(k)H^*(k)$, as defined in section 3.1. The isostatic response function is calculated as

$$R(k) = \langle B\,H^* \rangle / \langle H\,H^* \rangle$$

where * denotes the complex conjugate.

The functional relationship between G(k) and H(k) is given by the coherency, defined as

$$C^2(k) = \langle B\,H^*\,B\,H^* \rangle \left[\langle B\,B^* \rangle \langle H\,H^* \rangle \right]^{-1}$$

The coherency, a measure of the degree of correlation between the Bouguer anomaly and topography, is equivalent to the correlation coefficient of least squares analysis. As discussed in Bendat and Piersol (1966), if $C^2 = 0$ it is not possible to

define a response function between the two functions B and H. If $C^2 \neq 0$, however small is the value, a response function can be estimated with an accuracy which depends on the degrees of freedom of the estimate of each component of the spectrum.

By examining the coherency expression C^2, one can see that if the raw spectrum is used to estimate it, C^2 will be always equal to one for any single specified k. Therefore, a statistical approach must be used to understand the meaning of R(k).

The Bouguer anomalies and the topography are taken to be random gaussian variables (Bendat and Piersol, 1966). Therefore, the Fourier transforms of these quantities are also gaussian because the Fourier transform is a linear operator.

From the definition of χ^2 and its application, each $\hat{B}(k)$ estimated component of B(k) will have a distribution such as

$$\hat{B}(k) \; / \; B(k) = \chi^2_2/2$$

where χ^2_2 is the chi-square variable with n=2 degrees of freedom.

This distribution does not depend on the length of the series, that is, the error of the estimate will not change by increasing the number of observations. The average and variance of χ^2 are n and 2n respectively. Therefore, the error of B(k) is significant. The normalized standard error is

$$E = \sigma_{\hat{B}(k)} / \hat{B}(k) = \sqrt{2n} / n = \sqrt{2} / n^{1/2} \quad .$$

Because n=2, this implies that E = 1. Therefore, the standard deviation of the estimate is as large as its value. The error can be reduced by smoothing the spectrum. If the total length of the series is L, the smallest wavenumber will be $\Delta k = 1/L$ which is also known as the resolution of the spectrum. For each wavenumber $k = 1/L, 2/L, \ldots, N/L$ there is an independent estimate of the spectrum.

However, by taking the average of m components,

$$\hat{B}(k) = (1/m)[\, B(k) + B(k+1) + \ldots + B(k+m-1)]$$

then $\hat{B}(k)$ will be a χ^2 variable with n = 2m degrees of freedom. The resolution of the spectrum will decrease to $\Delta k' = m \Delta k$ but the standard deviation $E = \sqrt{1/(\Delta k' L)}$ is reduced to $\sqrt{1/m}$. In this case, the variance of the estimate is reduced at the expense of losing resolution.

In the present study, the procedure followed by Bloomfield (1975, chap.7, page 197) known as a modified Daniell filter was used. The spectrum was subdivided into bands of width Δk with log-scale length. The parameters assumed in the averaging procedure are presented in Table 3.1, together with the results

λ (km)	R(λ) (mGal m^{-1})	σ	C(λ)	m (each profile)
1280	0.0850	0.02	0.65	3
640	0.1102	0.03	0.68	3
420	0.1200	0.03	0.875	3
285	0.088	0.01	1.0	8
210	0.0186	0.003	0.85	8
180	0.0264	0.004	0.15	8
160	0.0058	0.0009	0.18	8
140	0.015	0.002	0.044	8
120	0.008	0.001	0.070	8
100	0.0064	0.0004	0.03	20
90	0.0004	$2x10^{-4}$	0.06	20
80	0.0005	$3x10^{-4}$	0.004	20
70	0.0003	$2x10^{-4}$	0.08	20
60	0.0004	$2x10^{-4}$	0.02	20
50	0.0007	$4x10^{-4}$	0.009	20
40	0.0005	$3x10^{-4}$	0.020	20
30	0.0002	10^{-4}	0.001	20
20	0.0001	10^{-4}	0.002	20

Table 3.1 - Results of the cross-spectral analysis of Bouguer anomalies and topography, averaged over five profiles. R = response function; C = coherency ; σ = standard deviation; λ = wavelength; m = smoothing factor.

of the response function, standard deviation of the estimate and coherency, averaged over five profiles.

The phase spectrum is obtained as

$$\Phi(k) = \arctan [\ \mathrm{Im}\ (B\ H^{*}) / \mathrm{Real}\ (B\ H^{*})]$$

where Im is the imaginary part and Real is the real part. $\Phi(k)$ is the measure of whether R(k) is a real function. The phase is nearly zero or ± 180 degrees if the imaginary part of R(k) is negligible.

The isostatic response function (or admittance function) of Bahia State is shown in Fig. 3.5. The bars indicate one standard deviation of each estimate, which is calculated as $\sigma^{2} = R(k)/(N\ m)$ where N is the number of profiles and m is the number of components of each estimate of R in a wavenumber bandwidth Δk. The phase and coherency spectra are shown in Fig. 3.6.

The response function of Bahia State presents a sharp decrease of energy at about $\lambda = 200$ km. Topographic features with wavelength shorter than 200 km are either "uncompensated" or they are compensated by other means which are not predicted by the linear model. The coherency spectrum also shows that the degree of linearity is distinctly low for $\lambda < 200$ km. Therefore, topographic and gravity signals at this bandwidth are not correlated. At long wavelengths ($\lambda > 600$ km), low energy is also observed due to numerical reasons. As shown in Fig. 3.3, the

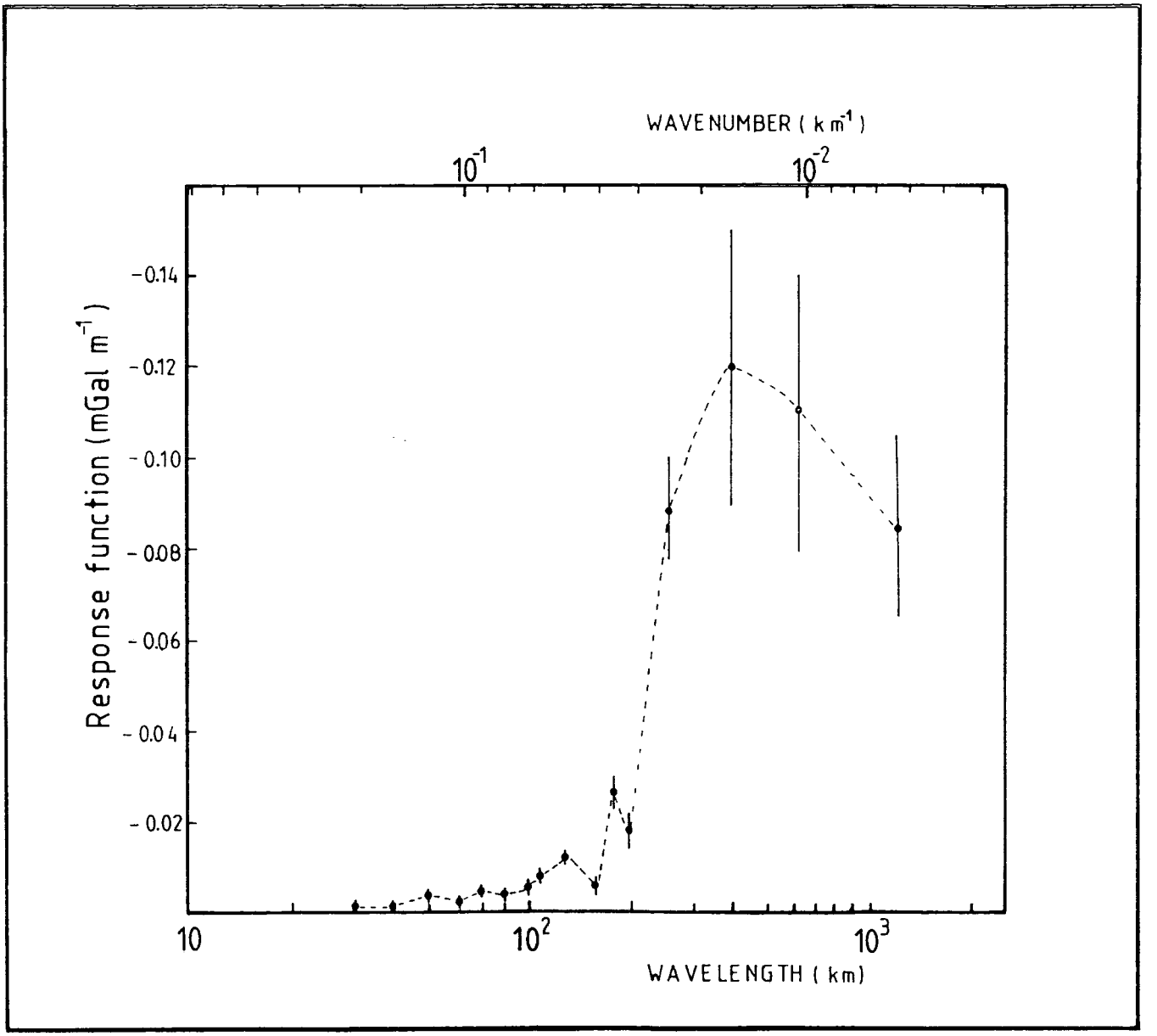

Fig. 3.5 - Response or Admittance function of Bahia State. The bars are the standard deviation.

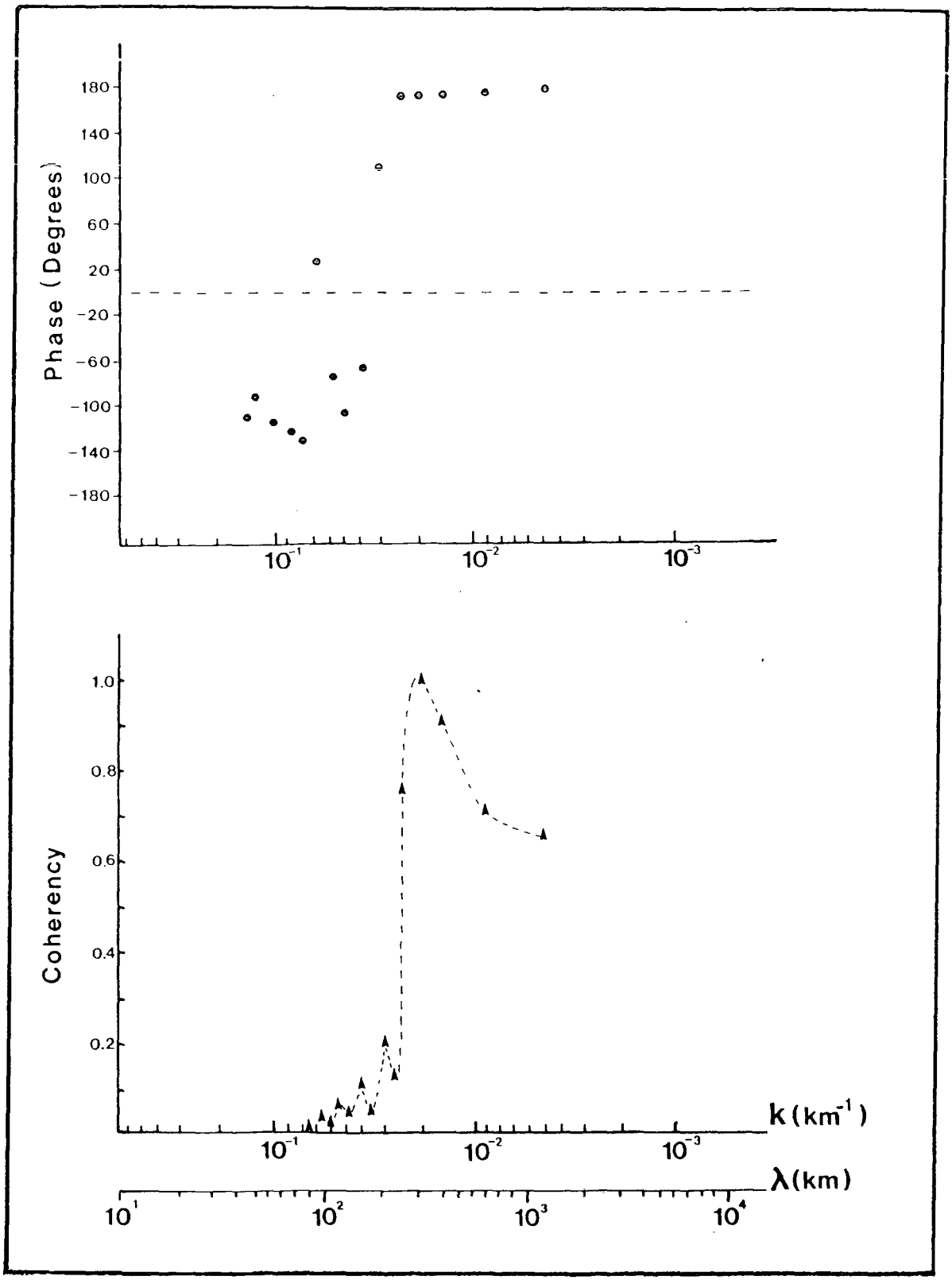

Fig. 3.6 - Phase and coherency spectra associated with the response function of Bahia State.

longest topographic feature, which extends from the centre of the craton to the eastern continental margin, does not define a complete wavelength. However, there is some correlation between this topographic feature and the Bouguer anomaly. One way to avoid numerically the decrease in energy for $\lambda > 600$ km is to "complete" the wavelength of this feature by extending the profile westwards. This can be done, for instance, by mirror-imaging the data in relation to the west end of the profile. However, the response function corresponding to this artificially created signal, does not have any real physical meaning. It is very unlikely that the gravity and topographic signatures to the west of Bahia State resemble those to the east. The western border of the São Francisco craton is the Brasilia fold belt and the eastern border is the Atlantic continental margin. For this reason, it was decided to calculate the response function keeping the "incomplete" wavelength. This does not result in any loss of information or misinterpretation as long as we bear in mind this limitation in the data. Also, as is shown in the next section, the response function at wavelengths larger than 1000 km does not provide much information regarding the possible compensation mechanism . The bandwidth, in which useful information regarding the compensation mechanism can be obtained, is between 200 to 1000 km. In particular, the response function of Bahia State shows a narrow bandwidth where the response is high and the coherency is nearly one. This interval is situated around 250 - 600 km.

The phase spectrum shows that the response function is a real function for $\lambda > 200$ km. For $\lambda < 200$ km, a random relationship between topography and Bouguer anomalies appear to exist, as expected if the gravity anomalies are caused by uncompensated sources.

3.2.2 Comparison between observed and theoretical isostatic response functions.

In order to interpret the isostatic response function of Bahia State, it is useful to compare it with theoretical response functions predicted by different lithospheric rheologies. This approach has been used by Banks et al. (1977), Banks and Swain (1977), McNutt and Parker (1978) and Stephenson and Lambeck (1985) in studying the isostasy of continental regions. Whilst Stephenson and Lambeck (1985) used a viscoelastic rheology, the other continental studies made use of the elastic plate model. In order to assess the possible mechanism of compensation of Bahia State region, thin elastic plate rheology is initially assumed, with the topographic masses compensated at the base of the crust.

The response function predicted by the thin elastic plate model overlying a fluid substratum is easily obtained in the wavenumber domain, following Banks et al. (1977). The one dimensional equation of the vertical deformation $w(x)$ of either

an elastic beam or a thin elastic plate, when loaded on top by a topography h(x) and density ρ_0 is given by the following differential equation (Hetenyi, 1946 ; Jeffreys, 1976)

$$D \frac{\partial^4 w}{\partial x^4} + (\rho_m - \rho_c)\, g\, w(x) = \rho_0 g\, h(x) \qquad (9)$$

where ρ_m = mantle density,

ρ_0 = density of topography (load),

ρ_c = crustal density,

g = gravity,

$D = E\, T_e^3 / 12(1-\nu^2)$ is the flexural ridigity of the plate,

E = Young modulus,

ν = Poisson ratio,

Te = plate thickness.

The Fourier transform of the above equation is

$$k^4\, D\, W(k) + (\rho_m - \rho_c)\, g\, W(k) = \rho_0\, g\, H(k)$$

and the Fourier transform of the deflection w(x) is thus

$$W(k) = \frac{\rho_0}{\Delta\rho}\left\{1 + \left[k^4 D/(\Delta\rho\, g)\right]\right\}^{-1} H(k) \qquad (10)$$

where $\Delta\rho = \rho_m - \rho_c$

$k = 2\pi / \lambda$

λ = wavelength

The gravitational effect due to the deformation W(k) at the base of the crust is linearly approximated as

$$B(k) = 2\tilde{\pi} G \Delta\rho \exp(-k z_m) W(k)$$

where z_m is the mean depth of the Moho. Substituting the equation for W(k) gives

$$B(k) = 2\tilde{\pi} G \Delta\rho \exp(-k z_m) \left\{ \frac{\rho_0}{\Delta\rho} \left[1 + \left(k^4 D / \Delta\rho g \right) \right]^{-1} \right\} H(k)$$

The response function is then

$$R(k) = B(k) / H(k) = 2\tilde{\pi} G \exp(-k z_m) \rho_0 \left[1 + \left(k^4 D / \Delta\rho g \right) \right]^{-1}$$

If D = 0, W(k), the deflection of the Moho, follows the simple Airy model of local compensation. If D $\neq$ 0, the compensation is accomplished in a regional way.

Four theoretical response functions were determined using elastic plate rheology for values of effective elastic thickness of 0, 20, 40 and 80 km. The other parameters used in the calculation were:

ν = 0.25, E = 10^{11} N m^{-2} , the depth of compensation z_m = 35 km, ρ_m = 3.3 g cm^{-3} , ρ_c = 2.8 g cm^{-3} and ρ_0 = 2.67 g cm^{-3}. The four

theoretical response functions are shown in Fig. 3.7, together with the response function of Bahia State.

There is little resemblance between the observed and the theoretical response functions. The observed response function suggests that the topographic features with wavelengths between 250 and 600 km are apparently "overcompensated". In other words, the compensating gravity field at these wavelength exceeds the one predicted by the local compensation model (Te = 0 km).

This comparison shows that the assumed elastic plate model with compensation at the Moho is not totally adequate to describe the way the topographic masses are compensated in this region. There are medium wavelength features of gravity anomalies which correlate with topography and those are not adequately accounted for by the linear model based on compensation only at the Moho. Further departure from the local compensation model is observed at short wavelengths ($\lambda < 200$ km). The gravity anomalies and topography are uncorrelated as shown in both the coherency and phase spectra.

From the four theoretical isostatic response functions, it can be observed that the response function at $\lambda > 1000$ km does not help to discriminate the mechanism by which the compensation is achieved. All curves tend assymptotically to the same value at $\lambda > 1000$ km. At such long wavelength, the topography will always

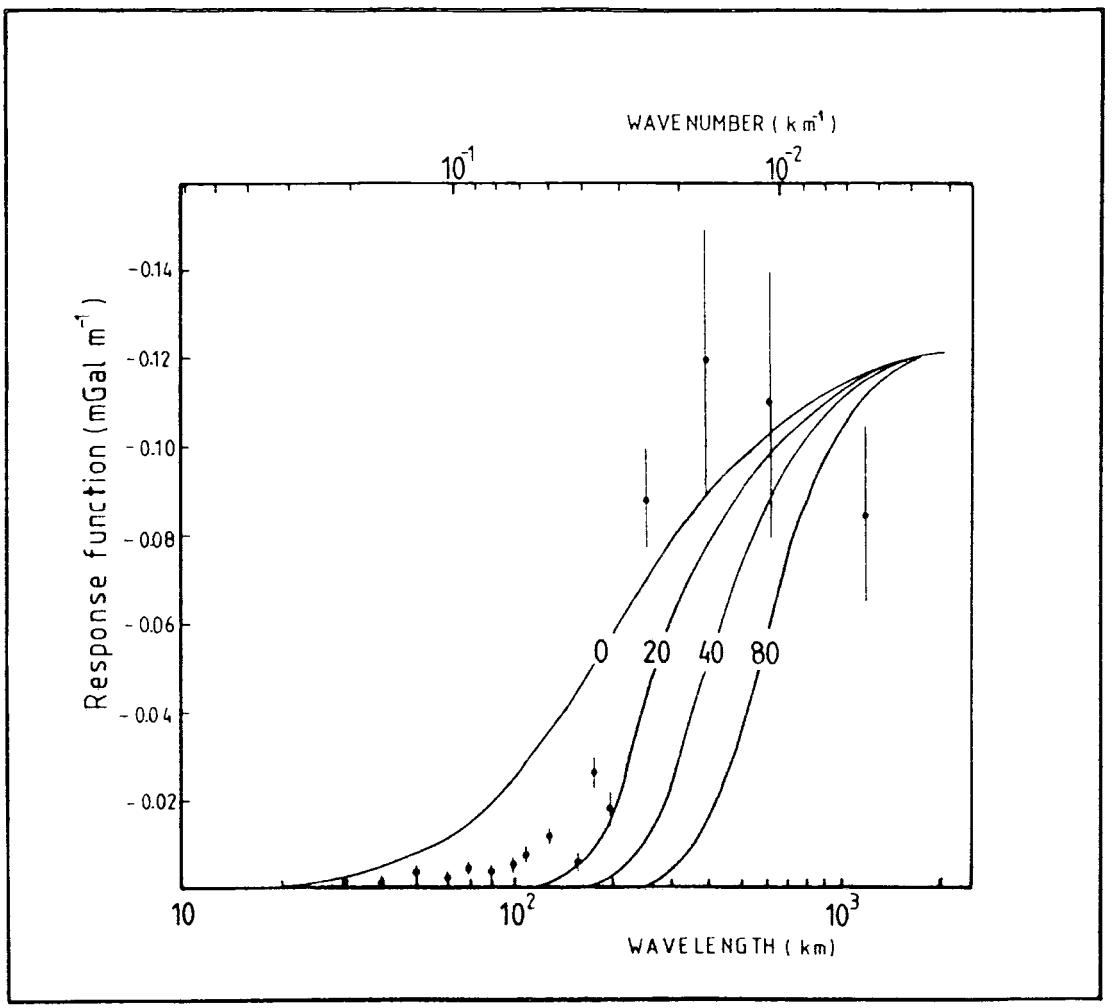

Fig. 3.7 - Comparison between observed and theoretical response functions predicted by the thin elastic plate rheology. Moho at 35 km; crustal density = 2.80 g cm^{-3} ; mantle density = 3.3 g cm^{-3} ; Te = 0, 20, 40, 80 km are the effective elastic thicknesses.

appear to be locally compensated, independent of the rigidity of the plate.

In order to explain the apparent "overcompensation" observed at wavelengths between 250 and 600 km, two approaches can be followed:

1) The first approach is to investigate whether the surface topography is the only source of load acting on the elastic plate and whether the compensation only occurs at the Moho. The primary assumption in obtaining the theoretical response functions shown in Fig. 3.6 is that the plate is only loaded from the top and that compensation occurs at a single depth, at the Moho. However, as pointed out by Forsyth (1981,1985) and McNutt (1983), low rigidities may be obtained if subsurface loads such as lateral density variation, low or high density bodies which correlate with the surface topography or compensation at different depths other than at the Moho are not taken into account in calculating the theoretical isostatic response function. Forsyth (1985) obtained the response function shown in Fig. 3.8a by assuming a plate loaded both on top by the observed topography and at the base of the crust by a low density body such as a crustal root. As the ratio between the amplitude of the bottom load and the amplitude of the surface load increases, the response function gradually increases towards the short wavelengths. A local maximum in the function is also observed. The overall shape of the response function is very similar to the one obtained for Bahia State,

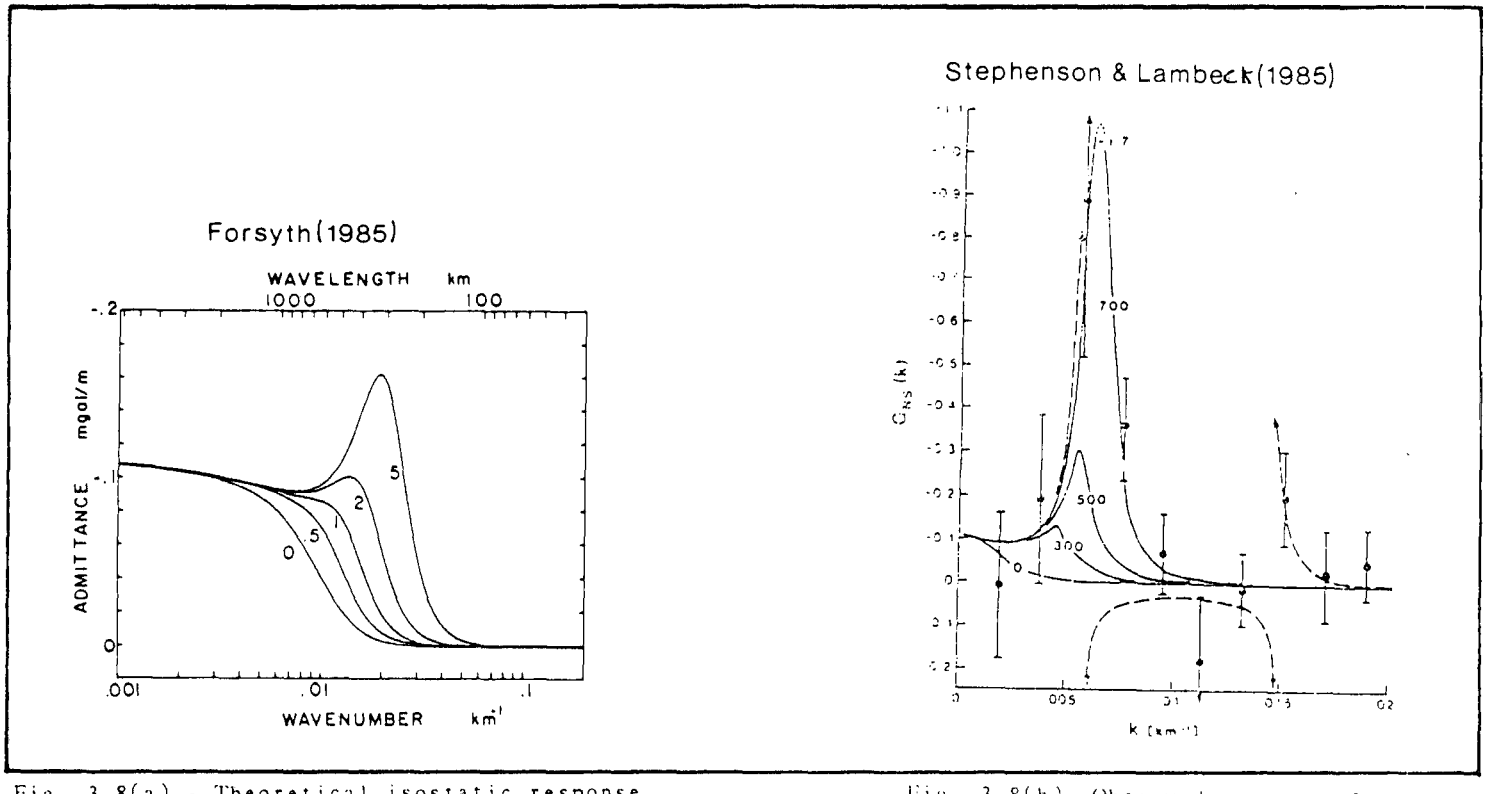

Fig. 3.8(a) - Theoretical isostatic response function for loading an elastic plate on top and at the Moho, simultaneously. The number in each curve is f, the ratio of the amplitude of the bottom load to the amplitude of the surface load . Moho at 35 km and plate thickness of 40 km.

Fig. 3.8(b)- Observed response function of central Australia and theoretical response function predicted by the viscoelastic model with $D = 10^{23}$ N m, including erosion and in-plane stresses.

except for $\lambda > 1000$ km for reasons which were previously discussed.

2) If the simple elastic plate rheology is not adequate to explain the observed response function, a more complicated rheology has to be considered, such as the viscoelastic model. The elastic plate model can be regarded as a special case of the viscoelastic model in which the viscous relaxation time constant is too large to observe any relaxation within geological time scale of less than 1000 Ma. The viscoelastic model has been used by Stephenson and Lambeck (1985) in interpreting the isostatic response function of central Australia (Fig. 3.7b). In their study, the observed response function was interpreted using a viscoelastic model with in-plane stresses, erosion and viscous relaxation. According to these authors, the in-plane stresses are associated with the buckling of the lithosphere during a compressional event in the Late Proterozoic (Lambeck, 1983). The use of this model is problematic due to the large number of assumptions which have to be made regarding the erosional process and the requirement of large in-plane stresses being preserved for period of time of 700 Ma or more.

To investigate the sources of departure of Bahia State compensation from the elastic plate rheology considered so far, the first approach is followed. The initial step is to calculate the "isostatic" anomalies predicted by the observed isostatic response function. This may indicate the possible sources of the apparent "overcompensation".

3.2.3 The "isostatic" anomalies

An obvious, but seldom followed procedure is to calculate the isostatic anomalies using the linear response function R(k) obtained from the cross-spectral analysis. The gravity effect predicted by the observed isostatic response function is then subtracted from the observed anomalies to obtain the isostatic anomalies (see section 3.1). The latter are expected to be uncorrelated with the topography. Fig. 3.9 shows the results of applying the calculated response function to three topographic profiles. The results obtained show:

1) The gravity effect associated with the longest topographic variation, which does not define a complete wavelength, is still present in the "isostatic" anomaly field. As discussed in section 3.1, R(k) is the spectral representation of the response function of a point load which is both symmetrical and real function. Therefore, R(k) is also symmetrical. By convolving R(k) with the topography, the predicted gravity field tends to look nearly symmetrical;

2) The isostatic response function has been derived from the correlation of topographic features and negative anomalies such as shown in profile 12.^{0} S. The two quantities are in phase and their wavelengths ($\lambda = 400$ km) coincides where an apparent "overcompensation" is observed (Fig. 3.5). For topographic features with $\lambda < 250$ km, such as the one presented in the profile 13.5^{0}S, no significant compensating gravity response is observed.

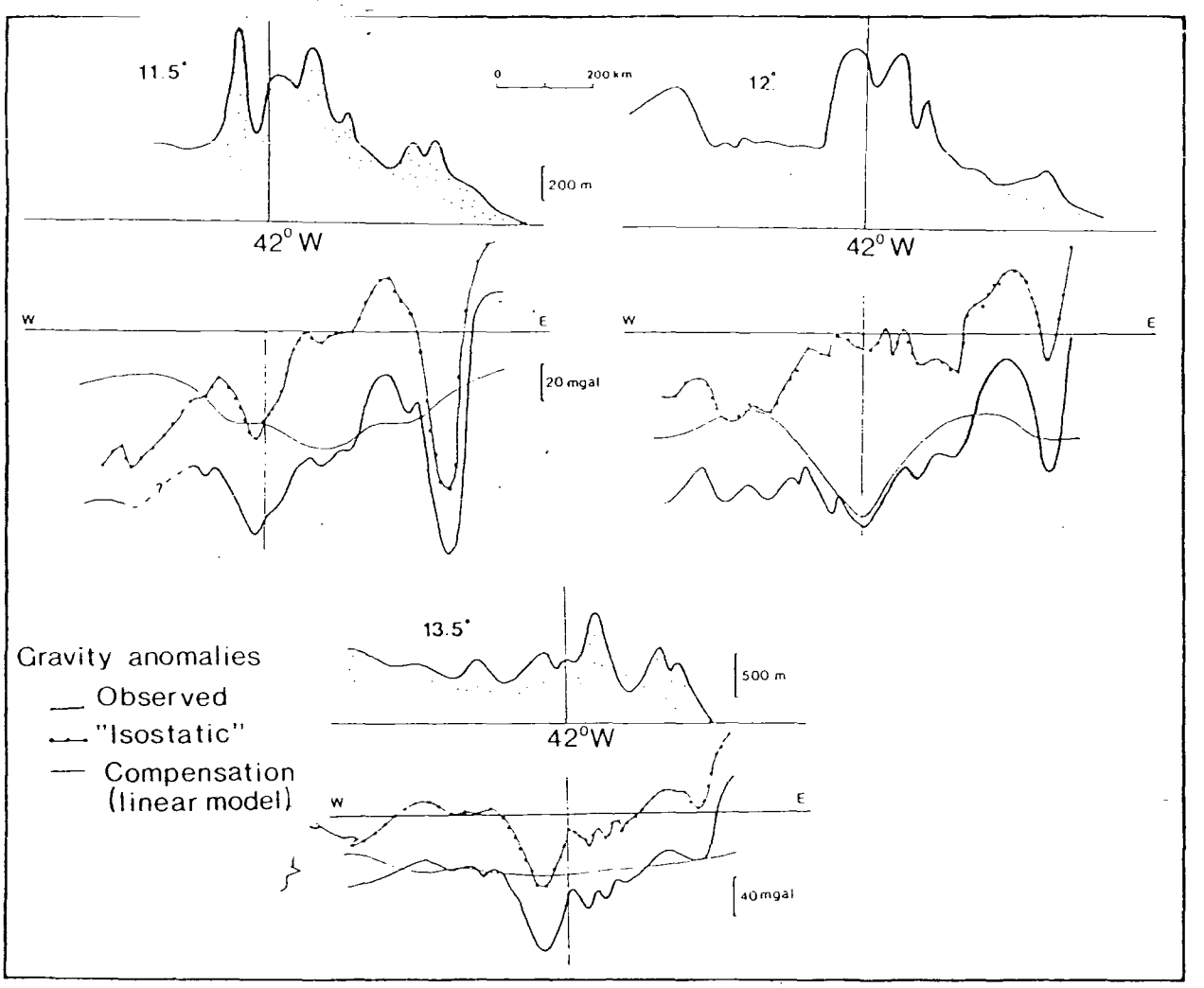

Fig. 3.9 - "Isostatic" anomalies predicted by convolving the topography and the observed response function of Bahia State.

Because of the symmetry of both the response function and derived "isostatic" anomalies, the results are not particularly helpful in finding out the sources of the apparent "overcompensation". If the compensating gravity effect predicted by the simple elastic model could be separated from the observed gravity field, then the source of the "overcompensation" may be more easily identified. This can be done either by convolving the theoretical response function with the topography, as carried out previously, or by solving the "forward" problem. The latter consists in loading an elastic plate with the observed topography, calculating the deflection, for instance at the Moho, and estimating the associated gravity effect.

As demonstrated before, the convolution technique has the drawback of generating a relatively symmetrical gravity field around the load. Therefore, the "forward" problem has been used instead. This problem has already been formulated when obtaining the response function predicted by the elastic plate model. The deflection of a thin elastic plate in equilibrium, is given by the differential equation (9). The deflection w(x) is written in the wavenumber domain as

$$W(k) = \frac{\rho_o}{\Delta\rho}\left[1 + \left(k^4 D / \Delta\rho\, g\right)\right]^{-1} H(k)$$

where $H(k)$ = Fourier transform of $h(x)$ the surface topography;

ρ_0 = density of the surface load;

$\Delta\rho$ = mantle density - crustal density;

D = flexural rigidity;

g = gravity .

The deflection of the Moho w(x) is obtained by calculating the inverse Fourier transform of W(k). The one dimensional gravity effect is accurately computed using the method proposed by Parker (1972) and it is given by

$$G(k) = -2\pi G \Delta\rho \exp(-k z_m) \sum_{n=1}^{M} \frac{k^{n-1}}{n!} F[w^n]$$

where z_m is the mean depth of the Moho.

$F[w^n]$ = Fourier transform of the n-th power topography

M = maximum order of the series

This procedure was applied to four topographic profiles and the calculated Bouguer anomalies are shown in Fig. 3.10, together with the topography and the observed gravity anomalies. The assumed values for the elastic plate model were: z_m= 35 km, $\Delta\rho$ = 0.5 g cm^{-3}; ρ_0 = 2.67 g cm^{-3} , M = 5 , ν= 0.25, E = 10^{11} N m^{-2} and Te = 0, 20 and 40 km. The computer routine used to calculate both the deflection of the Moho and its gravity effect is listed in Appendix B.

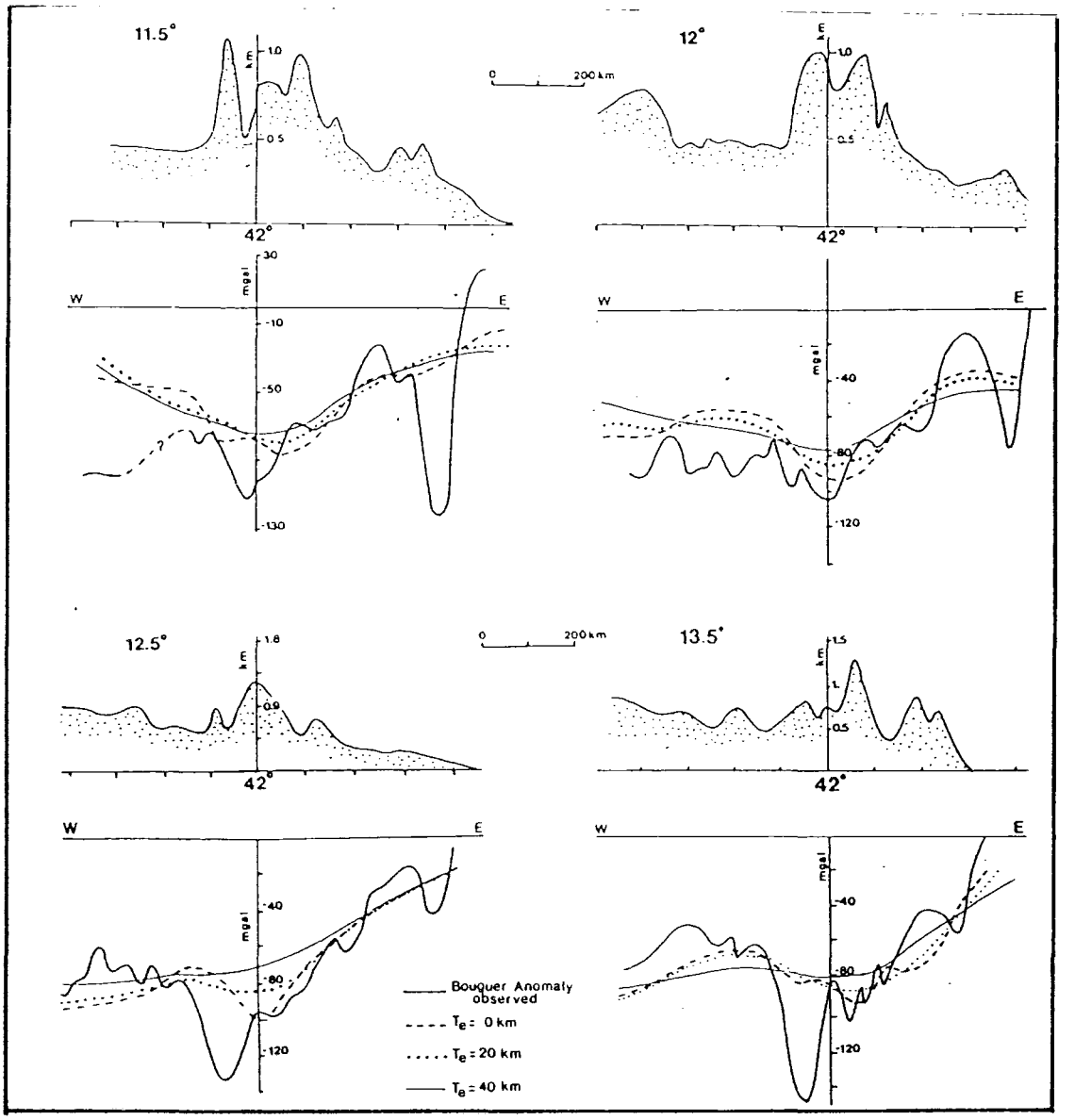

Fig. 3.10- Predicted gravity effect by loading the elastic plate with the observed topographic masses. The results are for different effective elastic thickness, Moho depth at 35 km.

A change in the depth of compensation z_m from 35 km to 30 or 40 km only affects the results by a few milliGal. This procedure gave more useful conclusions. The results are presented in Fig. 3.10 and they are summarized as follows:

1) The regional component of the observed gravity field is largely predicted by loading the elastic plate with the observed topography, independent of the rigidity of the plate;

2) For the western half of the 11.5°S and 12.° S profiles, the observed Bouguer anomalies are significantly lower than the calculated anomaly. Whereas the residuals are in the opposite sense for the two southern profiles (12.5°S and 13.5° S). This discrepancy in the Bouguer anomalies at the western part of the profiles is caused by the NS variation of the gravity field, within the São Francisco basin, as shown in Fig. 3.4, section 3.1;

3) The calculated regional gravity field is associated with a progressively shallowing of the Moho towards the east, if no lateral density variation occurs in the crust. However, it appears that the estimated relative shallowing of the Moho (~ 4.5 km) from the centre of the craton towards the continental margin is not enough to account for the observed positive gravity gradient of 0.2 mGal/km. The eastern end of the profiles, near the continental margin, presents a steep positive Bouguer anomaly gradient because of the proximity of the continental-oceanic crust boundary. In particular, this part of the Brazilian continental margin is relatively narrow. The transition from the continental crust to oceanic crust occurring

within a distance of about 50 km from the coastline (Rabinowitz and Cochran, 1978). Whilst the gravity measurements near the coast indicate a major variation in the thickness of the crust, the equivalent topographic (bathymetry) variation occurs further to the east. The proximity of the continental margin was not taken into account in calculating the compensating gravity effect by loading a continuous plate with the observed topography.

In order to estimate whether this limitation in the data explains part of the "overcompensation" at λ=400 km, a calculation of the response function was carried out by replacing the actual gravity gradient with the one predicted by loading the elastic plate with the observed topography. The results show that the response function is slightly amplified at wavelengths between 100 and 200 km, from 0.01 to 0.02 mGal/metre. However, no significant change is observed at λ=400 km. This means that the source of "overcompensation" is situated in the centre of the São Francisco craton.

3.3 The Surface and Subsurface Loads

3.3.1 Thickening of the crust

The first model to explain the apparent "overcompensation" places the load at deeper levels, possibly at the

Moho. Such load might be a relative thickening of the crust beneath the Espinhaço Fold System, which resulted from compressional events in the Middle Proterozoic. This low density "root", which is not associated with the surface load, responds isostatically producing the topography from below.

This type of subsurface load has already been discussed by McNutt (1983) and Forsyth (1985) in which the elastic plate is loaded on top and from below, with the subsurface load situated at the base of the crust. The theoretical isostatic response function is written as (Forsyth, 1985)

$$R(k) = -2\pi\rho_0 G \exp(-k z_m) \frac{\left\{D_2 W^2 + H^2 / D_1\right\}}{\left\{W^2 + H^2\right\}}$$

where $W(k)$ = spectral representation of the topography created from below

$H(k)$ = spectral representation of the topography on top of the plate;

$D_1 = 1 + (D k^4 / \Delta\rho g)$

$D_2 = 1 + (D k^4 / \rho_c g)$

ρ_m = mantle density

ρ_c = crustal density

$\Delta\rho = \rho_m - \rho_c$

This analysis allows for both subsurface and primary surface loads. The ratio of the weight of the applied load at the Moho

to the weight of the load applied at the surface is $r = \frac{W\ D_1\ \Delta\rho}{\rho_0\ H}$.

The results obtained by Forsyth (1985) for a 40 km thick elastic plate and different values of the ratio r are shown in Fig. 3.11. The curve for r= 3 agrees best with the observed response function. The subsurface load is, therefore, relatively more important than the actual surface load. The average altitude at the centre of the São Francisco craton is about 800 metres. For r=3, the average thickening of the crust beneath the Espinhaço Fold System would be estimated as 3-4 km to account for the observed topography.

3.3.2 Near surface mass deficiency

An alternative model to explain the observed isostatic response function of Bahia State, which does not exclude the previously discussed model, admits the subsurface load to be situated near the surface.

The topographic features observed in the Espinhaço Fold System are situated in the region of widespread acid volcanism, granite intrusion and a relatively thick accumulation (2-3 km) of metasediments. Therefore, compensation of the surface topography is partially achieved within the uppermost part of the crust. If the lithosphere behaves elastically, part of the topography is actually created as a flexural response of the plate due to the buoyant effect associated with low density rocks within the upper crust. In order to evaluate whether this

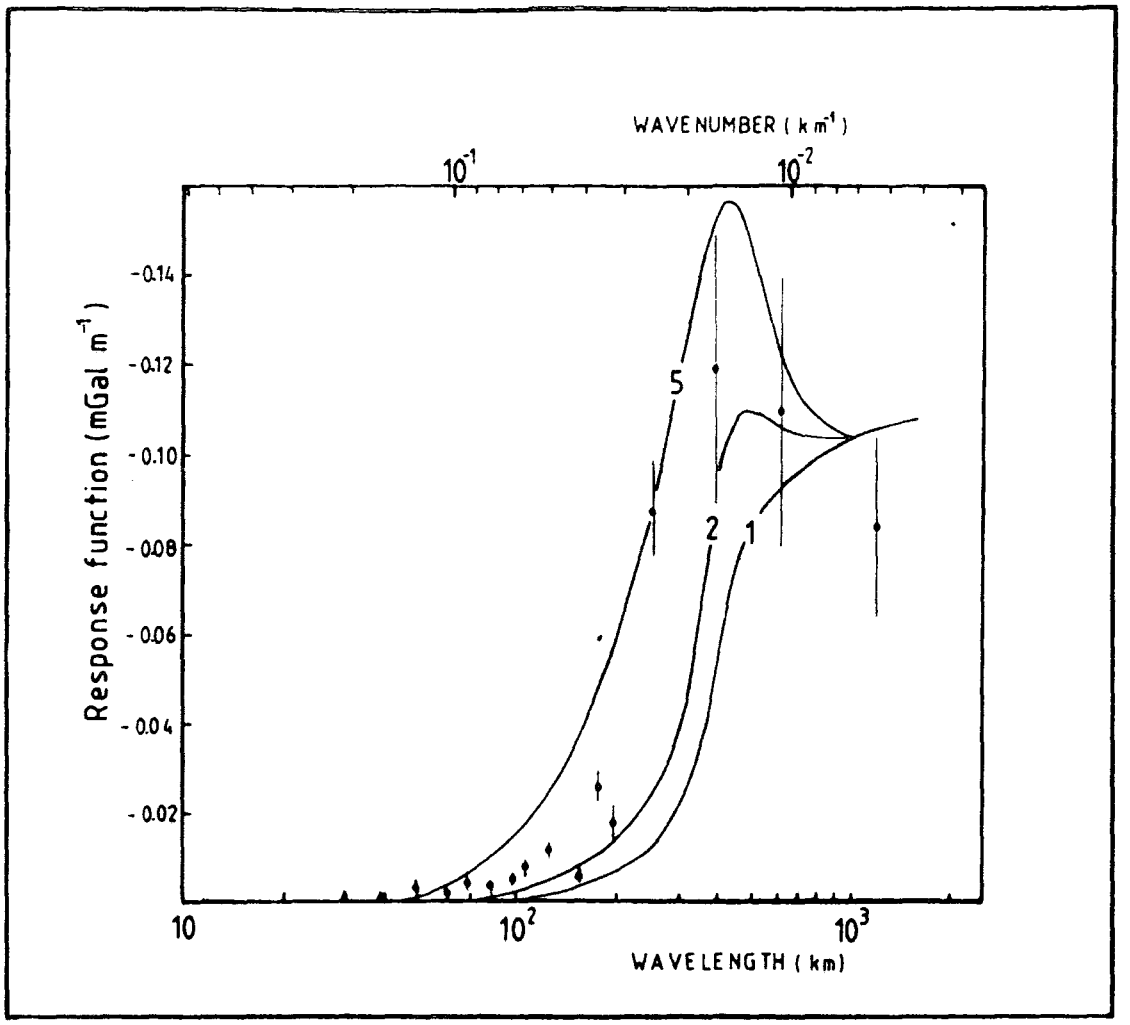

Fig. 3.11 - Isostatic response function predicted by an elastic plate loaded on top and at the base of the crust (crustal thickening). Effective elastic thickness is Te = 40 km. The curves are for different ratios between the surface and surface loads.

hypothesis may also explain the observed isostatic response function of Bahia State, the distribution of loads shown in Fig. 3.12 is analysed.

The observed topography is composed of an elevation created at the time of mountain formation and topography created from within. The density upper crustal density is assumed to be lower than the average density of the crust (ρ_c). Considering a thin elastic plate model, the total deformation w(x) at the base of the crust will be the combined effect of the deformation caused by the low density body within the plate and the deformation caused by the surface load.

The equation of deformation of an elastic plate loaded on top by h(x), in the wavenumber domain is

$$D\,k^4\,W_1(k) + \Delta\rho\,g\,W_1(k) = \rho_0\,g\,H(k)$$

where $\Delta\rho = \rho_m - \rho_c$ = density contrast between mantle and crust

ρ_0 = density of the load

H(k) = Fourier transform of h(x)

and

$$W_1(k) = \frac{\rho_0}{\Delta\rho}\left[1 + (D\,k^4 / \Delta\rho\,g)\right]^{-1} H(k)$$

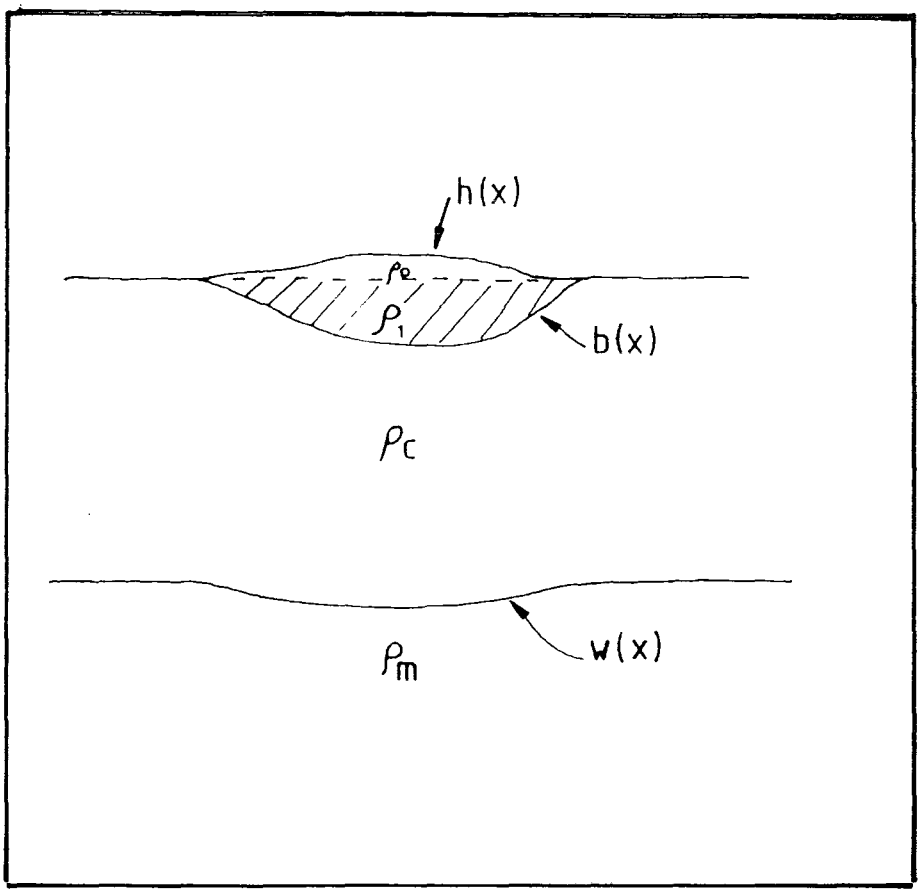

Fig. 3.12 - System of surface and subsurface loads in an elastic plate model. ρ_c= crustal density; ρ_m= mantle density; ρ_1= density of the subsurface load; ρ_o= density of surface load; h(x)=topography of the surface load; b(x) = depth of the subsurface load and w(x) = Moho deflection.

The deformation expected if the plate is loaded from within is

$$D\,k^4\,W_2(k) + \rho_m g\,W_2(k) = -\Delta\rho_1\,g\,B(k)$$

where $\Delta\rho_1 = \rho_c - \rho_1$

$B(k)$ = Fourier transform of $b(x)$, the depth of the low density body.

The deformation $W_2(k)$ is written as

$$W_2(k) = \frac{\Delta\rho_1}{\rho_m}\left[1 + (D\,k^4 / \rho_m g)\right]^{-1} B(k) \qquad (11)$$

The total deformation $W_2(k)$ is obtained by combining these two systems of loading. The gravity effect due to the total deformation at the Moho and the internal negative density contrast is written as

$$G_T(k) = -2\pi G\left\{\Delta\rho_1 B(k) + \Delta\rho \exp(-k\,z_m)\left[\frac{\rho_0}{\Delta\rho}\left(1 + \frac{D\,k^4}{\Delta\rho\,g}\right)^{-1} H(k) - \right.\right.$$

$$\left.\left. - \frac{\Delta\rho_1}{\rho_m}\left(1 + \frac{D\,k^4}{\Delta\rho\,g}\right)^{-1} B(k)\right]\right\} \qquad (12)$$

The first term of $G_T(k)$ is a linear approximation of the gravity effect of the low density body, which is reasonably good since features with wavelengths over 200 km are considered in the present study. Rewritting (12) as

$$G_T(k) = -2\tilde{\pi}\, G\, \Delta\rho_1 \left[1 - \frac{\Delta\rho}{\rho_m}\left(1+\frac{D\,k^4}{\Delta\rho\, g}\right)^{-1} \exp(-k\, z_m)\right] B(k) -$$

$$- 2\tilde{\pi}\, G \exp(-k\, z_m)\ \rho_0 \left(1+\frac{D\,k^4}{\rho_m\, g}\right)^{-1} H(k)$$

and writting the total observed topography as

$$T(k) = H(k) + W_2(k),$$

the isostatic function is estimated as

$$Q = \frac{\langle G_T(k)\ T^*(k)\rangle}{\langle T\ (k)\ T^*(k)\rangle}$$

Substituting B(k) with (11)

$$Q = \overbrace{-2\tilde{\pi}\, G\ \rho_0 \exp(-k\, z_m)\left(1+\frac{D\,k^4}{\Delta\rho\, g}\right)^{-1}}^{Q1} \frac{\langle H\, T^*\rangle}{\langle T\, T^*\rangle} -$$

cont.

$$\underbrace{-2\tilde{\pi}G\left\{\rho_m\left(1+\frac{D\,k^4}{\rho_m\,g}\right)-\Delta\rho\exp(-k\,z_m)\right\}\frac{\langle W\,T^*\rangle}{\langle T\,T^*\rangle}}_{Q2}$$

The term Q1 of this expression for Q is approximately the response function of a plate loaded from the top. However, T(k) contains W(k), the topography which is created from below, as a response of the negative density contrast within the plate. The term Q2 is the response associated with the internal load and its compensation.

The terms $\langle H\,T^*\rangle/\langle T\,T^*\rangle$ and $\langle W_2\,T^*\rangle/\langle T\,T^*\rangle$ are fractions of the total observed topography.

The term Q2 depends on k^4 . Therefore, unless the term

$$r\,(k) = \langle W_2 T^*\rangle/\langle T\,T^*\rangle$$

goes to zero as $k\to\infty$, Q2 will tend to infinity. In practice, B(k), and consequently $W_2(k)$, is band limited. For the present calculation, the spectral representation of the deformation w(x) was tapered to zero for $\lambda<200$ km to avoid the amplification caused by the term which depends on k^4 . Fig. 3.13(a,b,c) show the response function for three effective elastic thicknesses (Te= 20, 40, 80 km). The density contrast between the low

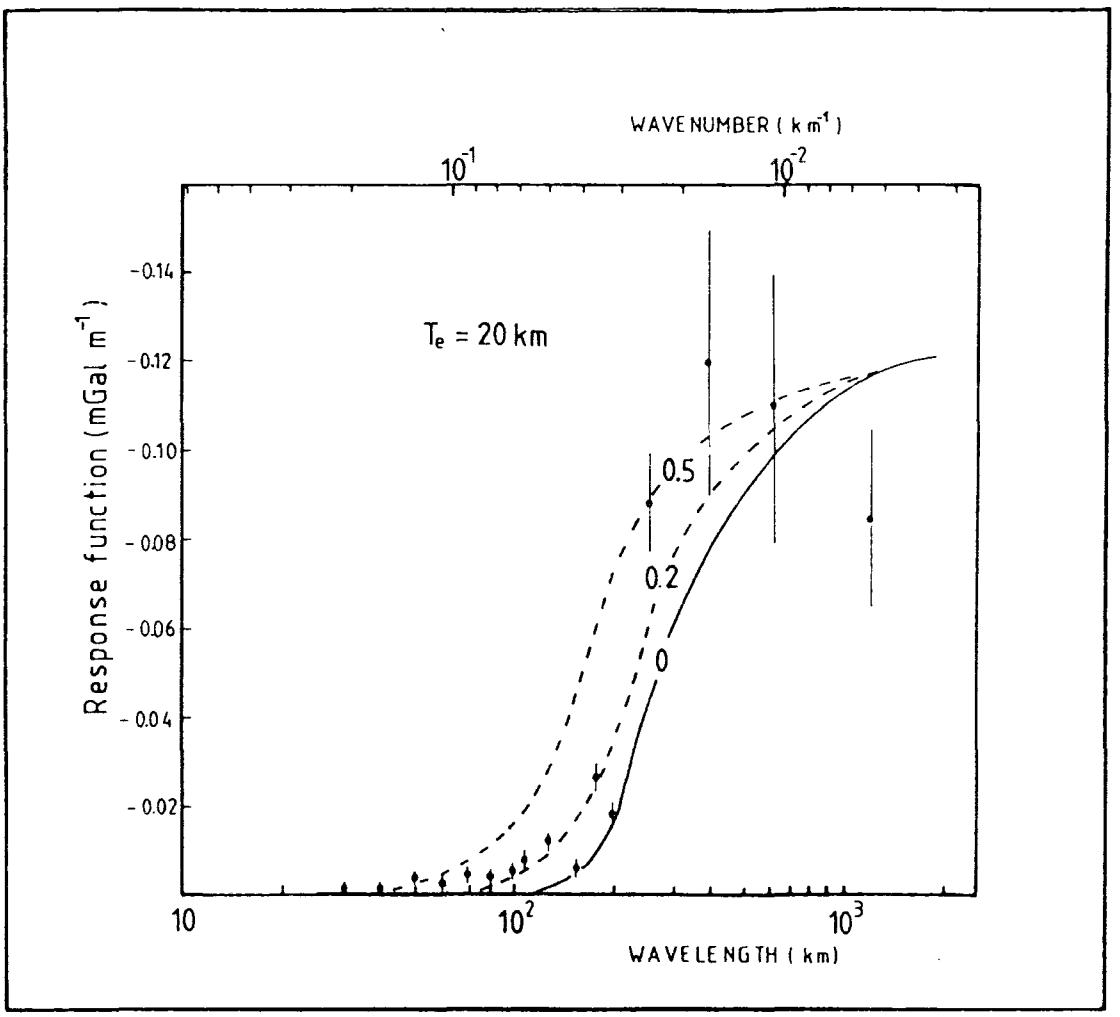

Fig. 3.13a - Isostatic response function predicted by an elastic plate with subsurface load defined as a low density body within the plate. The curves are for different ratios between the topography created from within and the total observed topography. Effective elastic thickness Te=20 km.

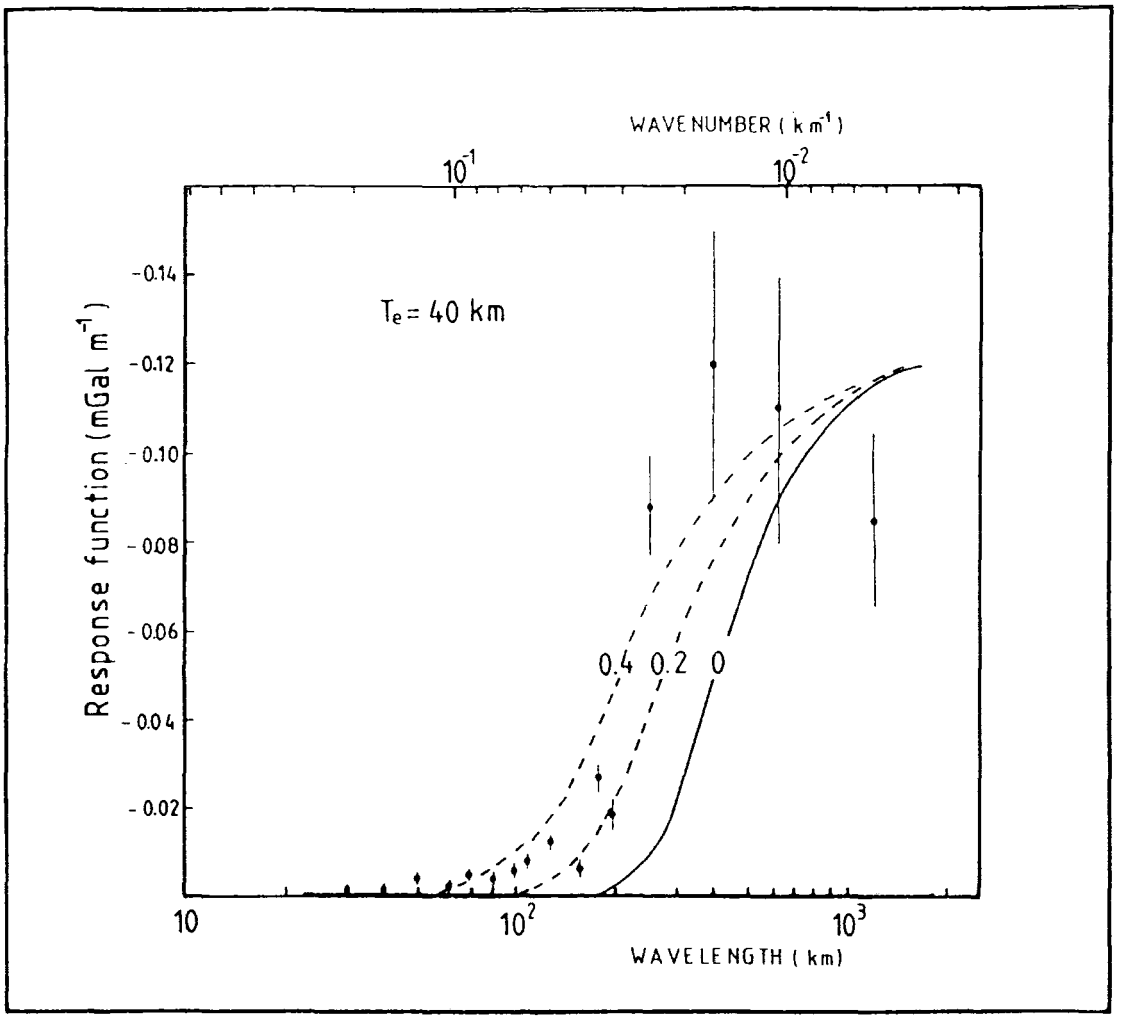

Fig. 3.13b - Idem Fig. 3.13a for Te=40 km.

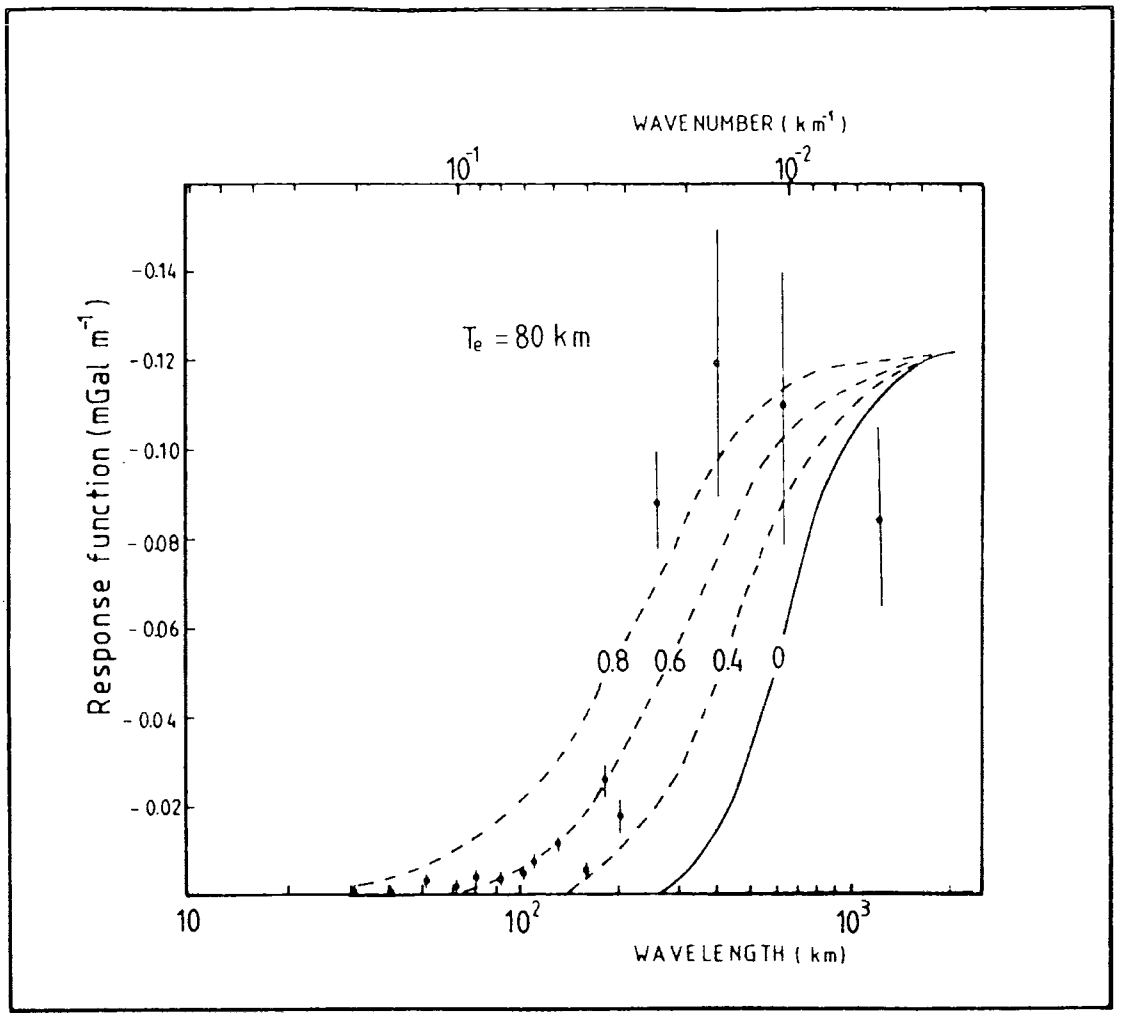

Fig. 3.13c - Idem Fig. 3.13a for Te=80 km.

density body and the crust was assumed as -0.1 g cm^{-3} . The curves are given for different ratio r between the topography produced from below and the total observed topography at the surface.

There is a better agreement between the observed response function and the response function predicted by the new model, for a 30-40 km thick elastic plate in which 40% of the observed topography is produced from within the plate (Fig. 3.13a). For an elastic plate 20 km thick, the ratio $W_2T^*/ T T^*$ decreases to 0.2 or 20% (Fig. 3.13b). This near surface source of "overcompensation" can only explain the observed isostatic response function at wavelength shorter than 300 km.

Considering that the average altitude of the Espinhaço Fold System is about 800 metres above sea level, the topography created from within, for a 40 km elastic plate, is about 320 metres. A thickness of 10 km of low density rocks (density contrast -0.01 g cm^{-3}) within the uppermost part of the crust is necessary to produce such uplift. This figure is obtained by using the expression (11) and such thickness of low density rocks is commonly associated with granitic batholiths. However, a 20 km thick elastic plate with r=0.2 may also explain the observed response function as well as a 40 km thick elastic plate. In this case the minimum thickness of the internal load required to produce 160 metres of uplift from within is about 5 km. This particular model ascribes a relatively low flexural

rigidity to an old Proterozoic region. An apparent low flexural rigidity can be obtained in ancient cratonic regions if enough stress relaxation occurred after the formation of the mountains. Granite intrusion and faulting could be part of such process. Radiometric dates (Tavora et al., 1967) suggest a thermal event, possibly associated with granite intrusion and faulting in the late Proterozoic (900-500 Ma), therefore after the Espinhaço orogeny which defined the main topographic features in the region. Lastly, Fig. 3.13c shows the results for an elastic plate with Te=80 km. In this case, a minimum of 60% of topography created from within (~480 metres) is required to explain the observed response function. A minimum thickness of 17 km of low density rocks in the upper crust is necessary to produce such uplift.

This near surface low density subsurface load does not predict the peak at λ = 400 km.

3.4 Discussion

The results of the application of the response function technique to the gravity and topographic data of the northern São Francisco craton firstly show a low isostatic response and an equally low coherency between topography and Bouguer anomaly at wavelengths shorter than 300 km. These results suggest a

strong lithosphere which supports small topographic features without significant deformation.

An apparent "overcompensation" at λ = 400 km in the observed response function can only be interpreted, in the context of the elastic plate rheology, if subsurface loads are taken into account. A comparison between the observed response function with those predicted by an elastic plate with surface load and compensation at the Moho shows no satisfactory agreement regardless of the flexural rigidity. This confirms Forsyth's suggestion that low flexural rigidities obtained for continental lithosphere, using the isostatic response function technique, may have resulted from dismissing sources of compensation other than at the Moho and by assuming that the observed topography is the only load acting on the plate.

Two subsurface loads which may explain the isostatic response function of Bahia State were considered. Firstly, a low density subsurface load at the base of the crust which is represented by a thickening of the crust beneath the Espinhaco Fold System. This subsurface load together with a partial surface load, predicts equally well the observed response function both at short and long wavelengths, and in particular the apparent "overcompensation" at λ = 400 km.

The second subsurface load considered is based on the geological and gravity evidence (see Chapter 4) that the

uppermost part of the crust in the Espinhaço Fold System is composed of 5 to 10 km of low density rocks, mainly granites, subordinate acid volcanics and low-grade metasediments. Therefore, it is very likely that a substantial fraction of the observed topography is compensated at shallow depths. However, this second subsurface load alone does not predict the peak in the response function at $\lambda = 400$ km. It is thus possible that two types of subsurface loads, a slight thickening of the crust and near surface mass deficiency, may be present in the centre of the northern São Francisco craton. Both subsurface loads contribute to create the topography as a flexural response. This appears to be a common situation in continental areas where high topographic terrains are associated with low density granitic intrusions. Combining these two subsurface loads, an elastic plate with effective elastic thickeness as high as 40 km, may explain the way the topography is compensated (or created) in this old cratonic area.

Evidence of an overprint of late thermal events and normal faulting suggests that stress relaxation could have occurred after the emplacement of the topographic masses and crustal deformation. Erosional processes have not been taken into account in the simple elastic plate rheology considered in this study. These complexities together with the lack of information on the relative importance of the two subsurface loads required to explain the observed isostatic response function only allow us to define a lower bound of the effective elastic thickness to be situated between 20 and 40 km.

CHAPTER 4

Gravity Study of the Paramirim Complex Granite

A large negative Bouguer anomaly, trending NNW, is found at the centre of Bahia State (Fig. 2.4). This anomaly covers an area of approximately 60 km (east-west) by 200 km (north-south). A detailed Bouguer anomaly map of the area concerned is presented in Fig. 4.1a. This same map is presented in Fig. 4.1b together with the same scale geological map. The amplitude of the anomaly is about -40 to -50 mGal and its main axis parallels the Espinhaço fold belt. The anomaly has a steep gradient reaching at least 2.5 mGal/km. The minimum of the anomaly lies along the western side of the Paramirim complex bordering the metasediments of the Espinhaço fold belt. Near the latitude 13.5° S, the minimum of the anomaly is shifted towards the centre of the Paramirim complex. To the north the anomaly terminates at Oliveira dos Brejinhos city. The south end has a gentle gradient and it extends southwards to Lagoa Real city in the Gavião block. The eastern limit lies at the contact between the Paramirim complex and the Diamantina tableland metasediments. On this side, near Ibipitanga city, the occurrence of a positive anomaly locally disturbs the NNW trending gradient. The western limit coincides with a major NNW oriented normal fault which extends continuously along the entire western side of the Espinhaço fold belt.

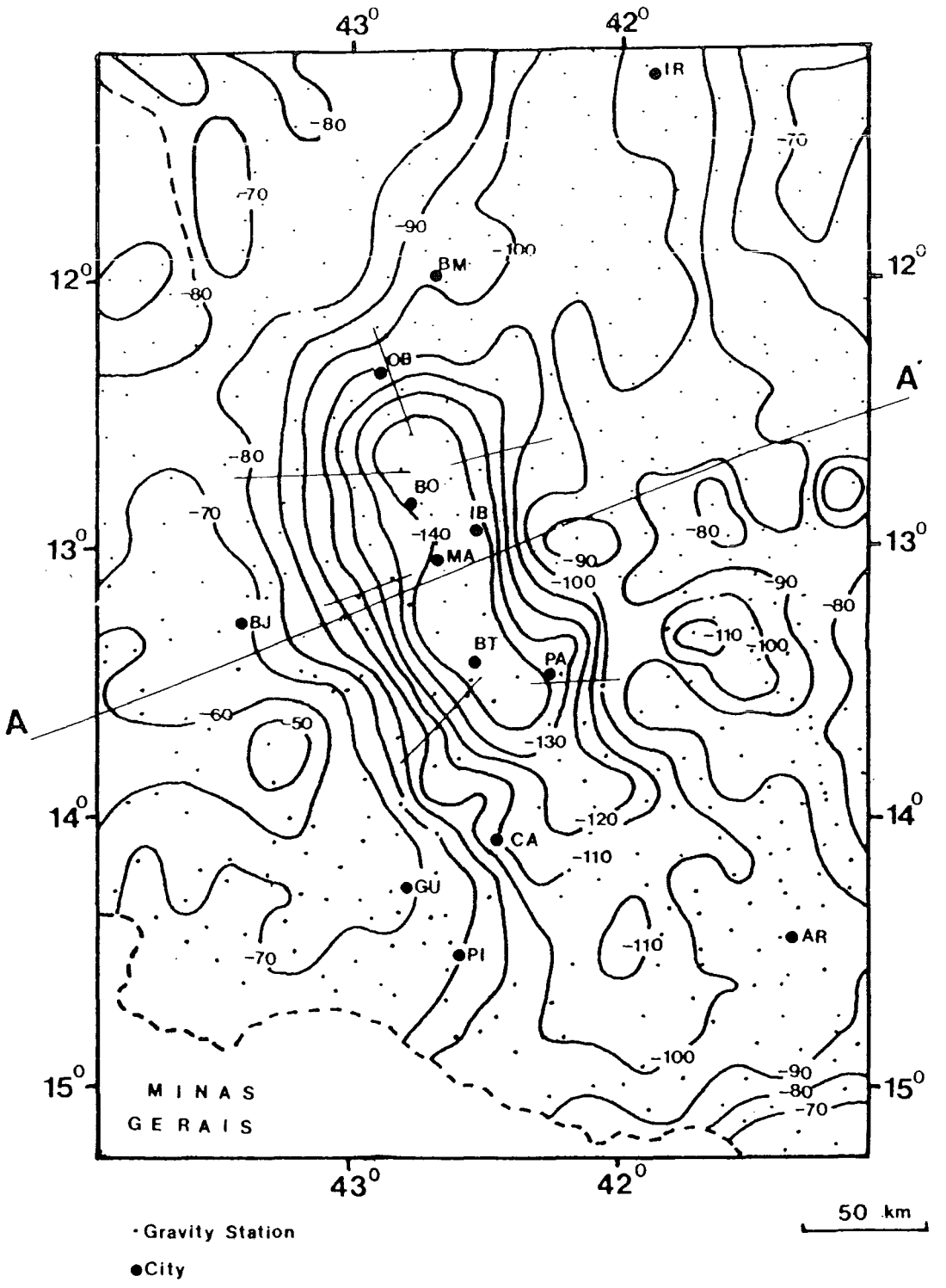

Fig. 4.1a- Espinhaço Fold System Bouguer anomaly map.
Cities are: OB - Oliveira dos Brejinhos
BO - Boquira; IB - Ibipitanga; MA - Macaúbas ; BT - Botuporã;
PA - Paramirim; JU - Jussiape; AB - Abaira; CA - Caetité;
LA - Lagoa Real; AR - Aracatu; GU - Guanambi, PI - Pindaí;
BJ - B. Jesus da Lapa; IR - Irecê; BM - Brotas de Macaubas.
A - A' is a gravity profile to be interpreted.
Contour interval 10 mGal; IGSN-71 ; IGF-1967.

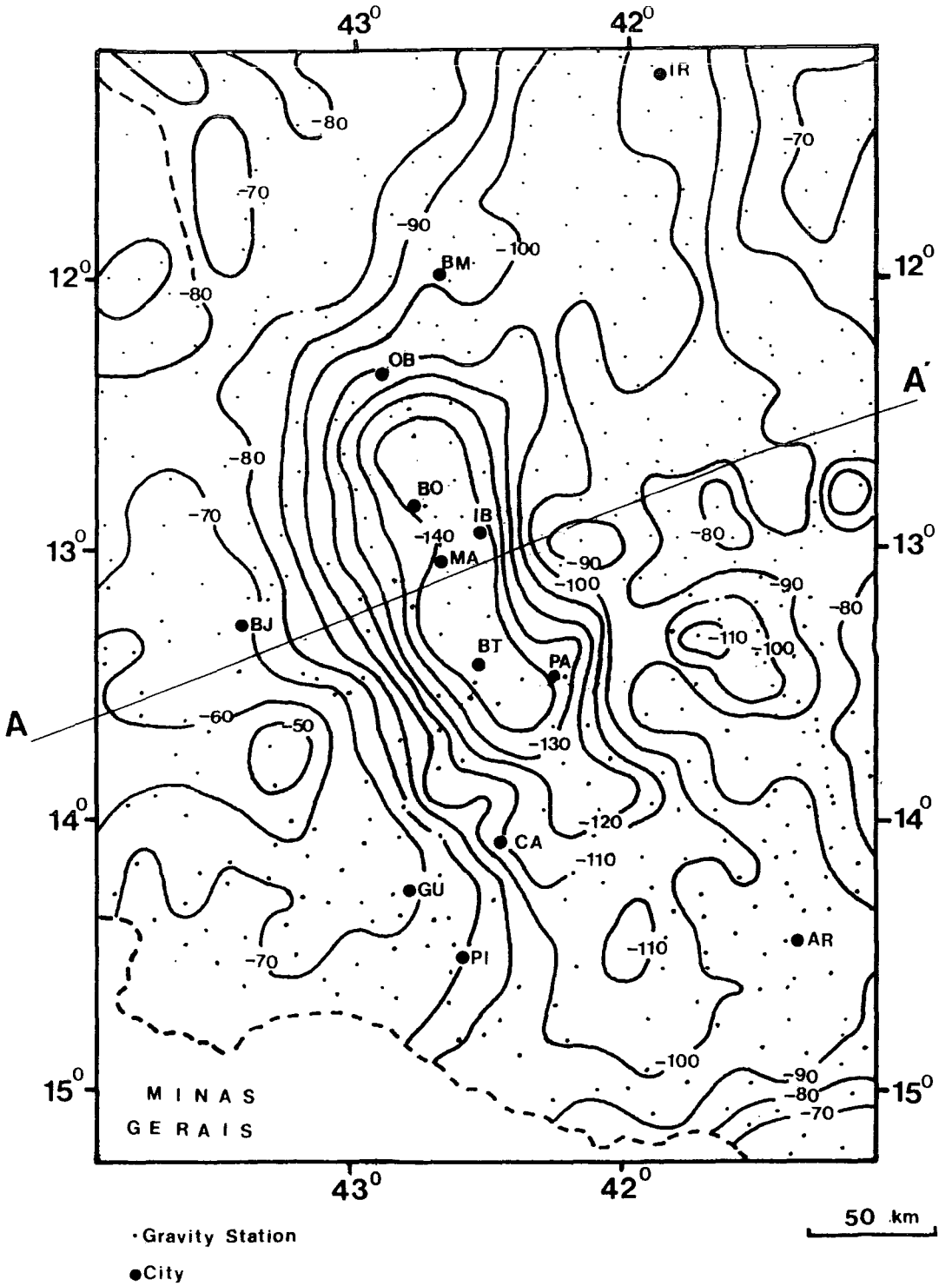

Fig. 4.1b- Bouguer and geological maps of the Espinhaço Fold System.

4.1 Geology of the Area

4.1.1 The Espinhaço Fold System and its sub-regions

A brief outline of the geology of the Espinhaço Fold System is presented in Chapter 2, section 2.2.3. A geological map of this region is shown in Fig. 4.2, which has been modified from the 1:1,000,000 scale map of Bahia State (Inda and Barbosa, 1978). The Espinhaço Fold System is subdivided into six sub-regions. The Archean sub-regions include the Paramirim, Gavião and Guanambi complexes and the Lagoa Real region. These terrains were later affected by Lower and Middle Proterozoic events, mostly igneous intrusion. In the Middle Proterozoic, intracratonic tectonic events formed the Espinhaço fold belt and the Diamantina tableland.

The basement of the Gavião block is composed of Archean gneisses, migmatites and plutonic rocks (granodiorites, monzonites and syenites). Volcanic-sedimentary complexes (schists, quartzites and iron banded quartzites) are extensively found in this region which is regarded as part of a greenstone belt (Mascarenhas, 1973). High grade metamorphism characterizes the migmatites and gneisses. The region was affected by the Transamazonian orogenic cycle (1.8-2.2 Ga). The structural pattern of the Gavião block is very complex, with overprints of several deformational phases. The youngest age so far observed is Lower Proterozoic suggesting that this region remained isolated

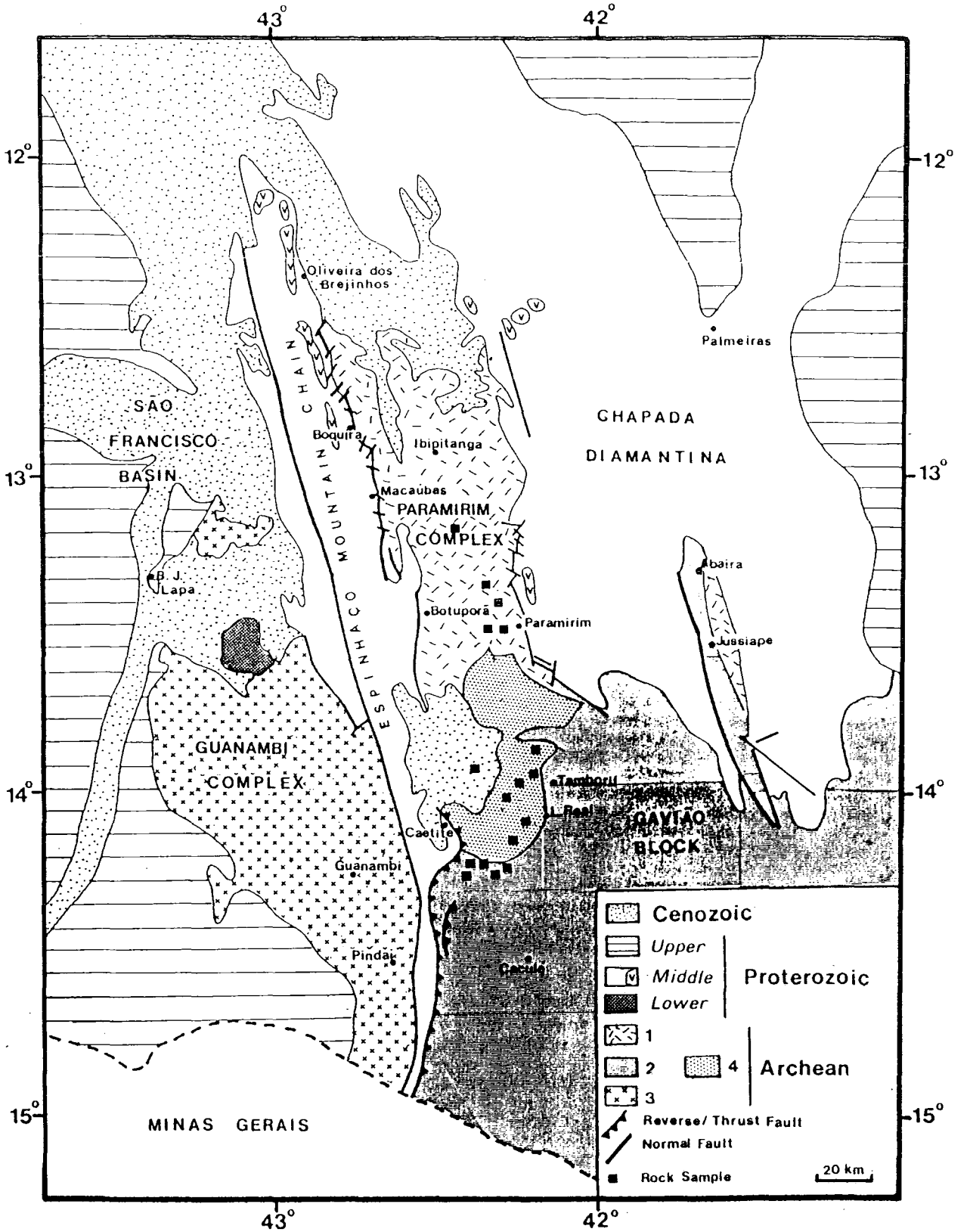

Fig. 4.2 - Geological map of the Espinhaço Fold System based on Inda & Barbosa (1978).
Archean : 1- Paramirim complex
2- Gavião block
3- Guanambi and Santa Izabel complexes
4- Lagoa Real region
Lower Proterozoic - syenitic intrusion
Middle Proterozoic - Espinhaço Supergroup
Upper Proterozoic - São Francisco Supergroup
Cenozoic - clastic sediments

from the later tectonic events which gave rise to the Espinhaço Fold System.

The same age pattern is observed in the Guanambi complex. This area of exposed Archean basement is situated to the west of the Espinhaço fold belt (Fig. 4.2) and it is essentially composed of gneisses and migmatites of granulite and amphibolite facies (Barbosa and Costa, 1973). Migmatites of intermediate composition are the dominant lithology and these display a complex structural pattern. The last major metamorphic and tectonic event in this region occurred in the Archean at 2.6 Ga (Cordani, 1973). In the Lower Proterozoic (2.0 Ma), a large circular syenitic body intruded the Guanambi complex southeast of the Bom Jesus da Lapa city (Fig. 4.2).

Between the Espinhaço fold belt and the Diamantina tableland, there is a zone of Archean basement, the Paramirim complex. According to Jardim de Sá et al. (1976a), the Paramirim complex is composed of gneisses and migmatites of granodioritic and tonalitic composition which are dated at 2.6 Ga. The metamorphism of high amphibolite facies is also Archean. Intrusive granitic bodies are very common. Potassic granites are subordinate in the complex. Exceptions are the isotropic remobilized K-rich granites which outcrop to the west of the Paramirim city.

The structural pattern of the Paramirim complex rocks show an apparent overprint of at least two deformational phases. The

older S-plane is shown in the folded banded gneisses and migmatites. The isoclinal folds do not present any dominant orientation. The younger (Middle Proterozoic?) S-plane, which trends NW, is extensively observed in the complex. Only the K-rich granites south of the latitude 13.5°S were not affected by the deformation.

Between the southern Paramirim complex and the northwestern border of the Gavião block, another segment of Archean terrain is observed. This region is identified as the Lagoa Real region in Fig. 4.2. The basement of this complex is composed of plagioclase and microcline gneisses, with widespread inclusion of albitite veins and intrusion of granitic bodies. The occurrence of uranium mineralization is associated with veins of albitite.

A thick accumulation of sediments took place on both sides of the Paramirim complex, during the Espinhaço orogenic cycle which lasted from 1.7 to 1.3 Ga (Jardim de Sá, 1981 and listed references). Deformation and metamorphism of the sediments occurred at the end of this cycle at about 1.3-1.2 Ga (Jardim de Sá et al., 1976a). The metasediments of the Espinhaço fold belt were strongly folded, with westward vergence. Whereas the metasediments in the western border of the Diamantina tableland are less folded and they present an eastward vergence. The deformation and the degree of metamorphism, within the western Diamantina tableland, decreases from west to east. As described in Chapter 2, the Middle Proterozoic upper sequence (Chapada

Diamantina group) was deposited in the northern part of the tableland, above the latitude 12.5° S. The sediments of this sequence present no metamorphism nor deformation. New tectonism followed the end of the Espinhaço orogeny, with normal faulting in the northern part of the Espinhaço fold belt.

The Espinhaço Fold System remained uplifted during the subsequent Upper Proterozoic sedimentation which occurred in the São Francisco basin to the west and in the Lençois basin to the east. A thin blanket of Cenozoic sedimentation occurs to the north of the Espinhaço Fold System. The thickness does not exceed 50 metres.

4.1.2 The acid volcanism and granitic intrusion.

Acid volcanics are observed at the eastern border of the Espinhaço fold belt and at the western side of the Diamantina tableland. They constitute the basal sequence of the Diamantina tableland. In the Espinhaço fold belt, the volcanics are found at the contact between the metasediments and the Paramirim complex. Granites are described as widespread in the southern Paramirim complex.

The origin of both the acid volcanism in the Espinhaço fold belt/Diamantina tableland and the granitic intrusion in the Paramirim complex have been discussed by McReath et al. (1981) and Jardim de Sa (1981). The composition of the major elements in

these volcanics is shown in Table 4.1.

In the Diamantina tableland, the acid volcanics belong to the Rio dos Remedios group, which were extruded during the initial stages of the Middle Proterozoic sedimentation (1.8-1.7 Ga). This group is found along the western border of the Diamantina tableland (Fig. 2.13). It extends for about 150 km and the thickness reachs up to 2.5 km in some places. McReath et al. (1981) describe the sequence as composed of dacites and rhyodacites of tholeiitic affinity. These rocks were metamorphosed (greenschist facies) and deformed at the end of the Espinhaço orogeny (1.3 Ga).

The volcanics of the Espinhaço fold belt are rhyolites and trachytes, with thickness ranging between 100 and 350 metres. They are possibly post-tectonic, according to K/Ar dates (1100 - 850 Ma) obtained by Tavora et al. (1967). Metamorphism has not been observed in these rocks.

The granites which intrude the Paramirim complex are slightly more acid than the volcanics, as shown in Table 4.1. Using the Rb/Sr method Jardim de Sá et al. (1976b)have dated some granites from the southern Paramirim complex at 1530 ± 33 Ma and 1087 ± 27 Ma. However, Tavora et al. (1967) have also dated two non-foliated granites from the basement adjacent to the Espinhaço fold belt at the latitude 12^{o} 45' S and they obtained K/Ar ages which range from 815 to 400 Ma. These young ages have been

	Acid volcanics		Monzonitic granites
	Diamantina tableland	Espinhaco fold belt	Paramirim complex
SiO_2	69.41	67.53	72.09
TiO_2	0.52	0.49	0.25
Al_2O_3	12.92	13.48	13.26
Fe_2O_3	5.03	5.76	2.82
MnO	0.14	0.14	0.14
MgO	0.67	0.36	0.51
CaO	2.06	0.09	1.23
Na_2O	3.46	3.88	3.32
K_2O	4.74	7.38	5.59
P_2O_5	0.19	0.06	0.03

Table 4.1 - Average abundance of major elements in the acid volcanics of the Espinhaço fold belt, western Diamantina tableland and granites of the Paramirim complex. From McReath et al. (1981).

interpreted as late thermal events which affected this region during the Brasiliano orogenic cycle (900 - 500 Ma).

The number of radiometric dates and the geological understanding of this region are still very poor. Jardim de Sá (1981) suggested that the remobilization of the Paramirim complex with granitic intrusion was synchronous with the acid volcanism in the western Diamantina tableland, possibly derived from crustal anatexis. This volcanism may have occurred at the early stages of the Espinhaço orogenic cycle. Metamorphism and deformation of the volcanics and metasediments are both dated at 1.3 Ga. The non-metamorphosed acid volcanics, which occur in the northern Espinhaço fold belt, are possibly post-tectonic.

4.2 Aeromagnetic Data

An aeromagnetic survey was carried out by the Brazilian Mineral Production Department (DNPM/CPRM - Brazil) and it covers almost the whole Espinhaço Fold System. [Fig. 4.3a] Magnetic anomaly of the same areal extent as the gravity anomaly is not observed. However, short wavelength magnetic anomalies occur over the Paramirim complex and are more conspicuously developed near its western boundary close to Espinhaço mountain chain, thus coinciding with the position of the minimum of the gravity anomaly. According to Jardim de Sa' *et al.* (1976b), petrographic evidence such as epidote and feldspar recrystalization are indicative of more

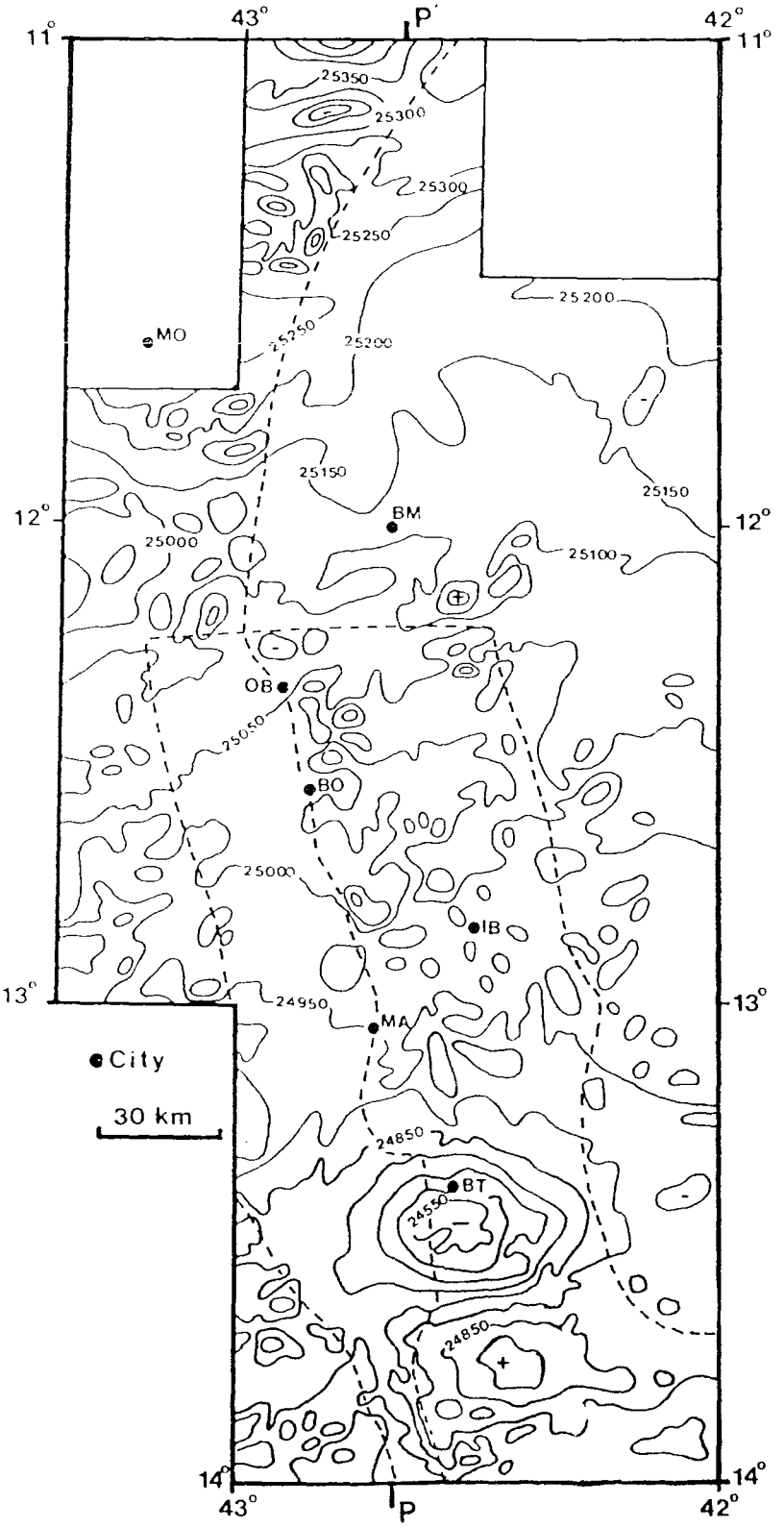

Fig. 4.3a - Aeromagnetic map of the Espinhaço Fold System.
Data source DNPM/Brazil.
Total component of the geomagnetic field.
Contour interval 50 nT.
The dashed line indicates the contact between the metasediments and the crystalline basement.
Cities as named in Fig. 4.1a and P-P' is the profile presented in Fig. 4.4

intense remobilization of the basement at the eastern border of the Espinhaço fold belt. Fig. 4.3b presents the aeromagnetic and geological maps on the same scale.

A large magnetic anomaly, to the south of he Botuporã city, is also situated along the Paramirim magnetically disturbed region. This magnetic anomaly has reversed polarity (negative in the north and positive in the south), which is opposite to the polarity of an anomaly induced over a magnetic body in the southern hemisphere. The minimum is about -300 nT and the maximum is 150 nT. The anomaly is situated at the region where large and circular granitic bodies were reported by Jardim de Sá et al. (1976b). It extends southwards and terminates at the contact between the granites and the Gavião block. The negative magnetic anomaly is situated at the southern end of the large negative gravity anomaly.

The aeromagnetic data were found useful in mapping the basement of this area, in particular, between 11° S and 12° 30' S, where the basement is covered by the Phanerozoic sediments and the Chapada Diamantina group metasediments. Over the Paramirim and Guanambi migmatitic terrains, the magnetic field is highly disturbed by short wavelength anomalies reflecting a heterogenous basement. Over the Espinhaço fold belt and Diamantina tableland the short wavelength magnetic anomalies are almost absent due to a deeper magnetic basement. The northern border of the Paramirim complex, as indicated by the aeromagnetic map, is situated to the north of

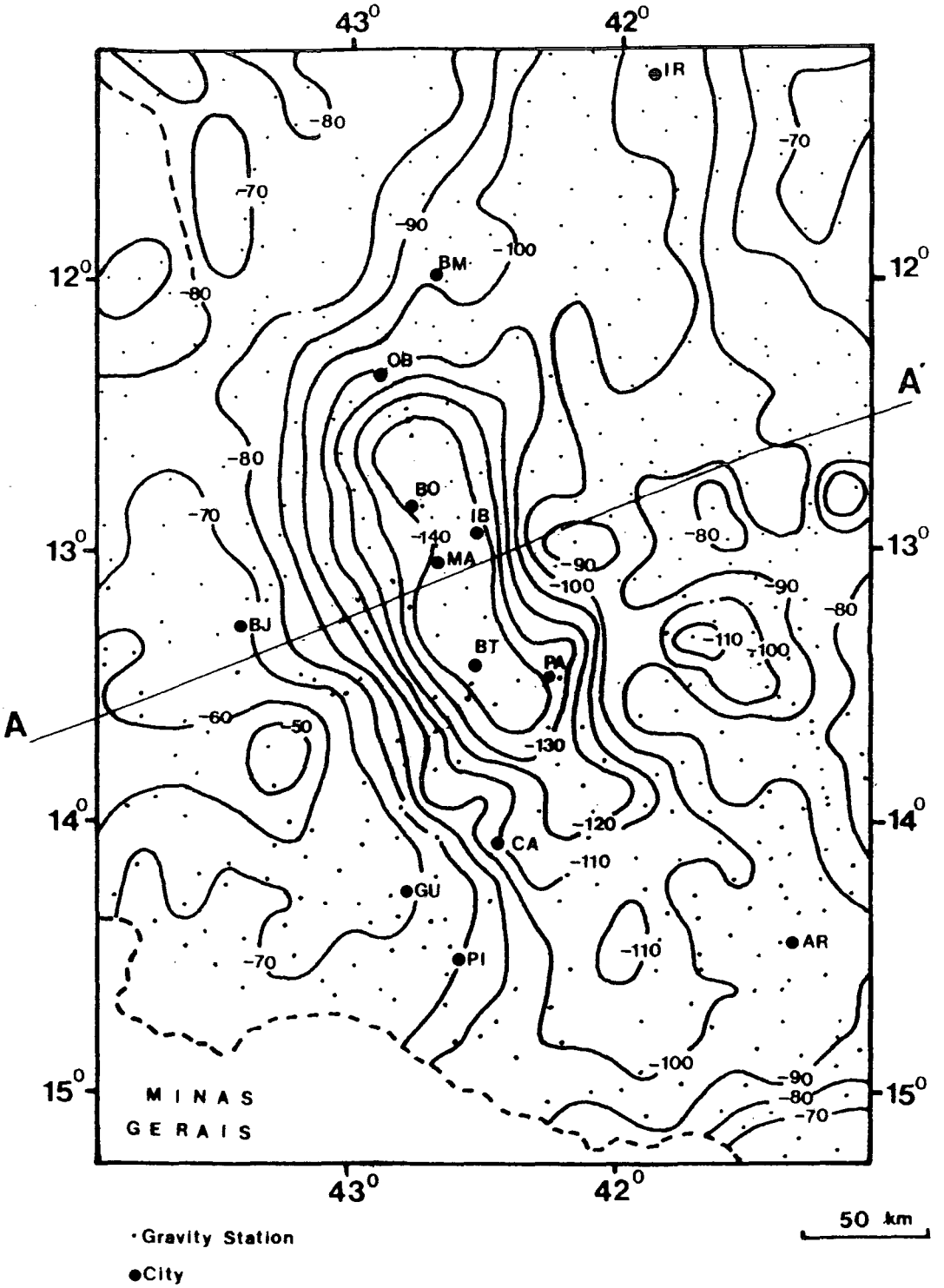

Fig. 4.3b - Bouguer and aeromagnetic maps of the Espinhaço Fold System.

Oliveira dos Brejinhos city between 42° 30' W and 43°W, where the short wavelength magnetic anomalies terminates (Fig. 4.4). Also at this latitude, the linear gravity gradient, which parallels the Espinhaço fold belt, swings to a NNE direction and coincides with a sequence of short wavelength magnetic anomalies which are ascribed to the contact of the basement to the west with the metasediments of the Espinhaço Supergroup to the east. Therefore, the northern limit of the large negative gravity anomaly coincides with the northern border of the Paramirim complex.

4.3 Density Data

Density measurements were carried out on 52 rock samples which were collected for radiometric dating (U.G.Cordani, personal communication). Their sites are shown in the Fig. 4.2. The samples are separated into two groups according to their geographical distribution and the listing of the density mesurements are presented in Table 4.2. The method of density measurement is described in Appendix A. The first group of samples is from the centre of the Paramirim complex. It is composed of granitic migmatites and gneisses which yielded an average density of 2.64 g cm^{-3} and two granites in the same area yielded a density of 2.60 g cm^{-3}. The 16 samples of the second group were taken from the Archean region to the south of the Paramirim complex, between Caetite and Lagoa Real cities. Homogeneous migmatites of granodioritic composition have a density

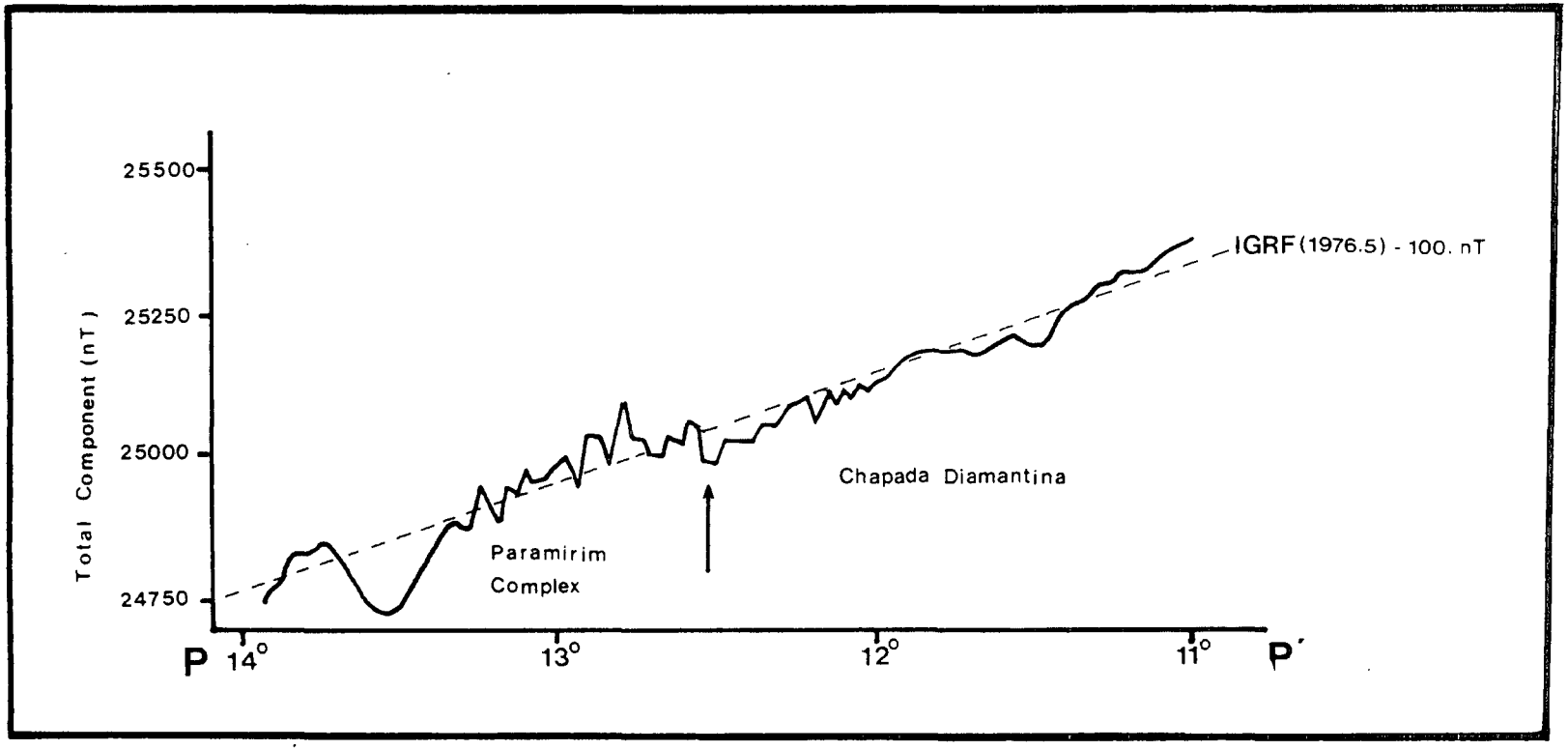

Fig. 4.4 - Total component of the geomagnetic field along P-P' profile. The arrow indicates the northern border of the Paramirim complex which is covered by the Middle Proterozoic and Cenozoic sediments. The dashed line is the International Geomagnetic Reference Field - 1965 (Barraclough et al.,1978) calculated for 1976.5, altitude 135 metres. Note that 100 nT has to be subtracted from the values predicted by the IGRF model in order to obtain the "minimum least-square" magnetic residual field.

South of Paramirim Valley (Lagoa Real city)

Rock no.	Density ($g\ cm^{-3}$)	Rock type
LR-11E	2.63	migmatite
LR-11D	2.63	migmatite
LR-11B	2.61	migmatite
LR-11A	2.64	migmatite
LR-11C	2.60	migmatite
LR- 1	2.69	granite
LR- 2	2.67	microcline augen gneiss
LR- 3B	2.79	plagioclase gneiss
LR- 5C	2.69	microcline augen gneiss
LR-10A	2.64	granite
LR-10F	2.68	granite
LR-10E	2.68	granite
LR-12A	2.65	migmatite
LR-12F	2.78	migmatite
LR-12C	2.62	migmatite
LR-12B	2.65	migmatite
LR-20B	2.70	gneiss
LR-20D	2.64	gneiss
LR-20F	2.63	gneiss
LR-20E	2.63	gneiss
LR- 22	2.64	migmatite
LR- 9	2.69	granulite
LR-18C	2.59	granite
LR-13G	2.71	microcline augen gneiss
LR-13D	2.74	gneiss
LR-13E	2.70	gneiss
LR-13A	2.80	gneiss
LR-16B	2.64	granite
LR-17B	2.65	granite
LR-17A	2.64	granite
SS-111	2.63	granite
GA- 9	2.80	granulite
AR- 35	2.72	gneiss
PC-421	2.62	granite
GA-393	2.64	migmatite

Rocks from Paramirim Valley

Rock no.	density ($g\ cm^{-3}$)	rock type
JM/BA/35A	2.66	granite gneiss
/35B	2.65	granite gneiss
/35C	2.65	granite gneiss
/35D	2.65	granite gneiss
/35E	2.63	granite gneiss
/36	2.80	gneiss
/37	2.78	gneiss
/38	2.59	gneiss
/39	2.64	migmatite
/40A	2.70	granite
/40B	2.59	granite
/40C	2.61	granite
/41	2.65	migmatite
/43A	2.95	diorite
/53A	2.73	gneiss
/171A	2.62	granite

Table 4.2 - Results of density measurements on crystalline rocks of the Paramirim complex and surrounding regions.

of 2.65 g cm^{-3} and the microcline augen-gneisses, plagioclase gneisses and granulites yielded densities ranging from 2.67 to 2.75 g cm^{-3}. Histograms of the density measurements listed in Table 4.2 are presented in Fig. 4.5. A gradual increase in density towards the Gavião block occurs as the lithology becomes dominated by high grade migmatites and rocks of tonalitic composition. Notwithstanding the limited number of samples considered in the present work, it can be stated that the Paramirim complex has lower average density (d=2.69 g cm^{-3}) than the high grade metamorphic terrains of the Eastern Bahia Shield, which is characterized by a density of 2.73 g cm^{-3} (see Fig. 2.2). The lack of a detailed density sampling across the region where the negative anomaly is observed limits the inference of the precise source of the anomaly. Neither density measurement on the metasediments nor on the acid volcanics are available.

4.4 Gravity Interpretation.

Geological and geochemical evidence together with aeromagnetic data and density measurements suggest that the large negative gravity anomaly is probably caused by low density granites. Other possible sources of this high amplitude negative anomaly are firstly discussed because the evidence presented in the previous sections does not rule out the possibility that the anomaly is caused either by the Espinhaço fold belt sediments or by a local thickening of the crust.

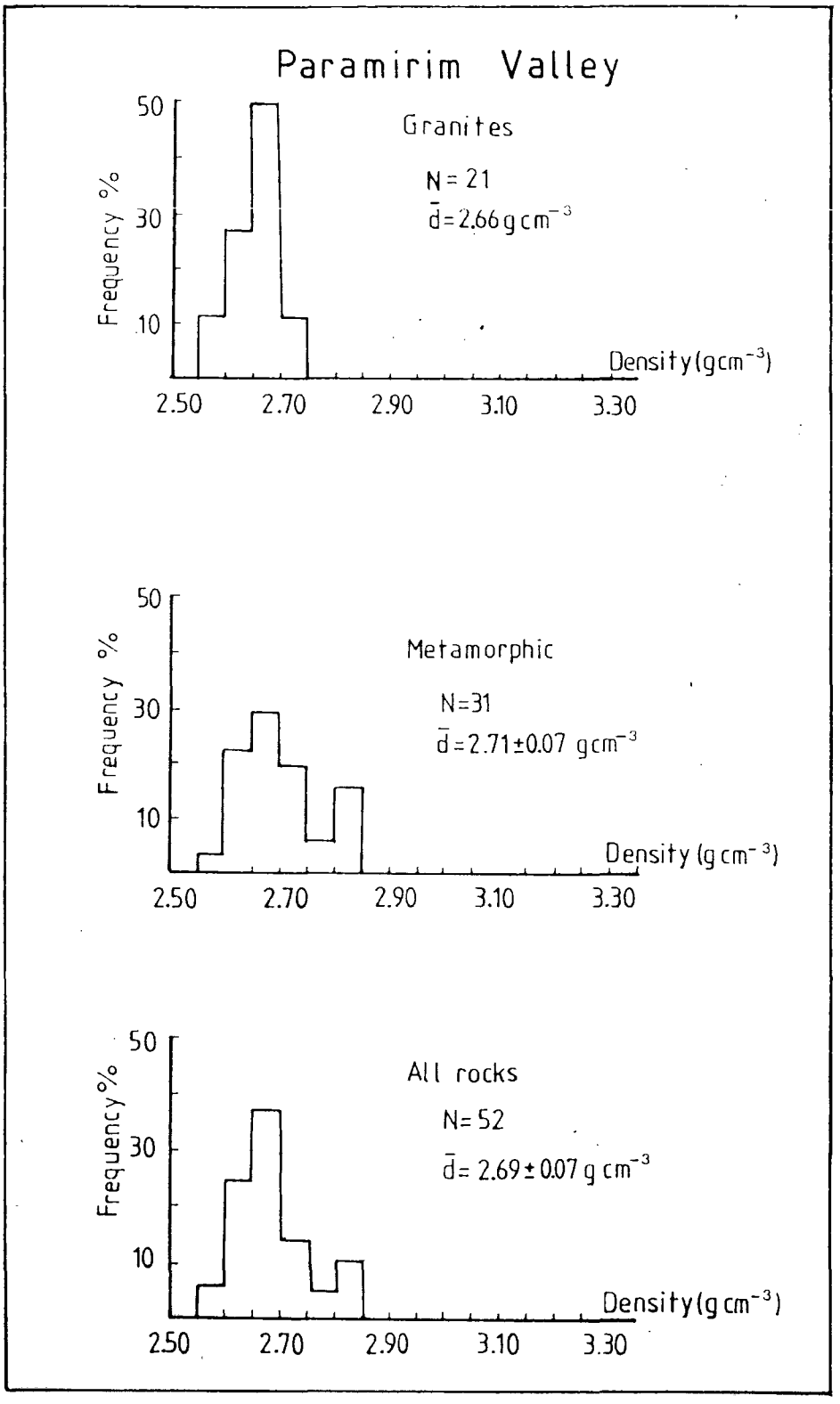

Fig. 4.5 - Histograms of density measurements on Paramirim complex crystalline rocks.

4.4.1 The source of the negative gravity anomaly

The first possible source, the Espinhaço fold belt metasediments, can be questioned on the grounds that the minimum of the anomaly occurs over the Paramirim region to the east of the sediments. This is clearly seem by comparing the Bouguer anomaly map with the geological one (Fig. 4.1b). Although no density measurements are available, it is also unlikely that the density of the highly folded Espinhaço metasediments is much lower than the average density of the basement rocks. Moreover, if the metasediments were the main source of the large negative anomaly, an equivalent gravity signature would be expected over the Diamantina tableland, where rocks of the same age are less strongly folded and less metamorphosed. Only small amplitude (<20 mGal) negative gravity anomalies are observed over the Diamantina tableland.

Another possible source of the large negative anomaly at deeper levels, would be a local thickening of the crust. Such a root could have been associated with the compressional events (Espinhaço orogeny) which occurred during the Middle Proterozoic. A deep seated source can be ruled out by using the gravity maximum depth formula proposed by Bott and Smith (1958). For an approximately two dimensional body, the maximum possible depth of the source of the anomaly is given by

$$h < 0.65 \frac{|g_{max}|}{|\partial g/\partial x|_{max}}$$

where g_{max} is the maximum amplitude of the anomaly and $\left|\partial g/\partial x\right|_{max}$ is the maximum gradient of the anomaly.

The steepest gradient of the anomaly is 2.5 mGal km^{-1} and it occurs over the centre of the Paramirim complex, in the direction of the Diamantina tableland. The maximum amplitude of the anomaly is about 50 mGal. With these figures, $z = 13$ km is obtained. The same estimate was carried out for other segments of the local anomaly (see Fig. 4.1) and an average maximum depth of 20 km was obtained. This rules out an origin of the anomaly at the base of the crust or near it. The source of the large negative gravity anomaly must therefore lie within the upper crust. The only obvious source of such a large negative gravity anomaly are near surface granites of lower density than the country rocks. Similar gravity signature is associated with granitic masses which are not conspicously exposed on the surface such as the Devonian Weardale and Wensleydale granites of NE England (Bott, 1967) and the Devon and Cornwall granites (Bott et al., 1958).

Having established the source of the gravity anomaly, the next step is to estimate the dimensions of the anomalous body. As discussed by Bott and Smithson (1967), useful quantitative information on the deep structure of granitic bodies can be inferred from gravity measurements. This can be carried out in spite of the ambiguity inherent in the gravity method, by placing bounds on physical properties of the body provided by independent data. However, before the granite is modelled, the problem of

estimating the regional gravity field is briefly discussed.

4.4.2 The regional gravity field.

The estimation of the regional gravity field of a large area with significant topographic variation requires the isostatic compensating effect to be taken into account.

The compensating gravity field predicted by an elastic plate loaded on top by the surface topography will be assumed as one possible approximation of the regional field. However, it was shown from the isostatic analysis that different "loads", other than the surface topography, are present in the region which contribute to the regional gravity field. These sources of long wavelength gravity anomalies are modelled here, together with the near surface low density granitic body.

Two profiles (A-A' and 12.5^{0}S) are shown in Figs. 4.6(a) and 4.6(b), together with the gravity compensating effect predicted by loading the elastic plate with the observed topography and assuming that the compensation takes place entirely at the Moho at a depth of 35 km. As already pointed out in Chapter 3, there is a long wavelength negative anomaly which is not predicted by the simple elastic model loaded only on top. This negative anomaly could be ascribed to a relatively lower density bodies within the uppermost part of the crust and/or to a thickening of the crust

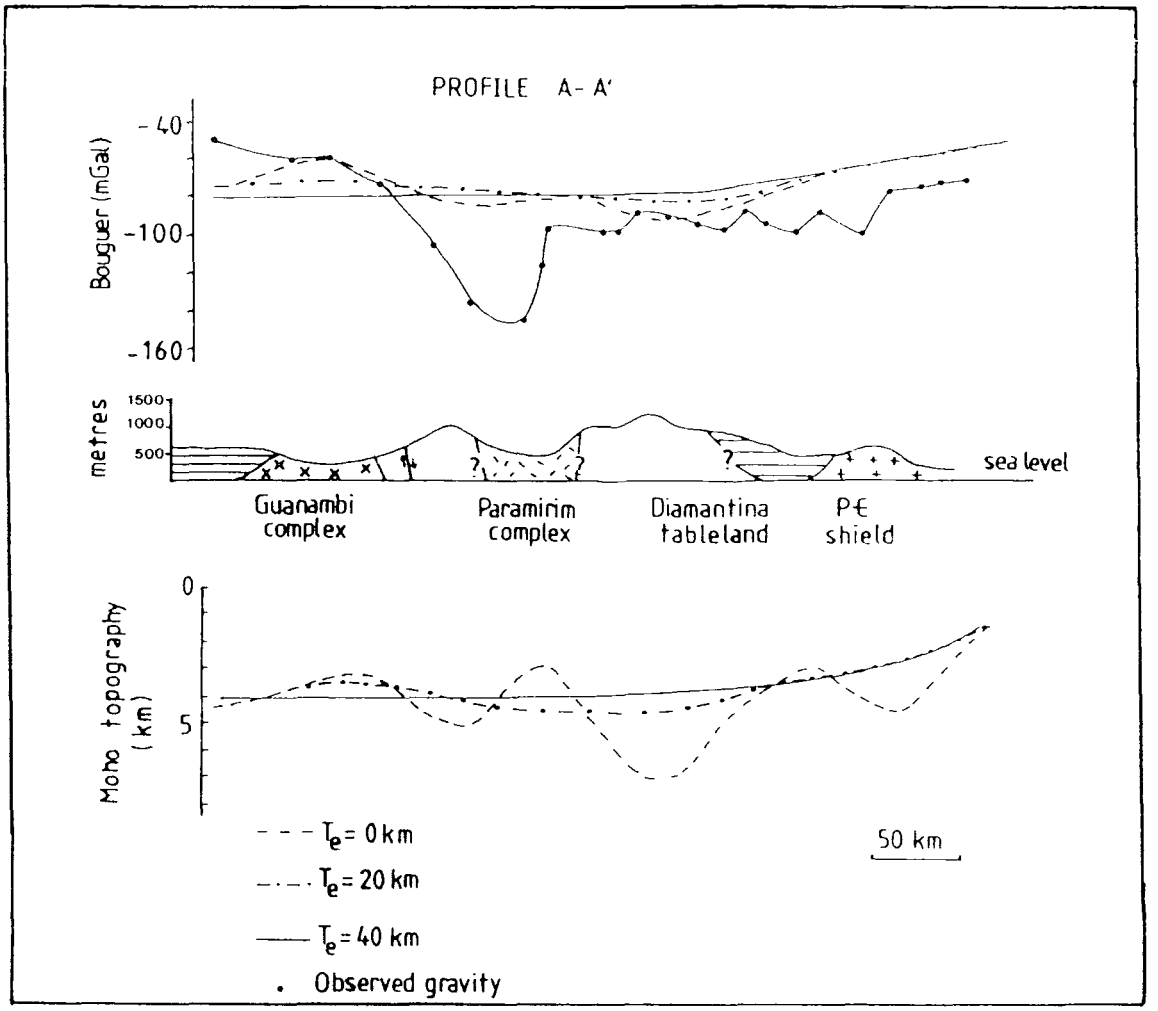

Fig. 4.6(a) - Moho topography and respective gravity effect predicted by an elastic plate loaded on top by the observed topography along the profile A-A' indicated in Fig. 4.1. A simplified geological cross section is also outlined.

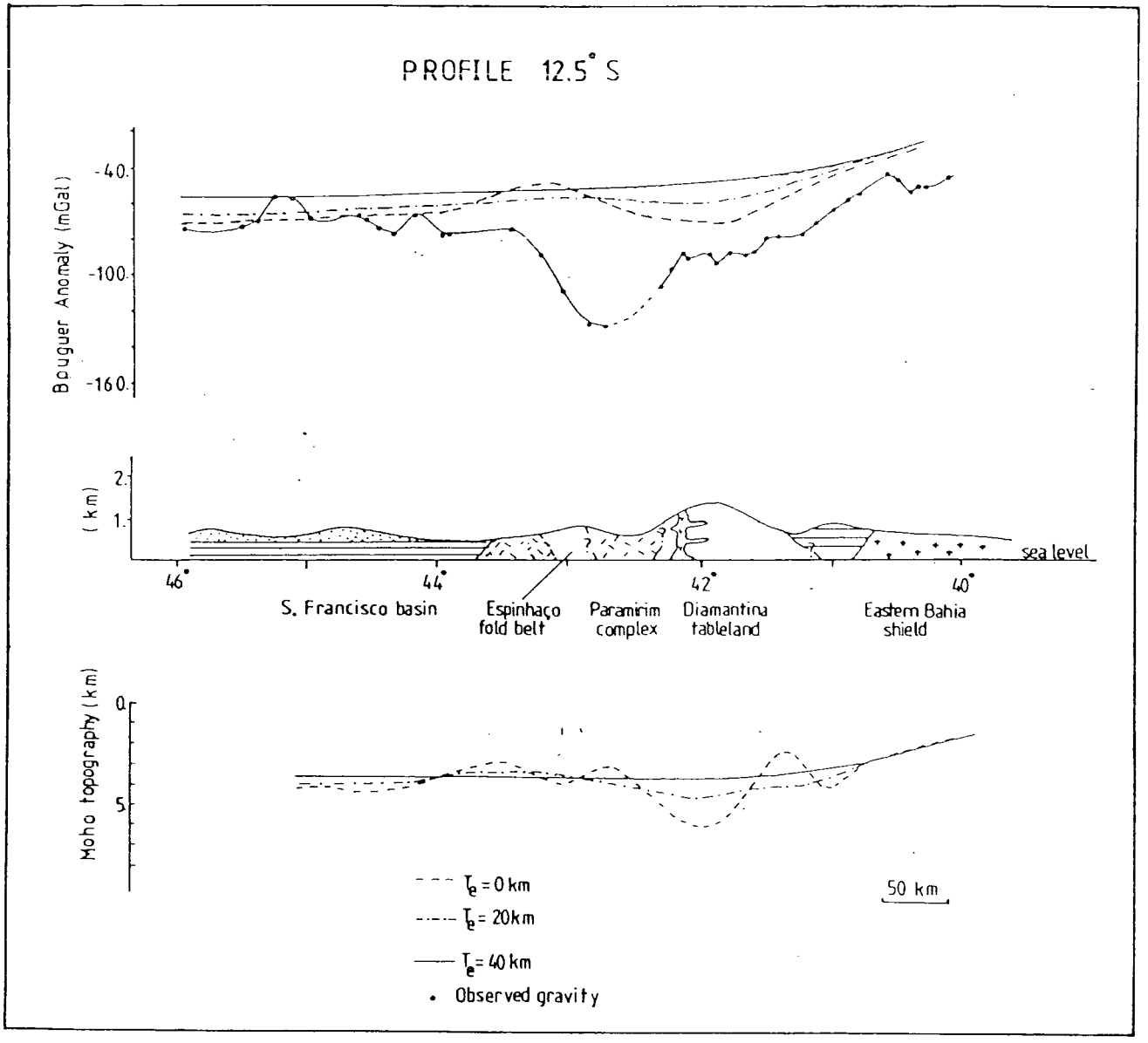

Fig. 4.6(b) - Idem for profile along 12.5°S.

underneath the Espinhaço Fold System.

As discussed in Chapter 3, it is not possible to choose without ambiguity a regional field based solely on the gravity data. Therefore, two extreme cases, crustal thickening and low density uppermost crust were considered when modelling the granite.

4.4.3 The granite modelling.

Since the gravity anomaly is finite along the NNW direction, a three dimensional model would be the most accurate geometric representation of the granitic body. However, the granite can be accurately approximated using a two dimensional model with end correction (2D model).

For the profile A-A' (Fig. 4.1), which is situated half way between the ends of the body, the results for the 2D gravity model differ from the simple 2D model by a few milliGals. Therefore, 2D modelling is suitable for this profile, in view of both the uncertainty in the densities and the errors of observation.

Although small outcropping granites are widespread in the Paramirim complex, the minimum of the anomaly occurs near the western border of this complex. However, the 1:1,000,000 scale geological map of Bahia State does not indicate any granitic body outcropping in the region where the minimum is situated.

Exceptions are the small granitic bodies observed at Boquira city (latitude 12.7° S) and the circular granitic bodies near Paramirim city in the south where the large negative magnetic anomaly is situated. As described by Espourteille and Fleisher (1980), the granites in Boquira city are small bodies intruding the basement. These bodies show no contact metamorphism and they are cut by normal faults. On the other hand, the Paramirim city granitic bodies are associated with well developed migmatitic aureoles and are not foliated. Further comparative study on these granites has not been carried out so far. Due to the lack of detailed geological information concerning the distribution of the granites in the region, the top of the granite was assumed to be at the sea level.

It is also assumed that there is a single body which produces the steep negative anomaly and no density variation within it. The lower bound in the density contrast can be estimated using the previous result (section 4.4.1) which shows the granite to be situated at a maximum depth of 20 km within the upper crust. The maximum amplitude of the anomaly is about 50 mGal. These figures suggest a minimum density contrast of about 0.06 g cm^{-3}. Any density contrast lower than 0.06 g cm^{-3} would require the bottom of the body, which has its top near the surface, to extend below the depth of 20 km. However, in this case, there is no solution which predicts the observed gradient of the anomaly.

The results of the gravity modelling are shown in Fig. 4.7(a) and Fig. 4.7(b). In Fig. 4.7(a), the granitic body was modelled as having density contrasts of -0.1 g cm^{-3} and -0.15 g cm^{-3}. The long wavelength negative anomaly, which is not predicted by an elastic plate loaded on top, was modelled assuming a relative thickening of the crust in the centre of the Espinhaco Fold System. Apart from the Moho deflection, predicted by loading the elastic plate with the observed topography, a maximum crustal thickening of 3 km for a 40 km thick plate and 2 km for a 20 km thick plate was necessary to produce the long wavelength negative anomaly. A relative thinning, from 40 km to 35 km, towards the Guanambi complex and the São Francisco basin, was also assumed to fit the observed westerly increase in the Bouguer anomaly. In this case, the depth to the bottom of the granitic body may vary from 13 km for a density contrast of -0.1 g cm^{-3} to 8 km if a density contrast of -0.15 g cm^{-3} is assumed instead. For this model of granite with no lateral density variation, the width of the top is about 35 km and the width of the base is 55 km. This is a granite of batholithic dimension and tabular form.

Bott and Smithson (1967) have suggested a method of evaluating whether the sides of the granite slopes inwards or outwards by using the gradient of the anomaly across the edges of the body. The lack of detailed gravity measurements across the gradient of the anomaly does not permit the utilization of this method. However, the observed gravity anomaly and the outcropping geology are most consistent with an outward sloping contact as shown in Fig. 4.7a.

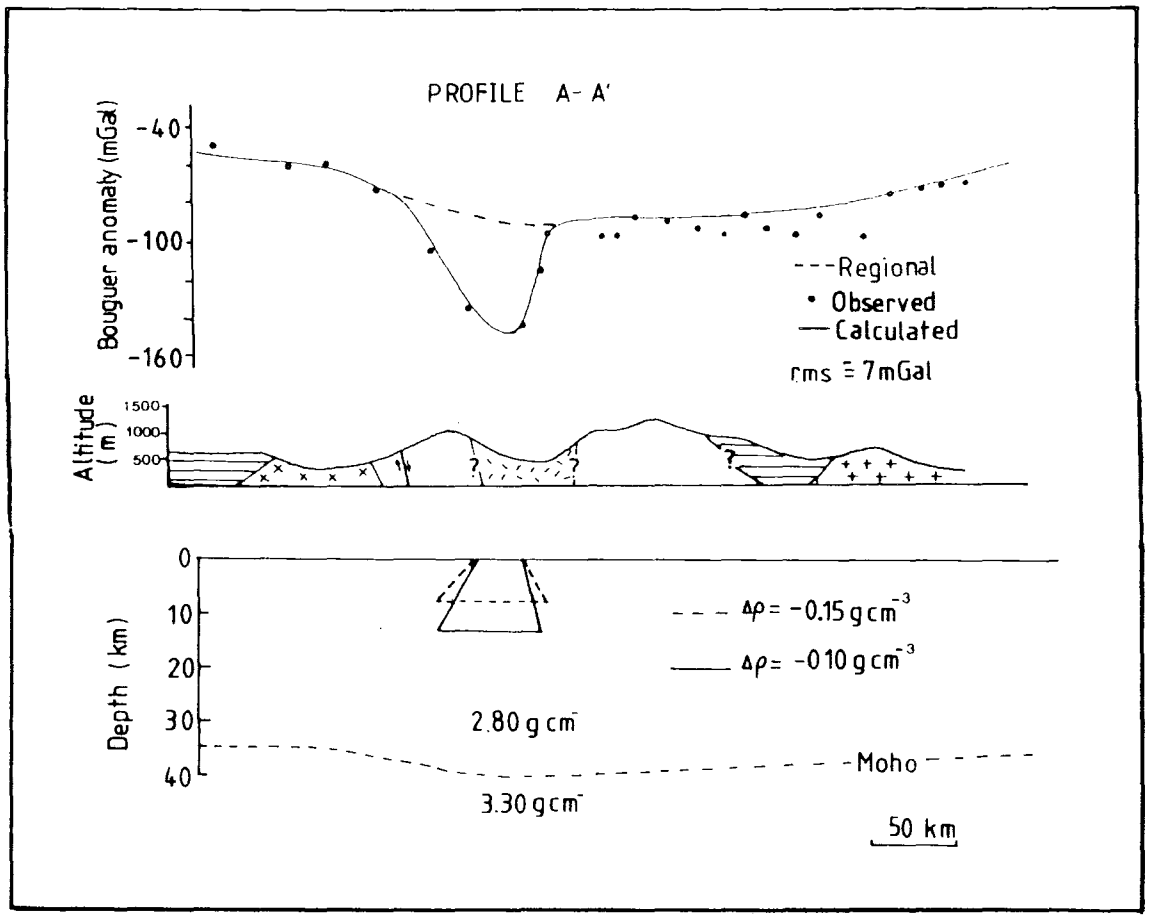

Fig. 4.7(a) - Gravity modelling of profile A-A'. Description in the text.

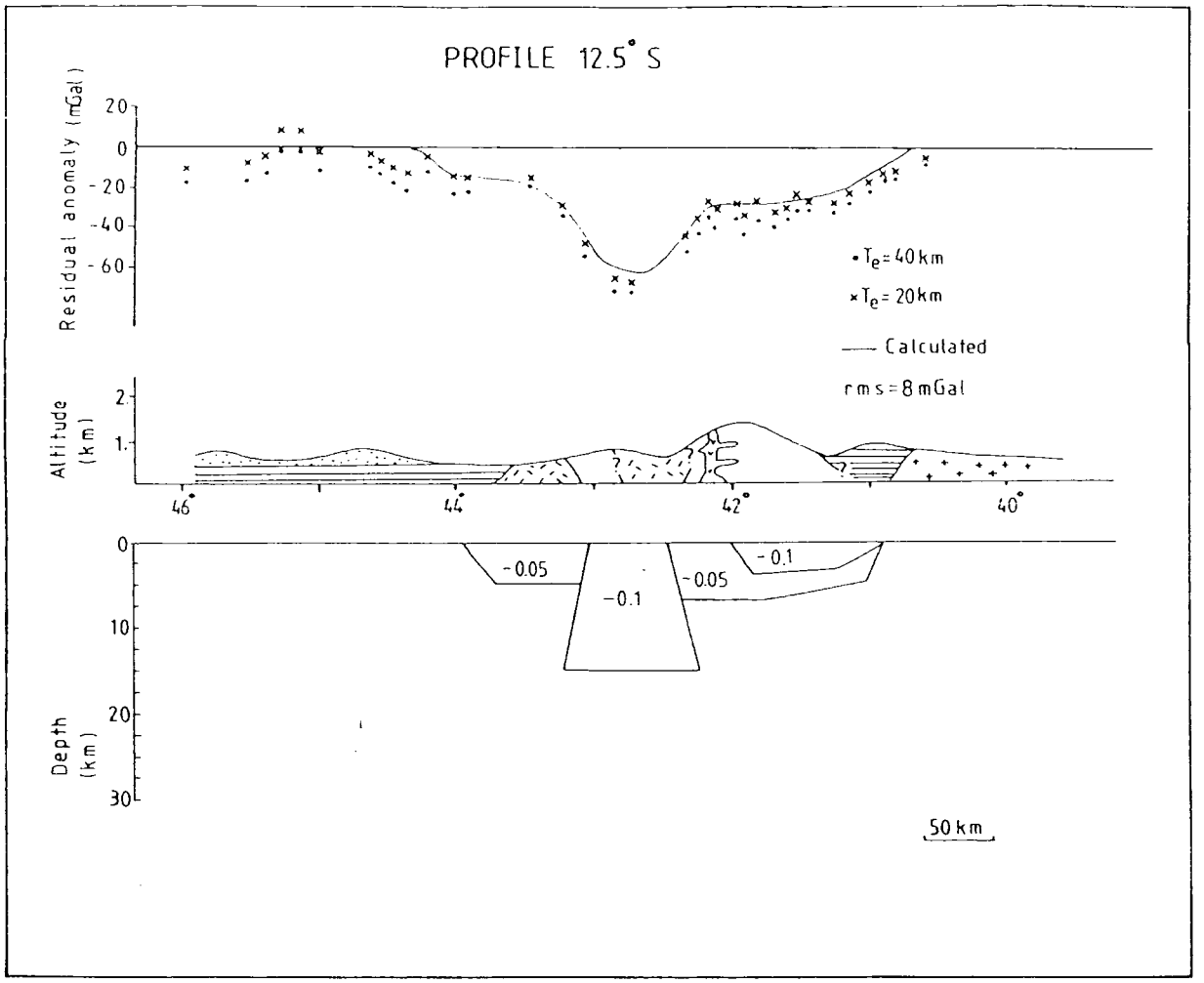

Fig. 4.7(b) - Idem for profile 12.5°S.

The western outward sloping side of the granite may, therefore, underlie the folded metasediments of the Espinhaço fold belt, whereas, the eastern side of the granite is situated underneath the centre of the Paramirim complex.

The profile 12.5°S, shown in Fig. 4.7b, is situated close to the northern edge of the large negative anomaly. In comparison with the anomaly shown in profile A-A', the amplitude of this local anomaly is less and its wavelength is greater. The long wavelength negative residual anomaly which is not predicted by the topographic loading on an elastic plate, has a maximum amplitude of -30 mGal over the Diamantina tableland. This gravity low coincides with the region in the Diamantina tableland where the upper Middle Proterozoic Diamantina group (argillaceous rocks and sandstones), has a maximum thickness of about 2-3 km. Density measurements on these rocks are not available. However, the rocks probably have lower density than the basement, since metamorphism and deformation are not significantly present in this region of the Espinhaço Fold System. The sedimentary cover together with the acid volcanics may produce this long wavelength negative anomaly. The gravity model along this profile is assumed as comprising the following: (1) 5 to 7 km of low density rocks (-0.05 g cm^{-3}) which are ascribed to acid volcanics and granitic rocks near the surface; (2) a sequence of about 2-3 km of low density sediments (-0.1 g cm^{-3}) and (3) a low density granitic

body (-0.1 g cm^{-3}). Modelling of the residual anomalies predicted by a 20 km thick elastic plate, suggests the thickness of the granite to be 15 km. Changing the density constrast to -0.15 g cm^{-3}, reduces the thickness to about 10 km. For a more rigid plate, the average thickness of the low density rocks would be slightly greater.

From the results presented in Fig. 4.7a and Fig. 4.7b, it is shown that the vertical thickness of the granitic body is not only dependent on the density contrast but it also depends on the model used to explain the long wavelength (regional) gravity anomaly. A thicker granitic model is required to fit the local negative anomaly if this regional anomaly is entirely ascribed to a low density upper crust.

4.5 Discussion.

The gravity interpretation of the large negative gravity anomaly over the Paramirim complex suggests that this anomaly is caused by a source situated within the upper crust. This source is probably granite of batholithic dimensions.

Granites are commonly found in the gneissic-migmatitic basement of the Paramirim complex (Jardim de Sá et al., 1976b). However, as shown by the gravity modelling, the low density granitic body, which produces the steep negative gravity anomaly, substantially

underlies both the Espinhaço fold belt and the western Paramirim complex. To the south of the latitude 13.5°S , the anomaly is centred over the Paramirim complex and it coincides with the region where Jardim de Sá et al. (1976a) have reported large circular K-rich granitic bodies. The available 1:1,000,000 scale geological maps of Bahia State and the geological literature of this region indicate small granitic bodies outcropping in the vicinity of Boquira city (12.7°S in Fig. 4.2) and a large circular granitic body at latitude 13.5° S near Paramirim city. Further evidence of granitic bodies outcropping in the region where the large negative gravity anomaly is situated has yet not been reported.

Geological information across the Espinhaço fold belt and the Paramirim complex, at the latitude of Boquira city, does not show granites intruding the metasediments but only the Archean basement. Where granites outcrop, they are frequently cut by normal faults which horizontally displace sections of the same body. According to Espourteille and Fleisher (1980), the normal faulting affecting the Espinhaço fold belt postdates the Espinhaço orogeny (1.3 Ga). The Espinhaço orogeny was accompanied by low grade metamorphism. However, metamorphism has not affected these granites. These observations suggest that the granites of Boquira city probably postdate the deformation of the fold belt. K/Ar radiometric ages obtained by Tavora et al. (1967) yielded values ranging from 400 to 815 Ma which may represent minimum ages. This is because K/Ar ages commonly reflect

overprint of younger events such as re-heating, mineralization, metamorphism or reworking (Fitch and Miller, 1973). The granites of Boquira city outcrop in a region where lead and zinc mineralization occurs.

The granites (samples X-33 and II-Liv) situated near Paramirim city were dated by Jardim de Sa' et al. (1976b) using Rb/Sr method and two ages were obtained: 1530 ± 33 Ma and 1087 ± 27 Ma. These ages reflect late and post-orogenic phases of the Espinhaço orogenic cycle (1.7 - 1.3 Ga).

In view of the lack of detailed geological information of the area, in particular concerning the granites, the relation between this postulated granite batholith with the Middle Proterozoic tectonic events, which affected the Espinhaço Fold System, is very uncertain. The uniformity and the apparent regular shape of the negative gravity anomaly strongly suggest a single event or closely related series of events of granitic intrusion. There are two possibilities to be discussed. Firstly, if the granite intrusion predates the Espinhaço orogeny, then the region where the granite is found should have remained a stable block throughout the deposition and folding of the sediments both in the Espinhaço fold belt and in the western Diamantina tableland. In this case, the metasediments very likely would have been folded against the uplifted granite. However, as shown in the schematic cross-section presented in Fig. 4.8, the axes of the folds in both the Espinhaço fold belt and Diamantina tableland are normal to the

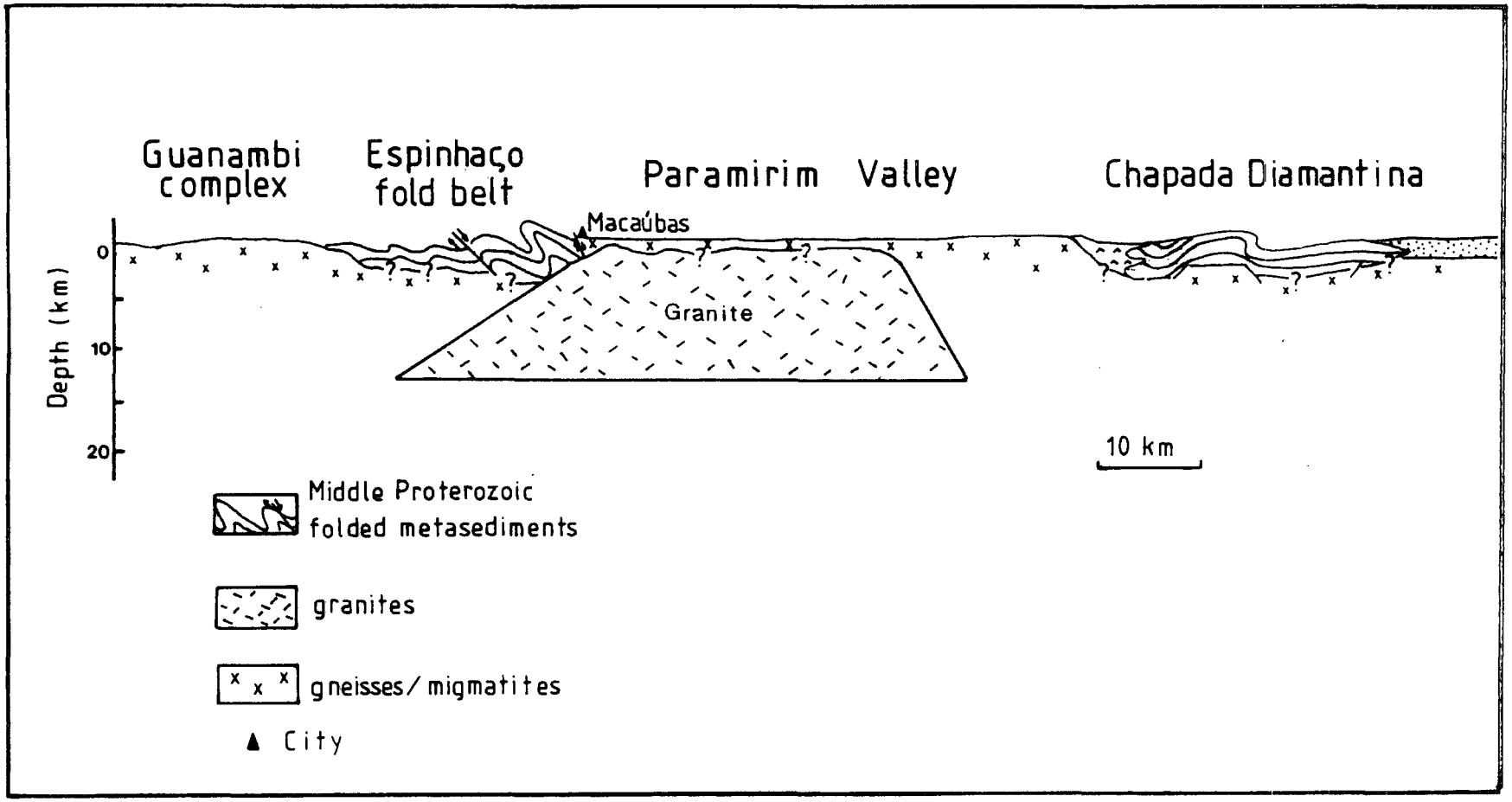

Fig. 4.8 - Schematic cross section showing the granitic batholith (no vertical exaggeration) in relation to the Espinhaço Fold System.

plane which defines the outward slopping sides of the granite. That is, there is a discordance between the emplaced granite and the deformed metasediments, with the granite cutting across the folding. This may suggest that the granite mainly postdates the Espinhaço orogeny. It is possible, therefore, that the syn or post tectonic granites observed to the south of the latitude 13.5° S are the exposed parts of the granitic batholith. The emplacement of the granite batholith may also have been controlled by conspicously assymetrical aspects of the Espinhaço fold belt relative to the Diamantina tableland. The degree of deformation and metamorphism is more intense in the fold belt, whereas the western Diamantina tableland is characterized by low-grade metamorphism and the metasediments are relatively less deformed. The centre of the large negative anomaly is situated at the western border of the Paramirim complex and near the contact with the Espinhaço fold belt, thus coinciding with the region where uranium, lead and zinc mineralizations amongst other mineralizations are found. Short wavelength magnetic anomalies, and in particular the local negative magnetic anomaly near Botupora city, are also situated in the centre of the negative gravity anomaly.

The young K/Ar ages obtained by Tavora et al. (1967) have been interpreted as reflecting thermal and hydrothermal events which postdate the Espinhaço orogeny (1.3 Ga). It is not possible to ascribe directly these ages to the time of the emplacement of the granitic batholith. However, it appears that the hydrothermal

events may be related to the granitic intrusion and this has to be verified with further geological studies in the area.

As discussed in Chapter 3, in interpreting the isostatic response function, this low density granitic batholith may also substantially explain the uplift of the Espinhaço Fold System and its isolation from subsequent Upper Proterozoic sedimentation which occurred in the Lençois basin to the east and in the São Francisco basin to the west (see Fig. 2.11).

CHAPTER 5

Gravity and Stratigraphic Studies of the Mesozoic to Tertiary Basins

Near the eastern coast of Bahia State, between 8^{o} S and 14^{o} S, a series of high amplitude negative Bouguer anomalies are associated with the Mesozoic to Tertiary sedimentary basins.

The largest negative anomalies occur over the onshore Reconcavo, Tucano and Jatoba basins (Fig. 5.1). These are separated from the continental margin Jacuipe and Sergipe-Alagoas basins by a segment of Precambrian terrain of approximately triangular shape. Apart from the Jatoba basin, the onshore basins apparently cross cut the Sergipano fold belt. To the north of the Jatoba basin is the system of Proterozoic wrench faults known as Pernambuco fault system. To the west of the onshore basins is the high grade metamorphic terrain of the Eastern Bahia Shield, within the São Francisco craton.

These Mesozoic to Tertiary sedimentary basins were formed in connection with the opening of the South Atlantic Ocean which was initiated in the Upper Jurassic - Lower Cretaceous. The sequence of the initial events which resulted in the separation of South America from Africa and the subsequent spreading of the new ocean

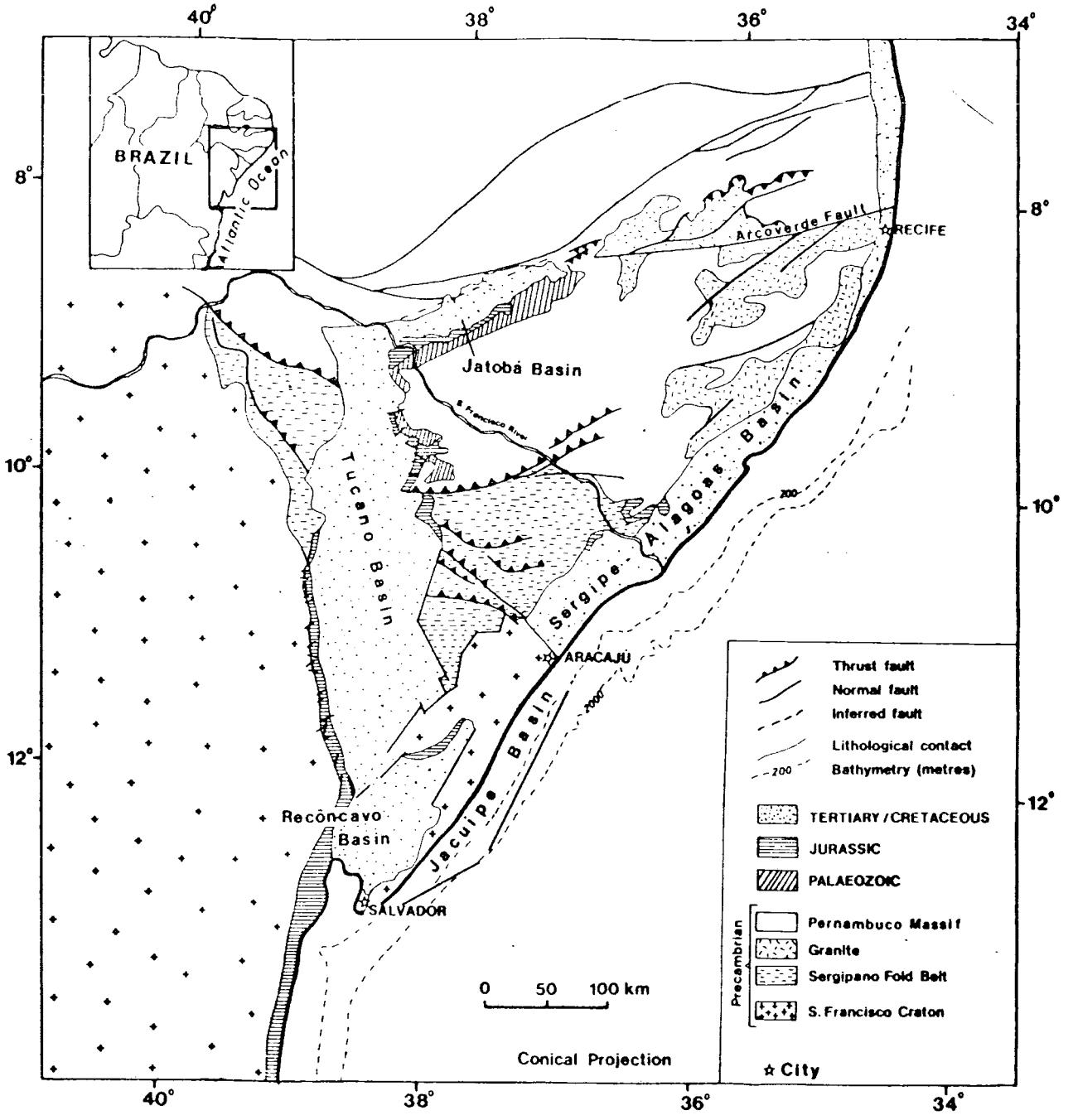

Fig. 5.1 - Geological map of the northeastern Brazil. Modified from Schobbenhaus et al. (1984) to show the Mesozoic to Tertiary sedimentary basins.

floor are documented in the stratigraphy of the onshore and the passive margin basins (Asmus and Ponte, 1973; Nairn and Stehli, 1973, Campos et al., 1974). In this study, the gravity interpretation of the onshore and offshore basins is integrated with stratigraphical and structural data and a connected model of formation of the onshore and offshore basins is proposed. The final results of this study have already been submitted and accepted for publication as a Letter to Nature, authors N. Ussami, G.D. Karner and M.H.P. Bott.

5.1 The structure and stratigraphy of the basins

The subsidence history of the eastern Brazilian continental margin basins involves the two characteristic stages of the evolution of an Atlantic-type passive margin (Asmus and Ponte, 1973): the rifting stage and the drifting stage.

The rifting stage is characterized by normal faulting, deposition of continental clastic sediments and igneous activity in most of the continental margin. Following this phase, evaporites and platform limestones were deposited in a period of tectonic quiescence and restricted marine conditions. A new phase of subsidence and sedimentation in open marine conditions followed the onset of the sea floor spreading in the subsequent drifting stage.

Using the magnetic anomalies M0, M4, salt boundary, anomaly 34 and also the Larson and Hilde (1975) Phanerozoic time scale, Rabinowitz and LaBrecque (1979) have dated the sequence of events of the formation of the South Atlantic. The rift stage started in the Upper Jurassic - Lower Cretaceous (135 Ma) and it lasted until the Aptian (110 Ma). Salt deposition occurred during the Aptian-Albian (Leyden et al., 1976). Open marine condition followed by sea floor spreading, started in the late Albian (105 Ma).

The stratigraphy of the basins along the continental margin of eastern Brazil records the sedimentation associated with each one of these events. However, igneous activity during the rifting stage occurred only to the south of the Espirito Santo basin (latitude 16^{0} S). Salt deposition is absent in the northern continental margin (see Fig. 5.2). Between the Espirito Santo and Sergipe-Alagoas basins, only anhydrite is found. Salt occurs to the south of the Espirito Santo basin on the Brazilian side and in the Gabon, Congo-Cabinda and Cuanza basins on the complementary African continental margin.

A comparison between the stratigraphy of the onshore Reconcavo, Tucano and Jatoba basins and the stratigraphy of the continental margin Sergipe-Alagoas and Gabon basins (Allard and Hurst, 1969) is shown in Fig. 5.3. The rift sequence is common to all basins. However, post-rift marine sequences are only observed in the continental margin basins.

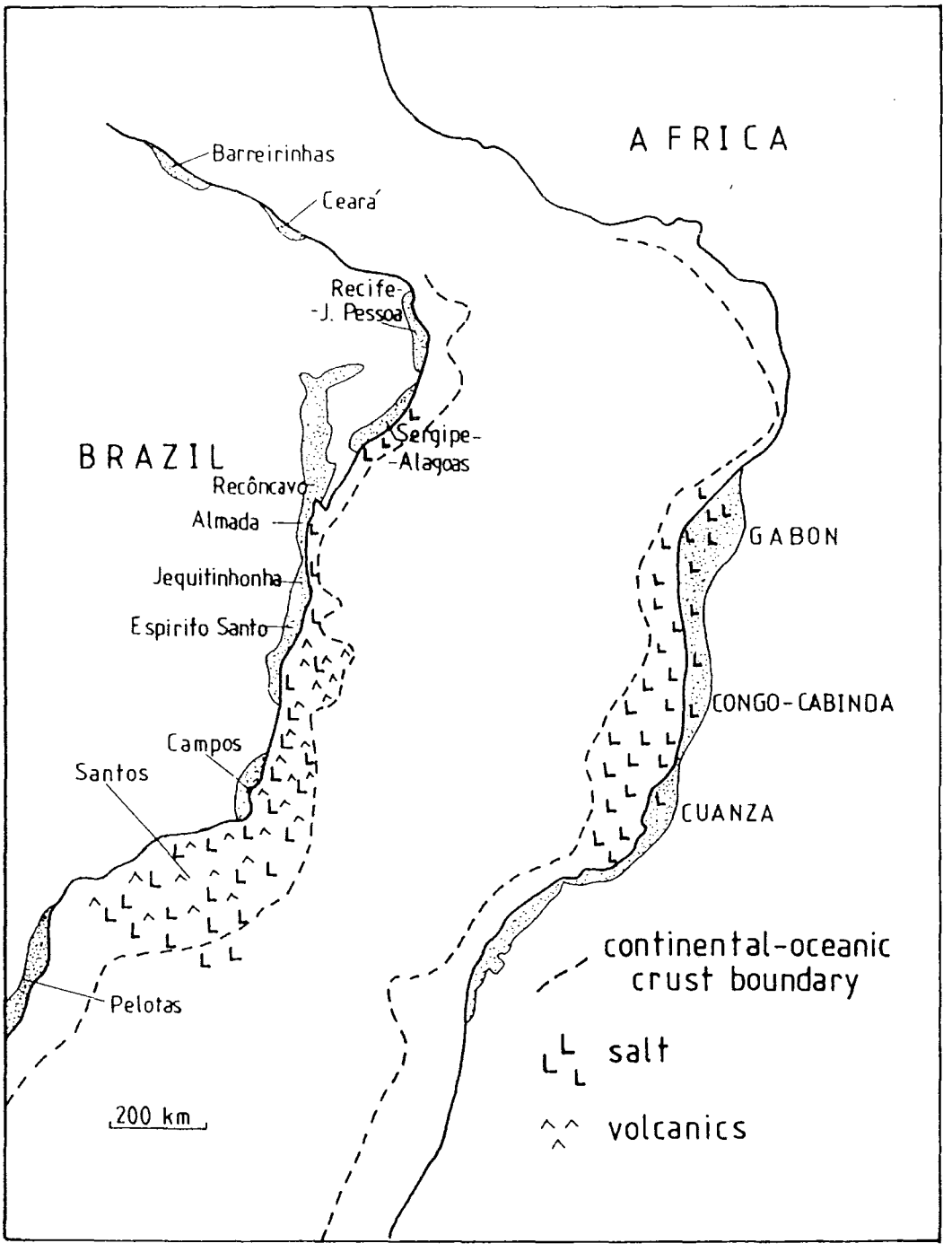

Fig. 5.2 - Distribution of the Mesozoic-Tertiary basins along the eastern Brazilian and centre-western African coast and continental margin. From Emery and Uchupi (1984) and Leyden et al. (1976).

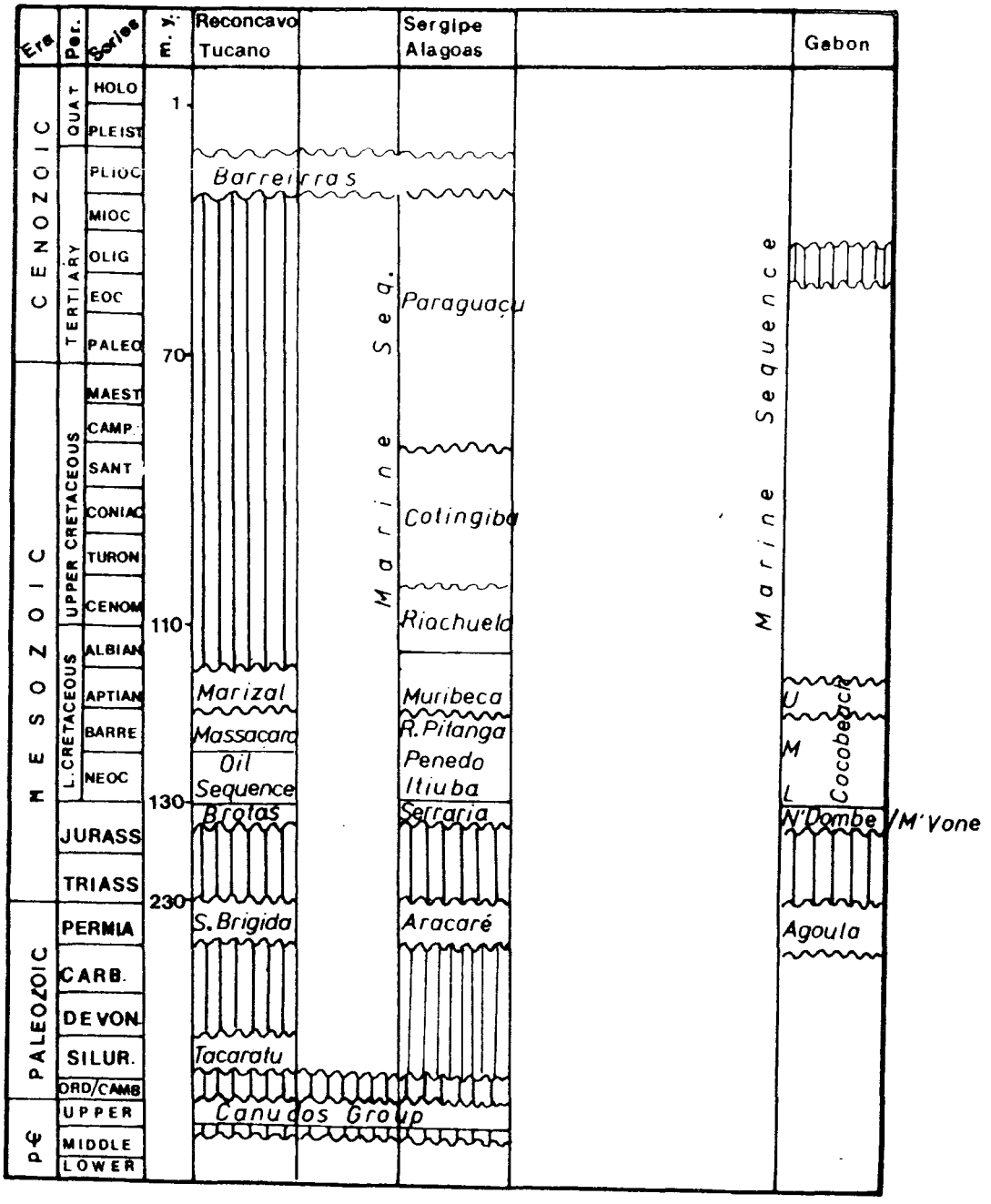

Fig. 5.3 - Comparison of the stratigraphy of the onshore Reconcavo, Tucano and Jatoba basins with the stragraphy of the offshore Sergipe-Alagoas (Brazilian margin) and Gabon basins (African margin). Based on Asmus and Ponte (1973) and Allard and Hurst (1969).

An account of the stratigraphical and structural aspects of these basins is presented in the next section.

5.1.1 Reconcavo, Tucano and Jatoba basins.

The Brazilian oil company (PETROBRAS) provided the stratigraphy of eleven wells from these onshore basins. Their sites are shown in Fig. 5.4 and the stratigraphy of each individual well is shown in Fig. 5.5. The wells identified by the letter 'M' were obtained from Inda and Barbosa (1978).

Variation of the pre-Jurassic basement is observed in these onshore basins. Upper Proterozoic metasediments were recovered in some wells drilled in the Reconcavo, central and southern Tucano basins. These metasediments are, according to Asmus and Ponte (1973), remnants of the Miaba/Vaza Barris group which correlates with the Ndjolè Series in Western Africa (Allard and Hurst, 1969). The Proterozoic basement in the northern Tucano and Jatoba basins is overlain by a thin blanket of Palaeozoic sediments. The Silurian-Devonian sequence (Tacaratu formation) is composed of continental facies sandstones with an estimated thickness of 250-300 metres. The Permian sequence (Santa Brigida formation) is composed of fluvial conglomeratic and fine sandstones. The maximum thickness is about 440 metres.

Unconformably over the Palaeozoic basement, the extensive Upper Jurassic - Lower Cretaceous sediments of the Brotas group were

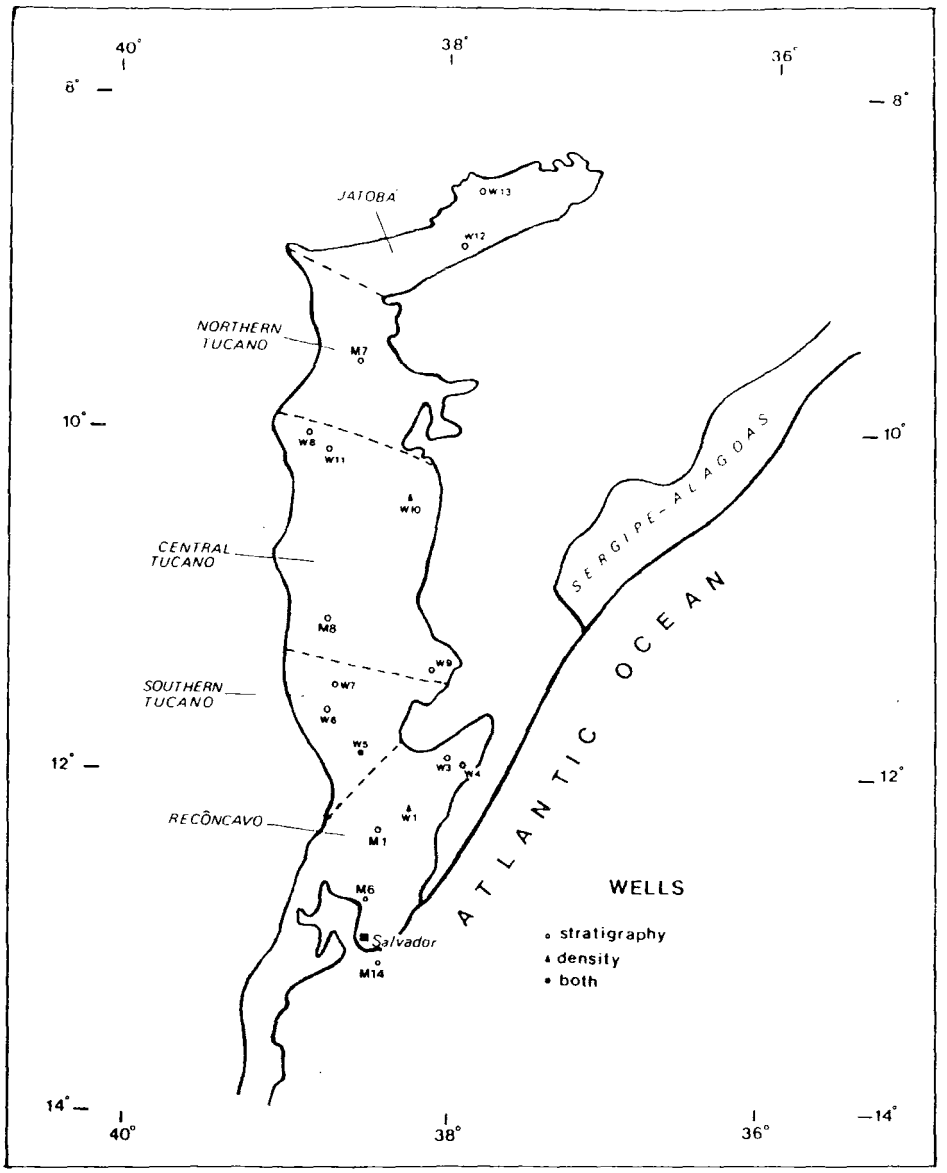

Fig. 5.4 - Distribution of the wells used in the present study.

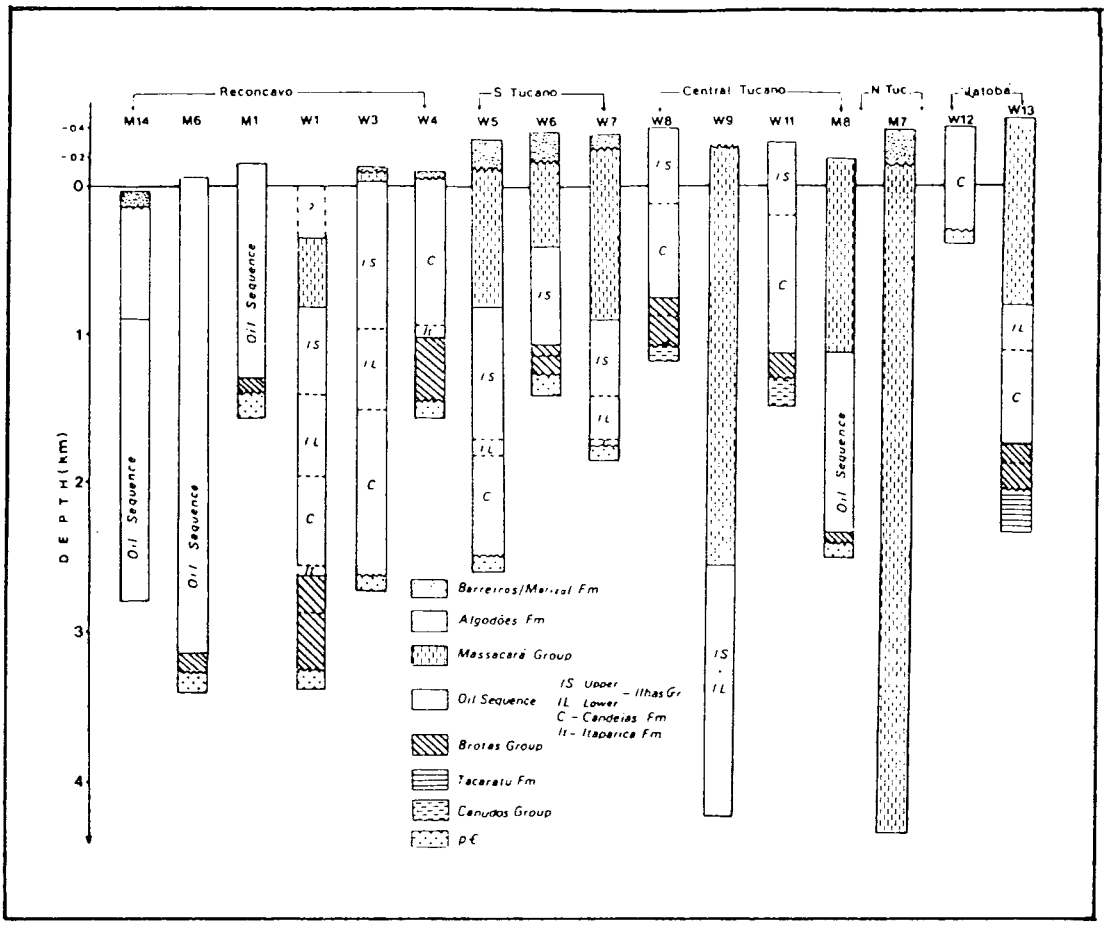

Fig. 5.5 - Stratigraphy and depth of 16 wells from the onshore Recôncavo, Tucano and Jatoba basins. p€ is the non-divided Precambrian basement; Upper Proterozoic (Canudos Group); Palaezoic (Tacaratu formation); Upper Jurassic (Brotas Group); Lower Cretaceous: Neocomian (Oil Sequence); Barremian (Massacará Group); Aptian (Marizal Formation) Tertiary (Barreiras Formation).

deposited. The basal sequence is the Aliança formation. It is composed of 300 metres of fluvial shale with limestone, siltstone and sandstone intercalation. At the top of the Brotas group are 150 metres of sandstones (Sergi formation) which were deposited in a shallow lacrustine environment. After the deposition of the Sergi formation, the rate of subsidence increased marking the initiation of the main rifting phase. An essentially lacrustine sedimentation of the lower Candeias and Itaparica formations, with maximum thickness of 300 metres, was deposited at that time. A thick fan of conglomerates, the Salvador formation, is observed at the eastern border of the Reconcavo basin and contiguous with the Salvador high (profile B-B' in Fig. 5.6a).

Rapid sedimentation followed throughout the Neocomian, with the deposition of both the upper Candeias formation and the Ilhas group with no discontinuity. The Candeias formation is composed of shales interbedded with siltstones and massive sandstones (Vieira et al., 1971) and it is evidently thickest (ca. 3500 metres) in the Reconcavo basin. The Ilhas group is composed of 325 to 2500 metres of sandstone, siltstone and subordinate shales. The group marks a transgressive period in a deltaic sequence. Growth faults with roll-over and shale diapirs developed during the sedimentation of this group (Ojeda, 1982). Inda and Barbosa (1978) have named the Neocomian sequence as the 'Oil Sequence'. This terminology is used in the wells of the Reconcavo and Central Tucano basins in Fig. 5.5.

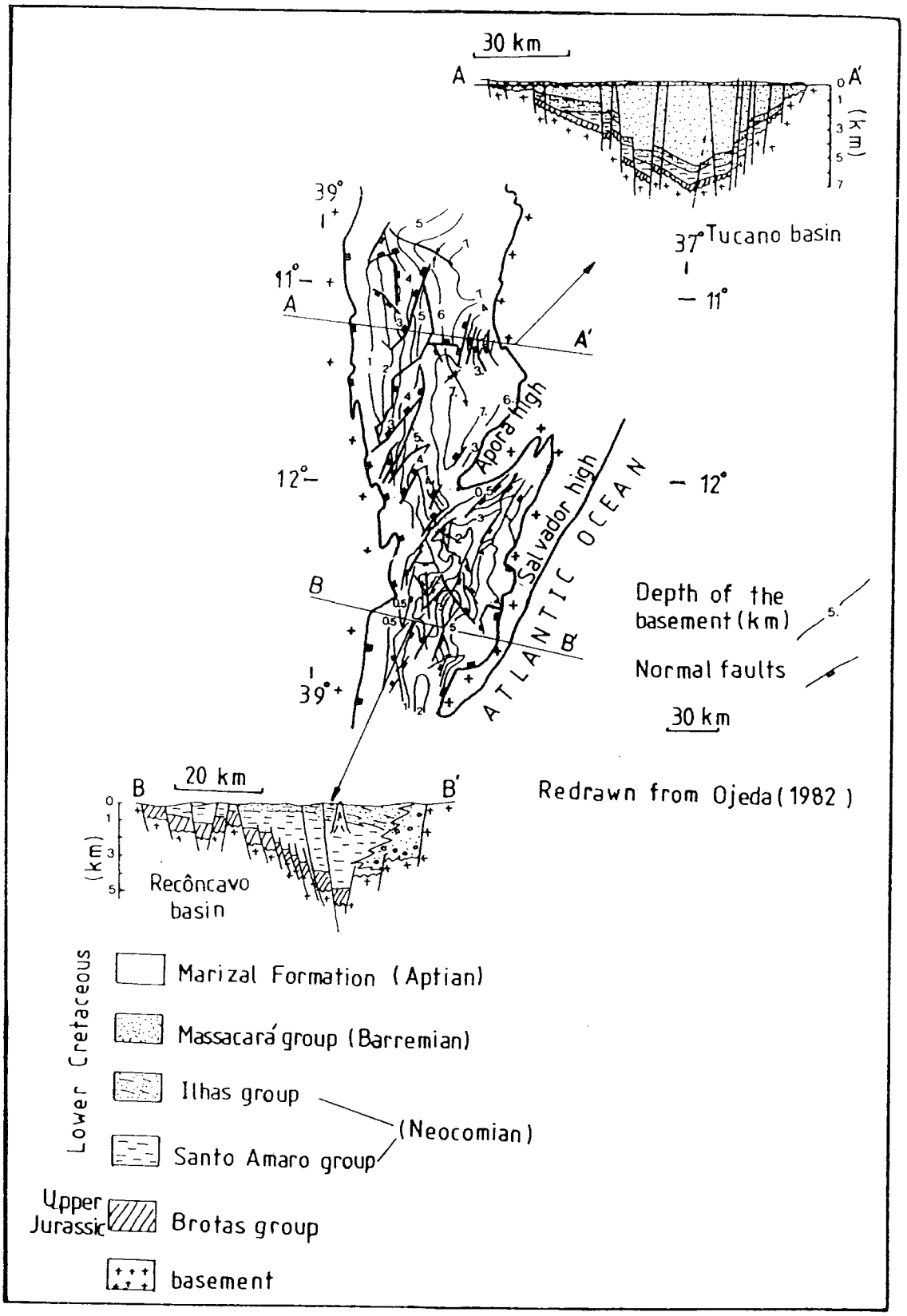

Fig. 5.6a - Structural and stratigraphical aspects of the Reconcavo and Tucano basins. Based on Ojeda (1982).

During the Barremian, thick and rapid fluvial sedimentation occurred in the Tucano basin (Massacara group) and a less thick sedimentation (São Sebastião group) in the Reconcavo basin. Both groups are composed of sandstones and siltstones with subordinate shales. As shown in Fig. 5.5, the Barremian dominates the sedimentation in the central and northern Tucano basins attaining at least 4 km in thickness, whereas in the Reconcavo basin, the thickness is less than 1.8 km.

An erosional period preceded the deposition of clastic sediments of the Marizal formation (Aptian - Albian) which is found in all basins. In the Tucano basin this formation attains a thickness of 150 to 300 metres whereas in the Reconcavo basins the thickness does not exceed 50 metres. The sedimentation then ceased until the Pliocene when a maximum of 50 metres of sandstones and clays of the Barreiras formation were deposited.

The structural aspects of the onshore Reconcavo, Tucano and Jatoba basins have been discussed by Ojeda (1982), Cohen (1985) and Szatmari et al. (1985) based on information provided by seismic data and commercial wells. Normal faults border these onshore basins which have the internal configuration of half-grabens. The Reconcavo basin (Fig. 5.6a) is a southeastern dipping half-graben. According to Cohen (1985), the Reconcavo basin formed during two main faulting episodes. The first episode was in the Upper Jurassic-Lower Cretaceous when left-lateral transform faulting, parallel to the present continental margin, occurred at that

latitude. Three directions of faulting originated from this movement: the conjugate Reidel shears trending N30°E and N37°W and tension faults trending N13°W. In the Middle Cretaceous (Aptian - Albian), a NW-SE extension may have reactivated the pre-existing faults, with essentially dip-slip movement. The maximum depth of the basin is about 5 km. This basin is separated from the present continental margin (Jacuipe basin) by a segment of Precambrian named Salvador high. The Apora high separates the Reconcavo basin from the southern Tucano basin.

The faulting pattern in the southern Tucano basin is characterized by N40 E trending faults. The deepest section of the basin (4 km) is situated next to the northern border of the Apora high.

Central Tucano basin is separated from the southern Tucano by the Itapecuru arch, at the latitude 11.5° S approximately (Fig. 5.6a). The central Tucano half-graben dips eastwards and the thickness of sediments reaches 7 km.

To the north of the inferred Vaza Barris fault (Fig. 5.6b) is the northern Tucano basin which is a prolongation of the Jatoba basin. The northern Tucano basin is a half-graben with westward polarity. A minimum of 4 to 5 km of sediments fills the deepest part of the basin.

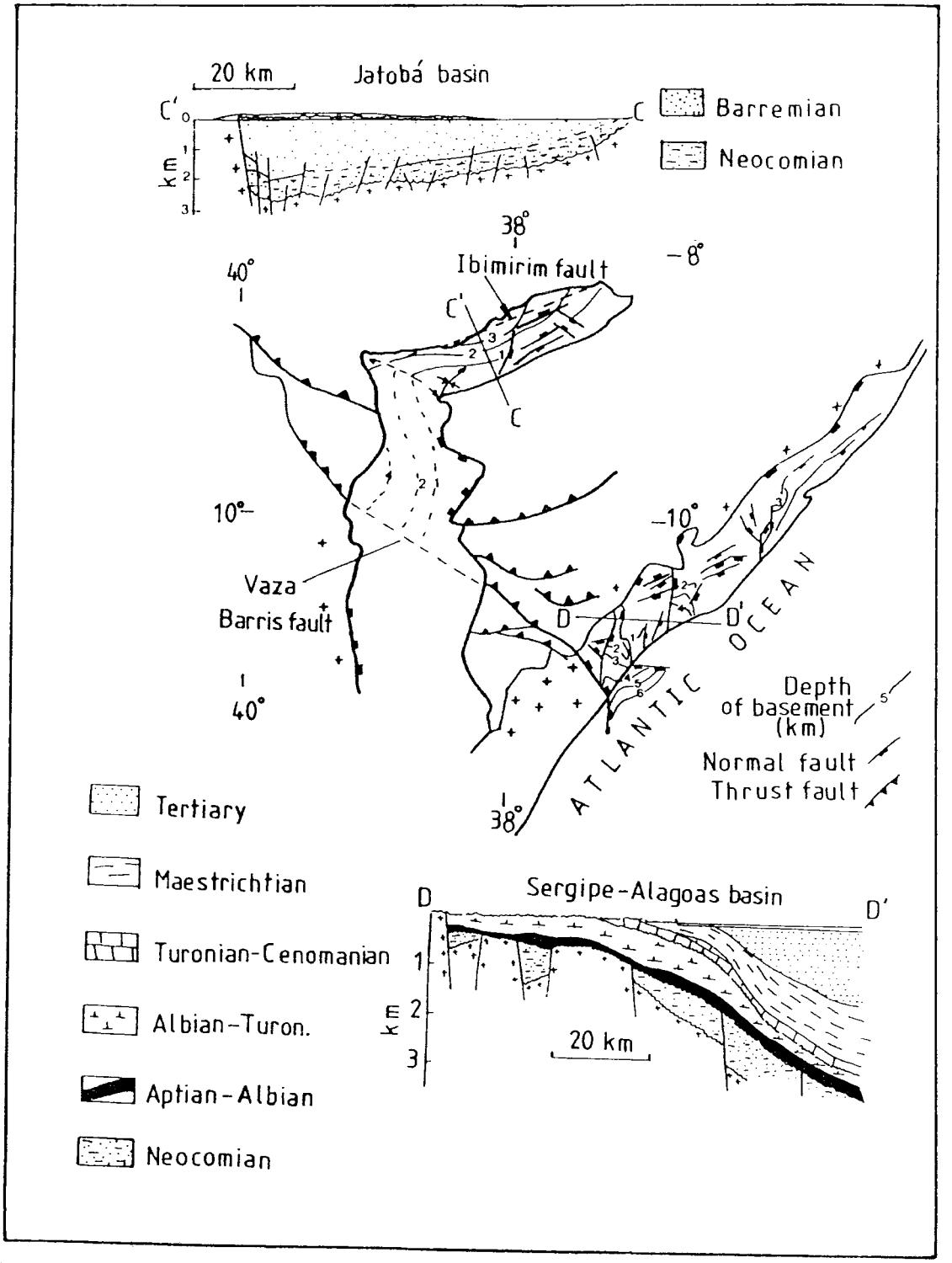

Fig. 5.6b - Structural and stratigraphical aspects of the Jatoba (Correira, 1965) and Sergipe-Alagoas basins (Asmus and Ponte, 1973).

The Jatoba basin is situated in the Pernambuco Massif. It is separated from the northern Tucano basin by the São Francisco arch. A section across the basin (C-C' in Fig. 5.6b), based on two wells and refraction seismic (Correia, 1965), shows the half-graben dipping northwards. The northern border of the Jatoba basin is the Ibimirim fault. This fault belongs to the Pernambuco wrench fault system, which may have been reactivated in the Lower Cretaceous (Beurlen, 1967).

5.1.2 The Sergipe-Alagoas basin

The basement of the Sergipe-Alagoas basin is composed of Upper Proterozoic rocks (Vaza Barris group) overlain by Palaeozoic rocks, of similar nature to the basement of the northern Tucano and Jatoba basins.

The Upper Jurassic-Lower Cretaceous sedimentation (Igreja Nova Subgroup) is similar to that of the onshore basins (Asmus and Ponte, 1973). It thickness is about 300 metres of which 200 metres are red shales and 100 metres are sandstones. Continuous sedimentation progressed throughout the Neocomian. The syn-rift sediments locally reach a thickness of 6000 metres in the Mosqueiro graben, to the south of profile D-D' (Fig. 5.6b). A period of tectonic quiescence followed the Barremian deposition in the onshore basins but the sedimentation continued in the Sergipe-Alagoas basin, where limestones rich in non-marine ostracods were deposited (Asmus and Ponte, 1973). A further

period of rapid subsidence occurred in both the onshore and the Sergipe-Alagoas basins in the lower Aptian. During this time, clastics sediments with rapid facies changes (Muribeca formation) were deposited. A new period of tectonic stability followed the lower Aptian event, with the deposition of 100-200 metres of shaly sequence in the Sergipe Alagoas basin. Shallow marine transgression and regression occurred during the Aptian-Albian, which allowed the deposition of anhydrite and associated evaporites in restricted parts of the Sergipe - Alagoas basin. Carbonate facies sediments were deposited during transgressive periods.

The drifting stage of the South Atlantic evolution started in the late Albian. In the Cenomanian a thin deposition of calcareous muds of the Cotinguiba formation occurred. 200 to 1000 metres of limestones shales were deposited in the Turonian-Coniacian but very little deposition occurred in the Santonian. The subsidence of the basin increased in the Campanian-Maestrichtian and a thick sedimentation (1500 metres) took place in a neritic environment. During the Paleocene-Eocene, thick and dominantly clastic sediments were deposited progressively towards the southeast offshore part of the basin. Onshore, continental fluvial sediments of the Barreiras formation were deposited in the Pliocene (ca. 50 metres). The thickness of post-rift sediments reaches a maximum of 4 km in the offshore part of the basin.

The structural aspects of this basin are shown in Fig. 5.6b, based on Asmus and Ponte (1973). Normal faulting with formation of horsts and grabens characterizes the initial stages of sedimentation. This is observed both in the onshore and offshore parts of the basin. As shown in Fig. 5.6b, in some structural highs (horsts) syn-rift sediments are absent. The seaward dipping of the basin is approximately NW-SE. The maximum total subsidence of the basin is observed to the south of latitude 10^{0} S. In plan view, the pattern of normal fault distribution is very complex.

5.2 Gravity interpretation

5.2.1 The Bouguer anomaly map of the onshore basins

The Bouguer anomaly map of the onshore Reconcavo, Tucano and Jatoba basins was obtained using gravity data provided by PETROBRAS (Fig. 5.7). Data reduction has already been discussed in Chapter 2. The Bouguer anomaly map shown in Fig. 5.8 was obtained by interpolating the gravity values using the routine provided by GPCP (1973). This procedure was applied to regions where the data coverage is uniform whereas manual interpolation was carried out where the distribution of the stations was poor. The results based on manual interpolation are presented as dashed contours.

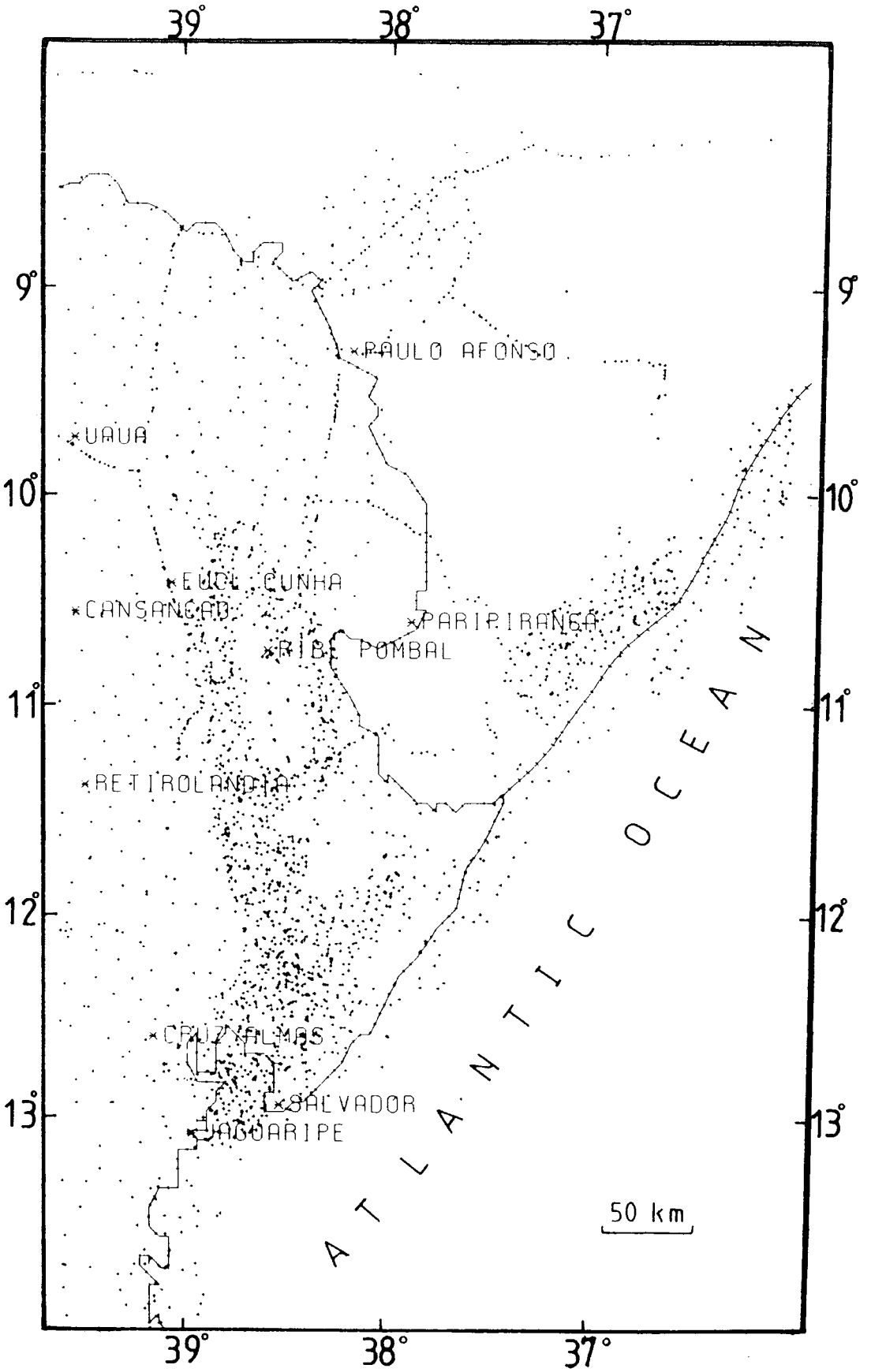

Fig. 5.7 - Distribution of the gravity stations utilized in this study. Data source PETROBRAS.

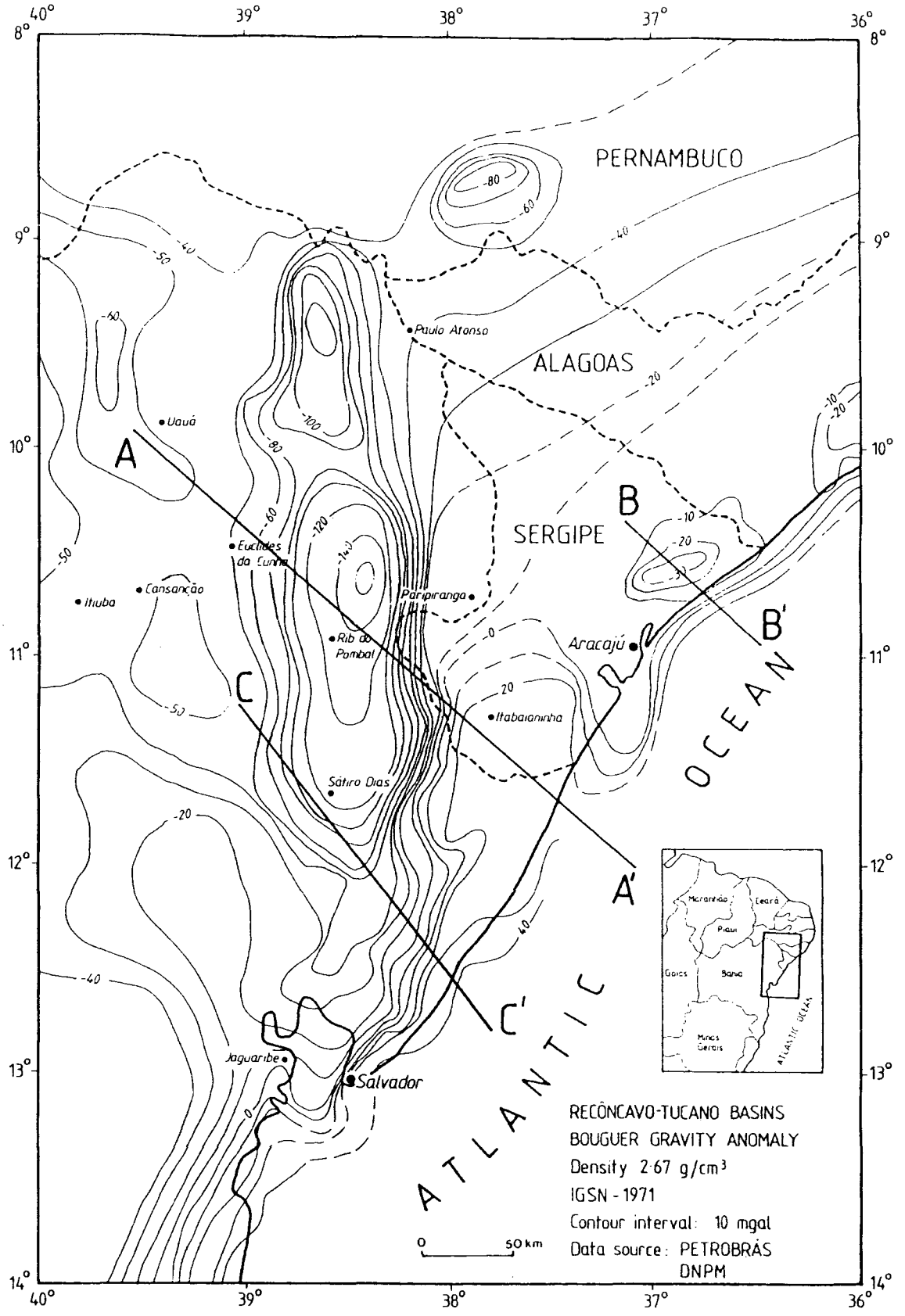

Fig. 5.8 - Bouguer gravity map of the northeastern Brazilian coast. A-A', B-B' and C-C' are the profiles which gravity model is presented in Fig. 5.13 , Fig. 5.14, Fig. 5.12c respectively.

Three topographic, free-air and Bouguer profiles, across the northern Tucano, central Tucano and Reconcavo basins are shown in Fig. 5.9. High amplitude negative anomalies are observed in both the free-air and Bouguer anomaly profiles. The amplitude of the negative anomaly is about 120 mGal in the central Tucano basin with a gradient of about 7 mGal/km. The negative anomaly in the northern Tucano basin has an amplitude of 80 mGal and the steepest gradient is about 5 mGal/km. In the Reconcavo basin, the amplitude of the anomaly is only 40 mGal and the steepest gradient is about 3 mGal/km. Gravity survey over the Jatoba basin is restricted to the region close to the northern Tucano basin. The amplitude of the negative anomaly is 30 mGal. Near the coastline, to the north of the Aracaju city (Fig. 5.8), a series of 20 mGal amplitude negative anomalies are associated with the sediments of the Sergipe-Alagoas basin.

Gravity data of the offshore regions were obtained from the 1:6,000,000 free-air anomaly map of the Brazilian continental margin (Rabinowitz and Cochran, 1978) shown in Fig. 5.10a. Accuracy in positioning the gravity values is relatively poor from this map. The error of the free-air anomaly may be as high as 10 mGal as described in Rabinowitz and Cochran (1978). The relative positions of the two steep short wavelength anomalies, the negative anomaly which is situated over the Jacuipe basin and the positive anomaly associated with the offshore extension of Sergipe-Alagoas basin, are reasonably well controlled by the bathymetry. Both anomalies have an amplitude of 75 mGal.

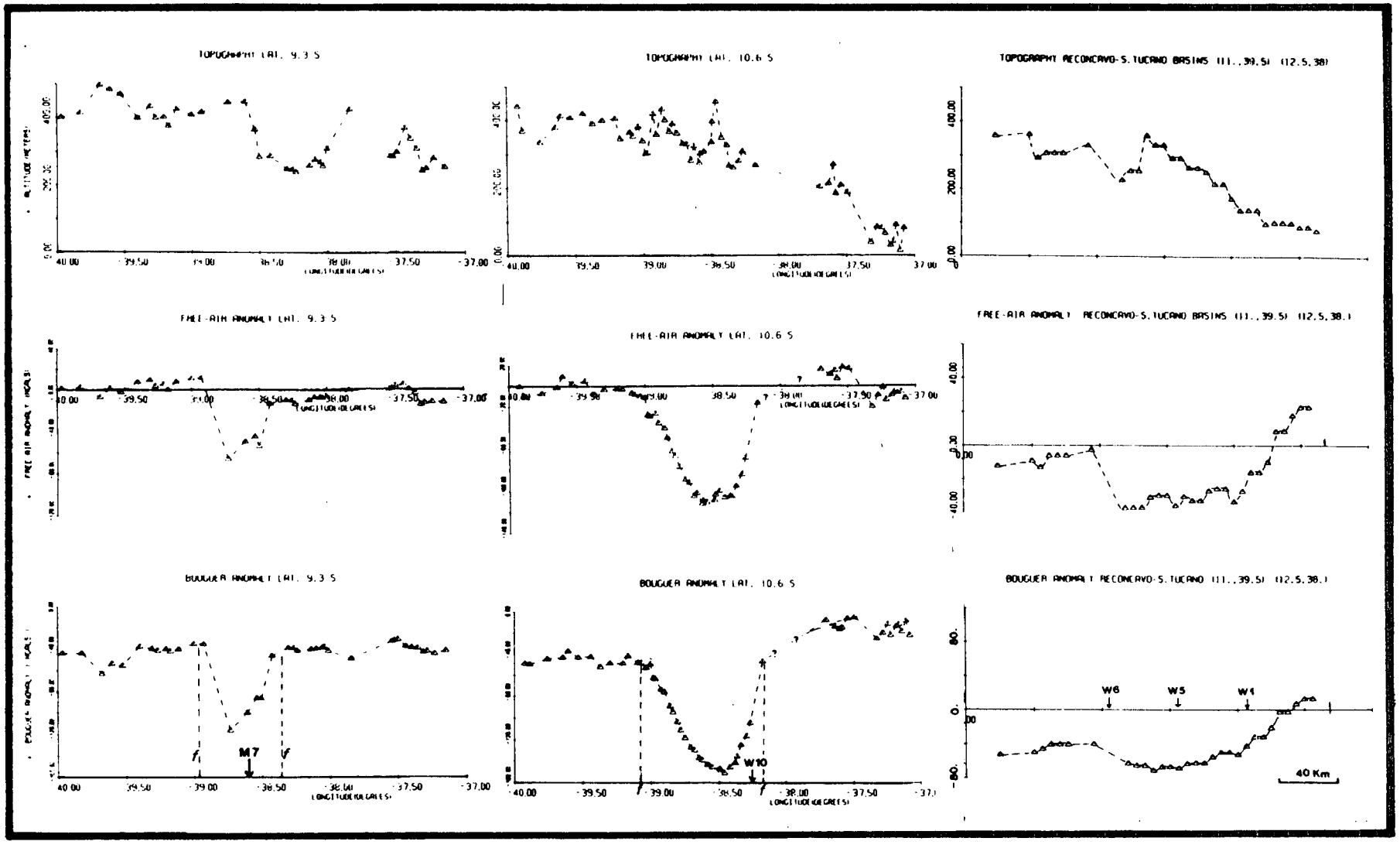

Fig. 5.9 - Three topographic, Free-air and Bouguer profiles across the onshore basins. f indicates the position of the borders of the basins.

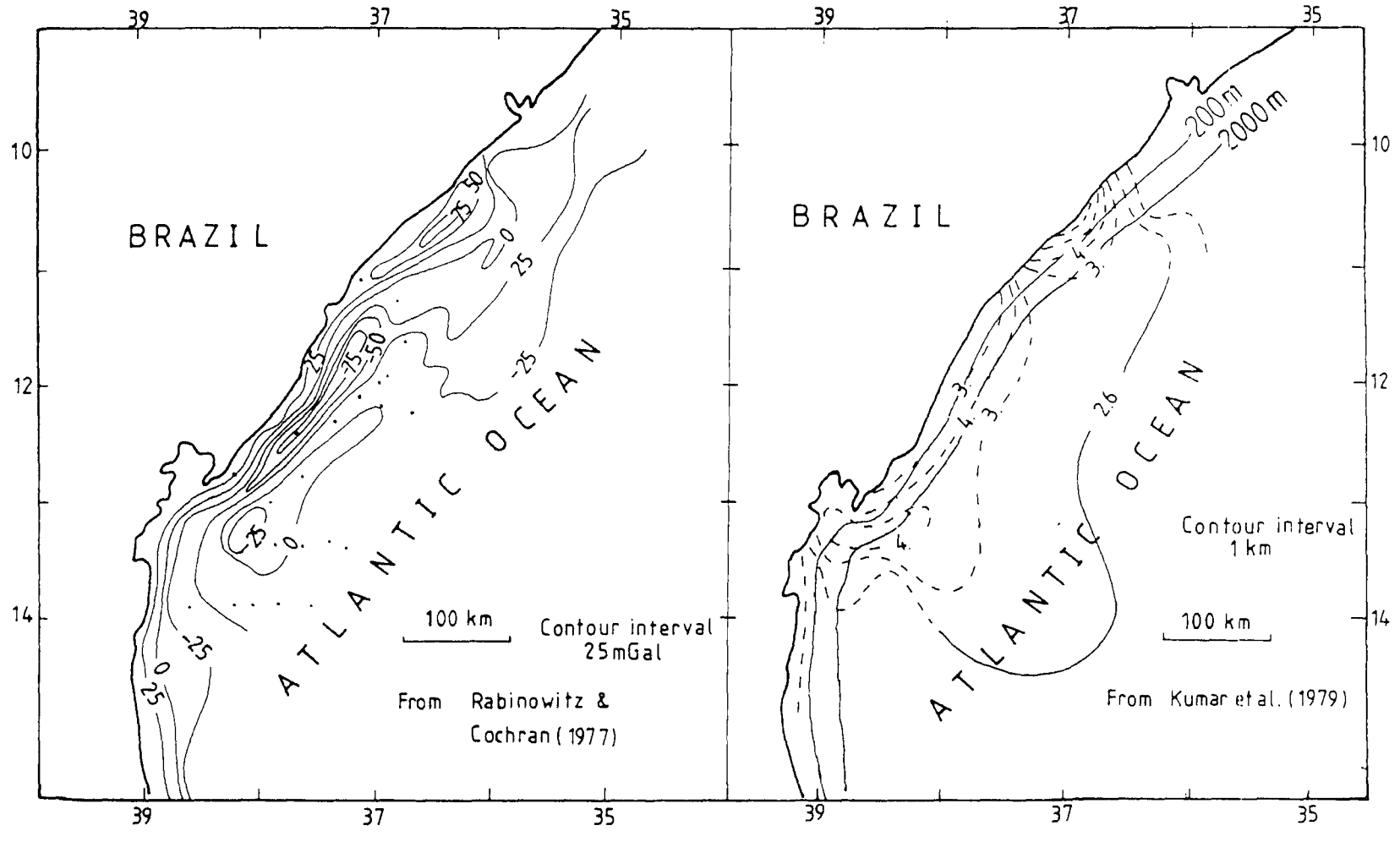

Fig. 5.10 - Free-air and sediment isopach maps of the Brazilian continental margin. (a) Free-air anomalies. Contour interval 25 mGal. (b) Sediment thickness. Contouring in km.

An isopach map of the distribution of sediments along the Brazilian continental margin (Fig. 5.10b) was published by Kumar et al. (1979). This map is based on compilation of several single channel seismic reflection profiles, sonobuoys and two-ship refraction seismic surveys in the area. Dashed contours indicate regions where the basement control is poor. In these cases, the depth of the basement was estimated from other sources such as structural maps of the offshore basins, provided by Petrobras.

5.2.2 Density data.

Four density profiles from commercial wells drilled by PETROBRAS are presented in Fig. 5.11. Their locations, except for the well W2, are shown in Fig. 5.5 and they provide the vertical density distribution in the southern Tucano, Reconcavo and central Tucano basins. The corresponding stratigraphical information of the gamma-gamma density logs from wells W1 and W5 is shown in Fig. 5.5. Stratigraphical information about the wells W10 and W2 is not available to us. However, the lithology of the Tucano basin up to the depth of 4-5 km is basically composed of sandstones and siltstones of the Massacara group, as evidenced by other wells shown in Fig. 5.5. An average density of 2.40 g cm^{-3} is ascribed to the first 3 kilometres of sediments of wells W1 and W2. Below this depth, the density probably increases steadily with depth due to compaction of the sediments and possible changes of lithology.

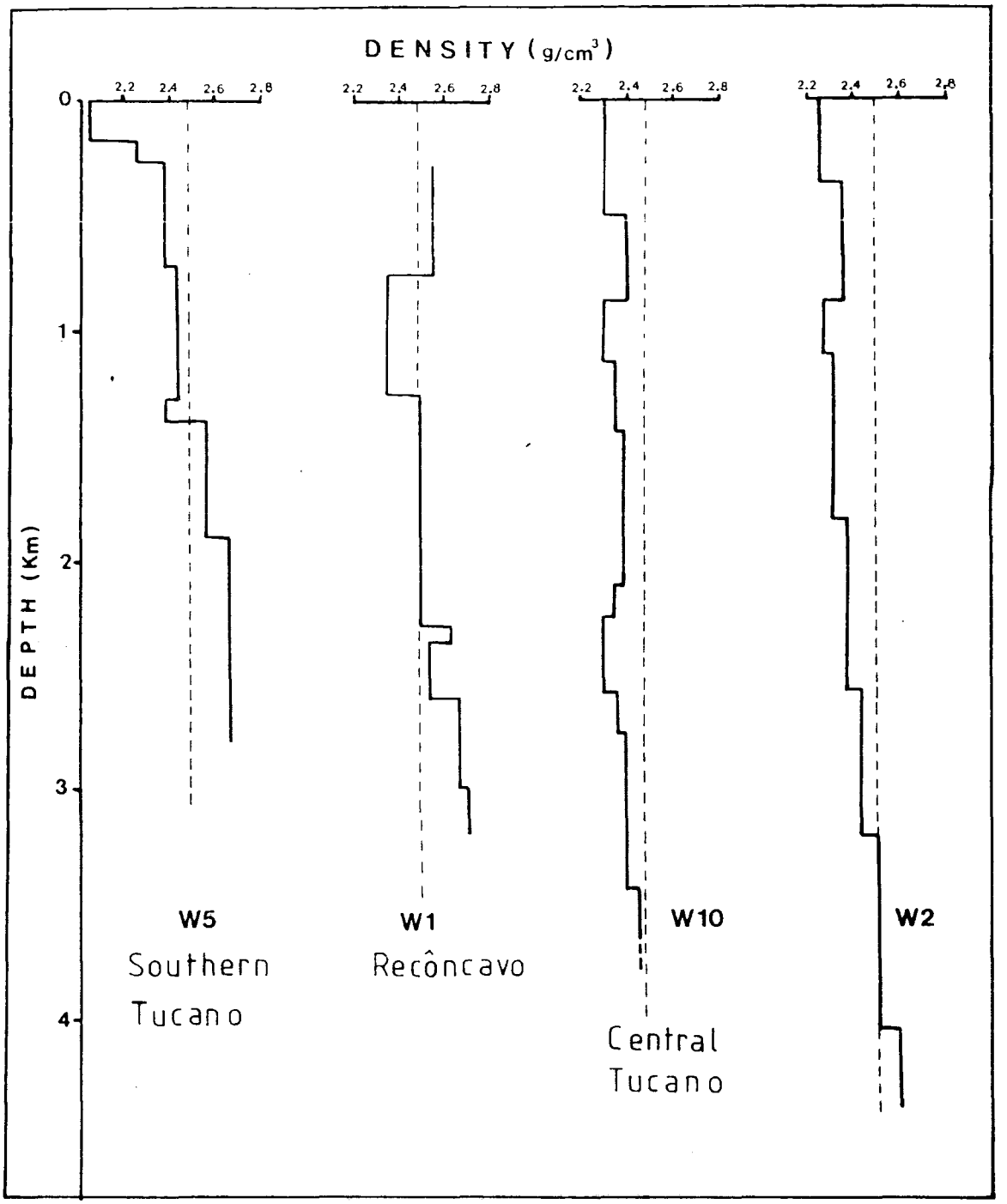

Fig. 5.11 - Density log of four wells of the onshore basins. The location of each well, except for W2, is shown in Fig. 5.5.

The wells of the southern Tucano and Reconcavo basins present a more diverse lithology which is also reflected in the density profile. The Barremian sequence is relatively thin in comparison with the same sequence in the central and northern Tucano basins. There is an increase in density from under 2.4 g cm^{-3} to 2.5 g cm^{-3}, at the depth of 1.3 km. Below this depth, the density increases rapidly with depth towards 2.6 g cm^{-3}. A significant proportion of shale in the Neocomian sequence may explain the relatively higher density in the southern Tucano and Reconcavo basin.

5.2.3 The gravity models.

The negative anomalies over the basins are associated with low density sediments which infill the basins. As shown in Fig. 5.9, the steep gradient of the negative gravity anomalies coincides with the faulted border of the basins.

In this section, gravity modelling of the basins and deep crust is discussed in detail. Two dimensional gravity models are used throughout. This is an adequate approximation for these rift-type structures.

Fig. 5.12a and 5.12b present the profiles perpendicular to the central and northern Tucano basins, respectively. The vertical density distribution is reasonably well controlled, except at the

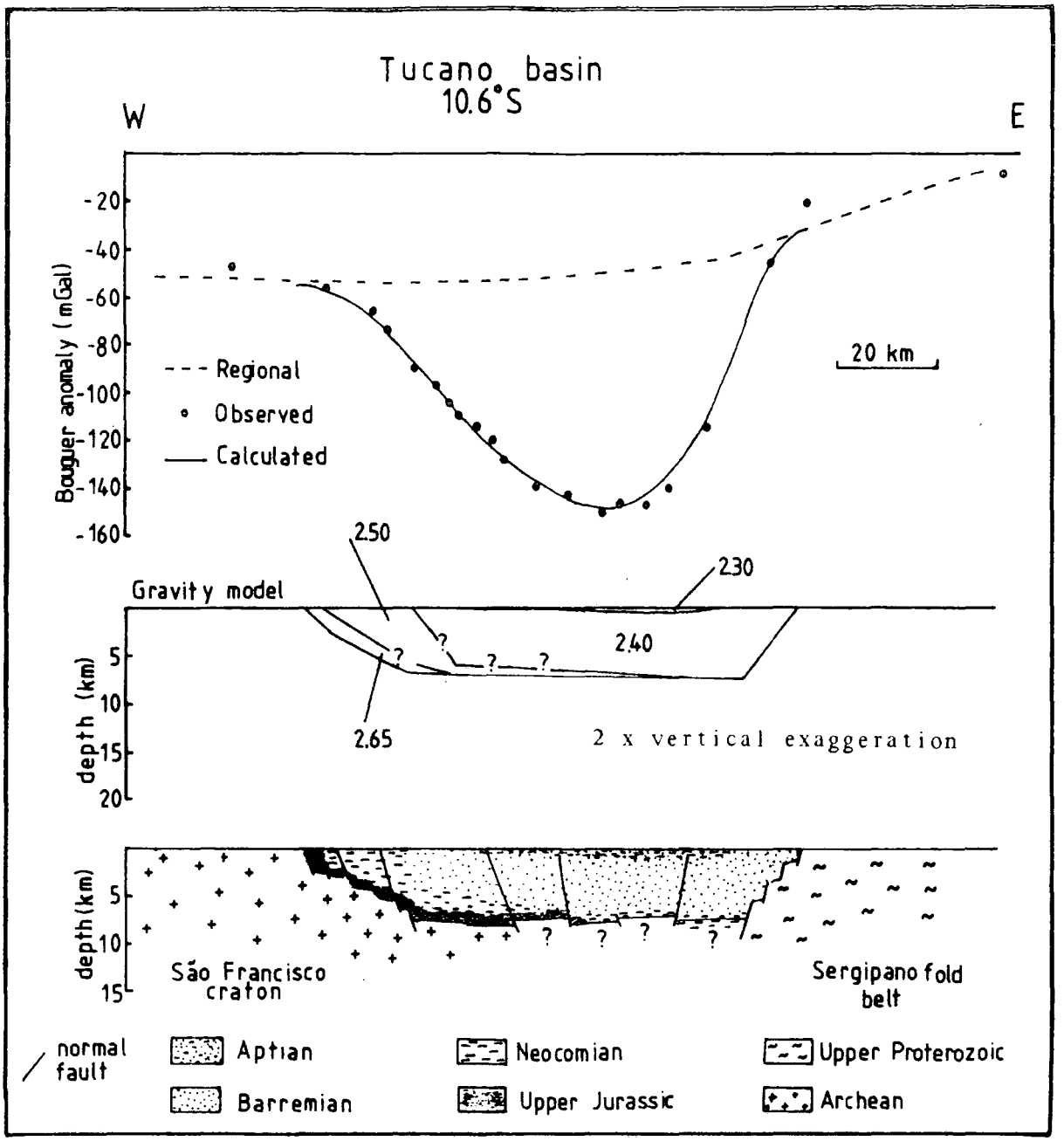

Fig. 5.12a - Gravity and geological model of the central Tucano basin. The numbers indicate the density in g cm^{-3} .

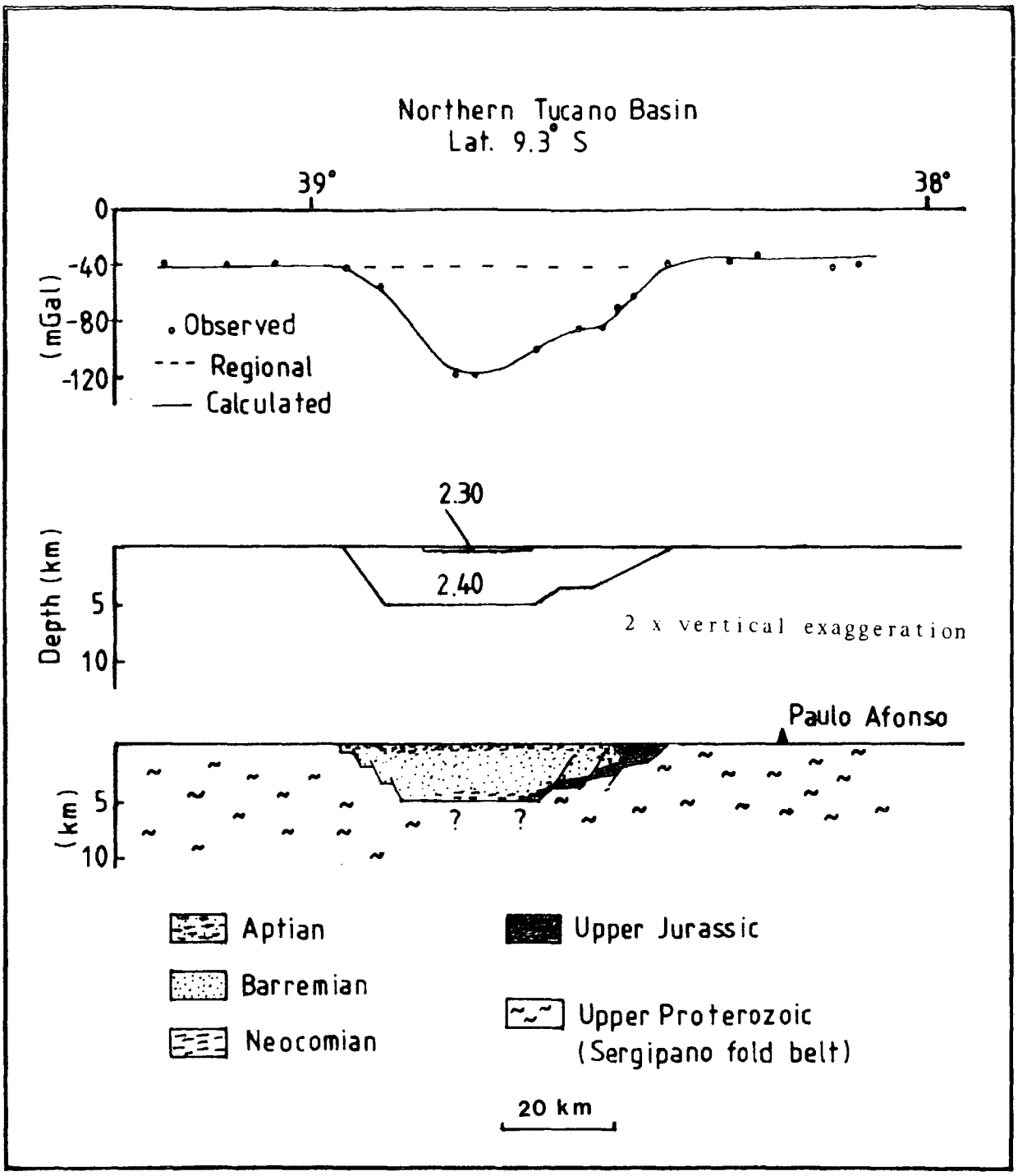

Fig. 5.12b - Gravity and geological model of the northern Tucano basin. The numbers indicate the density in g cm^{-3} .

deep parts of the basins. The high amplitude negative anomaly of about 100 mGal over the central Tucano basin is explained by 7 km of syn-rift sediments. In the northern Tucano basin, the 80 mGal amplitude negative anomaly is fully accounted for by 5 km of syn-rift sediments. The geological models are based on the structural map of the basin published by Ojeda (1982). In the central Tucano basin, the Upper Jurassic-Neocomian sediments outcrop only on the western and less steep border of the basin whereas in the northern Tucano basin the oldest sediments occur on the eastern border. The Barremian sediments dominate the deepest part of the basins. The observed gravity field over these basins shows no evidence of flanking positive anomalies. The regional gravity field suggests a gradual shallowing of the Moho towards the continental margin to the east.

The gravity model of the Reconcavo basin is shown in Fig. 5.12c. The gravity anomalies over this basin (profile C-C' in Fig. 5.8) were interpreted as a sequence of 4-5 km of low density syn-rift sediments. A better control of both the vertical density distribution and the depth to the basement is provided by the wells indicated in the same figure. The gravity model agrees with the structural information of the basin obtained by independent data (Ojeda, 1982). The eastern half of the Reconcavo basin is situated over a slightly attenuated crust (about 5 km). In contrast to the Tucano basin, the Neocomian sequence dominates the Reconcavo basin.

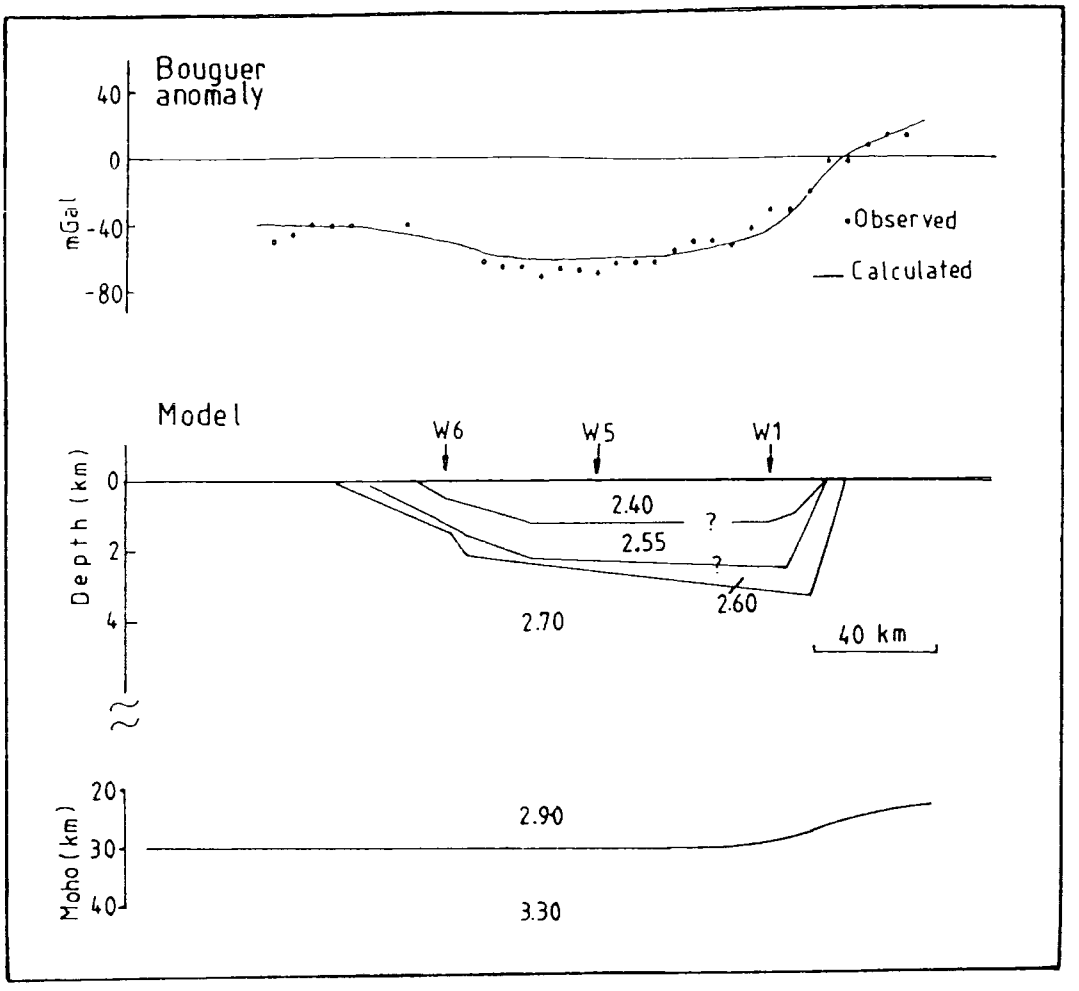

Fig. 5.12c- Gravity model of the Recôncavo basin. Profile C-C' of Fig. 5.8. Density in g cm^{-3} . The arrows indicate the wells W1, W5, W6 used to obtain the depth of the Lower Cretaceous sequences.

Fig. 5.13 shows the profile A-A' which is indicated in Fig. 5.8. This profile cuts obliquely the Tucano basin and is perpendicular to the continental margin Jacuipe basin. A simplified gravity model of the onshore Tucano and offshore Jacuipe basin is shown together with the modelling of the Moho. The Jacuipe basin is the least well known basin. Information about the stratigraphy and density of the sediments of this section of the continental margin was not available. Therefore, a density value of 2.30 g cm^{-3} was assumed in the present modelling. The steep negative free-air anomaly of 75 mGal in amplitude was modelled as a local wedge of low density sediments which forms the Jacuipe basin. A depth of about 4 km is estimated for this basin. The gravity model shows a lack of positive anomalies flanking the borders of the Tucano basin suggesting a flat Moho topography beneath the basin. To the east of the Tucano basin, the positive gradient of the gravity field towards the continental margin is modelled as due to a relative shallowing of the Moho. The thickness of the continental crust is highly attenuated under the Jacuipe basin.

The gravity model of the Sergipe-Alagoas basin (profile B-B' in Fig. 5.8) is based on the structural map of the basin published by Asmus and Ponte (1973). The gravity data over the offshore part of the basin were obtained from the Free-air anomaly map of Rabinowitz and Cochran (1978). The gravity model of this basin, which is presented in Fig. 5.14, suggests a crustal attenuation of 18 km occurring over a distance of 15-20 km. The outline of the

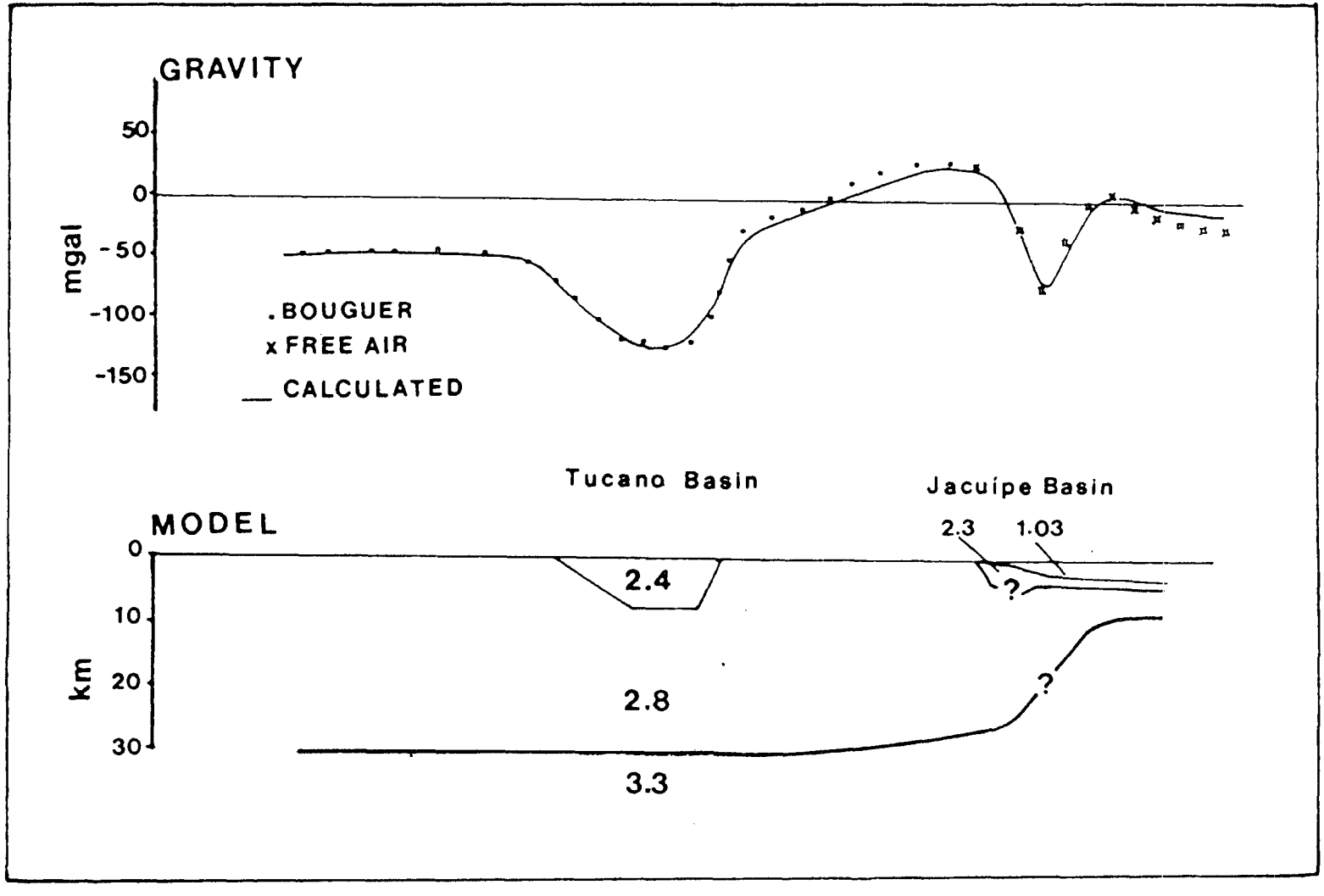

Fig. 5.13 - Simplified gravity model of Tucano and Jacuípe basins. Profile A-A' in Fig. 5.8. Density in g cm^{-3}.

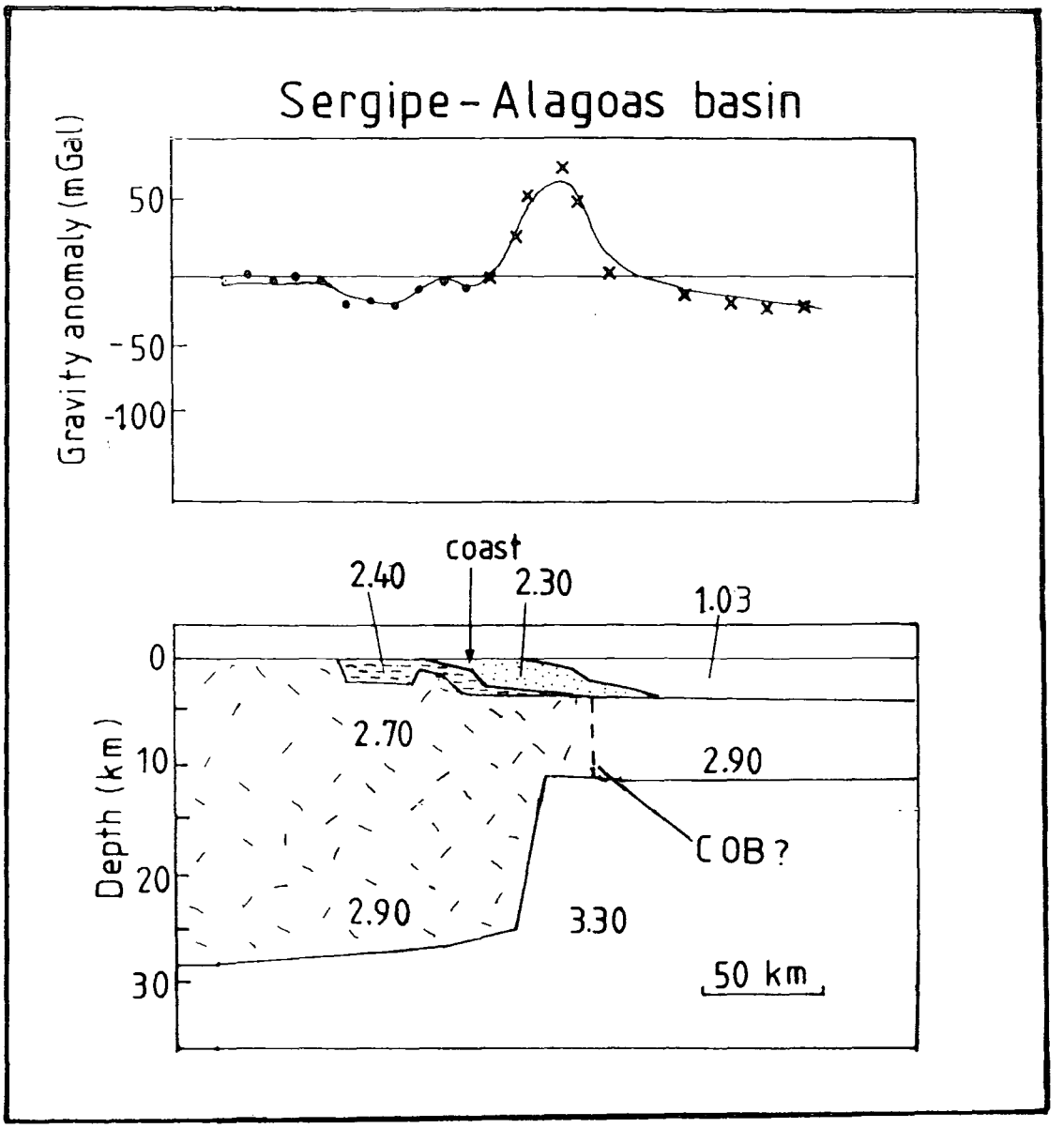

Fig. 5.14 - Gravity model of the Sergipe-Alagoas basin. Profile B-B' in Fig. 5.8. Density in g cm^{-3} .

Moho topography, shown in Fig. 5.13 and Fig. 5.14, indicates a very rapid transition from normal continental crust towards an attenuated (transitional?) continental crust or oceanic crust. The exact position of the continental oceanic crustal boundary is not known. However, based on magnetic anomalies, Rabinowitz and LaBrecque (1979) and Rabinowitz (1982) have suggested that the oceanic crust starts at about 2000 metres water depth.

5.2.4 The isostatic compensation of the onshore basins.

The lack of positive anomalies flanking the borders of the onshore basins suggests that the compensation of the low density sediments is not accomplished locally (Airy isostasy) but the basins may be sustained without local compensation by a strong lithosphere. The observed negative anomalies are totally accounted for by the sediments which infill the basins.

In order to estimate the flexural rigidity of the lithosphere in the region, and the way in which the sediments are compensated, an elastic plate rheology was assumed. By following the same procedure outlined in Chapter 3, section 3.2.2, the compensating gravity effect of the low density sediments which infill the basin can be predicted by calculating the deflection of the Moho and its gravity effect. The one dimensional equation of deformation W(k) of an elastic plate with a negative load on top caused by the sedimentary basin, is written in the wavenumber domain as

$$D\ k^4\ W(k) + \rho_m g\ W(k) = -\Delta\rho_1 g\ B(k)$$

where $B(k)$ is the spectral representation of the depth of the basin, $\Delta\rho_1$ is the density contrast between the sediments and the crust, $\Delta\rho$ is the density contrast between the mantle and the crust and D is the flexural rigidity. The deformation $W(k)$ is written as

$$W(k) = \frac{\Delta\rho_1}{\rho_m}\left[1 + \left(D\ k^4 / \rho_m\ g\right)\right]^{-1} B(k)$$

By calculating the inverse Fourier transform of $W(k)$ the deflection of the Moho $w(x)$ is easily obtained. The gravity effect can be calculated using Parker's method (1972) as already discussed in Chapter 3 section 3.2.2.

$$g(x) = F^{-1}\ [\ G_T(k)]$$

where

$$G_T(k) = -2\pi\ G\Delta\rho \exp(-k\ z_m)\ \sum_{n=1}^{M} \frac{k^{n-1}}{n!} F\ [\ w(x)^n\ ],$$

F is the Fourier transform

F^{-1} is the inverse Fourier transform

z_m is the depth of the Moho, G is the gravitational constant and M is the maximum order of the series.

The Moho topography and respective gravity effect are shown in Fig. 5.15 for different values of the effective elastic thickness Te. The compensating gravity effect predicted by a local compensation is shown for an elastic plate with zero thickness. For low flexural rigidity lithosphere, the observed gravity field should present positive anomalies flanking the sides of the basins as in Fig. 5.15a. The minimum elastic thickness in which no significant Moho upwarp is predicted is approximately 50-80 km. For this effective flexural rigidity, a maximum upwarp of the Moho of about 2 km is obtained (Fig. 5.15b). The long wavelength gravity effect of 10 mGal will only appear as a regional component of the gravity field. Therefore, the lithosphere is rigid enough to sustain the basin without any significant deflection.

An effective elastic thickness of 40 km suggests that the thermal structure of the lithosphere under the onshore basins has not been modified significantly during and after the formation of the basins. This result agrees with the subsidence history of the onshore basins which is characterized by short lived subsidence and little, if any, thermal subsidence.

5.3 The mechanism of formation of the onshore basins.

Recent studies of passive margins basins (Steckler and Watts, 1978; Royden and Keen, 1980; De Charpal et al., 1978) have demonstrated the applicability of McKenzie's model (McKenzie,

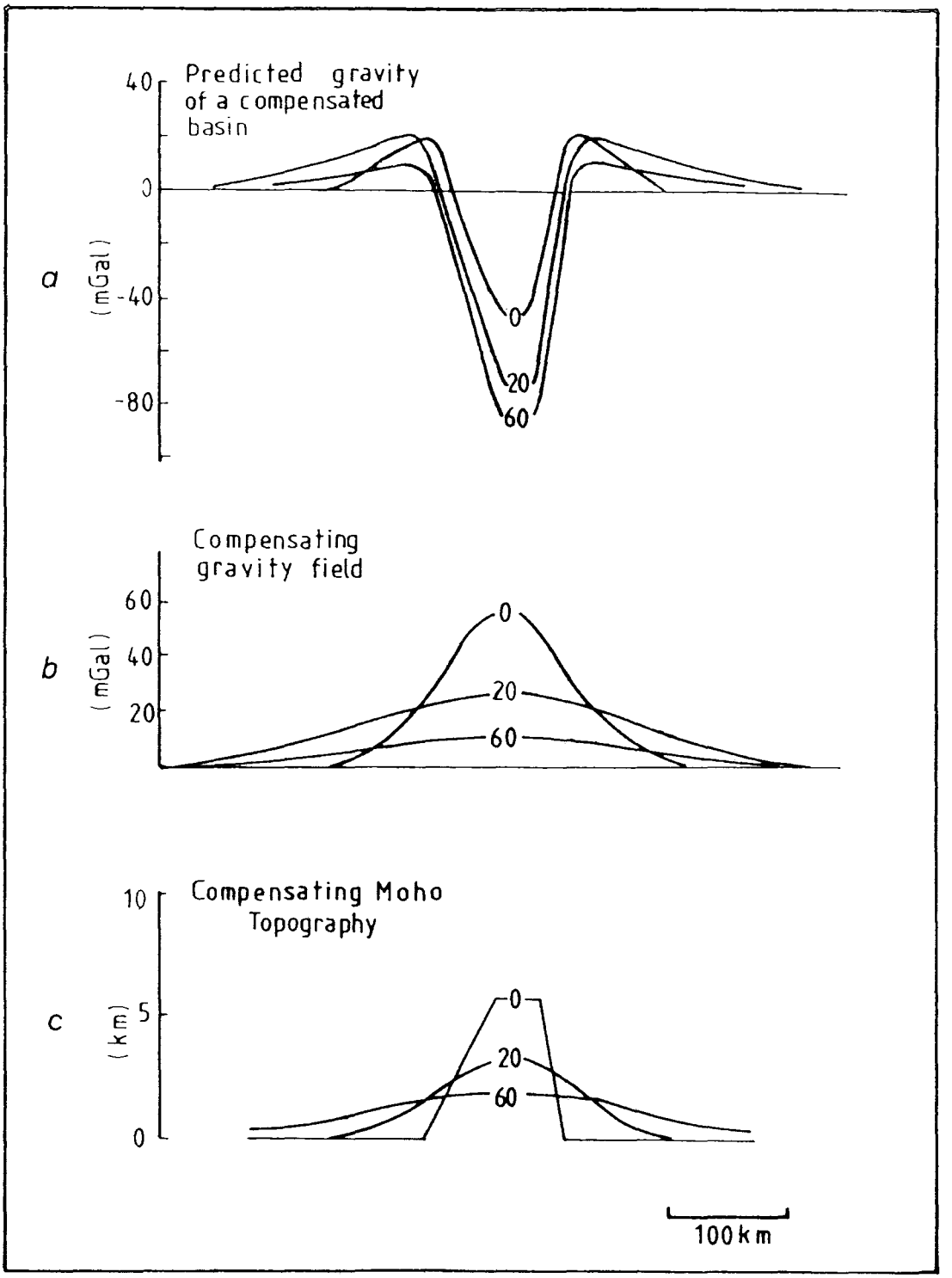

Fig. 5.15 - Flexural response at the Moho and respective gravity effect predicted by the compensation of the Tucano basin (Fig. 5.12a) in an elastic plate of different effective elastic thicknesses, which are given in km.

1978) in quantitatively evaluating and predicting the history of subsidence of the continental margins. The rifting stage initiates with lithospheric extension and crustal attenuation due to stretching. An increase in the thermal gradient is caused by the passive upwelling of the asthenosphere. The crust extends uniformly by normal faulting, of possible listric type in the brittle upper crust and by ductile deformation of the lower crust. The initial isostatic subsidence is dependent on the initial crustal and lithospheric thicknesses and on the amount of extension. The rift phase is regarded as instantaneous (less than 25 Ma) and it is followed by further subsidence caused by the isostatic response to the cooling and thermal contraction of the lithosphere, after the cessation of the extensional regime and the onset of sea floor spreading. The thermal subsidence, which can be amplified by sedimentary loading, is characterized by a rate of subsidence which decreases exponentially with a time constant of 50 - 100 Ma.

This simple model of extension and subsequent modifications (Watts et al., 1982; Royden and Keen, 1980; Hellinger and Sclater, 1983) fails to explain the way the onshore Tucano and Jatoba basins were formed. The stratigraphy of these basins shows that they are characterized by short lived subsidence which terminated in the Aptian. The sedimentation of the onshore basins was synchronous with the rift phase of the offshore Sergipe-Alagoas and Gabon basins. However, when the offshore basins went into the thermal phase of subsidence, the onshore basins stopped subsiding.

This subsidence pattern is also compatible with the present crustal structure inferred from the gravity interpretation. The absence of detectable Moho topography beneath the onshore basins suggest that the local thermal structure was not significantly altered during their formation. Crustal attenuation occurred further to the east, beneath the offshore basins, where the deposition of 3-4 km of syn-rift sediments is followed by further subsidence of about 4 km after the initiation of sea floor spreading.

Therefore, a problem of balancing the upper crust and lower crust deformation exists if the opening of these onshore and offshore basins is analysed within the context of uniform extension. However, if a different mode of lithospheric extension, such as the "simple shear" model proposed by Wernicke (1981,1985) and Wernicke and Burchfiel (1982) is considered, balancing of differential stretching of the upper crust in the region and lower crust and lithosphere in another region can be achieved across a low angle detachment fault. The idea presents a mechanical solution to many geological problems where upper crust extension in one region needs to be balanced against lower lithosphere deformation in another region.

In the context of the opening of the South Atlantic, such a detachment fault allowed the opening of the onshore basins during the rifting stage without significant deformation of the lower crust underneath. The lower crust extension which compensates

this upper crust extension was occurring, at the same time, further to the east in the region of the present continental margin.

The existence of a detachment is reinforced by the temporal link between the evolution of the onshore basins and the continental margin basins. Synchronous sedimentation occurred in the onshore and offshore basins during the rifting stage (Upper Jurassic - Lower Cretaceous to Aptian). In the late Aptian, sedimentation stopped in the onshore basins and it went into the thermal phase in the offshore basins at the time of the onset of sea floor spreading.

It is possible that the detachment fault, which is postulated to explain the formation of the Brazilian onshore and offshore basins, represents the basal contact between the Sergipano fold belt and the São Francisco craton (Fig. 5.1). The Sergipano fold belt is composed of at least 5 km of greenschist to amphibolite facies metasediments which were thrusted and folded against the São Francisco in the Upper Proterozoic (Jardim de Sá et al., 1981). The NW Vaza Barris thrust fault (see Fig. 5.6b) appears to control the separation of the onshore central Tucano from the northern Tucano sub-basin and the Sergipe-Alagoas basin from the Jacuipe basin, in the offshore region. Apparently, the onshore basins cross cut the Upper Proterozoic Sergipano fold belt. However, the net displacement of the hanging wall, which led to the opening of the onshore basins, and in particular of the Tucano

basin, was parallel to the NNW thrust faults. This observation suggests a close relationship between the distribution of these onshore basins and the tectonic fabric of the Proterozoic fold belt.

The sequence of evolution of the onshore and offshore basins can be visualized by reconstructing the pre-drift configuration of this part of the the Brazilian continental margin. The African counterpart of this segment of the Brazilian continental margin is the present continental margin off Gabon. The plate reconstruction using the isobath of 2000 metres is shown in Fig. 5.16. An approximate outline of the African equivalent of the Sergipano fold belt is also presented in the same diagram. The correlation of this fold belt in Brazil and Africa was carried out by Allard and Hurst (1969). The pre-Jurassic basement of Gabon basin is composed of Upper Proterozoic remnants (Allard and Hurst, 1969) and Palaeozoic marine sediments (Klasz, 1978). In contrast to its Brazilian counterpart which is the Jacuipe basin, the Gabon basin (Fig. 5.17) is a well developed passive margin basin with a total width of 200 km perpendicular to the margin. The thickness of syn-rift sediments is as much as 6 km in some parts of the basin and 3 to 4 km of post-rift sediments are cut by massive salt diapirs (Driver and Pardo, 1974; Brink, 1974). The postulated sequence of evolution of this part of the Brazilian and African continental margin is illustrated in Fig. 5.18(a,b,c,d).

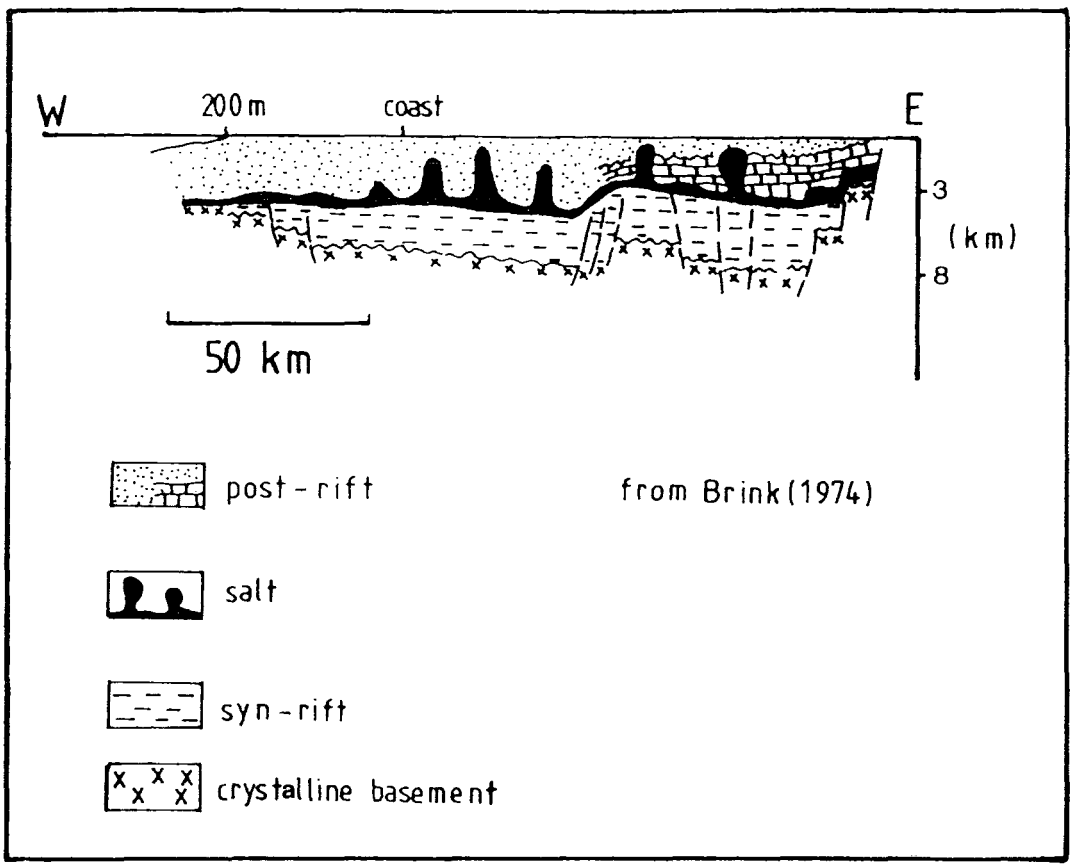

Fig. 5.16 - Simplified cross section across the Gabon basin based on Brink (1974).

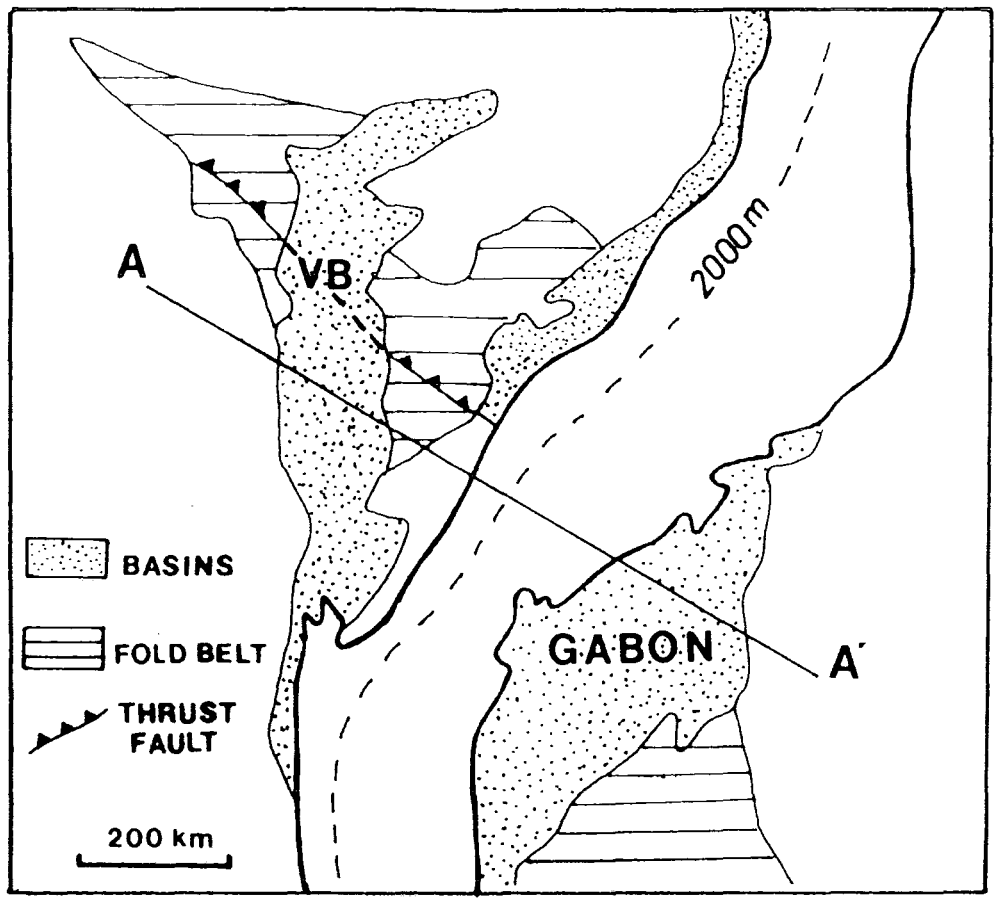

Fig. 5.17

- Pre-drift reconstruction of the Brazilian and African continental margins. A-A' is the profile considered in Fig. 5.18.
VB = Vaza Barris Fault.

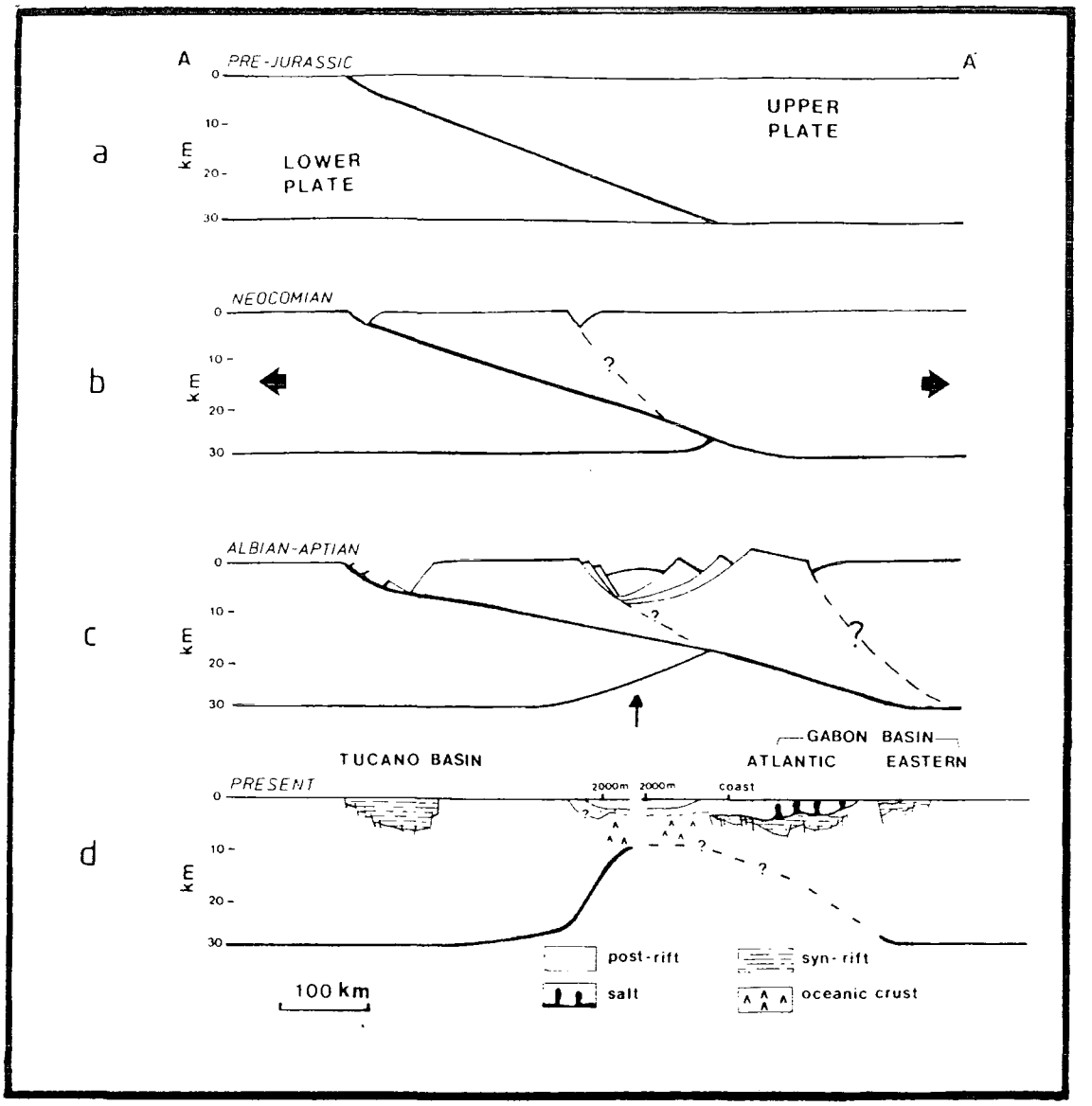

Fig. 5.18 - Model of evolution of the Brazilian and African continental margins and South Atlantic opening. The arrow in (c) indicates the approximate position of initiation of sea floor spreading.

In Fig. 5.18a the postulated detachment is supposed to cut the entire crust, dipping towards the African continent. The lower "plate" represents the South American continent whereas the upper "plate" contains the Sergipano fold belt and the African continent. The extension started in the Upper Jurassic and continued throughout the Lower Cretaceous (Fig. 5.18b) with the opening of the Tucano basin and, synchronouly, the opening of the Jacuipe and Gabon basins in the region of the present continental margins. The opening of the Tucano basin was controlled by a low angle detachment fault, with a relative eastward movement of the upper plate and collapse of the hanging wall. Faulting was restricted to the upper crust. The upper crustal extension was taken up by lower lithospheric extension in the region where the South Atlantic was starting to form.

At the end of the Albian (Fig. 5.18c), the extension ceased and the Tucano basin stopped subsiding. The final break up and subsequent sea floor spreading apparently started near the present Brazilian coast which resulted in an assymetric distribution of continental margin basins at this latitude.

Fig. 5.18d shows the present distribution of basins at the margin of the Brazilian and African continents.

5.4 Conclusions

A short lived subsidence (< 25 Ma) with an accumulation of up to 7 km of sediments, with no evidence of lower crustal attenuation nor thermal subsidence, characterizes the evolution of the onshore Reconcavo, Tucano and Jatoba basins. These basins were formed during the rifting stage of the South Atlantic opening. A model of basin formation based on an uniform extension of the lithosphere fails to explain the linked evolution of the onshore and offshore basins at this latitude of the Brazilian continental margin. A mechanism in the lines of Wernicke's simple shear model in which upper crust extension in one region is connected to and balanced against lower lithospheric extension in another region by intracrustal detachment appears to be more adequate to explain the way the onshore basins were formed. This detachment may have also played an important role in controlling the distribution of basins off Brazil and Africa.

CHAPTER SIX

Conclusions and Discussion

6.1 The Isostatic Analysis of Bahia State

The results of the application of the isostatic response function analysis to Bahia State gravity and topographic data show that, by taking into account both the surface and subsurface loads, an elastic plate with a minimum thickness of 20 to 40 km explains the compensation of the northern São Francisco craton. This result confirms Forsyth's explanation why abnormally low flexural rigidities were obtained in previous application of the same technique to continental areas (Banks et al., 1977; McNutt and Parker, 1978). Low flexural rigidities were obtained because the observed isostatic response function has been interpreted in the context of an elastic plate loaded only on top and because the compensation of the surface topography was assumed to be at a single depth, at the Moho. In the particular case of Bahia State isostatic response function, the result obtained cannot be interpreted within the context of a plate loaded from the top only. Subsurface loads must be present in the centre of the São Francisco craton.

Based on the geological history of the Espinhaço Fold System, two possible subsurface loads, which are not mutually exclusive,

were considered in interpreting the observed isostatic response function. Firstly, the observed topography may be partly or wholly compensated near the surface by a low density upper crust (5-10 km) composed mainly of granites with subordinate acid volcanics and metasediments. The Paramirim complex granite discussed in Chapter 4 is a major part of this subsurface load. The amplification of the observed response function of Bahia State at λ=400 km may be caused by a second subsurface load associated with a thickening of the crust beneath the Espinhaço Fold System.

Both subsurface loads produce topography from within as a flexural response to the buoyant effect of the low density upper crust and crustal root at the base of the crust.

The result of this study is consistent with the apparent increase of flexural rigidity with the thermal age of lithospheric plates. This is shown by plotting the result of the present study with the results obtained by Karner et al. (1983) (Fig. 6.1). The minimum thickness of the elastic plate inferred in the present study may be between 20 and 40 km and the age of the last thermal event is between 1.0 and 0.5 Ga. However, because the isostatic response function presents the same ambiguity of the gravity method, the lack of independent constrain such as the topography of the Moho or the average depth of the low density rocks in the Espinhaço Fold System limits the inference of both the upper bound of the flexural

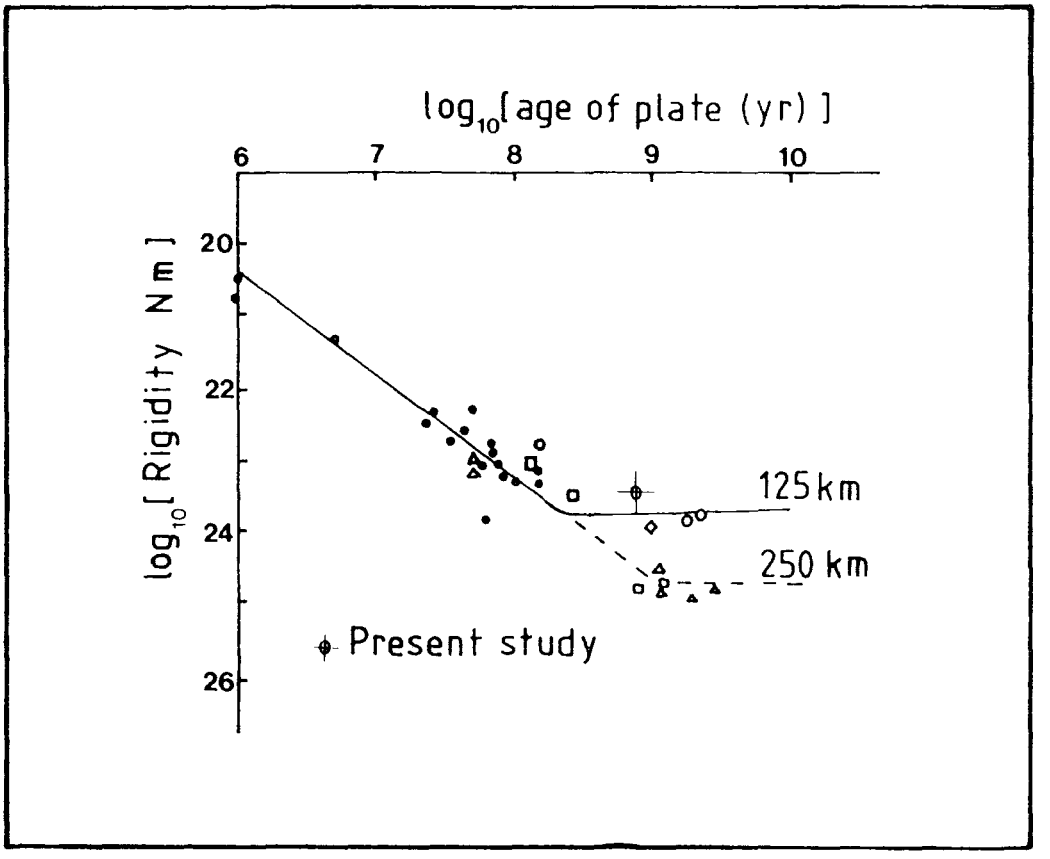

Fig. 6.1 - Flexural rigidity of the northern São Francisco craton in comparison with the results of oceanic and continental flexural studies after Karner et al. (1983). Dots for oceanic studies and open symbols for continental studies.
Continuous and broken curves are the values of flexural rigidity as a function of the thermal age of the plate, predicted by a cooling 125 km and 250 km thick plate model.

rigidity and the relative importance of the two subsurface loads considered in this study. A seismic survey across the Espinhaço Fold System is therefore necessary before a definitive conclusion about the compensation mechanism and the flexural rigidity of the lithosphere in this region are drawn.

6.2 Gravity Study of the Paramirim Complex Granite.

The large and high amplitude negative gravity anomaly, which is situated at the western border of the Paramirim complex and near the Espinhaço fold belt, is interpreted as having been produced by a granite of batholithic dimension. A deep seated source of anomaly such as an abnormally thickening of the crust was ruled out by using the criterion of maximum depth of the anomalous gravitating body. There is not a correlation between the metasediments and this local negative anomaly. This rules out the possibility of sediments being the main source of this anomaly.

The only plausible source of the negative anomaly is, therefore, a granitic intrusion which is not conspicously exposed in the region where the negative gravity anomaly is observed. The possibility of granites being the main cause of the anomaly is reinforced by the widespread presence of granites in the gneissic and migmatitic basement of the Paramirim complex. The intrusion of the granites is possibly associated

with the acid volcanism which affected both the Espinhaço fold belt and the Diamantina tableland in the Middle Proterozoic (McReath et al., 1981).

Assuming that the regional field is produced by a slight thickening of the crust, a two dimensional modelling of the granite yielded an estimated thickness of 13 km for a density contrast of -0.1 g cm^{-3}. This depth decreases to about 8 km if a density contrast of -0.15 g cm^{-3} is assumed instead. These figures may increase by 2 km if the source of the regional field is entirely ascribed to a near surface low density rocks. The granite extends laterally from underneath the Espinhaço fold belt towards the centre of the Paramirim complex (35 km). It is very likely that the sides of the granite slope outwards. Considering that the granite batholith extends for about 200 km along its NW strike, the estimated volume of low density granitic rocks is about $7x10^4$ km^3.

The lack of detailed geological information does not allow us to relate with certainty the time of intrusion of this granitic batholith with the Espinhaço orogeny. It is possible that the large circular non-foliated K-rich granites found to the southwest of Paramirim city are the exposed part of the granite batholith. If so, the radiometric dates obtained by Jardim de Sá et al. (1976a) suggest that the granite could be either syntectonic or it postdates the Espinhaço orogeny (1.3 Ga). The discovery of this non-exposed granite may provide new evidence

to clarify some geological aspects of the area.

A detailed gravity survey, combined with a careful density sampling, across the Espinhaço Fold System is a suggestion for further work to improve the details of this dubiously exposed anomalous body. This work should be combined with a detailed geological study of the region to search for the granite and determine its age. An interpretation of the large negative magnetic anomaly to the south of Paramirim city may also provide further constrain on the deep structural relation between the granite and the country rocks.

6.3 Gravity and Stratigraphic Studies of the Mesozoic to Tertiary basins.

The history of subsidence of the onshore Reconcavo, Tucano and Jatoba basins indicates that these basins were entirely formed during the rifting stage of the South Atlantic opening. Up to 7 km of sediments were deposited in less than 25 Ma during the Upper-Jurassic to the Aptian. The continental margin basins record the syn-rift sedimentation and is followed by thermal subsidence which started with the onset of the sea-floor spreading in the late Albian. The onshore basins are characterized by negative gravity anomalies which range from 50 to 110 mGal and there is no indication of flanking positive anomalies. This suggests a lack of significant Moho upwarp

beneath the Reconcavo, Tucano and Jatoba basins. 7 km of sediments, which account totally for the observed negative gravity anomaly, are supported by a stronger lithosphere. Such inference from the gravity study indicates that the thermal structure beneath these basins was not altered during and after their formation. This agrees with the subsidence history of these onshore basins which records little, if any, thermal subsidence. Crustal attenuation, syn-rift sedimentation and post-rift sediments associated with thermal subsidence are only observed in the continental margin basins. There is, therefore, a relay in the lithospheric extension between the onshore and offshore basins. This suggests that the Brazilian onshore and offshore basins, and their counterpart African basins were formed by non-uniform extension during the rifting of the South Atlantic Ocean.

A model in the lines of Wernicke (1982, 1985) in which the balance of deformation is accomplished across a major detachment (or decollement) fault is a possible mechanism to explain the non-uniform extension during rifting. This also confirms Bott's (1982) suggestion that, during rifting, upper crustal extension may occur beyond the limit of 50-100 km where lower crust deformation takes place. Any attempt to balance the lower crust and upper crust extension within a narrow region around the continental margin is likely to be unsuccessful if relay in upper crust and lower lithosphere extension has occurred. In the context of balancing the extension across continental

margins, the pre-drift reconstruction is necessary, since, as a general rule, complementary rifted margins are not symmetrical. With the onset of sea floor spreading, the basin which was formed by upper crustal extension may be left on one side of the rifted margin whereas the basin overlying a more attenuated lower crust is now found on the complementary margin.

In the particular case of the Brazilian onshore and offshore basins and the complementary Gabon basin, it appears that the distribution of these basins was controlled by detachment faults. It is still unclear whether these detachments are reactivation of pre-existing faults or whether they are created during the extensional regime. Information on the characteristics of extended crust, topography of the Moho and on how these detachments are accomodated at deeper levels are still to be obtained from deep seismic sounding across continental margins.

As further work, along the line of the present study, it would be useful to carry on a comparative quantitative subsidence study of the Brazilian and African basins system at this latitude of the South Atlantic margin in order to estimate whether the upper crustal extension, which formed the onshore Brazilian basins, was taken up by lower crustal extension in the Gabon basin. In this case, there should be as surplus of lower crustal attenuation and post-rift sedimentation compared with the amount of stretching predicted either by fault

reconstruction or the amount of syn-rift sedimentation in the Gabon basin.

Another question raised in analysing the mechanism of continental rifting leading to formation of a new ocean floor concerns with the mechanical and thermal factors which control the position of lithospheric break-up and the initiation of sea floor spreading. Has the postulated detachment somehow controlled the position of the initiation of sea floor spreading to occur near the present Brazilian coastline?

REFERENCES

Allard, G.O.; Hurst, V.J. (1969)
Brazil-Gabon geologic link supports continental drift. Science, 163, 528-532.

Almeida, F.M.M. de (1977)
O Craton do São Francisco. Revta. bras. Geoc., 7(4), 349-364.

Almeida, F.F.M.; Hasui, Y.; Brito Neves, B.B.; Fuck, R.A.(1981)
Brazilian Structural Provinces: An Introduction. Earth Sci. Rev., 17, 1-29.

Amaral, G.; Kawashita, K. (1967)
Determinacao da idade do grupo Bambui pelo metodo Rb/Sr in Anais do XXI Congresso Brasileiro de Geologia, SBG, Belo Horizonte, 214-217.

Artemjev, M.E.; Artyushkov, E.V. (1971)
Structure and isostasy of the Baikal rift and the mechanism of rifting. J. geophys. Res., 76, 1179-1211.

Asmus, H.E.; Ponte, F.C. (1973)
The Brazilian Marginal Basins in The Ocean Basins and Margins: The South Atlantic, edited by A.E.M. Nairn and F.G. Stehli, Plenum Press, N.Y., vol.1, 87-133.

Bally, A.W. (1981)
Atlantic Type Margins in Geology of Passive Continental Margins AAPG Eastern Section Meeting Course Note Series no. 19, 1-48, AAPG, Tulsa.

Banks, R.J.; Parker, R.L.; Huestis, S.P. (1977)
Isostatic Compensation on a Continental Scale: Local versus Regional Mechanisms. Geophys. J. R. astr. Soc., 51, 431-452.

Banks, R.J.; Swain, C.J. (1978)
The Isostatic Compensation of East Africa. Proc. R. Soc. Lond. A, 364, 331-352.

Barbosa, O.; Costa, L.A.M. (1973)
Relatorio do Projeto Leste do Tocantins/Oeste do Rio São Francisco. DNPM/CPRM/Prospec S.A. (unpublished report)

Barraclough, D.R.; Harwood, J.M.; Leaton, B.R.; Malin, S.R.C. (1978)
A Definitive Model of the Geomagnetic Field and its Secular Variation for 1967. I. Derivation of Model and Comparison with the IGRF. Geophys. J. R. astr. Soc., 55, 111-121.

Bendat, J.S.; Piersol, A.G. (1966)
Measurement and Analysis of Random Data. John Wiley & Sons, N.Y., 390 pp.

Beurlen, K. (1967)
A Estrutura Geologica do Nordeste do Brasil in Anais do XXI Congresso Brasileiro de Geologia. SBG, Curitiba, 151-158.

Blitzkow, D.; Gasparini, P.; Mantovani, M.S.M.; Sa', N.C. de (1978)
Crustal Structures of SE Minas Gerais, Brazil deduced from gravity measurements. Revta. bras. Geoc., 9, 39-43.

Bloomfield, P. (1975)
Fourier Analysis of Time Series: An Introduction. John Wiley & Sons, N.Y., 258 pp.

Bott, M.H.P.; Smith, R.A. (1958)
The estimation of the limiting depth of gravitating bodies. Geophys. Prosp., 6, 1-10.

Bott, M.H.P.; Day, A.A.; Masson-Smith, D. (1958)
The Geological interpretation of Gravity and Magnetic surveys in Devon and Cornwall. Phil. Trans. R. Soc. A, 251, 161-191.

Bott, M.H.P.; Smithson, S.B. (1967)
Gravity investigations of subsurface shape and mass distribution of granite batholiths. Geol. Soc. Am. Bull., 78, 859-878.

Bott, M.H.P. (1967)
Geophysical investigation of the northern Penine basement rocks. Proc. Yorks. geol. Soc., 36, 139-168.

Bott, M.H.P. (1982)
Stress Based Tectonic Mechanism at Passive Continental Margins in Dynamics of Passive Margins edited by R.A. Scrutton Geodynamics Series v. 6, AGU, 147-153.

Brink, A.H. (1974)
Petroleum Geology of Gabon Basin. Bull. Am. Ass. Petrol. Geol., 58, 216-235.

Brito Neves, B.B. de; Cordani, U.G.; Torquato, J.R.F. (1980)
Evolução geocronologica do Precambriano do Estado da Bahia in Geologia e Recursos Minerais do Estado da Bahia, edited by H.A.V. Inda and F.B. Duarte, SME/CPM, Salvador, vol. 3, 1-101.

Burke, K.; Dewey, J.F.; Kidd, W.S.F. (1977)
World distribution of sutures - the sites of former oceans. Tectonophysics, 40, 69-99.

Campos, C.W.M.; Ponte, F.C.; Miura, K. (1974)
Geology of Brazilian continental margin in The Geology of Continental Margins edited by C.A. Burk and C.L. Drake. Springer & Verlag, N.Y., 447-461.

Cloud, P.; Dardenne, M. (1968)
Proterozoic age of the Bambui group in Brazil. Geol. Soc. Am. Bull., 84, 1673-1676.

Cohen, C.R. (1985)
Role of fault rejuvenation in hydrocarbon accumulation and structural evolution of Reconcavo basin, Northeastern Brazil. Bull. Am. Ass. Petrol. Geol., 69, 65-76.

Cordani, U.G. (1973)
Evolução Geologica Precambriana da Faixa Costeira do Brasil entre Salvador e Vitoria. (unpublished thesis). Universidade de São Paulo, 98 pp.

Cordani, U.G.; Iyer, S.S. (1979)
Geochronological investigation on the Precambrian granulitic terrain of Bahia, Brazil. Precambrian Res., 9, 255-274.

Correira, E.G. (1965)
Contribuição da refração sismica no delineamento do arcabouco estrutural da Bacia de Jatoba. (Petrobras internal report), 27pp.

Dardenne, M.; Walde, H.G. (1979)
A estratigrafia dos grupos Bambui e Macaubas no Brasil central. Bol. Nucl. Minas Gerais. Soc. Bras. Geol. Belo Horizonte 1, 43-52.

De Charpal, O.; Guennoc, P.; Montadert, L.; Roberts, D.G. (1978)
Rifting, crustal attenuation and subsidence in the Bay of Biscay. Nature, 275, 706-711.

DNPM/CPRM (Departamento Nacional da Produção Mineral) (1980)
Report on the Bambui Drilling Project. Belo Horizonte.

Dorman, L.M.; Lewis, B.T.R. (1970)
Experimental isostasy. 1. Theory of the determination of the earth's isostatic response to a concentrated load. J. geophys. Res., 75, 3357-3365.

Driver, E.S.; Pardo, G. (1974)
Seismic Traverse across the Gabon continental margin in The Geology of Continental Margins edited by C.A. Burk and C.L. Drake. Springer & Verlag, N.Y., 293-295.

Emery, K.O.; Uchupi, E. (1984)
The Geology of the Atlantic Ocean, Springer Verlag, N.Y., 1050 pp.

Enmark, T. (1981)
A Versatile Interactive Computer Program for Computation and Automatic Optimization of Gravity Models. Geoexploration, 19, 47-66.

Espourteille, F.; Fleisher, R. (1980)
A Mina de Boquira in Geologia e Recursos Minerais do Est. da Bahia edited by H.A.V. Inda and F.B. Duarte - CPM/SME, Salvador, vol. 3, 104-124.

Fitch, F.J.; Miller, J.A. (1973)
Dating granites by the Potassium-Argon method in Spec. Publ. Geol. Soc. S. Africa 3 Simposium on granites, gneisses and related rocks edited by L.A. Lister, 219-225.

Forsyth, D.W. (1979)
Lithospheric Flexure. Rev. geophys. Space Phys., 17, 1109-1114.

Forsyth, D.W. (1981)
Can the strength of the lithosphere be inferred from the average relationship between topography and gravity anomalies? (abstract) Eos Trans. AGU, 62, 1032.

Forsyth, D.W. (1985)
Subsurface loading and estimates of the flexural rigidity of continental lithosphere. J. geophys. Res., 90, 12623-12632.

Gibbs, R.A. (1968)
The densities of Precambrian rocks from northern Manitoba. Can. J. Earth Sci., 5, 433-438.

Giese, P.; Schutte, J. (1975)
Preliminary results of seismic measurements in the Brazilian Coastal Mountains. (unpublished report, Univ. Freiberg)

Gomes, R.A.A.D.; Motta, A.C. (1978)
Projeto levantamento gravimetrico no Est. da Bahia Preliminary report. Text and maps. DNPM/CPRM, Salvador, 139 pp.

GPCP (1973)
A General Purpose Contouring Package. Calcomp, California.

Hasui, Y.; Cordani, U.G. (1968)
Idade K/Ar de rochas eruptivas Mesozoicas do Oeste Mineiro e sul de Goias in Anais do XXII Congresso Brasileiro de Geologia, Belo Horizonte, 139-143.

Hellinger, S.J.; Sclater, J.G. (1983)
Some comments on 2-layer extensional models for the evolution of sedimentary basins. J. geophys. Res., 88, 8251-8269.

Hetenyi, M. (1946)
Beam on Elastic Foundation, University of Michigan Press, Ann Arbor, 255 pp.

Hettich, M. (1977)
Glaciação Proterozoica no centro norte de Minas Gerais. Revta. bras. Geoc., 7, 85-101.

Inda, H.A.V.; Barbosa, J.F. (1978)
Texto Explicativo para o Mapa Geologico do Est. da Bahia 1:1,000,000 scale map. CPM/SME Salvador, 137 pp.

Inda, H.A.V.; Schorscher, H.D.; Dardenne, M.A.; Schobbenhaus, C.; Haralyi, N.L.E.; Branco, P.C.A.; Ramalho, R. (1984)
O craton do São Francisco e a faixa de dobramentos Araçuai in Geologia do Brasil explanatory text of 1:2,500,000 scale map edited by Schobbenhaus, C.; Campos D.A.; Derze, G.R.; Asmus, H.E., DNPM, Brasilia, 193-248.

Jardim de Sa', E.F.; Bartels, R.L.; Brito Neves, B.B.; McReath, I. (1976a)
Geocronologia e o modelo tectonomagmatico da Chapada Diamantina e Espinhaço Setentrional in Anais do XXIX Congresso Brasileiro de Geologia, Ouro Preto SBG, vol. 4, 205-227.

Jardim de Sá, E.F.; McReath, I.; Brito Neves, B.B.; Bartels, R.L. (1976b)
Novos dados geocronologicos sobre o craton do São Francisco no Est. da Bahia in Anais do XXIX Congresso Brasileiro de Geologia, Ouro Preto, vol 4., 184-204.

Jardim de Sá, E.F. (1981)
A Chapada Diamantina e a Faixa Sto. Onofre: um exemplo de tectonica intra-placa no Proterozoico medio do Craton do Sao Francisco in Geologia e Recursos Minerais do Estado da Bahia, SME/CPM, Salvador, vol 4, 111-120.

Jardim de Sa', E.F.; Legrand, J.M.; Hackspacher, P.C. (1981)
Contraste de estilos estruturais e matamorficos na faixa dobrada Sergipana. Revta. bras. Geoc., 11, 126-137.

Jeffreys, H. (1976)
The Earth. Cambridge University Press, London, 420 pp.

Karner, G.D.; Watts, A.B. (1982)
On isostasy at Atlantic-type continental margins. J. geophys. Res., 87, 2923-2948.

Karner, G.D.; Steckler, M.S.; Thorne, J.A. (1983)
Long-term thermo-mechanical properties of the continental lithosphere. Nature, 304, 250-253.

Karner, G.D.; Watts, A.B. (1983)
Gravity anomalies and flexure of the lithosphere at mountain ranges. J. geophys. Res., 88, 10449-10477.

Keen, C.E. (1982)
The Continental Margins of Eastern Canada: A Review in Dynamics of Passive Margins edited by R.A. Scrutton Geodynamics Series v. 6, AGU, 45-58.

Kirby, S.H. (1983)
Rheology of the lithosphere. Rev. geophys. Space Phys., 21, 1458-1487.

Klasz, I. de (1978)
The Western African sedimentary basins in Phanerozoic geology of the world The Mesozoic, A edited by M. Moullade and A.E.M. Nairn, Elsevier, Amsterdam, 371-399.

Kumar, N.; Leyden, R.; Carvalho, J.; Francisconi, O. (1979)
Sediment isopach map: Brazilian Continental Margin. AAPG Brazil Continental Margin Map Series no. 1.

Lambeck, K. (1983)
Structure and evolution of the intracratonic basins of central Australia. Geophys. J. R. astr. Soc., 74, 843-886.

Lanczos, C. (1961)
Linear Differential Operators. D. Van Nostrand, London, 564 pp.

Larson, R.L.; Hilde, T.W.C. (1975)
A revised time scale of magnetic reversals for the Early Cretaceous, Late Jurassic. J. geophys. Res., 80, 2586-2594.

Leyden, R.; Asmus, H.; Zembruscki, S.; Bryan, G. (1976)
South Atlantic Diapiric Structures. Bull. Am. Ass. Petrol. Geol., 60, 196-212.

Lesquer, A.; Almeida, F.F.M.; Davino, A.; Lachaud, J.C.; Maillard, P. (1981)
Signification structurale des anomalies gravimetriques de la partie sud du Craton de Sao Francisco (Bresil). Tectonophysics, 76, 273-293.

Lewis, B.R.R.; Dorman, L.M. (1970)
Experimental isostasy. 2. Isostatic model for USA derived from gravity and topographic data. J. geophys. Res., 75, 3367-3386.

Lima, E.A.M.; Leite, J.F. (1978)
Projeto Estudo Global dos Recursos Minerais da Bacia Sedimentar do Parnaiba. Mettalogenetic and Geological integration. DNPM/CPRM, Recife, 16 volumes.

Louden, K.E.; Forsyth, D.W. (1982)
Crustal structure and isostatic compensation near Kane fracture zone from topography and gravity measurements I. Spectral analysis approach. Geophys. J. R. astr. Soc., 68, 725-750.

Mascarenhas, J.F. (1973)
A geologia do centro-leste do Est. da Bahia in Anais do XXVII Congresso Brasileiro de Geologia, SBG, Aracaju, 36-66.

McKenzie, D.; Bowin, C. (1976)
The relationship between bathymetry and gravity in the Atlantic Ocean. J. geophys. Res., 81, 1903-1915.

McKenzie, D. (1978)
Some remarks on the development of sedimentary basins. Earth planet. Sci. Lett., 40, 25-32.

McNutt, M.K.; Parker, R.L. (1978)
Isostasy in Australia and the evolution of the compensation mechanism. Science, 119, 773-775.

McNutt, M.K. (1980)
Implications of regional gravity for state of stress in the earth's crust and upper mantle. J. geophys. Res., 85, 6377-6396.

McNutt, M.K. (1983)
Influence of Plate Subduction on isostatic compensation in Northern California. Tectonics, 2, 399-415.

McReath, I.; Jardim de Sa, E.F.; Fryer, B.J. (1981)
As vulcanicas acidas Proterozoicas da região da Bacia do Rio Paramirim, Bahia in Geologia e Recursos Minerais do Est. da Bahia, SME/CPM, Salvador, vol. 4, 121-134.

Montes, A.S.L.; Montes, M.L.; Dardenne, M.A. (1981)
A Região da Serra de Jacobina, um paleorelevo ativo durante a sedimentação dos grupos Chapada Diamantina e Bambui in Anais dos Simposio sobre o craton do São Francisco e sua faixas marginais edited by J.F. Mascarenhas, SGB/CPM, Salvador, 79-85.

Mooney, M. (1952)
Magnetic susceptibility measurements in Minnesota, Part I: Technique of measurements. Geophysics, 28, 531-543.

Motta, A.C.; Gomes, R.A.A.D.; Delgado, I.M.; Siqueira, L.P.; Pedreira, A.J. (1981)
Feições gravimetricas e magneticas do craton do Sao Francisco in Anais do Simposio sobre o craton do São Francisco e sua faixas marginais edited by J.F. Mascarenhas, SBG/CPM, Salvador, 17-33.

Nairn, A.E.M.; Stehli, F.G. (1973)
A model for the South Atlantic in The Ocean Basins and Margins: The South Atlantic. edited by A.E.M. Nairn and F.G. Stehli, Plenum Press, N.Y., vol.1, 1-20.

Oyeda, H.A.O. (1982)
Structural Framework, Stratigraphy and evolution of Brazilian Marginal basins. Bull. Am. Ass. Petrol. Geol., 66, 732-749.

Parker, R.L. (1972)
The rapid calculation of potential anomalies. Geophys. J. R. astr. Soc., 31, 447-455.

Rabinowitz, P.D.; Cochran, J.R. (1978)
Free air gravity anomalies of the continental margin off Brazil AAPG Brazil Continental Margin Map Series, no. 1 (AAPG, Tulsa)

Rabinowitz, P.D.; La Brecque, J. (1979)
The Mesozoic South Atlantic Ocean and evolution of its continental margins. J. geophys. Res., 84, 5973-6002.

Rabinowitz, P.D. (1982)
Gravity Measurements Bordering Passive Continental Margins in Dynamics of Passive Margins edited by R.A. Scrutton Geodynamics Series v. 6, AGU , 91-115.

Richardus, P.; Adler, R.K. (1972)
Map Projections for geodesists, cartographers and geographers. North Hollland Publ. Co., Amsterdam.

Royden, L.; Keen, C. (1980)
Rifting process and thermal evolution of the continental margin of eastern Canada determined from subsidence curves. Earth planet. Sci. Lett., 51, 343-361.

Schobbenhaus, C.; Campos, D.A.; Derze, G.R.; Asmus, H.E. (1984)
Geologia do Brasil. 1:2,500,000 scale map, DNPM, Brasilia.

Scrutton, R.A. (1982)
Passive Continental Margins: A Review of Observations and Mechanisms in Dynamics of Passive Margins edited by R.A. Scrutton Geodynamics Series v. 6, AGU , 5-11.

Sighinolfi, G.P.; Conceição, T.M.L. (1974)
Petrologia e geoquimica de riolitos precambrianos do oeste da Bahia (abstract) in Anais dos XXVII Congresso Bras. Geol., Porto Alegre, 406-407.

Singleton, R.C. (1969)
An Algorithm for Computing the Mixed Radix Fast Fourier Transform. IEEE Trans. Audio Electroacoustics, AU-17, 2, 93-103.

Steckler, M.; Watts, A. (1978)
Subsidence of the Atlantic type continental margin off New York. Earth planet. Sci. Lett., 41, 1-13.

Stephenson, R.; Lambeck, K. (1985)
Isostatic response of the lithosphere with In-plane stress: application to central Australia. J. geophys. Res., 90, 8581-8588.

Szatmari, P.; Milani, E.; Lana, M.; Conceição, J.; Lobo, A. (1985)
How South Atlantic rifting affects Brazilian oil reserves distribution. Oil Gas J., 14 june, 107-113.

Tavora, F.J.; Cordani, U.G.; Kawashita, K. (1967)
Determinações de idades Potassio-Argonio em rochas da região central da Bahia in Anais do XXI Congresso Bras. Geol., Salvador, 159-165.

Ussami, N.; Padilha, A.L. (1982)
Density and magnetic susceptibility measurements on crystalline rocks of Bahia State.(unpublished report, Instituto Astronomico e Geofisico, Univ. of Sao Paulo)

Viana, C.F.; Gama Jr., E.G.; Simões, I.A.; Moura, J.A.; Fonseca, J.R.; Alves, R.J. (1971)
Revisão estratigrafica da Bacia Reconcavo/Tucano. Bolm. tec. Petrobras, 14, 157-192.

Walcott, R.I. (1970)
Flexural rigidity, thickness and viscosity of the lithosphere. J. geophys. Res., 75, 3941-3954.

Watts, A.B. (1978)
An analysis of isostasy in the world's oceans. 1. Hawaiian - Emperor Seamount chain. J. geophys. Res., 83, 5989-6004.

Watts, A.B.; Karner, G.D.; Steckler, M.S. (1982)
Flexure and the evolution of sedimentary basins. Phil. Trans. R. Soc., 249-282.

Wernicke, B. (1981)
Low angle normal faults in the Basin and Range Province: nappe tectonics in an extending orogen. Nature, 291, 645-647.

Wernicke, B.; Burchfiel, B.C. (1982)
Modes of extensional tectonics. J. Struct. Geol., 4, 105-115.

Wernicke, B. (1985)
Uniform-sense normal simple shear of the continental lithosphere. Can. J. Earth Sci., 22, 108-125.

APPENDIX A

Density and Magnetic Susceptibility measurements on crystalline basement rocks of Bahia State

The results of density and magnetic susceptibility measurements on 158 rocks, from different sites in Bahia State, are here summarized. The rock samples were collected for radiometric dating by the Geochronological Research Centre of São Paulo University. The collection and the field description of the samples were carried out by Haroldo Sa' and Ernesto Alves (private communication). The maps of the location of the collected samples are presented in Fig. A.1.

A.1 Methodology

A.1.1 Density measurements

Since metamorphic and igneous rocks do not give a difference higher than 0.02 g cm^{-3} between "dry" and "saturated" densities, all the measurements were carried out on dry rocks.

The density measurement was carried out by weighting the rock sample, of about 10 cm^3, in both air and water. The results have an accuracy of ± 0.01 g. The scale was verified using a quartz crystal of known density of 2.650 g cm^{-3}.

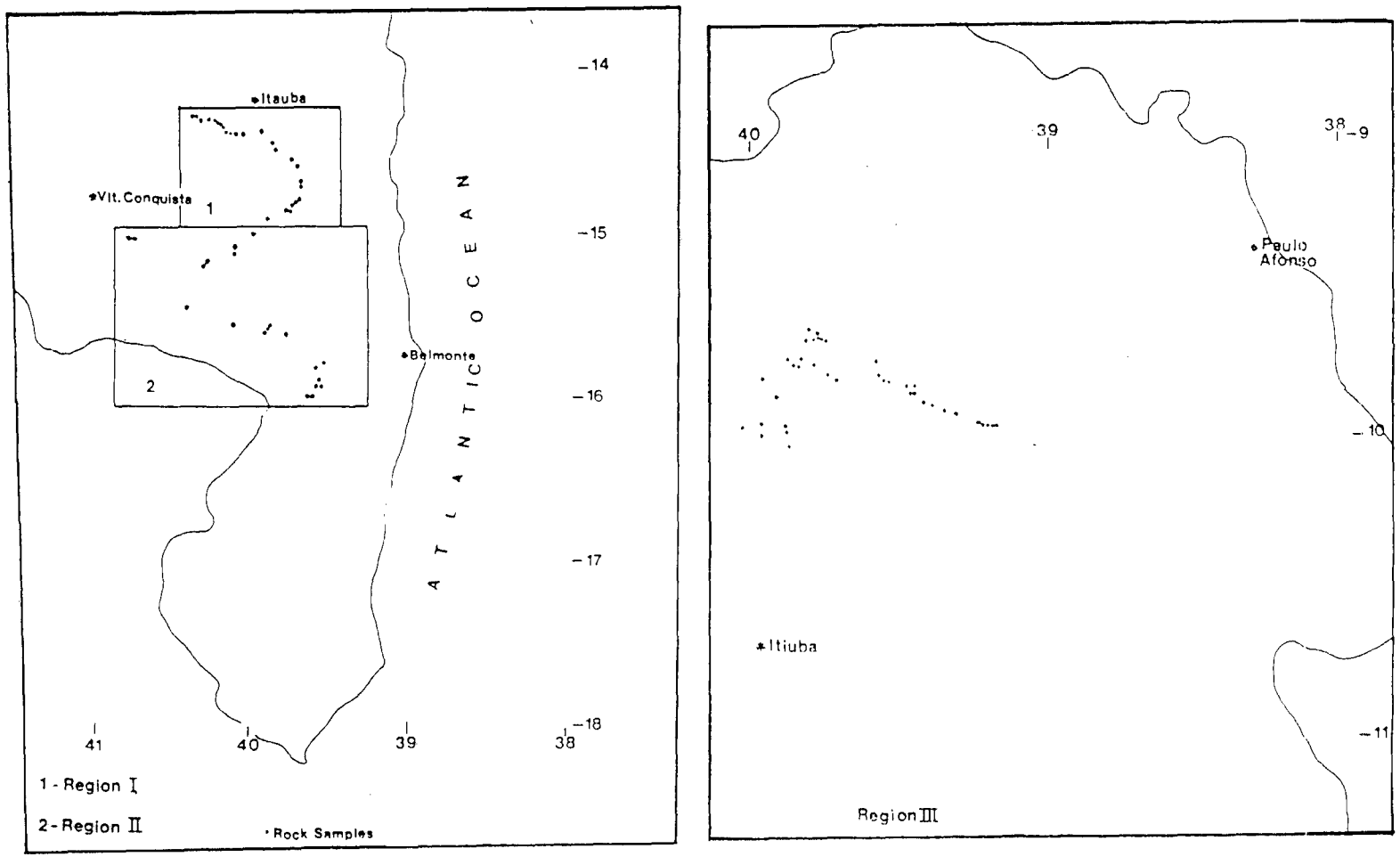

Fig. A.1 - The sites of the rock samples.

Region I : Jequié - Mutuípe Zone
Region II : Araçuai Fold System
Region III : Contendas - Uauá - Jacobina Fold Zone

The density value was obtained using the following formula:

$$d_r = M_1 [M_1 - M_2]^{-1} d_w$$

where M_1 = mass of the sample in the air (grams)

M_2 = mass of the sample in water (grams)

$d_w = 1.03 \text{ g cm}^{-3}$.

The estimated error is about $\pm 0.02 \text{ g cm}^{-3}$.

A.1.2 Magnetic susceptibility measurements

The magnetic susceptibility measurements were carried out using a commercial susceptibilimeter Bison, based on Mooney's magnetic susceptibiliter bridge (Mooney, 1952). The accuracy is about 10%.

A.2 Lithology

The rocks were collected from three different regions in Bahia State (Fig. A.1). The first region, is the Jequie-Mutuipe zone, within the Eastern Bahia Shield (see chapter 2, section 2.2.4). The rocks are high grade granulites, gneisses and migmatites, probably of Archean or Lower

Proterozoic age. The gneisses show a high degree of feldspathization.

The region 2 is the Araçuai Fold System. The rock samples are greenschist faceis gneisses, migmatites, granites and syenites.

Half of the samples used in this study were collected from Contendas-Uauá-Jacobina fold zone. This zone is composed of high grade metamorphic rocks (granulites, migmatites and amphibolites) and syenites, granodiorites and and gabbros of the Lower Proterozoic.

A.3 Results

The results are listed in Table A.1 and A.2, together with the lithology and coordinates of the rock samples. In Fig. A.2, the results are presented in histograms for density and magnetic susceptibility, for each of the previously described regions.

The average value and the respective standard deviation were calculated for each histogram of density measurements and the results can be summarized as follows:

REGION I

Rock no.	Coordinates Lat.	Long.	Density g cm^{-3}	Mag.susc. x10^{-6} emu	Rock type
JM/BA/260A	-14.3455	-40.3148	2.66	57	granite
JM/BA/260B	-14 3455	-40.2917	2.68	220	granite
JM/BA/261A	-14.3636	-40.2685	2.68	462	gneiss
JM/BA/261B	-14.3636	-40.2685	2.64	323	gneiss
JM/BA/262	-14.3636	-40.2129	2.98	42	amphibolite
JM/BA/263	-14.3636	-40.1759	2.62	196	gneiss
JM/BA/264	-14.3727	-40.1620	2.69	529	granulite
JM/BA/265	-14.3818	-40.1620	2.61	592	granulite
JM/BA/266	-14.3909	-40.1528	2.63	103	granulite
JM/BA/267A	-14.4000	-40.1389	2.66	686	granulite
JM/BA/267B	-14.4000	-40.1389	2.65	903	granulite
JM/BA/267C	-14.4000	-40.1389	2.64	846	granulite
JM/BA/268	-14.4273	-40.1111	2.70	700	granulite
JM/BA/269	-14.4455	-40.1019	2.69	2249	granulite
JM/BA/270	-14.4455	-40.0833	2.66	2332	granulite
JM/BA/271	-14.4500	-40.0648	2.69	2044	granulite
JM/BA/272	-14.4500	-40.0463	2.80	3185	granulite
JM/BA/273	-14.4455	-40.0000	2.73	1863	granulite
JM/BA/274	-14.4364	-39.8935	2.67	273	granulite
JM/BA/275	-14.5091	-39.8148	3.02	835	granulite
JM/BA/276	-14.5455	-39.8009	2.61	518	pegmatite
JM/BA/277	-14.6136	-39.6944	2.72	693	granulite
JM/BA/278	-14.6500	-39.6667	2.88	4810	granulite
JM/BA/279	-14.7455	-39.6482	2.74	51	granulite
JM/BA/280	-14.7727	-39.6482	3.04	58	granulite
JM/BA/281A	-14.8545	-39.6620	2.86	73	granulite
JM/BA/281B	-14.8545	-39.6620	2.81	-	granulite
JM/BA/281C	-14.8545	-39.6620	2.81	471	migmatite
JM/BA/281D	-14.8545	-39.6620	2.74	1480	pegmatite
JM/BA/282A	-14.8727	-39.6806	2.88	55	agmatite
JM/BA/282B	-14.8727	-39.6806	2.67	1411	agmatite
JM/BA/283	-14.9000	-39.7037	3.10	4088	diabase
JM/BA/284	-14.9182	-39.7130	2.85	17	gneiss
JM/BA/285	-14.9182	-39.7407	2.99	630	migmatite
JM/BA/286A	-14.9636	-39.8611	2.96	7697	migmatite gneiss
JM/BA/286B	-14.9636	-39.8611	2.68	1683	feldspathic gneiss
JM/BA/286C	-14.9636	-39.8611	2.66	734	feldspathic gneiss
JM/BA/286D	-14.9636	-39.8611	2.68	719	feldspathic gneiss
JM/BA/286E	-14.9636	-39.8611	2.67	686	feldspathic gneiss
JM/BA/286F	-14.9636	-39.8611	2.62	298	pegmatite
JM/BA/286G	-14.9636	-39.8611	2.60	24	pegmatite
JM/BA/286H	-14.9636	-39.8611	2.74	533	feldspathic gneiss
JM/BA/287A	-15.0541	-39.9537	2.65	87	feldspathic gneiss
JM/BA/287B	-15.0541	-39.9537	2.62	422	feldspathic gneiss

REGION II

Rock no.	Coordinates Lat.	Long.	Density g cm^{-3}	Mag.susc. 10^{-6} emu	Rock type
JM/BA/288	-15.1351	-40.0741	2.64	2	gneiss
JM/BA/289	-15.1712	-40.0741	2.78	-	cataclastic gneiss
JM/BA/290A	-15.2432	-40.2639	2.70	22	biotite gneiss
JM/BA/290B	-15.2432	-40.2639	2.70	30	biotite gneiss
JM/BA/290C	-15.2432	-40.2639	2.65	14	gneiss
JM/BA/290D	-15.2432	-40.2639	2.68	11	gneiss
JM/BA/290E	-15.2432	-40.2639	2.63	69	gneiss
JM/BA/290H	-15.2432	-40.2639	2.65	21	pegmatoid
JM/BA/291C	-15.2252	-40.2487	2.68	21	gneiss
JM/BA/291F	-15.2252	-40.2487	2.65	2	gneiss
JM/BA/292E	-15.4955	-40.3796	2.73	25	micaschist
JM/BA/292G	-15.4955	-40.3796	2.74	26	micaschist
JM/BA/293A	-15.6036	-40.0833	2.65	1511	gneiss
JM/BA/293B	-15.6036	-40.0833	2.62	376	gneiss
JM/BA/294	-15.6396	-39.8704	2.86	19	syenite
JM/BA/295	-15.6577	-39.8889	2.67	12	gneiss
JM/BA/296A	-15.6216	-39.8611	2.65	261	gneiss
JM/BA/296C	-15 6216	-39 8611	2.63	488	gneiss
JM/BA/297	-15 6667	-39.7500	2.70	2	gneiss
JM/BA/298B	-16 0541	-39.6157	2.66	18	granite
JM/BA/299B	-16.9910	-39.5185	2.68	12	migmatite
JM/BA/299C	-15.9910	-39.5185	2.94	46	migmatite
JM/BA/300A	-15.9910	-39.5370	2.78	172	migmatite
JM/BA/300B	-15.9910	-39.5370	2.82	2321	migmatite
JM/BA/301	-15.8829	-39.5648	2.73		granite
JM/BA/302B	-16.0541	-39.5926	2.63	6	granite
JM/BA/303	-15.9910	-39.5556	2.71	26	migmatite
JM/BA/304A	-15.9550	-39.5463	2.66	20	migmatite gneiss
JM/BA/304B	-15.9550	-39.5463	3.00	78	migmatite gneiss
JM/BA/305A	-15.8454	-39.5185	3.01	70	migmat te
JM/BA/305B	-15.8454	-39.5185	2.71	20	migmat te
JM/BA/305C	-15.8454	-39.5185	2.65	11	migmat te
JM/BA/306	-15.0773	-40.6944	2.66	17	migmat te gneiss
JM/BA/307B	-15.0727	-40.7222	2.67	41	gneiss

Table A.1 - Listing of density and magnetic susceptibility measurements. Region I and Region II.

REGION III

Rock no.	Coordinates Lat.	Long.	density g cm^{-3}	mag.suscep. 10^{-6} emu	rock type
JM/BA/340A	- 9.9459	-39.9630	2.64	679	granite
JM/BA/340B	- 9.9459	-39.9630	3.06	1107	amphibolite migmat.
JM/BA/340C	- 9.9459	-39.9630	2.78	2960	migmatite
JM/BA/340D	- 9.9459	-39.9630	2.66	1999	migmatite
JM/BA/340E	- 9.9459	-39.9630	2.66	388	migmatite
JM/BA/341	- 9.7297	-39.8704	2.70	507	granite
JM/BA/342	- 9.6667	-39.8056	2.74	2725	migmatite
JM/BA/343	- 9.6306	-39.7963	2.80	7132	gneiss
JM/BA/344A	- 9.6667	-39.7407	2.75	1517	mylonite
JM/BA/344B	- 9.6667	-39.7407	2.70	148	cataclasite
JM/BA/345	- 9.7477	-39.8519	2.71	15	gneiss
JM/BA/346A	- 9.7838	-39.7315	2.63	12	migmatite
JM/BA/346B	- 9.7838	-39.7315	2.72	329	migmatite
JM/BA/346C	- 9.7838	-39.7315	2.71	142	migmatite
JM/BA/346D	- 9.7838	-39.7315	2.71	28	migmatite
JM/BA/347	- 9.8018	-39.7037	2.72	161	gneiss
JM/BA/348A	- 9.8018	-39.6300	2.64	20	gneiss
JM/BA/348B	- 9.8018	-39.6300	2.58	9	leptite
JM/BA/349A	- 9.8018	-39.5463	2.64	158	feldspathic gneiss
JM/BA/349B	- 9.8018	-39.5463	2.62	322	gneiss
JM/BA/350A	- 9.7477	-39.7778	2.64	894	granite
JM/BA/350B	- 9.7477	-39.7778	2.65	785	granite
JM/BA/350C	- 9.7477	-39.7778	2.78	3350	migmatite
JM/BA/350D	- 9.7477	-39.7778	2.81	71	gabbro-norite
JM/BA/350E	- 9.7477	-39.7778	2.87	173	gabbro-norite
JM/BA/350F	- 9.7477	-39.7778	2.73	23	garnet leptite
JM/BA/350G	- 9.7477	-39.7778	2.83	4318	granodiorite
JM/BA/351A	-10.0180	-39.8704	2.67	0	garnet leptite
JM/BA/351B	-10.0180	-39.8704	2.65	16	granodiorite
JM/BA/352C	-10.0180	-39.8704	2.62	16	syenite
JM/BA/353	- 9.7477	-39.8333	2.64	696	granitoid
JM/BA/354	- 9.7297	-39.8241	2.68	192	gneiss
JM/BA/355A	- 9.9550	-39.8796	2.63	92	migmatite
JM/BA/355B	- 9.9550	-39.8796	2.67	10	migmatite
JM/BA/355C	- 9.9550	-39.8796	2.64	1769	migmatite
JM/BA/355D	- 9.9550	-39.8796	2.88	5957	migmatite
JM/BA/356	- 9.9685	-39.8796	2.79	1131	hornblendite
JM/BA/357	- 9.7928	-39.9537	2.64	1489	hornblendite
JM/BA/358	- 9.8559	-39.9074	3.07	9995	migmatite
JM/BA/359	- 9.9820	-39.9630	2.93	258	migmatite

REGION III

Rock no.	Coordinates Lat.	Long.	Density g cm^{-3}	Mag.Susc. 10^{-6} emu	Rock type
JM/BA/360	- 9.9550	-40.0278	2.74	3675	granite
JM/BA/361	- 9.6486	-39.7685	2.76	1710	syenite
JM/BA/362	- 9.6576	-39.7593	2.64	546	diorite
JM/BA/363	- 9.6667	-39.7500	2.75	1165	syenite
JM/BA/364	- 9.6667	-39.7500	2.77	2008	migmatite
JM/BA/365	- 9.7387	-39.5741	2.74	3068	gneiss
JM/BA/366	- 9.7928	-39.5648	2.71	56	amphibolite
JM/BA/367	- 9.8018	-39.5463	2.67	1714	migmatite
JM/BA/368	- 9.8108	-39.5278	2.68	925	gneiss
JM/BA/369	- 9.8300	-39.4722	2.66	801	gneiss
JM/BA/370	- 9.8468	-39.4630	3.06	419	diabase
JM/BA/371	- 9.8559	-39.4537	3.12	430	diabase
JM/BA/372A	- 9.8559	-39.4537	2.60	289	syenite
JM/BA/372B	- 9.8559	-39.4537	2.80	721	syenite/amphibolite
JM/BA/373	- 9.8559	-39.4537	3.02	53	amphibolite
JM/BA/374	- 9.8559	-39.4537	3.08	742	diabase
JM/BA/375A	- 9.8829	-39.4167	2.65	575	gneiss
JM/BA/375B	- 9.8829	-39.4167	3.03	973	diabase
JM/BA/376	- 9.8829	-39.4167	2.71	1924	migmatite
JM/BA/377A	- 9.8919	-39.3889	2.70	1251	gneiss
JM/BA/377B	- 9.8919	-39.3889	3.07	1383	diabase
JM/BA/378	- 9.9099	-39.3426	3.03	1092	gabbro
JM/BA/379	- 9.9189	-39.3056	3.14	419	gabbro
JM/BA/380	- 9.9550	-39.2269	2.63	14	granodiorite
JM/BA/381A	- 9.9640	-39.2130	2.63	39	amphibolite
JM/BA/381B	- 9.9640	-39.2130	-	11	leucogneiss
JM/BA/382A	- 9.9640	-39.1944	2.81	258	migmatite
JM/BA/382B	- 9.9640	-39.1944	2.91	246	migmatite
JM/BA/383	- 9.9640	-39.1852	2.67	1953	migmatite
JM/BA/384	- 9.9640	-39.1756	2.69	3376	gneiss
JM/BA/385	- 9.9640	-39.1667	2.61	258	gneiss
JM/BA/386A	- 9.8288	-39.4444	2.78	2489	gneiss
JM/BA/386B	- 9.8288	-39.4444	2.70	999	gneiss
JM/BA/386C	- 9.8288	-39.4444	2.67	1299	gneiss
JM/BA/386D	- 9.8288	-39.4444	2.73	2968	gneiss
JM/BA/386E	- 9.8288	-39.4444	2.69	1389	gneiss
JM/BA/387	- 9.1574	-39.9009	3.07	64	gabbro
JM/BA/388	- 9.1574	-39.9009	3.10	83	gabbro
JM/BA/389	- 9.1574	-39.9009	-	88	gabbro
JM/BA/390	- 9.1574	-39.9009	2.91	88	coarse gabbro
JM/BA/391	- 9.1574	-39.9009	2.62	322	coarse gabbro
JM/BA/392	- 9.1574	-39.9009	3.04	73	gabbro

Table A.2 - Listing of density and magnetic susceptibility measurements for Region III.

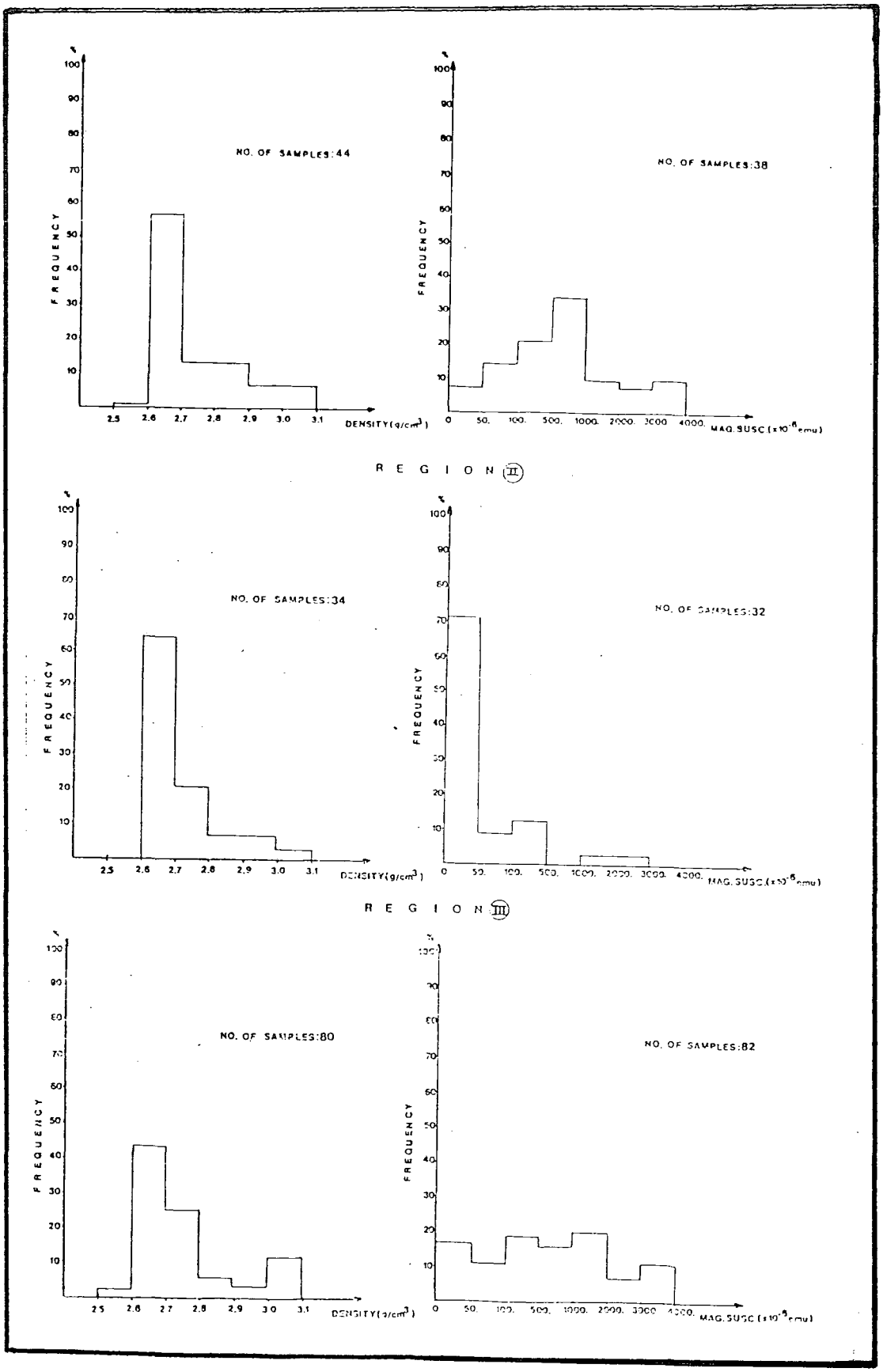

Fig. A.2 - Histogram of the results presented in Tables A.1 and A.2.

	$\bar{d}$	σ	N
Region I	2.70	0.06	44
Region II	2.71	0.06	34
Region III	2.71	0.06	80

For the average density, the formula is

$$\bar{d} = \frac{\sum_{i=1}^{M} Fi\ Xi}{\sum_{i=1}^{M} Fi}$$

and the respective standard deviation is given by:

$$\sigma^2 = \frac{\sum_{i=1}^{M} (Xi - \bar{d})^2\ Fi}{\sum_{i=1}^{M} Fi}$$

where

M = number of density intervals in the histogram;

Fi = frequency of density intervals in the histogram;

Xi = median value of the density at the i-th interval.

The density interval assumed in calculating both the average and the standard deviation is 0.05 g cm^{-3} . The rocks were subdivided into two groups in the final calculation of the average density. The first group included rocks with maximum density of 2.85 g cm^{-3} . The second group is composed of rocks with density higher than 2.85 g cm^{-3} . Because these high density rocks may represent a minor fraction of the upper crust composition, a weight of 0.5 was given to these rocks and 0.95 to rocks with density lower than 2.85 g cm^{-3} .

The results suggest that all regions have the same average density. However, the magnetic susceptibility of these rocks varies significantly. In particular, the magnetization of the region II is very low. The rocks in this region are mostly banded gneisses in which the melanocratic fraction is very small and the rock is essentially composed of plagioclase. The regions I and II present the same magnetically heterogeous basement.

APPENDIX B

Computer Programs

The computer programs used throughout the development of this research project are here listed.

The routine which calculates the Fast Fourier Transform is not listed since it is already published elsewhere. The reference of the subroutine which calculates the multivariate FFT is Singleton (1969).

The computer package which calculates the auto and cross spectra, prior to obtaining the response function is entirely based on Bloomfield (1975). Therefore, only the main programs which were modified are here listed. Reference to the already published subroutines is made when appropriate.

The 2D gravity modelling was carried out using the software available in the Department of Geological Sciences of Durham University and a program already published by Enmark (1981).

The Bahia State gravity data, with complete documentation, are available at the Instituto Astronomico e Geofisico of São Pãulo University (São Paulo, Brazil).

```
      SUBROUTINE CONI1(PHI,THET,PHI0,X,Y)
C THIS ROUTINE PROJECTS THE ELLIPSOIDAL COORDINATES PHI(LAT) AND
C THET(LONG) INTO X AND Y COORDINATES OF A CONICAL SECTION WITH ONE
C STANDARD PARALLEL PHI0.
C THE FORMULA WERE OBTAINED FROM:
C RICHARDUS,P. AND ADLER,R.K.-1972-"MAP PROJECTIONS"
C NORTH HOLLAND PUBL. CO.
C
C INPUT DATA:
C      PHI= LATITUDE IN DEGREES
C      THET= LONGITUDE
C      PHI0= STANDARD PARALLEL (LATITUDE) IN DEGREES
C
C OUTPUT DATA
C      X=NORTH COORDINATE IN THE CONICAL  PROJECTION ( IN METERS )
C      Y=EAST COORDINATE IN THE CONICAL PROJECTION ( IN METRES )
C

      DATA A,B,F/6378388.,6356911.9,297./
      A2=A*A
      B2=B*B
      EPS1=(A2-B2)/A2
      EPS=SQRT(EPS1)
      EPSM=0.5*EPS
      DEGRAD=ATAN(1.)/45.
      ARG1=45.-0.5*PHI
      ARG1=ARG1*DEGRAD
      ARG2=45.-0.5*PHI0
      ARG2=ARG2*DEGRAD
      TAN1=TAN(ARG1)
      TAN2=TAN(ARG2)
      TAN3=TAN1/TAN2
      IF(TAN3.LT.0.)TAN3=-TAN3
      PHI01=PHI0*DEGRAD
      PHI1=PHI*DEGRAD
      SIN1=SIN(PHI1)
      SIN10=SIN(PHI01)
      Z1=1.+EPS*SIN1
      Z2=1.-EPS*SIN1
      Z=Z1/Z2
      Z10=1.+EPS*SIN10
      Z20=1.-EPS*SIN10
      Z0=Z10/Z20
      ZZ=Z/Z0
      ZZ=ZZ**EPSM
      TZ=TAN3*ZZ
      ZZF=TZ**SIN10
      DEN=1.-EPS1*SIN10*SIN10
      ENE=A/SQRT(DEN)
      RHO=ENE*COTAN(PHI01)
      THET1=THET*DEGRAD
      ARG3=THET1*SIN10
      COEF=RHO*ZZF
      X=RHO-COEF*COS(ARG3)
      Y=COEF*SIN(ARG3)
      RETURN
      END
```

Program to produce the contour maps of Bahia State. The same program can be used to contour the Bouguer, free-air and the topographic maps starting from non-uniform data distribution. The computer software to interpolate the data and to produce the plot is the

*GPCP (A General Purpose Contouring Program-1971)
revised version 1973

which is available at Newcastle University computer.

```
 $RUN *GPCP 9=-HELP 1=BAHIA/CONI1 2=DATA/COORD2  SPRINT=-S3
 JOB  GPK2 BOUGUER ANOMALIES- DENS=2.67 G/CM3  -BAHIA/BRASIL
 FLEX
 PAGE   28.
 SIZE 5080050800    1.   1.0  -700000.20000    663914.   -672672.20000    700000.
 EDIT    2.
 CNTL  .07    .05     0     5
 CNTL (2F10.0,6F2.0,8A1)
 CNTL     1     2     0     0
 PAUS
 FLEX
 PAGE   28.
 SIZX 5080050800    1.   1.0  -700000.20000    663914.   -672672.20000    700000.
 EDIT    1.
 CNTL  .02    .12     0     5
 CNTL (2F10.0,2F8.2,F5.2,F8.2,F5.2,F5.0,8A1)
 CNTL     2     1     6     0
 BEND
 PRNT
 BLNK     1    40
 BND     211752.   -666016.    423492.   -668512.    425238.   -557328.
 BND     320242.   -444848.    240674.   -388592.    241408.   -305456.
 BND     321874.   -306288.    320895.   -389424.    240674.   -388592.
 BND     320242.   -444848.    428723.   -335456.    322853.   -223232.
 BND     324156.   -112560.    379548.    -13664.    406819.     -3008.
 BND     490911.    150544.    408855.    135264.    458369.    162160.
 BND     437413.    217840.    396807.    440000.    331328.    496304.
 BND     165014.    386896.    110227.    442592.   -110118.    414864.
 BND    -109792.    331776.         0.    332000.         0.    221280.
 BND    -109357.    221056.   -109792.    331776.   -110118.    414864.
 BND    -219582.    331136.   -328066.    219344.   -437413.    217840.
 BND    -435675.    107200.   -432200.   -114048.   -215238.   -222176.
 BND     107185.   -332304.    106313.   -554208.    212626.   -554832.
 BND     211752.   -666016.
 BLNK
 PAUS
 PHS4
 BOLD     2
 BLEV   10.
 PLOT
 LINE     0   5.6 15.5  5.5 15.6 0.10 0.02 0.0     -3
 LINE     0   5.5 15.6  5.5 15.8 0.10 0.02 0.0     -3
 LINE     0   5.5 15.8  5.5 16.0 0.10 0.02 0.0     -3
                    .
                    .
                    .
                    .
 LINE     0   5.8 15.3  5.7 15.4 0.10 0.02 0.0     -3
```

```
LINE     0  5.7 15.4  5.6 15.4 0.10 0.02 0.0    -3
SYMB     0 22.3 14.2   0. 0.17  17.              *SALVADOR
SYMB     0 23.1 22.0   0. 0.17  17.              *PAULO AFONSO
SYMB     0 22.2 18.9   0. 0.17  17.              *RIB. POMBAL
SYMB     0 21.2 19.6   0. 0.17  17.              *EUCL.CUNHA
                        .
                        .
                        .
                        .
                        .
                        .
SYMB     0 19.9  3.2   0. 0.17  17.              *MUCURI
SYMB     0 20.3  3.5   0. 0.17  17.              *N.VICOSA
SYMB     0 21.3  8.0   0. 0.17  17.              *BELMONTE
SYMB     0 21.2 11.4   0. 0.17  17.              *ITACARE
SYMB     0 2.78  4.0   0. 0.20  28.              STATIONS REFERRED TO IGSN-71
SYMB     0 2.78  3.6   0. 0.20  30.              ***THEORETICAL GRAVITY***
SYMB     0 2.78  3.2   0. 0.20  30.                ***FORMULA - 1967***
SYMB     0 11.3  3.5   0. 0.20  30.              CONICAL PROJECTION
SYMB     0 11.3  3.0   0. 0.20  30.              CONTOUR INTERVAL 10. MGALS
SYMB     0 22.8  8.0  70. 0.25  30.              A T L A N T I C   O C E A N
SYMB     0 8.78  8.0   0. 0.20  30.              M I N A S   G E R A I S
SYMB     0 2.78  6.0   0. 0.30  30.              BOUGUER ANOMALY MAP
SYMB     0 2.78  5.3   0. 0.20  30.              DENSITY:2.67 G/CM3
SYMB     0 3.97 0.59   0. 0.25   3.              47W
SYMB     0 6.10 0.59   0. 0.25   3.              46W
SYMB     0 8.19 0.59   0. 0.25   3.              45W
SYMB     010.29 0.59   0. 0.25   3.              44W
SYMB     021.20 25.3   0. 0.25   3.              39W
                       .
                       .
                       .
                       .
SYMB     023.40 25.3   0. 0.25   3.              38W
SYMB     025.60 25.3   0. 0.25   3.              37W
SYMB     0 0.99 22.6   0. 0.25   3.              9S
SYMB     0 0.87 20.5   0. 0.25   3.              10S
SYMB     0 0.87 18.3   0. 0.25   3.              11S
END
STOP
```

```
C  THIS PROGRAM  CALCULATES AND RECORDS THE FOURIER COEFFICIENTS
C  OF A EQUISPACED SERIES OF BOUGUER ( OR TOPOGRAPHIC ) DATA.
C
C  FILE 1 - TO INPUT THE DATA
C  FILE 2 - OUTPUT OF REAL AND IMAGINARY PART OF THE FOURIER
C           COEFFICIENTS
C  FILE 3 - OUTPUT OF THE SQUARED AMPLITUDE OF THE SPECTRUM
C
C
C  THE FOLLOWING SUBROUTINES ARE USED:
C
C    FFT - FROM SINGLETON (1969)
C  DATOUT - FROM BLOOMFIELD (1975)
C
      DIMENSION A1(1000),B1(1000),X(1000)
C
C     READ THE ORIGIN X0 AND SPACING DX OF THE DATA
C     IN THE PROFILE
C
      READ(1,*)X0,DX
C
      I=1
      AA=0.
C
C  READ THE BOUGUER ( OR TOPOGRAPHIC DATA )
C
 50   READ(1,*,END=99)X(I),A1(I)
      AA = AA + A1(I)
      B1(I)=0.
      I=I+1
      GO TO 50
 99   NX=I-1
      AA = AA/NX
C
C CALCULATE THE 1-D  FAST FOURIER TRANSFORM
C
      CALL FFT(A1,B1,NX,NX,NX,1)
C
C RECORD THE RESULTS ACCORDING TO THE FORMAT REQUIRED
C IN THE FOLLOWING AUTO AND CROSS SPECTRA CALCULATION
C SUBROUTINE DATOUT IS FROM BLOOMFIELD (1975).
C
      NPGM=NX/2+1
      DO 10 I=1,NPGM
      A1(I)=A1(I)/SQRT(NX)
      B1(I)=-B1(I)/SQRT(NX)
 10   CONTINUE
C
C A1 IS THE REAL PART
C B1 IS THE IMAGINARY PART
C
      CALL DATOUT(A1,NPGM,X0,DX,3)
      CALL DATOUT(B1,NPGM,X0,DX,3)
C
C CALCULATE AND RECORD THE SQUARED AMPLITUDE OF THE SPECTRUM
C
      DO 20 I=1,NPGM
      A1(I)=A1(I) * A1(I) + B1(I) * B1(I)
 20   CONTINUE
      CALL DATOUT(A1,NPGM,X0,DX,2)
       STOP
       END
```

```
C  PROGRAM PROG.AUTO MODIFIED FROM BLOOMFIELD (1975).
C  THIS PROGRAM CARRIES OUT PERIODOGRAM SMOOTHING TO
C  OBTAIN A SPECTRUM ESTIMATE. THE SPECTRUM ESTIMATE IS COMPUTED
C  BY REPEATED SMOOTHING WITH MODIFIED DANIELL WEIGHTS.
C  THE PROGRAM IS CONTROLLED BY THE FOLLOWING VARIABLES:
C
C  NK   THE NUMBER OF SMOOTHING PASSES
C
C  K    AN ARRAY OF THE SMOOTHING PARAMETERS
C
C  NOTE: THE PERIODOGRAM TO BE SMOOTHED IS READ IN
C        BY SUBROUTINE DATIN. SUBROUTINES MODDAN,
C        DATIN AND DATOUT IN BLOOMFIELD (1975)
C
C
C  FILE 1 - INPUT OF VARIABLES WHICH CONTROLS THE PROGRAM
C  FILE 2 - OUTPUT OF THE VARIABLES READ IN FILE 1
C  FILE 7 - INPUT THE SQUARED AMPLITUDE OF THE SPECTRUM
C           TO BE SMOOTHED
C  FILE 8 - OUTPUT OF ORIGINAL SERIES
C  FILE 10 - OUTPUT OF SMOOTHED SERIES
C
      DIMENSION X(1000),Y(1000),K(10),FX(1000),NP(100),ALOGN(1000)
      DATA PI/3.141593/
      CALL DATIN (X,NPGM,START,STEP,7)
C
C  READ:
C    NOBS=LENGTH OF THE ORIGINAL SERIES(PERIODOGRAM RESCALED)
C         IT IS ASSUMED THAT THE INPUT PERIODOGRAM HAS BEEN CALCULATED
C         AS A SQUARED AMPLITUDE RATHER THAN THE TRUE PERIODOGRAM
C
C   NP2 = NOBS/2+1
C
C    NK = ARRAY OF SMOOTHING PASSES
C
C     K = ARRAY OF SMOOTHING PARAMETERS
C
      READ(1,1)NOBS,NP2,NK,(K(I),NP(I), I=1,NK)
1     FORMAT(10X,1315)
      READ(1,2)DX
2     FORMAT(F10.2)
      WRITE(2,6)NK
6     FORMAT(' NUMBER OF MODIFIED DANIELL PASSES IS',I5,/,
     *'VALUES OF K ARE - ')
      WRITE(2,1)(K(I),NP(I), I=1,NK)
      M=1
      DO 50 I=1,NK
      NPG=NP(I)
      CALL MODDAN(X,Y,NPG,M,K(I),1.)
50    M=NPG+M-1
      START=0.
      STEP=2.*PI/FLOAT(NP2)
      CALL DATOUT(X,NPGM,START,STEP,8)
      CALL DATOUT(Y,NPGM,START,STEP,10)
      STOP
      END
```

```
C
C THIS PROGRAM SMOOTHES THE CROSS-PERIODOGRAM
C OF TWO SERIES. THE SPECTRUM ESTIMATES ARE COMPUTED
C BY REPEATED SMOOTHING WITH MODIFIED DANIEL WEIGHTS
C PROGRAM WRITTEN BY BLOOMFIELD,P.(1975)-FOURIER ANALYSIS
C                     OF TIME SERIES:AN INTRODUCTION-PP. 232
C
C THE PROGRAM IS CONTROLLED BY THE FOLLOWING VARIABLES,
C WHICH ARE READ IN BY THE PROGRAM.
C
C  NK  THE NUMBER OF SMOOTHING PASSES
C
C  K   AN ARRAY OF THE SMOOTHING PARAMETERS
C
C  NOTE:THE TRANSFORMS AND THE AUTO-SPECTRUM ESTIMATES OF
C       THE TWO  SERIES ARE READ IN BY SUBROUTINE DATIN
C       SUBROUTINE GRAPH ALREADY LISTED IN PAGE B-
C
C  SUBROUTINES USED DURING THE PROGRAM FROM BLOOMFIELD (1975)
C
C     DATIN  - TO READ THE FOURIER TRANSFORMS AND THE AUTO
C              SPECTRA OF THE TWO SERIES TO BE CROSS-
C              -CORRELATED
C
C     DATOUT - TO RECORD THE RESULTS
C
C     MODDAN - SUBROUTINE TO SMOOTH THE PERIODOGRAM
C
C
C     GRAPH (SEE PAGE B-18 )
C
C  FILES USED THROUGHOUT THE PROGRAM:
C
C     FILE 1 - INPUT PARAMETERS FOR SMOOTHING
C
C     FILE 5 - INPUT DEVICE NUMBER
C
C     FILE 6 - OUTPUT DEVICE NUMBER
C
C     FILE 7 - FOURIER COEFFICIENTS OF SERIES 1
C
C     FILE 8 - FOURIER COEFFICIENTS OF SERIES 2
C
C     FILE 9 - PLOT FILE
C
C     FILE 11 - OUTPUT OF THE RESULTS (RESPONSE FUNCTION
C               COHERENCY AND PHASE SPECTRA)
C

      DIMENSION SP1(1000),SP2(1000),TR1(1000),TI1(1000),
     *TR2(1000),TI2(1000),K(10),Y(1000),FX(1000),NP(100),Q(1000)
      DATA PI/3.141593/
      CALL DATIN(TR1,NPGM1,START,STEP,7)
      CALL DATIN(TI1,NPGM1,START,STEP,7)
      CALL DATIN(TR2,NPGM2,START,STEP,8)
      CALL DATIN(TI2,NPGM2,START,STEP,8)
      IF(NPGM1.EQ.NPGM2)GO TO 20
      WRITE(6,2)NPGM1,NPGM2
2     FORMAT('*ERROR-TRANSFORM LENGTHS',2I5,' DIFER.')
      STOP
```

```
20    CONTINUE
      N=NPGM1
      CALL DATIN(SP1,N1,START,STEP,12)
      CALL DATIN(SP2,N2,START,STEP,10)
      IF((N1.EQ.N) .AND. (N2.EQ.N))GO TO 66
      WRITE(6,3)N,N1,N2
3     FORMAT('*ERROR - TRANSFORM LENGTH',I5,'NOT THE SAME
     *AS SPECTRA LENGTHS',2I5)
      STOP
66    CONTINUE
      READ(1,1)NOBS,NP2,NK,(K(I),NP(I),I=1,NK)
1     FORMAT(10X,13I5)
      READ(1,11)DX
11    FORMAT(F10.2)
      NP2=(N-1)*2
      DO 30 I=1,N
      CR=TR1(I)*TR2(I)+TI1(I)*TI2(I)
      CI=TI1(I)*TR2(I)-TR1(I)*TI2(I)
      TR1(I)=CR
      TI1(I)=CI
30    CONTINUE
      WRITE(6,6)NK
6     FORMAT(' NUMBER OF MODIFIED DANIELL PASSES IS',I5,/,
     *'VALUES OF K ARE -')
      WRITE(6,1)(K(I),NP(I),I=1,NK)
      M=1
      DO 40 I=1,NK
      NN=NP(I)
      CALL MODDAN(TR1,Y,NN,M,K(I),1.0)
      CALL MODDAN(TI1,Y,NN,M,K(I),-1.0)
40    M=NN+M-1
      CALL POLAR (TR1,TI1,N)
      DO 50 I=1,N
      Q(I)=SP1(I)/TR1(I)
      TR2(I)=TR1(I)/SP2(I)
50    TR1(I)=TR1(I)/SQRT(SP1(I)*SP2(I))
      START=0.
      STEP=PI/FLOAT(N-1)
      WRITE(11,777)
777   FORMAT(' COHERENCY SPECTRUM')
      CALL DATOUT( TR1,N,START,STEP,11)
      WRITE(11,888)
888   FORMAT(' PHASE SPECTRUM ')
      CALL DATOUT( TI1,N,START,STEP,11)
      WRITE(11,999)
999   FORMAT(' RESPONSE FUNCTION')
      CALL DATOUT( TR2,N,START,STEP,11)
      XL=NOBS*DX
      STEP2=1./XL
      DO 60 I=2,N
      ALAMB=NOBS/(I-1)
      ALAMB=ALAMB*DX
 60   FX(I)=ALOG10(ALAMB)
C
C  GRAPH THE RESPONSE FUNCTION
C
      WRITE(6,441)
441   FORMAT(1X,'GRAPHIC OUTPUT FOR RESPONSE FUNCTION')
      CALL GRAPH(N,FX,TR2)
C
```

```
C  GRAPH THE COHERENCY FUNCTION
C
      WRITE(6,222)
222   FORMAT(1X,'GRAPHIC OUTPUT FOR COHERENCY')
      CALL GRAPH(N,FX,TR1)
C
C GRAPH THE PHASE
C
      WRITE(6,333)
333   FORMAT(1X,'GRAPHIC OUTPUT FOR PHASE')
      CALL GRAPH(N,FX,TI1)
      STOP
      END
```

```
C      PROGRAM TO CALCULATE THE RESPONSE FUNCTION AS A
C      FUNCTION OF WAVELENGTH (SEE BANKS ET AL., 1977
C      FOR REFERENCE) PREDICTED BY AN ELASTIC PLATE
C      LOADED ON TOP AND COMPENSATION AT DEPTH TC.
C
C      SUBROUTINES USED:
C
C          PLATE
C
C          GRAPH (SEE PAGE B-18  )
C
C          FREQ
C
C      FILES USED:
C
C          FILE 1 - TO INPUT THE PARAMETERS OF THE MODEL
C
C          FILE 6 - OUTPUT  OF THE RESULTS
C
C          FILE 9 - PLOT FILE
C
C
C     INPUT DATA:
C
C          NX - NUMBER OF DATA POINTS IN THE PROFILE
C          RHO0 - DENSITY OF THE LOAD ( G/CC)
C          RHO1 - DENSITY OF THE CRUST (G/CC)
C          RHO2 - DENSITY OF THE MANTLE (G/CC)
C          RL - FLEXURAL RIGIDITY OF THE PLATE (N.M)
C          TC - DEPTH OF COMPENSATION  (KM)
C          DX - SPACING BETWEEN THE POINTS OF THE PROFILE
C               IN KM.
C
C      OUTPUT :
C
C          NX2 - NUMBER POINTS IN THE SPECTRUM
C
C          FQX - FREQUENCY IN 1/KM
C
C          FQX2 - LOG10 OF WAVELENGTH (KM)
C
       DIMENSION FQX(1000),RESP(1000),FQX2(1000)
C
C READ THE PARAMETERS OF THE MODEL
C
       READ(1,*)NX, RHO0, RHO1, RHO2, RL, TC, DX
       NX2 = NX/2 +1
C
C CALCULATE THE ASSOCIATED WAVENUMBER AND WAVELENGTH
C
       CALL FREQ( NX, FQX , FQX2 , DX)
C
C CALCULATE THE THEORETICAL RESPONSE FUNCTION
C
       CALL PLATE(NX2,FQX,RHO0,RHO1,RHO2,RL,TC,DX,RESP)
C
C GRAPH OF THE RESPONSE FUNCTION AS A FUNCTION OF THE
C WAVELENGTH
C
       CALL GRAPH(NX2,FQX2,RESP)
```

```
C
C OUTPUT THE PARAMETERS OF THE MODEL
C
      WRITE(6,44)NX,RHO0,RHO1,RHO2,RL,TC
 44   FORMAT('NX=',I5,'RHO0=',F7.4,'RHO1=',F7.4,'RHO2=',F7.4,
     *'RL=',E7.2,'TC=',F7.4)
C
C PRINT THE RESULTS
C
      WRITE(6,41)
 41   FORMAT(' WAVELENGTH(KM)    ADMITTANCE(MGAL/M)')
      DO 55 I=2,NX2
 55   WRITE(6,20)FQX2(I),RESP(I)
 20   FORMAT(F10.2,5X,G15.5)
      GO TO 1212
999   CONTINUE
      STOP
      END
C
C
C
      SUBROUTINE FREQ(NX,FQX,FQX2,DX)
      DIMENSION FQX(1),FQX2(1)
      CONS=8*ATAN(1.)
      NX2=NX/2+1
      DO 10 I=1,NX2
      FQX(I)=CONS*(I-1)/NX
10    CONTINUE
      DO 20 I=2,NX2
      ARG=NX/(I-1)
      ARG=ARG*DX
      FQX2(I)=ALOG10(ARG)
20    CONTINUE
      RETURN
      END
C
C
      SUBROUTINE PLATE(NX2,FREQ,RHO0,RHO1,RHO2,RL,D1,DX,RESP)
C
C THIS ROUTINE CALCULATES THE RESPONSE FUNCTION OF AN  ELASTIC PLATE
C LOADED ON TOP AND COMPENSATION AT DEPTH D1.
C ARGUMENTS ARE:
C RHO0=DENSITY OF THE MATERIAL INFILLING DEPRESSION (LOWER CRUST)
C       IN G/CM3
C RHO1=CRUSTAL DENSITY IN G/CM3
C RHO2=DENSITY OF THE MANTLE IN G/CM3
C RL=FLEXURAL RIGIDITY IN N.M
C D1=DEPTH OF COMPENSATION IN KM.
C DX=SPACING OF THE GRAVITY DATA(KM)
C RESP(I)=RESPONSE FUNCTION IN MGAL/M
C
C HERE THE SUBROUTINE STARTS:
      DIMENSION FREQ(1),RESP(1)
      DD=D1/DX
      A1=RHO2-RHO0
      A2=RHO1-RHO0
      DIF=RHO2-RHO1
      CONS=6.2830*6.67*RHO0*980.
      DO 10 I=1,NX2
      F=FREQ(I)/DX
```

```
      FREQ2=F*F
      A=A1*980.+RL*FREQ2*FREQ2*1.E-13
      B=DIF*EXP(-FREQ(I)*DD)+A2
      RESP(I)=CONS*B/A
      RESP(I)=RESP(I)*0.001
10    CONTINUE
      RETURN
      END
```

```
C- THIS PROGRAM CALCULATES THE DEFLECTION AT THE MOHO
C- AND ITS GRAVITY EFFECT PREDICTED BY AN THIN AND
C- CONTINUOUS ELASTIC PLATE LOADED ON TOP.
C- THE DEFORMATION IS OBTAINED FROM THE ONE DIMENSIONAL
C- DIFFERENTIAL EQUATION OF THE DEFORMATION OF AN
C- ELASTIC PLATE LOADED ON TOP, IN THE EQUILIBRIUM. SEE
C- BANKS ET AL. (1977) FOR REFERENCE.
C- THIS PROGRAM USES THE FAST FOURIER TRANSFORM ROUTINE
C- BY SINGLETON (1979).
C-
C- THE INPUT PARAMETERS ARE:
C-
C-  X    - COORDINATES OF THE EQUISPACED
C-         TOPOGRAPHIC DATA ( IN KM ).
C-
C-  H    - EQUISPACED TOPOGRAPHIC DATA (IN KM).
C-
C- DX    - DISTANCE BETWEEN THE TOPOGRAPHIC DATA ( IN KM ).
C-
C- RHO0 - DENSITY OF THE TOPOGRAPHIC LOAD (IN G/CC).
C-
C- RHOC - DENSITY OF THE CRUST (IN G/CC).
C-
C- RHOM - DENSITY OF THE MANTLE (IN G/CC)
C-
C-   TE - EFFECTIVE ELASTIC THICKNESS IN KM.
C-
C-   TC - DEPTH OF THE COMPENSATION IN KM.
C-
C-    M - ORDER OF THE SERIES EXPANSION ( PARKER'S METHOD ).
C-
C-   X0 - MINIMUM X-COORDINATE FOR PLOTTING
C-
C-   XL - MAXIMUM X-COORDINATE FOR PLOTTING
C-
C- THE OUTPUT PARAMETERS ARE:
C-
C-  NX   - NUMBER OF DATA POINTS.
C-
C-  RM1 - MOHO TOPOGRAPHY IN KM.
C-
C-  DELG- GRAVITY EFFECT ASSOCIATED WITH THE MOHO TOPOGRAPHY
C-        IN MGAL.
C-
C- I/O DEVICES USED IN THE PROGRAM:
C-
C-   FILE 1 - READ THE COORDINATES AND TOPOGRAPHY.
C-   FILE 5 - READ THE REMAINING INPUT DATA
C-   FILE 6 - WRITE THE RESULTS: COORDINATES, INPUT TOPOGRAPHY,
C-            MOHO DEFLECTION AND THE GRAVITY EFFECT.
C-   FILE 9 - PLOTFILE TO BE USED IN RUNNING DURH:EASYPLOT
C-
      DIMENSION X(1000),DELG(1000),H(1000),RM1(1000),RM2(1000)
      DIMENSION FQX(1000),HI(1000),FILT(1000)
C-
C- INPUT THE PARAMETERS OF THE MODEL
C-
      READ(5,*)DX,RHOC,RHOM,TE,TC,M
      I=1
C-
```

```
C- READ THE COORDINATES AND TOPOGRAPHY
C-
 100    READ(1,*,END=99)X(I),H(I)
        I=I+1
        HI(I)=0.
        GO TO 100
 99     NX=I-1
C-
C- READ THE MINIMUM AND MAXIMUM COORDINATES FOR PLOTTING
C-
        READ(5,*)X0,XL
C-
C- GRAPH THE INPUT TOPOGRAPHY
C-
        CALL GRAPH(NX,X,H,X0,XL,DX)
C-
C-START CALCULATING THE MOHO DEFLECTION
C-
C-CALCULATE THE FOURIER TRANSFORM OF THE TOPOGRAPHY
C-
            CALL FFT(H,HI,NX,NX,NX,1)
            CALL FREQ(FQX,NX,DX)
C-
C- CALCULATE THE GREEN FUNCTION OF THE DIFFERENTIAL
C- EQUATION OF THE DEFORMATION OF A CONTINUOUS AND
C- THIN ELASTIC PLATE
C-
            CALL ISO(FILT,NX,RHOC,RHOM,TE,FQX)
C-
       CONS=RHO0/(RHOM-RHOC)
       DO 20 I=1,NX
       RM1(I) = CONS*H(I)*FILT(I)
 20    RM2(I)=CONS*HI(I)*FILT(I)
C
C GET THE MOHO TOPOGRAPHY BY INVERSE FOURIER TRANSFORM
C
       CALL FFT(RM1,RM2,NX,NX,NX,-1)
       DO 25 I=1,NX
 25    RM1(I)=RM1(I)/NX
C
C CALCULATE THE GRAVITY EFFECT OF THE MOHO TOPOGRAPHY USING
C PARKER'S METHOD(1972) EXPANDED UP TO 5TH. ORDER
C
            CALL GPARK(DELG,RHOC,RHOM,FQX,NX,TC,RM1,M)
C
C RECORD THE RESULTS
C
       WRITE(6,40)DX,RHO0,RHOC,RHOM,TE,TC,M,NX
 40    FORMAT(' DX=',F6.2,2X, 'RHO0=',F6.2,2X,'RHOC=', F6.2,2X,
      *' RHOM=',F6.2,2X,'TE=', F5.1,2X,'TC=',2X, 'M=',I3, 2X,'NX=',
      *I3)
       WRITE(6,50)
50     FORMAT('COORD',2X,'ALTITUDE',2X,'MOHO',2X,'GRAVITY')
       DO 30 I=1,NX
       WRITE(6,*)X(I),H(I),RM1(I),DELG(I)
30     CONTINUE
C
C - GRAPH OF THE GRAVITY EFFECT
C
       CALL GRAPH(NX,X,DELG,X0,XL,DX)
```

```
C
C - GRAPH OF THE MOHO
C
      CALL GRAPH(NX,X,RM1,X0,XL,DX)
      STOP
      END
C
C
       SUBROUTINE FREQ(FQX,NX,DX)
       DIMENSION FQX(1)
       PI=ATAN(1.)*4
       NN2=(NX+2)/2
       DEN = NX * DX
       DO 10 I=1,NN2
       FQX(I) = 2*PI*(I-1)/DEN
10     CONTINUE
       DO 30 I=1,NN2
       J=NX-I+1
30     FQX(J)=FQX(I+1)
       RETURN
       END
C
       SUBROUTINE ISO(FILT,NX,RHOC,RHOM,TE,FQX)
       DIMENSION FILT(1),FQX(1)
       RHO = RHOM-RHOC
       T3=TE*TE*TE
       RIG=1.E+7/(12*(1-0.25*0.25))
       DD=RIG*T3
       DEN=RHO*980.
       FACT=DD/DEN
       DO 10 I=1,NX
       FQ2=FQX(I)**2
       FQ4=FQ2*FQ2
       FILT(I)=1+(FQ4 * FACT)
 10    FILT(I)=1./FILT(I)
       RETURN
       END
C
       SUBROUTINE GPARK(DELG,RHOC,RHOM,FQX,NX,TM,ZR,M)
       DIMENSION DELG(1),FQX(1),ZR(1)
       DIMENSION W1(1000),W2(1000),AUX1(1000),AUX2(1000),FW(1000)
       DATA G/6.67/
       PI=ATAN(1.)*4
       RHO=RHOM-RHOC
C
C
        DO 10 I=1,NX
        AUX1(I)=1.
        W1(I)=0.
        W2(I)=0.
        FW(I)=1.
  10    CONTINUE
 C
 C
        SUM=1.
         DO 20 K=1,M
         SUM = SUM * K
               DO 40 I=1,NX
               AUX1(I) = AUX1(I) * ZR(I)
               AUX2(I) = 0.
```

```
   40          CONTINUE
C
   CALL FFT(AUX1,AUX2,NX,NX,NX,1)
C
          DO 50 I=1,NX
          W1(I) = AUX1(I) * FW(I)/SUM + W1(I)
          W2(I) = AUX2(I) * FW(I)/SUM + W2(I)
          FW(I) = FW(I) * FQX(I)
   50     CONTINUE
   20                          CONTINUE
C
                DO 60 I=1,NX
                EXPO=TM*FQX(I)
                EXPO=EXP(-EXPO)
                W1(I) = W1(I) * EXPO
                W2(I) = W2(I) * EXPO
   60           CONTINUE
C
C CALCULATE THE GRAVITY ANOMALIES IN THE SPACE DOMAIN
C
          CALL FFT(W1,W2,NX,NX,NX,-1)
                  CONS= 2*PI*G*RHO
                  DO 70 I=1,NX
  70                 DELG(I) = -CONS * W1(I)/NX
         RETURN
         END
C
C
       SUBROUTINE GRAPH(I,XI,ALTI,X0,XL,DX)
       DIMENSION XI(1),ALTI(1)
       DIMENSION HEAD(65),DEV(5)
       WRITE(6,10)
  10   FORMAT(1X,'GIVE THE FOLLOWING QUANTITIES:',/,1X,
      *43HHEAD=TITLE FOR THIS PLOT - MAX. 65 CHARACT. )
       READ(5,20)HEAD
  20   FORMAT(65A1)
 260   WRITE(6,30)
  30   FORMAT(35HGIVE THE DEVICE NAME:TEK,11,PTR,VDU)
       READ(5,40)DEV
  40   FORMAT(5A1)
       WRITE(6,50)
  50   FORMAT(1X,37HLETSIZ=LABEL LETTER SIZE(0.1 TO 0.5"),/,1X,
      *'PSIZE=REDUCTION FACTOR(0.1 TO 1.0 INCHES)',/,1X,
      *'SYMSIZ=PLOT SYMBOL SIZE(0.1 TO 0.5 INCHES)',/,1X,
      *'XLEN=X-AXE LENGTH (UP TO 36. INCHES)',/,1X,
      *'YLEN=Y-AXE LENGTH (DEPENDES ON THE OUTPUT DEVICE)',/,1X,
      *'NXDIV,NYDIV=NO. OF DIVISIONS IN X AND Y DIRECTIONS',/,1X,
      *'IDEF=1 IF THE MAXIMUM AND MINIMUM VALUES FOR X & Y WILL BE GIVEN'
      *,/,1X,'     =2 IF NOT AND THE PROGRAMS COMPUTES THEM TO GIVE A NICE
      *PLOT')
       READ(5,*)TSIZ,PSIZE,SYMS,XLEN,YLEN,NXDIV,NYDIV,IDEF
       IF(IDEF.NE.1)GO TO 60
       WRITE(6,70)
   70  FORMAT(1X,'GIVE THE FOLLOWING VALUES:',/,1X,
      *'XMIN,XMAX=MINIMUM AND MAXIMUM VALUES FOR X ',/,1X,
      *'YMIN,YMAX=SAME FOR Y')
       READ(5,*)XMIN,XMAX,YMIN,YMAX
   60  CONTINUE
  281  WRITE(9,80)HEAD,DEV
   80  FORMAT(' &OPTS',/,6X,'HEAD=',1H',65A1,2H',,/,6X,'DEV=',1H',
```

```
     *5A1,2H',,/,6X,
     *55HXLAB='                          DISTANCE IN                KM',
     *',',/,6X,
     *28HYLAB(1,1)='                     ',
     *',',/,6X,9HGRID='NO',',')
  282 WRITE(9,90)TSIZ,PSIZE,SYMS,XLEN,YLEN,NXDIV,NYDIV
   90 FORMAT(6X,'LETSIZ=',F4.2,',',/,6X,'PSIZE=',F5.2,',',/,6X,
     *'SYMSIZ=',F5.2,',',/,6X,'XLEN=',F6.2,',','YLEN=',F6.2,',',/,6X,
     *'NXDIV=',I3,',',/,6X,'NYDIV=',I3,',')
      IF(IDEF.NE.1)GO TO 100
      WRITE(9,110)XMIN,XMAX,YMIN,YMAX
  110 FORMAT(6X,'XMIN=',G10.2,',',/,6X,'XMAX=',G10.2,',',/,6X,'YMIN=',
     *G10.2,',',/,6X,'YMAX=',G10.2,',')
  100 WRITE(9,150)
  150 FORMAT(6X,'NY=1',',',/,6X,'NSYMB=2',',')
      WRITE(9,120)
  120 FORMAT(' &END')
      K1=(X0-XI(1))/DX + 1
      K2=I-(XI(I) - XL)/DX
      WRITE(8,*)K1,K2
      DO 130 K=K1,K2
      WRITE(9,*)XI(K),ALTI(K)
  130 CONTINUE
      WRITE(9,145)
  145 FORMAT('$ENDFILE')
      RETURN
      END
```

```
      SUBROUTINE GRAPH(I,XI,ALTI)
C
C  SUBROUTINE TO PRODUCE THE CONTROL CARDS TO RUN
C  THE PROGRAM DURH:EASYPLOT IN ORDER TO GET THE
C  SIMPLE PLOT OF "ALTI" AS FUNCTION OF "XI".
C
C  SEE DOCUMENTATION OF DURH:EASYPLOT FOR COMMENTS.
C
      DIMENSION XI(1),ALTI(1)
      DIMENSION HEAD(65),DEV(5)
      WRITE(6,10)
   10 FORMAT(1X,'GIVE THE FOLLOWING QUANTITIES:',/,1X,
     *43HHEAD=TITLE FOR THIS PLOT - MAX. 65 CHARACT. )
      READ(5,20)HEAD
   20 FORMAT(65A1)
  260 WRITE(6,30)
   30 FORMAT(35HGIVE THE DEVICE NAME:TEK,11,PTR,VDU)
      READ(5,40)DEV
   40 FORMAT(5A1)
      WRITE(6,50)
   50 FORMAT(1X,37HLETSIZ=LABEL LETTER SIZE(0.1 TO 0.5"),/,1X,
     *'PSIZE=REDUCTION FACTOR(0.1 TO 1.0 INCHES)',/,1X,
     *'SYMSIZ=PLOT SYMBOL SIZE(0.1 TO 0.5 INCHES)',/,1X,
     *'XLEN=X-AXE LENGTH (UP TO 36. INCHES)',/,1X,
     *'YLEN=Y-AXE LENGTH (DEPENDES ON THE OUTPUT DEVICE)',/,1X,
     *'NXDIV,NYDIV=NO. OF DIVISIONS IN X AND Y DIRECTIONS',/,1X,
     *'IDEF=1 IF THE MAXIMUM AND MINIMUM VALUES FOR X & Y WILL BE GIVEN
     *,/,1X,'     =2 IF NOT AND THE PROGRAMS COMPUTES THEM TO GIVE A NICE
     *PLOT')
      READ(5,*)TSIZ,PSIZE,SYMS,XLEN,YLEN,NXDIV,NYDIV,IDEF
      IF(IDEF.NE.1)GO TO 60
      WRITE(6,70)
   70 FORMAT(1X,'GIVE THE FOLLOWING VALUES:',/,1X,
     *'XMIN,XMAX=MINIMUM AND MAXIMUM VALUES FOR X ',/,1X,
     *'YMIN,YMAX=SAME FOR Y')
      READ(5,*)XMIN,XMAX,YMIN,YMAX
   60 CONTINUE
  281 WRITE(9,80)HEAD,DEV
   80 FORMAT(' &OPTS',/,6X,'HEAD=',1H',65A1,2H',,/,6X,'DEV=',1H',
     *5A1,2H',,/,6X,
     *55HXLAB='                                LOG10(WAVELENGTH) KM',
     *',',/,6X,
     *28HYLAB(1,1)='                    ',
     *',',/,6X,9HGRID='NO',',')
  282 WRITE(9,90)TSIZ,PSIZE,SYMS,XLEN,YLEN,NXDIV,NYDIV
   90 FORMAT(6X,'LETSIZ=',F4.2,',',/,6X,'PSIZE=',F5.2,',',/,6X,
     *'SYMSIZ=',F5.2,',',/,6X,'XLEN=',F6.2,',','YLEN=',F6.2,',',/,6X,
     *'NXDIV=',I3,',',/,6X,'NYDIV=',I3,',')
      IF(IDEF.NE.1)GO TO 100
      WRITE(9,110)XMIN,XMAX,YMIN,YMAX
  110 FORMAT(6X,'XMIN=',G10.2,',',/,6X,'XMAX=',G10.2,',',/,6X,'YMIN=',
     *G10.2,',',/,6X,'YMAX=',G10.2,',')
  100 WRITE(9,150)
  150 FORMAT(6X,'NY=1',',',/,6X,'NSYMB=2',',')
      WRITE(9,120)
  120 FORMAT(' &END')
      DO 130 K=1,I
      WRITE(9,*)XI(K),ALTI(K)
  130 CONTINUE
      WRITE(9,145)
  145 FORMAT('$ENDFILE')
      RETURN
      END
```